TECHNOLOGY AND INNOVATION

PROJECT NUMBER: PNC377-1516 June 2018

Optimising remotely acquired, dense point cloud data for plantation inventory

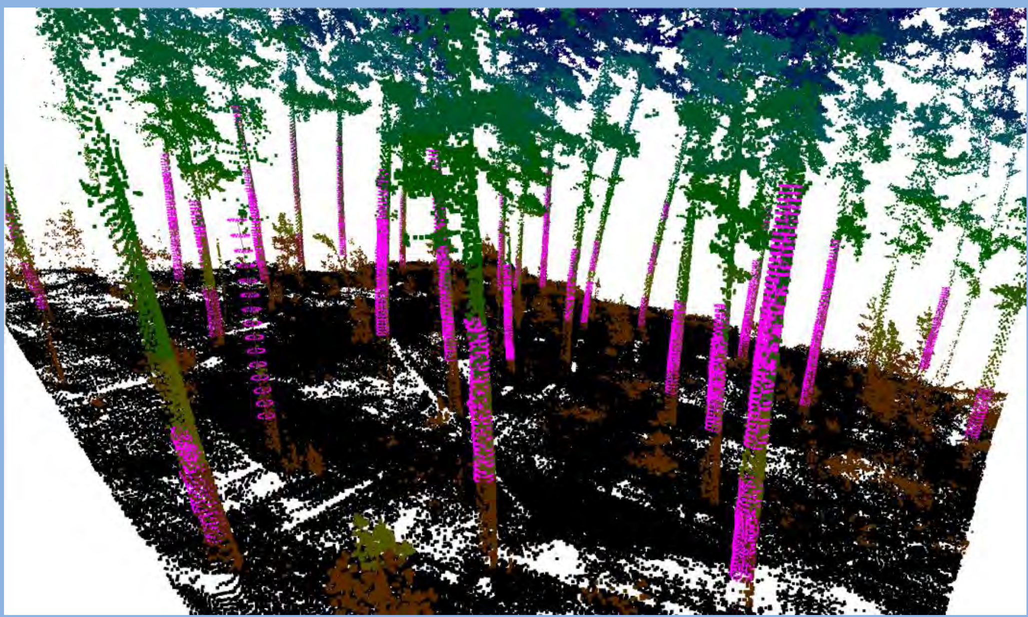

This report can also be viewed on the FWPA website: www.fwpa.com.au

FWPA Level 11, 10-16
Queen Street Melbourne VIC 3000, Australia
T +61 (0)3 9927 3200 F +61 (0)3 9927 3288
E info@fwpa.com.au

Optimizing remotely acquired, high resolution remotely sensed data for plantation inventory

Prepared for

Forest & Wood Products Australia

Final Report editors: Dr Michael Watt[1] & Dr Christine Stone[2]

[1]Geomatics,Scion
[2]Forest Science, NSW Department of Primary Industries - Forestry

Publication: Optimizing remotely acquired, dense point cloud data for plantation inventory

Project Number: **PNC377-1516**

IMPORTANT NOTICE

This work is supported by funding provided to FWPA by the Australian Government Department of Agriculture and Water Resources (DAWR).

ISBN: 978-1-925213-81-2

Researchers:

Christine Stone, Gabriele Caccamo (Forest Science, NSW Department of Industry Forestry); Jon Osborn, Arko Lucieer, Irfan Iqbal, Colin McCoull, Stephen Harwin, Darren Turner, Alex Pishchugin, Deepak Gautam, Saroj Sharma (Geography and Spatial Sciences, University of Tasmania); Winyu Chinthammit, Simon Hogwood (Human Interface Technology Laboratory, School of Engineering & ICT, University of Tasmania); Sean Krisanski, Mohammed Sadegh Taskhiri, Maciej Matuszak (Information and Communication Technology, University of Tasmania); Mitch Bryson (Australian Centre of Field Robotics, University of Sydney); Mike Watt, Grant Pearse, Joel Gordon, Dave Pont, Andrew Gordon, Ralf Gommers (Scion); David Herries, Susana Gonzalez, Barabara Del Perugia, Bruce Hill, Elizabeth Lee (Interpine).

Steering Committee:

Mike Sutton (Chair, Forestry Corporation NSW), Tony O'Hara (Hancock Victoria Plantations), Don Aurik (Timberlands Pacific), Lee Stamm (Hancock Queensland Plantations), Jan Rombouts (OneFortyOne), Rob Musk (Sustainable Timber Tasmania); Aaron Gunn (Blakely-Pacific NZ), Mark Forward (Nelson Forests NZ), Jo Drabsch (Rayonier NZ), David Crawley (PF Olsen NZ), Pete Watt (Indufor Asia Pacific), Sean McBride (Juken NZ), Bev Taylor (Ernslaw One), Sheldon Ellis (PanPac); Ian Hinton (Timberlands NZ), Brian Rawley (Silmetra).

Acknowledgements

The authors wish to thank Mike Sutton, Duncan Watt, Damien Petfield (Forestry Corporation NSW); Don Aurik (Timberlands Pacific); Peter McLoughlin (Norske Skog Paper Mills, Boyer); Lee Stamm (Hancock Queensland Plantations); Pete Watt (Indofur Asia Pacific) for their assistance with the study sites, provision of data and results and technical advice during the course of this project.

Final report received by FWPA in June 2018

Cover image: Modelled stem diameters applied by Mitch Bryson (Australian Centre of Field Robotics) to a dense point cloud acquired by Geomatic Technologies using a Riegl VUX-1LR laser scanner mounted on a helicopter flying over a *Pinus radiata* plantation. Data displayed in the open-source pointcloud viewer software "Meshlab".

Contents

Summary for Industry

Overview

This collaborative "Trans-Tasman" research project evaluated a series of novel, advanced remote sensing systems that capture accurate, 3D dense point cloud data in order to assess their potential for delivering operational plantation resource assessment tools. The project brought together internationally recognised expertise in remote sensing, Airborne Laser Scanning (ALS) and UAV technologies and robotics located within the TerraLuma group at the University of Tasmania, the New Zealand forest research agency Scion, the Australian Centre for Field Robotics, University of Sydney and NSW Department of Primary Industries. An important aspect of this project was also the collaborative engagement with the participating companies including Interpine and Indufor Asia Pacific.

The emerging diversity of platforms, sensors, algorithms and efficient processing workflows presents multiple opportunities across the forestry sector for more accurate and reliable resource information. This project represents the most recent FWPA and grower investment in a series of R&D projects focused on the evaluation of the advancing developments in remote sensing applications for the Australian forestry sector. We demonstrate that the improvements in the quality and density of data captured by these systems can be harnessed to significantly improve stand and tree-level assessment.

The overall aim of this project was to evaluate the acquisition, processing and analysis of dense point cloud data for the extraction of meaningful resource information acquired from light aircraft and UAV platforms.

Specifically the key tasks were to:

1) Evaluate whether UAV acquired ultra-high density point cloud datasets are suitable for tree-level on-screen visual assessment and 3D construction modelling for accurate estimation of stem attributes i.e. virtual plot inventory.

2) Develop efficient workflow processing pipelines for the analysis of dense point cloud data suitable for integration into operational LiDAR modelling systems for wood volumes and product prediction.

3) Develop and evaluate novel metrics extracted from dense ALS point clouds acquired by small aircraft and their impact on the recently implemented spatial plot imputation process for estimating resource volume and product mix.

In order to undertake these tasks and fulfil the proposed project deliverables, three Work Packages were developed by the project team, i.e.; i) 3D visualisation for interactive assessment of individual tree stems; ii) unmanned aircraft systems (UAS) LiDAR for dense point cloud acquisition and iii) Individual tree detection, 3D tree reconstruction, and automated extraction of improved point cloud metrics for forest inventory (e.g. use of voxelised metrics). These Work Packages represented the structure of the specific sub-projects that were undertaken, either individually or in combination to address the objectives and deliverables identified for this project.

Key findings

- *3D visualisation for interactive assessment of individual trees (section 2.1)*

Section 2.1 addresses 3D visualisation and assessment of individual trees using dense point cloud data. It includes a review of existing third-party software with functionality to import and visualise dense point cloud data and to automatically or semi-automatically segment tree stem and branches from that data. This section reports on trials of two third-party software using project data. It then describes the work undertaken to develop a proto-type immersive virtual reality application that allows users to visualise and interact with dense point cloud data, to measure key metrics such as tree height and DBH, and to view segmented stem data imported from other software. This section concludes with recommended next steps towards application development, testing and operationalisation. These tasks will be pursued in a new FWPA-funded, 12 month project “Enhanced forest inventory practice using immersive visualisation and measurement of dense point cloud data” (PNC464-1718), led by Dr Winyu Chinthammit at the University of Tasmania which commenced in July 2018.

- *Determination of optimal data acquisition parameters for UAS LiDAR tree inventory in pre-harvest Pinus radiata (Section 3.1)*

In order to gain the highest possible accuracy out of a UAS LiDAR scanner and the integrated positioning sensors there is a need for the operators to calibrate each component of the system. This Section (3.1) consisted of a series of objectives and tasks aimed at identifying optimal UAS LiDAR data acquisition parameters for forest inventory using a low-cost UAS LiDAR (Velodyne ‘Puck’) system which was built by the TerraLuma research group at the University of Tasmania. This process included developing a calibration workflow for lever arm determination and boresight calibration. When fully calibrated the UAS Velodyne system produced an absolute accuracy of between approximately 3 cm to 7 cm. Therefore, while this UAV system can accurately detect the stems and crowns of individual trees, it may be beyond the capacity of this instrument to accurately measure tree dimensions such as stem diameters.

An analysis of stem tree strikes revealed that best results were obtained if the system was flown close to the canopy, e.g. at altitudes of 35 m – 40 m for a 25 m canopy. It was also observed that an oblique mounting angle of the scanner did not improve the penetration of pulses hitting the stems or ground, however, a high side overlap and overlapping flight paths at perpendicular flight angles did result in maximizing stem strikes.

Finally, a flight planning software application was also developed that calculates point spacing, flight strip overlap, beam size on the ground etc., which assists in optimal flight planning and laser scanner configuration.

- *Optimal acquisition specifications for the Riegl VUX-1LR scanner over a Pinus radiata plantation (Section 3.2)*

The study for this section evaluated the acquisition specifications for a helicopter mounted Riegl VUX-1LR laser scanner that was flown over several study sites in Carabost State Forest, a plantation, near Tumut in southern NSW and managed by the Forestry Corporation of NSW. The flight path was flown over each study site in four directions (NS, EW, NWSE, SWNE) with a 15 m swath. For each study site the process was repeated three times at the altitudes of 30 m, 60 m and 90 m.

This flight pattern resulted in the collection of very large LiDAR datasets and before response metrics could be compared the data sets had to be pre-processed and thoroughly checked through a formal quality assurance and control process. Accompanying this section are two attachments. The first describes the essential process of establishing ground control points required for this type of very high resolution 3D data. The second attachment details the operational procedures associated with data quality assurance and control and provides examples of the high quality products that can be derived from these datasets.

The pulse and return density of this LiDAR dataset was very high: between 5,000 and 9,000 pulses/m^2 and over 8,000 pulses/m^2 respectively. From a height analysis based on local maxima of a 0.3 m resolution Canopy Height Model (CHM), the 90m and 60 m heights gave a positive result while the 30 m height presented an inaccurate canopy representation. The analysis of potential tree tops, based on peaks at different height peaks computed from the CHM indicated that the best flight altitude was 60 m. A stem detection methodology also confirmed the optimal flight altitude to be 60 m producing an accuracy of 91.9%.

- *A comparison of helicopter-based VUX-1LR LiDAR with below canopy UAV photogrammetry and manual measurements (Section 3.3)*

The aim of this study was to compare estimates of tree diameter at breast height derived from data acquired by a helicopter mounted Riegl VUX-1LR laser scanner (i.e. the same Carabost dataset acquired at 30 m, 60 m, and 90 m altitudes that was used in Section 3.2) with estimates derived from a point cloud created using below-canopy UAV photogrammetry. Manual DBH measurements were used as a baseline for comparison and analysis. The greatest correlation of remotely sensed DBH to manually measured DBH came from the below-canopy-canopy UAV photogrammetry, followed by the 60 m flying height with the VUX-1LR LiDAR sensor. The superior performance of the VUX-1LR data captured at 60 m compared to either 30 m or 90 m concurs with the results obtained in Section 3.2. Therefore where sub-canopy data is desired, it is recommended to fly at 60 m altitude with the VUX-1LR laser scanner.

The ultimate goal of using a sub-canopy UAV fitted with a stereo camera is for this process to be done with the user specifying a plot radius and plot centre and allowing the UAV-camera system to acquire point cloud data for each tree stem autonomously.

- *Algorithms and 3D modelling techniques for tree detection and tree-level volume estimates (Section 4.1)*

The research in this section focussed on the development of post-processing algorithms that can work with high-resolution aerially acquired pointcloud data to detect and segment individual trees, while making direct, automated measurements of stem parameters that are of interest to resource foresters. Two separate sets of algorithms/workflows have been developed in parallel: a “top-down” approach to tree detection and stem-fitting and a “bottom-up” approach to tree detection and stem profile measurements. These algorithms are adapted to resolutions of approximately 200-700—points/m^2, building upon existing techniques used for both traditional high-resolution terrestrial and low-resolution airborne LiDAR pointclouds. Results using the Riegl VUX-1 laser scanner pointclouds demonstrate the ability to accurately count and locate trees, while measuring diameters along the length of the stem that can be used for estimating tree taper and volume.

We also propose a prototype workflow pipeline that merges the two different approaches into a single workflow that would allow for efficient processing of dense pointclouds for providing tree stem maps and basic inventory attributes over both plot-scale and larger areas (Section 4.1, Figure 6). This workflow would initially perform tree detection based on canopy peak detection models and the RANSAC-based model fitting algorithms, which are assumed to be fast and scalable to larger LiDAR datasets. These detections would then provide refined candidate search regions in the pointcloud data that could be passed to the "Cloud2Stem' algorithms for a more accurate and computationally-intense search for tree stems from which stem attributes such as stem diameters, volume and taper could be extracted.

- *Comparison of models describing forest inventory attributes using standard and voxel-based LiDAR predictors across a range of pulse densities (Section 4.2)*

In addition to tree-scale characterisation using LiDAR data acquired from laser scanners with improved capacity and performance, these sensors mounted on light aircraft also hold considerable potential for improving the accuracy of area-based forest inventories. This study presents the evaluation of voxel-based metrics which are more commonly associated with the analysis of terrestrial LiDAR data. This was accomplished by comparing predictions of forest attributes made using voxel-based metrics, more standard LiDAR metrics and a combination of both classes of metrics.

A high-density LiDAR dataset was acquired using a helicopter-mounted Riegl VUX-1LR over *P. radiata* stands, near Tumut in southern NSW. Both the relative importance of pulse density and metric type were evaluated. The Section also provides a general description of voxelisation and the different types of voxel metrics. The results clearly demonstrated the utility of voxel-based metrics for the prediction of key plantation inventory attributes. Gains in predictive precision afforded by voxel-based metrics over the use of standard LiDAR metrics were substantial for predictions of basal area, stand density and volume and moderate for predictions of top height. The relative invariance of model precision to pulse density demonstrated that precision gains can be achieved using voxel-based metrics at pulse densities typical of current operational LiDAR acquisitions ($\cong$ 5 pulses/m^2).

The voxel-based metrics, described in Section 4.2, have now been implemented in the latest version of LAStools (RapidLASSO) and a summary of this implementation is provided at the end of the Section.

Discussion & Recommendations

This project has successfully evaluated in multiple dense point cloud datasets acquired by several different remote UAV and airborne platforms in order to determine their suitability for improving tree and stand-level inventory. A key deliverable has been the preliminary evaluation of 3D visualisation software for interactive assessment of individual trees. The recently funded FWPA project PNC464-1717 (Enhanced forest inventory practice using immersive visualisation and measurement of dense pointcloud data) will ensure the continued research momentum associated with developing an operational software solution for on-screen visualisation and measurement of tree plots and individual trees using dense point cloud data. This 'virtual' assessment will improve resource estimate accuracies and reduce OH&S risks compared to manual field-based inventory. The ability to obtain large numbers of tree-level estimates (approaching total tree census) will improve the resource estimates, in part, through the derivation of a quantifiable systematic bias as opposed to the subjective assessment bias arising from visual field-based plot assessment.

A topic not evaluated in this project was the application of multi-/hyper-spectral remotely acquired data. The added spectral information in combination with 3D structural data presents numerous opportunities for detecting and mapping features such as weeds and tree level health. The potential of fusing different data sources has been presented in a recent project application for funding from the National Institute for Forest Products (NIFPI).

It would be highly desirable for work to continue on the remote systems trialled in this project, for example, the sub-canopy stereo-camera UAS. With further development, the acquisition of a sub-canopy stem pointcloud data is expected to become largely automated and approach the accuracies of manual tree measurement. Alternatively, while present acquisition costs associated with the airborne VUX1- laser sensor are high, improved efficiencies will reduce costs and permit tree-level assessment over large areas.

The UAS Velodyne laser prototype presents a cheaper option to the VUX1 systems and while we have demonstrated significant improvement in inventory estimates obtained from incorporating voxel metrics in area based analysis using ALS data, it is desirable to also evaluate the performance of voxel metrics to UAS data. Similarly, point cloud individual tree and crown detection algorithms should also be tested on UAS LiDAR datasets.

The efficiency and accuracy of algorithms and 3D modelling techniques for tree-level estimates will continue to improve and become more applicable to spatially accurate, dense point clouds, such as the data acquired by survey grade VUX1 sensors. Recent state-of-the art machine learning methods (e.g. deep and active learning methods) are having enormous impact in topics such as image interpretation, artificial intelligence and robotics, and are starting to be applied in areas such as remote sensing. These methods can work with very large datasets by providing flexible internal models that learn to recognise and segment objects from sensor data. What distinguishes these methods from traditional machine learning or imputation techniques is that the "features" or "variables" used within the classification or regression algorithms are learnt from the data itself rather than having to be designed or hand-tuned by a human expert. Using dense point cloud data, these novel approaches could be used to improve automated stem quality assessments including detection of multi-leaders, sweep and position of major branches.

1. Introduction

1.1 Background

Conventional forest inventory methods involve the installation of sufficient ground based sample plots, on a random or systematic basis, to estimate required stand variables within predefined error limits. These methods are labour intensive and costly. Remote sensing technologies, however, are evolving rapidly. An emerging diversity of platforms, sensors, algorithms and efficient processing workflows presents opportunities across the forestry sector for more reliable or more-effective resource information.

Complementing these opportunities has been the continued investment in FWPA's Research, Development and Extension Program in the area of technology transfer and adoption (FWPA Strategic Plan 2014-2019) which has resulted in a series of progressive R&D projects focused on the evaluation and application of remote sensing technology for the Australian forestry sector.

In an initial project, (PNC305-12-13: Operational deployment of ALS derived information into softwood resource systems) a data workflow solution using Airborne Laser Scanner (ALS) data was presented based on nearest neighbour plot imputation. This approach enabled the integration of LiDAR derived information into company regulation systems. Numerous softwood plantation companies in Australia and New Zealand are now implementing this LiDAR based plot-imputation approach for their inventory and product yield estimates.

In addition, two separate applications, based on ALS data, were initiated in the PNC305-1215 project: i) an automatic tree crown detection algorithm for accurate tree count estimates (Kathuria *et al*. 2016) and ii) development of an efficient sampling design strategy, called Nearest Centroid sampling, which has been shown to be considerably more efficient than conventional grid-sampling schemes (Melville *et al.* 2015; Melville & Stone 2016). The tree detection algorithm has now been incorporated into an easy to use software application called "PointcloudITD" by Dr Mitch Bryson (Australian Centre for Field Robotics, University of Sydney). This tree crown detection application is now available on the FWPA web site at: http://www.fwpa.com.au/resources/resources/1461-deployment-and-integration-of-cost-effective-high-spatial-resolution-remotely-sensed-data-for-the-australian-forestry-industry.html. In the case of the Nearest Centroid sampling methodology, this has been scripted into a new R package called "NC sampling" and is now available in the open access R Library.

More recently, the FWPA project PNC326-1314 "Deployment and integration of cost, effective, high spatial resolution, remotely sensed data for the Australian forestry industry" was submitted in December 2017. A key finding of this FWPA project was the robust performance of the applications using point cloud data acquired from aerial photography (AP). A detailed evaluation of point clouds obtained from several AP platforms and coincident LiDAR data acquired over both *P. radiata* and *E. globulus* plantations revealed that this imagery can be processed through a modern photogrammetric solution to produce accurate canopy surfaces. If a sufficiently accurate Digital Terrain Model is available (often provided from prior LiDAR acquisition), then an accurate Canopy Height Model (CHM) can be derived (Stone *et al.* 2016).

Metrics can then be easily extracted from the CHM. Estimates of inventory attributes and resultant high spatial resolution maps derived from the AP data was shown to compare very favourably with estimates derived from LiDAR data (Caccamo *et al*. 2018). A key advantage of using AP to acquire CHMs is that AP data are cheaper to acquire than airborne LiDAR data so provide a cost-effective solution for inventory updates.

The final component of FWPA PNC326-1314 was to evaluate the potential of virtual reality technology for remote cruising of individual *P. radiata* trees from dense point clouds. This preliminary study by Dr Winyu Chinthammit (University of Tasmania) revealed that the technology to support immersive interaction with remotely sensed point clouds is available. In addition it was demonstrated that very dense 3D point clouds can be imported into current Virtual Reality systems, that tree architecture segmented from the 3D point clouds using separate software can be integrated within the same immersive environment, and that tools can be developed to allow users to interactively measure stem and tree structure.

An important aspect of this current FWPA project has been its multi-disciplinary approach which has brought together a "Trans-Tasman" team of experts from several research institutions including, the University of Tasmania, University of Sydney, Scion in NZ and NSW Department of Primary Industries. Some of these scientists are researchers from outside the forestry research community but are now gaining familiarity with the remote sensing issues related to the commercial forestry sector. One of the project achievements was the successful secondment of the Scion scientist, Dr Joel Gordon, who spent three weeks working alongside Dr Mitch Bryson at the Australian Centre for Field Robotics, University of Sydney during May in 2017. Together they worked on developing novel tree detection and segmentation algorithms, using the same dense LiDAR datasets acquired for the project. Mitch took a "Top-down" approach while Joel took a "Bottom-up" approach through the application of the SCION-developed software package "Cloud2Stem" (Section 4.1). This secondment was mutually beneficial and illustrates the collaborative culture promoted during the project.

In addition, this project significantly benefited from the consultation and engagement with the participating commercial companies, in particular Interpine. This collaboration has resulted in a paradigm shift in company awareness and the integration of high resolution, spatially explicit information into their resource management systems.

Airborne laser scanning – improved sensors

As mentioned, ALS is now routinely applied to improve inventory precision, with the application of ALS to forest inventory demonstrating gains over conventional forest inventory in both Australia and New Zealand. However, although ALS is fast becoming standard practice for forest inventory, rapid developments in LiDAR sensors require continuing evaluation to determine how this technology can be fully utilised. For example, early ALS surveys within New Zealand used the OPTECH ATLM3100EA sensor which was released in 2006. Although this sensor was very useful for introducing the forest industry to LiDAR much of the research and methods developed around this sensor is now outdated and needs to be revisited with the newer sensors that are available.

Compared to newer sensors the ATLM3100EA has limited capability. This sensor is only capable of receiving 4 returns per outgoing pulse and the minimum distance between returns is 3 m. With the sensors now available such as the Optech Orion HD300, Optech Pegasus

HD500, Riegl LMS-Q1560 or Trimble AX60, this separation distance has been reduced to 0.4-0.7 m and up to 15 returns are received for each outgoing pulse. This echo separation or distance between vertical range measurements impacts on the definition of the vegetation canopy and therefore the stability and reliability of sub canopy metrics used for later analysis. In contrast to the ATLM3100EA, which could only track one outgoing pulse at a time, more modern sensors are able to track 24 outgoing pulses which markedly improves the data received from the sensor. In addition, modern sensors now have a superior mirror design to the ATLM3100EA which results in a far more even point distribution across the swath.

The result of these changes in sensor technology is clearly evident when viewing the data. At the same target pulse density the level of detail obtained around individual trees is far greater for the newer sensors (Fig 1, bottom) than that of the ATLM3100EA (Figure 1, top). This enhanced detail opens up the possibility for development of novel LiDAR metrics that can more accurately characterise branching patterns and the percentage of structural grade, that are only poorly defined using the ATLM3100EA. As the ATLM3100EA provided a limited level of detail and was unable to store the full LiDAR waveform, this sensor was suited to the area based approach (ABA) using discrete returns, adopted by the forest industry. The richer level of detail available from newer sensors combined with the ability to store the full LiDAR waveform warrants a re-examination of how much could be gained through analyses using the individual tree data.

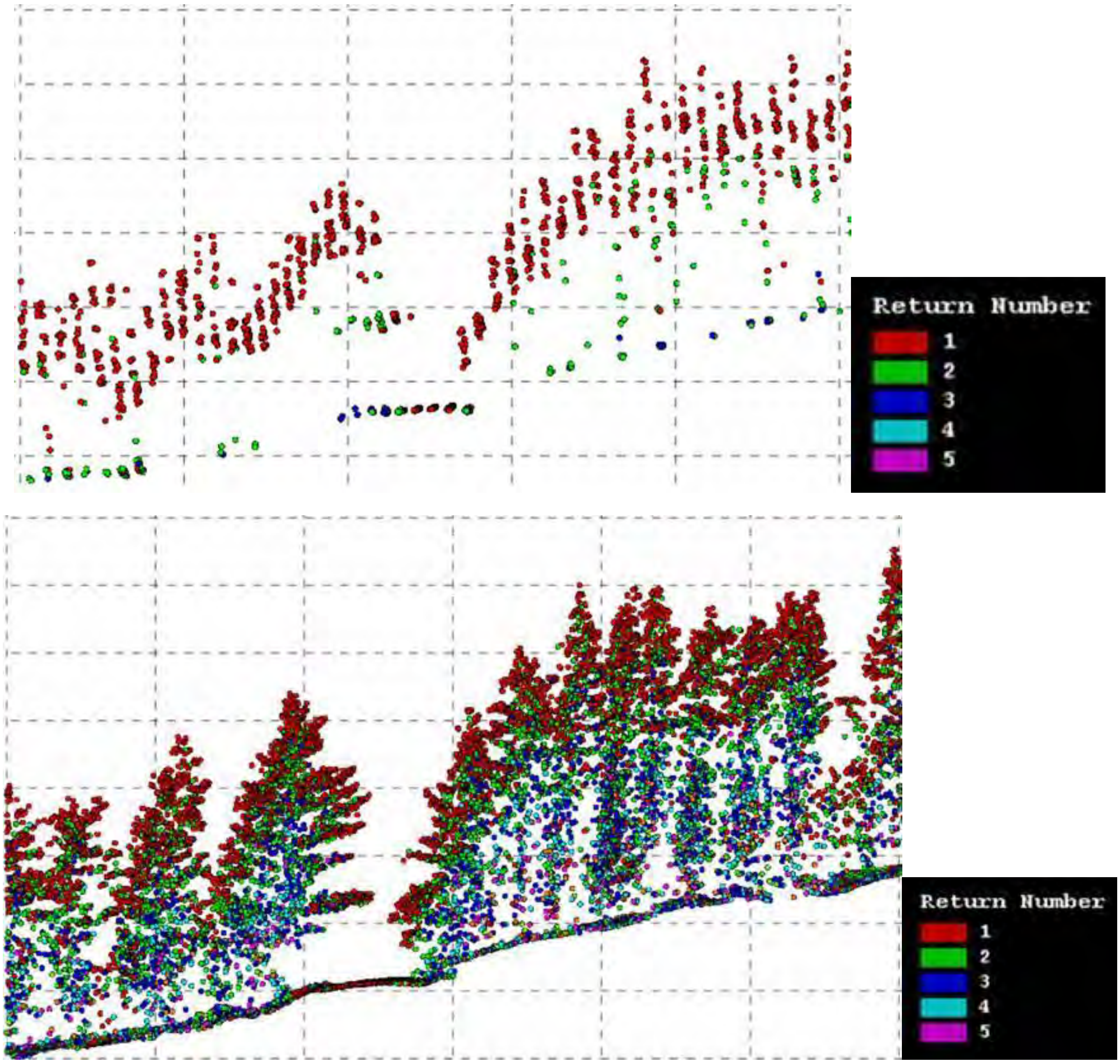

Figure 1: LiDAR profile of the same area, by return number, undertaken using (top) OPTECH ATLM3100EA in 2010 and (bottom) Riegl LMS-Q780 in 2015. In both figures the target pulse density was four pulses per m^2. Source: Interpine.

In this project we had the opportunity to test the state-of-the-art Riegl VUX1-LR laser sensor which was mounted on a helicopter. This survey grade laser scanner is capable of acquiring very accurate, ultra-dense, 3D point clouds having an effective measurement rate of up to 750,000 measurements per second. These datasets now present the real opportunities for 3D visualisation and assessment of individual tree stems (Figure 2).

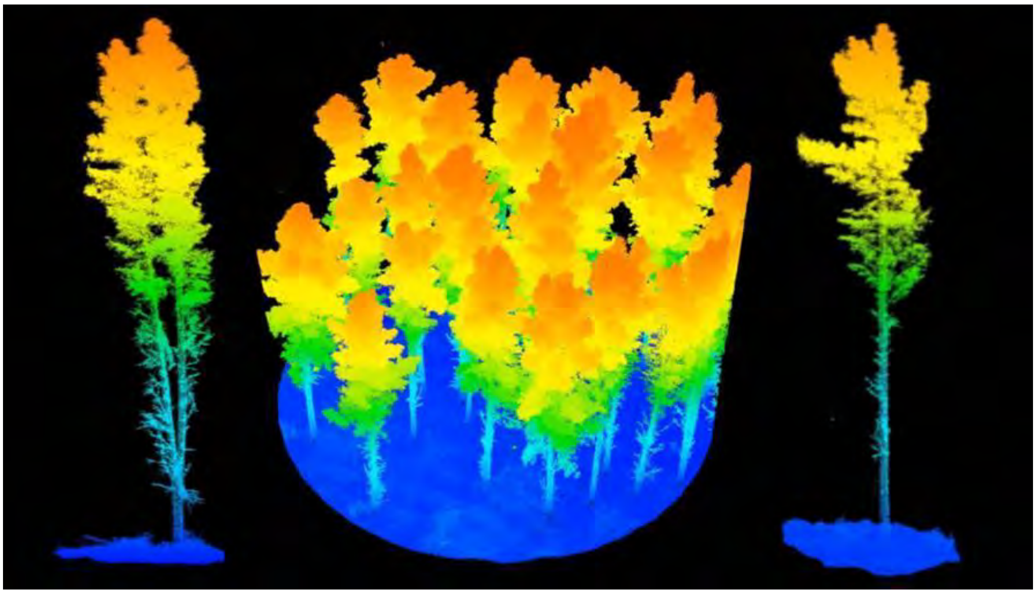

Figure 2: Example of the quality of 3D point cloud data captured by a Riegl VUX1-LR sensor mounted on a helicopter that was flown over *P. radiata* stands in Carabost state forest, near Tumut, southern NSW. Data is displayed in the 3D visualisation software Quick Terrain Modeler.

Parallel to the advances in ALS technology has been the recent advances in unmanned aircraft systems (UAS) and their integration with small, light-weight laser scanners. In general, these systems are much cheaper to operate than fixed wing aircraft or helicopters and avoid the need for plot access as is required by TLS. As for the new ALS sensors, UAV mounted LiDAR scanners have the capacity to acquire very dense, 3D point clouds, albeit over smaller areas compared to ALS platforms. Recently, Riegl introduced a VUX-1 scanner mounted on a RiCopter UAV platform which is capable of acquiring highly accurate, ultra-dense point cloud data (Brede *et al.* 2017). These units are very expensive. However, the UAV-LiDAR prototype developed for the FWPA project PNC305-1213 was built by the TerraLuma team at University of Tasmania much more cheaply with a laser scanner Velodyne VLP-16 'Puck' ($12,5000) that can be operated at oblique angles and generate point densities > 100 points m^{-2}. There is of course a trade-off between the cost of the instrumentation and the density and accuracy of the point cloud data. Therefore, for the cheaper UAV laser systems in particular, calibration and acquisition specifications need to be determined to ensure optimal deployment and maximum potential accuracies.

Dense LiDAR point cloud visualization and 3D modelling

A common aim connecting this project with previous FWPA projects has been to incorporate 3D remotely-sensed information, irrespective of the acquisition or processing methodology, into forestry management systems. This is a key enabler of precision forestry (Holopainen *et al.* 2014), enabling, for example, tree attributes to be precisely summarised within compartments. However, it is also disruptive, requiring forest managers to deal with high spatial resolution 3D point clouds in addition to the more conventional 2D sources of data (e.g. GIS). This requires familiarisation with 3D point cloud visualisation and processing software packages.

Numerous commercial and open source software products are now available that support 3D visualisation of point cloud data and the (semi) automatic segmentation of objects of interest, including trees, e.g. 3DForest (Trouchta *et al*. 2017) and LiForest (True Reality Geospatial Solutions). 3D point clouds generally provide geometric information (x, y, z) and per-point attributes such as intensity or colour. Traditionally there are a range of geometric primitives that can be applied, for example, a hierarchical collection of cylinders which can be used to model and reconstruct objects with complex geometry. This approach for displaying LiDAR data involves a visualisation software engine, which in effect involves translating the LiDAR data to the language of points, lines, triangles and polygons (Ghosh & Lohani 2014). More recently, point-based rendering techniques can now cope with massive 3D point clouds and enable an interactive visualisation and exploration of the data (Richter & Dőllner 2014).

Both the stem visualisation and 3D modelling procedures are very dependent on the quality of the point cloud. Stand attributes such as mean tree height can be determined directly from ALS data, however stem diameter can only be inferred from the ABA using ALS data. There are few examples of ALS systems directly estimating individual stem dimensions. Terrestrial LiDAR scanning (TLS) instruments, on the other hand have been used to acquire very dense point cloud data for over a decade. Much of the relevant literature on modelling dense LiDAR datasets, therefore, relates to TLS studies. High quality TLS point clouds have been successfully modelled to reconstruct the 3D structure of tree stems. Stem diameters are typically derived from TLS by fitting circles, cylinders or free form curves to the point cloud and these optimization procedures are critical for stem detection. Optimisation of the fit is typically achieved through a least squares adjustment or Hough transform (Hough 1962; van Leeuwen & Nieuwenhuis 2010). Other stem profile detection procedures based on cylinder fitting have been reported by Eysen *et al.* 2013; Raumonen *et al*. 2013; Hackenberg *et al.* 2014; Krooks *et al.* 2014; and Srinivasan *et al.* 2015 where the axis of a stem segment and its radius correspond to a cylinder. Liang *et al.* (2014), for example, modelled stem curves from the selected points using a series of TLS derived 3D cylinders and reported an accuracy of approximately 1 cm.

The Autostem™ Forest software (Treemetrics Ltd., Ireland) utilizes the tree-detection and diameter-fitting algorithms developed by Bienert *et al*. (2007) and was evaluated by Murphy *et al.(* 2010) in two *P. radiata* plantations located near Mt Gambier (S.A.) and Bunburry (W.A). In this software package, tree stems are detected using a slice of the point cloud data at a specified height and point clusters that can fit a circle (or circle-arc) are identified (Henning & Radtke, 2006; Bienert *et al.* 2007). A short vertical cylinder is applied at this height. Decimetre slices are then taken successively up or down the cylinder to obtain new sets of data points for circle fitting. A polynomial diameter smoothing function is then applied. Stem profiles at different height intervals can be determined with knowledge of the approximate position diameter returned by the tree detection process. Gaps in the stem data are addressed through the application of local taper models (Bienert *et al.* 2007). Sweep is determined based on the estimated tree centre points for each slice.

Other approaches have included voxel-based processing (Gorte & Pfeifer 2004); tree meshing (Antonarakis *et al.* 2009) or a combination of these procedures (e.g. Moskal & Zheng 2012). Dassot *et al.* (2012), for example, utilized the software PolyWorks (InnovMetric Software Inc.), software used in product manufacturing, through a process that involved polyline and cylinder fitting. They also applied polygonal meshing which links data points with triangles to obtain continuous surfaces without assumptions about the actual shape.

Branch recognition in point clouds obtained from laser scanning has proven to be more challenging. The Autostem software used by Murphy *et al.* 2010 did not provide information on branch size. Bucksch & Lindenbergh (2008) developed the CAMPINO (Collapsing And Merging Procedures In Octreee-graphs) algorithm for geometric tree skeleton reconstruction of 2 m tall apple trees using a point cloud with approximately 10,000 points per tree. The resultant skeletonisation of the tree structure allows for the measure of branch lengths and diameters for various branch orders.

In all cases, however, it is desirable that these quantitative structure models are comprehensive; precise; compact (i.e. easily stored, manageable and any attribute can easily be extracted after construction); automatic and fast (Raumonen *et al.* 2013). The extracted stem level measurements can then be linked with localised taper functions to estimate log product recoveries or extract individual stem profile descriptions (e.g. Murphy *et al*. 2010).

1.2 Key project tasks and deliverables

The overall aim of this project was to evaluate the feasibility of efficiently harnessing the 3D information captured by new LiDAR (laser scanning) technology capable of acquiring dense point cloud data for improved resource assessment by commercial plantation growers. This research aimed not only to develop methods that could reduce the reliance on inventory plots but more broadly to determine how information derived from high density LiDAR can be used to improve inventory precision.

The project proposed four deliverables, i.e.:

1) Provide recommended specifications and procedures for optimal data acquisition and on-screen 3D visualisation and assessment of individual tree stems using point cloud data captured by a multi-rotor LiDAR-UAV.

2) Provide recommendations on the feasibility of generating accurate 3D models of tree stems for product mix assessment using ultra-dense point clouds acquired by a LiDAR UAV.

3) Provide recommendations on any operational constraints for practical forest operations using LiDAR acquired from a UAV.

4) Provide recommended specifications and procedures for the data acquisition, processing and analysis of dense point clouds acquired by light aircraft for plantation resource assessment and mapping.

In order to fulfil the proposed project deliverables three Work Packages were developed by the project team, each with specific tasks. The three Work Packages were: i) 3D visualisation for interactive assessment of individual tree stems; ii) UAS LiDAR for dense point cloud acquisition and iii) Individual tree detection, 3D tree reconstruction, and automated extraction of forest inventory metrics.

The sections presented in this Final Report present the approaches, methodologies and results that have been produced from these Work Packages and either individually or in combination present the defined project deliverables.

References

Antonarkis, A.S., Richards, K.S., Brasington, J., Bithell, M. (2009) Leafless roughness of complex tree morphology using terrestrial lidar. *Water Resources Research* 45: DOI: 10.1029/2008WR007666.

Bienert, A., Scheller, S., Keane, E., Mohan, F., Nugent, C. (2007) Tree detection and diameter estimation by analysis of forest terrestrial laser scanning point clouds. *Proceedings of the ISPRS Workshop on Laser Scanning*, pp. 50-55. Sept 12-14, 2007 Finland.

Brede, B., Lau, A., Bartholomeus, H.M. & Kooistra, L. (2017) Comparing Riegl RiCopter UAV derived canopy height and DBH with terrestrial LiDAR. *Sensors* **17:** Article no. 2371; doi:10.3390/s17102371.

Bucksch, A. & Lindenbergh, R. (2008) CAMPINO – A skeletonization method for point cloud processing. *ISPR Journal of Photogrammetry & Remote Sensing* 63: 115-127.

Caccamo, G., Iqbal, I.A., Osborn, J., Bi, H., Arkley, K., Melville, G. & Stone, C. (2018) Comparing yield estimates derived from LiDAR and aerial photogrammetric point cloud data with cut-to-length harvester data in a *Pinus radiata* plantation in Tasmania. *Australian Forestry* **81:** https://doi.org/10.1080/00049158.2018.1458582.

Dassot, M., Colin, A., Santenoise, P., Fournier, M., Constant, T. (2012) Terrestrial laser scanning for measuring the solid wood volume, including branches, of adult standing trees in the forest environment. *Computers and Electronics in Agriculture* 89: 86-93.

Eysen, L., Pfeifer, N., Ressl, C., Hollaus, M. Grafl, A. *et al*. (2013) A practical approach for extracting tree models in forest environments based on equirectangular projections of terrestrial laser scans. *Remote Sensing* 5: 5424-5448.

Ghosh, S., Lohani, B. (2014) Development and comparison of aerial photograph aided visualization pipelines for LiDAR datasets. *International Journal of Digital Earth* 8: 656-677.

Gorte, B., Pfeifer, N. (2004) Structuring laser-scanned trees using 3D mathematical morphology. *Proceedings XX ISPRS Congress* pp. 929-933. Istanbul Turkey 2004.

Hackenberg, J., Morhart, C., Sheppard, J., Spiecker, H., Disney, M. (2014) Highly accurate tree models derived from terrestrial laser scan data: A method description. *Forests* 5: 1069-1105.

Henning, J.G., Radtke, P.J. (2006)Detailed stem measurements of standing trees from ground-based scanning lidar. *Forest Science* 52: 67-80.

Holopainen, M., Vastaranta, M. & Hyyppä, J. (2014) Outlook for the next generation's precision forestry in Finland. *Forests* **5:** 1682-1694.

Hough, P.V.C. (1962) Method and means for recognizing complex patterns. US Patent 3,069,654.

Kathuria, A., Turner, R., Stine, C., Duque-Lazo, J. & West, R. (2016) Development of an automated individual tree detection model using point cloud LiDAR data for accurate tree counts in a *Pinus radiata* plantation. *Australian Forestry* **79:** 126-136.

Krooks, A., Kaasalainen, S., Kanara, V., Joensuu, M., Raumonen, P. *et al*. (2014) Predicting tree structure from tree height using terrestrial laser scanning and quantitative structure models. *Silva Fennica* 48: article id 1125.

Liang, X., Kankare, V., Yu, X., Hyyppä, J., Holopainen, M. (2014) Automated stem curve measurement using terrestrial laser scanning. *IEEE Transactions on Geoscience and Remote Sensing* 52: 1739-1748.

Melville, GJ., Stone, C. (2015) Application of LiDAR data to maximise the efficiency of inventory plots in softwood plantations. *New Zealand Journal of Forestry Science* **45:** doi:10.1186/s40490-015-0038-7.

Melville, G. & Stone, C. (2016) Optimising nearest neighbour information – a simple, efficient sampling strategy for forestry plot imputation using remotely sensed data. *Australian Forestry* **79:** 217-228.

Moskal, L.M., Zheng, G. (2012) Retrieving forest inventory variables with terrestrial laser scanning (TLS) in urban heterogeneous forest. *Remote Sensing* 4: 1-20.

Murphy, G.E., Acuna, M.A., Dumbrell, I. (2010) Tree value and log product yield determination in radiata pine (*Pinus radiata*) plantations in Australia: comparisons of terrestrial laser scanning with a forest inventory system and manual measurements. *Canadian Journal of Forest Research* 40: 2223-2233.

Raumonen, P.K., Kaasalainen, M., Akerblom, M., Kaasalainen, S., Kaartinen, H. *et al* (2013) Fast automatic precision tree models from terrestrial laser scanner data. *Remote Sensing* 5: 491-520.

Richter, R. & Döllner, J. (2014) Concepts and techniques for integration, analysis and visualization of massive 3D point clouds. *Computers, Environment and Urban Systems* 45: 114-124.

Srinivasan, S., Popescu, S.C., Eriksson, M., Sheridan, R.D., Ku, N.-W (2015) Terrestrial laser scanning as an effective tool to retrieve tree level height, crown width, and stem diameter. *Remote Sensing* 7: 1877-1896.

Stone, C., Webster, M., Osborn, J. & Iqbal, I. (2016) Alternatives to LiDAR-derived canopy height models for softwood plantations: a review and example using photogrammetry. *Australian Forestry* **79:** 271-282.

Trochta, J., Krůček, M., Vrška, T., Král, K. (2017) 3D Forest: An application for descriptions of three-dimensional forest structures using terrestrial LiDAR. PLoS ONE 12(5): e0176871.hhttps://doi.org.10.1371/journal.pone.0176871.

Van Leeuwen, M., Nieuwenhuis, M. (2010) Retrieval of forest structural parameters using LiDAR remote sensing. *European Journal of Forest Research* 129: 749-770.

2. 3D visualisation for interactive assessment of individual trees

Osborn J.[1], *Chinthammit W.* [1], *Pishchugin A.* [1], *Lucieer A.* [1], *Herries D.* [2], *Stone C.*[3]

[1] *School of Technology, Environments and Design, University of Tasmania, E-mail: Jon.Osborn@utas.edu.au*

[2] *Interpine Innovation, Interpine Group Ltd*

[3] *Forest Science, NSW Department of Primary Industries*

Introduction

There is increasing capability to capture forest structure as dense point clouds using either mobile or static terrestrial laser scanners, terrestrial photogrammetry, UAS laser scanning and photogrammetry, or using high resolution airborne laser scanning or photogrammetry. This creates the potential to capture rich forest plot data as a point cloud and then undertake cruising measurements either automatically or semi-automatically in an office environment. In turn, this has the potential to lead to more accurate, complete and verifiable tree-level inventory data and to reduce the time, cost and workplace health and safety risks associated with manual field-based cruising.

The potential to apply Virtual Reality (VR) methods to forestry has been recognised for some time. Orland & Uusitalo (2001) and Bishop *et al.* (2005) examined the relationship between VR visualisation design and the requirements of forest management; Blaise *et al.* (2004) experimented with 3D visualisation of individual trees and forest landscapes. It is recent developments in data capture technology and the increasing capability, availability and affordability of VR platforms that prompts current interest in the application of VR to forest measurement.

Objectives

The objectives of this component of the research were threefold:

1. To identify and review existing software with functionality likely to support visualisation of dense point clouds and capability to allow automatic or semi-automatic extraction of inventory plot metrics. This component of the work was conducted in two phases. The first phase was to identify and review existing third-party software. The second phase was to trial two contending software options using dense point cloud data acquired from a previous FWPA research project (PNC326-1314) and from the current project (PNC377-1516).

2. To review immersive virtual reality technology and methods for interactive cruising. This component of the work was progressed through new collaborations with the University of Tasmania's Human Interface Technology Laboratory (HIT Lab) and was conducted in four stages:
   i. A scoping project to identify current and emerging software and hardware solutions that would support advanced immersive visualisation of dense point clouds.

ii. A prototype demonstration of immersive visualisation of forest point cloud data acquired by the project and using existing UTAS HIT Lab resources.

iii. Identification of additional requirements in order to develop forest measurement capability, particularly to identify existing software that has the potential to allow foresters to directly interact (visualise and measure) within a point cloud in an immersive environment, or to scope the development of software to meet those needs.

iv. Investigation of the possibilities for data generated by automated tree-metric extraction software to be integrated into an immersive VR environment.

3. Subject to the findings in (1) and (2) above, to identify pathways to operationalise the automated extraction of plot metrics and the use of immersive VR technology and methods.

The research to achieve these objectives has been supported and extended across two FWPA projects. Early work, including the initial review of forest point cloud visualisation and automated segmentation and measurement software and the development of task-specific immersive point cloud measurement capability, was supported by funding allocated to FWPA PNC326-1314 and by an FWPA supported extension to that project, and has been reported in Chinthammit *et al*. (2017). Later work, including trials of visualisation software and automated measurement software using project generated data has been supported by funding allocated to the current project, PNC377-1516, and progressed through new collaborations established by that project's research team and industry partners with UTAS HIT Lab researchers The current report summarises the combined outcomes of this work.

Outcomes and Deliverables

1. A review of current software: visualisation automated extraction of plot-level inventory metrics

The first component of this work comprised a review of third-party software products designed to support automatic segmentation of stem metrics from point cloud data. Five products were reviewed:

i. 3DForest (Trochta *et al*. 2017)[1]
ii. LiForest (True Reality Geospatial Solutions)[2]
iii. CompuTree (Association De Recherche Technologie Et Sciences)[3]
iv. Fusion_LDV (U.S. Department of Agriculture)[4]
v. Web-LiDAR (U.S. Department of Agriculture)[5]

Of these, two were selected for further testing using point cloud data collected for FWPA projects PNC326-1314 and PNC377-1516. One set of data tested were from a Timberlands Pacific NE Tasmania study site, referred to here as the Springfield site and comprising mature, thinned and pruned *Pinus radiata.* Those data were collected using terrestrial laser scanning (Leica Nova MS50 scanning total station), UAS photogrammetry and UAS Velodyne laser scanning. The second set of data tested were from a study site near Tumut, NSW, referred to here as Snow217. Those data were collected using a Riegl VUX-1 scanner on fixed-wing

[1] Homepage: http://www.3dforest.eu/
[2] White paper: http://www.liforest.com/wp-content/uploads/2016/07/LiForest2.1-Whitepaper.pdf
[3] Homepage: http://computree.onf.fr/?lang=en
[4] Homepage: http://forsys.cfr.washington.edu/fusion.html
[5] See: https://www.scribd.com/document/215650128/Web-LiDAR-forest-inventory-TreeTop-application

aircraft. This site comprised very old (84 years), thinned, *Pinus radiata.* The two software products selected for further review using these project data were 3DForest and LiForest.

The findings from these reviews are available to project industry partners on request. The following provides an overview, intended to summarise the capabilities of available tree segmentation algorithms and software current at the time of the review, and to illustrate their performance on dense point cloud data used in current FWPA research projects.

In broad terms, the software reviewed clearly indicates the current interest, and the substantial progress being made in, automated extraction (segmentation) of tree metrics from dense point cloud data. The software included both commercial and open source providers. The maturity of the products varied across most of the parameters tested, including: data import options (LAS, LAZ, CSV, PTS, etc.), functionality, ease of use, reliability (software stability), processing speed, visualisation tools (including stereoptic 3D visualisation), and data output options (.TXT, .PLY, PCD, etc.).

On balance, two of the software products were selected for use in additional trials using our own data. These two were 3DForest and LiForest. The following figures (Figures 1 – 6) illustrate the user interfaces and data extracted from our project datasets using 3DForest software.

(a) 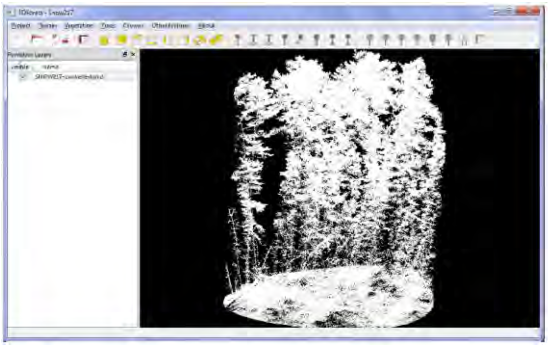 (b) 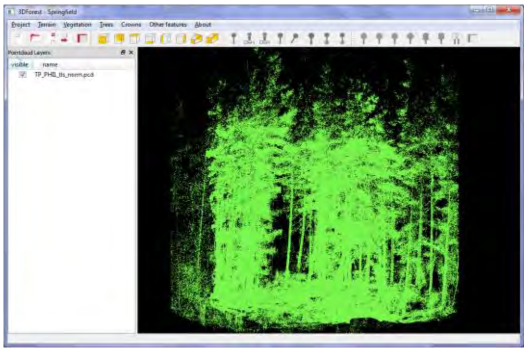

Figure 1: (a) VUX-1 (Snow217) ALS data and (b) Springfield data imported into 3DForest.

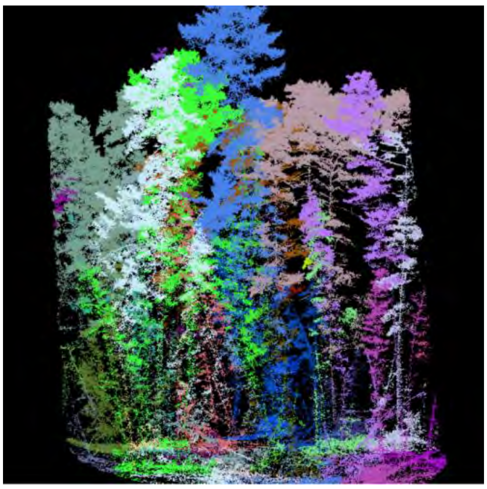

Figure 2: Point cloud segmentation of VUX-1 (Snow217) data using 3DForest.

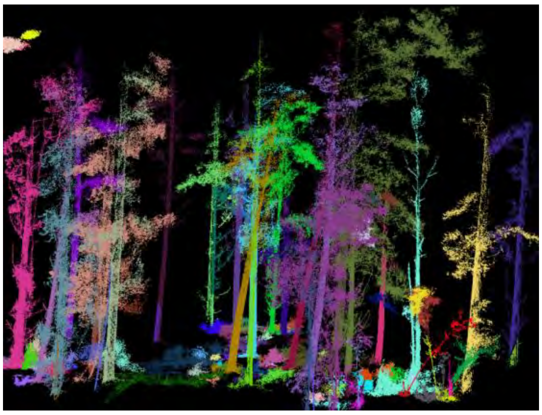

Figure 3: Point cloud segmentation of Springfield data using 3DForest,

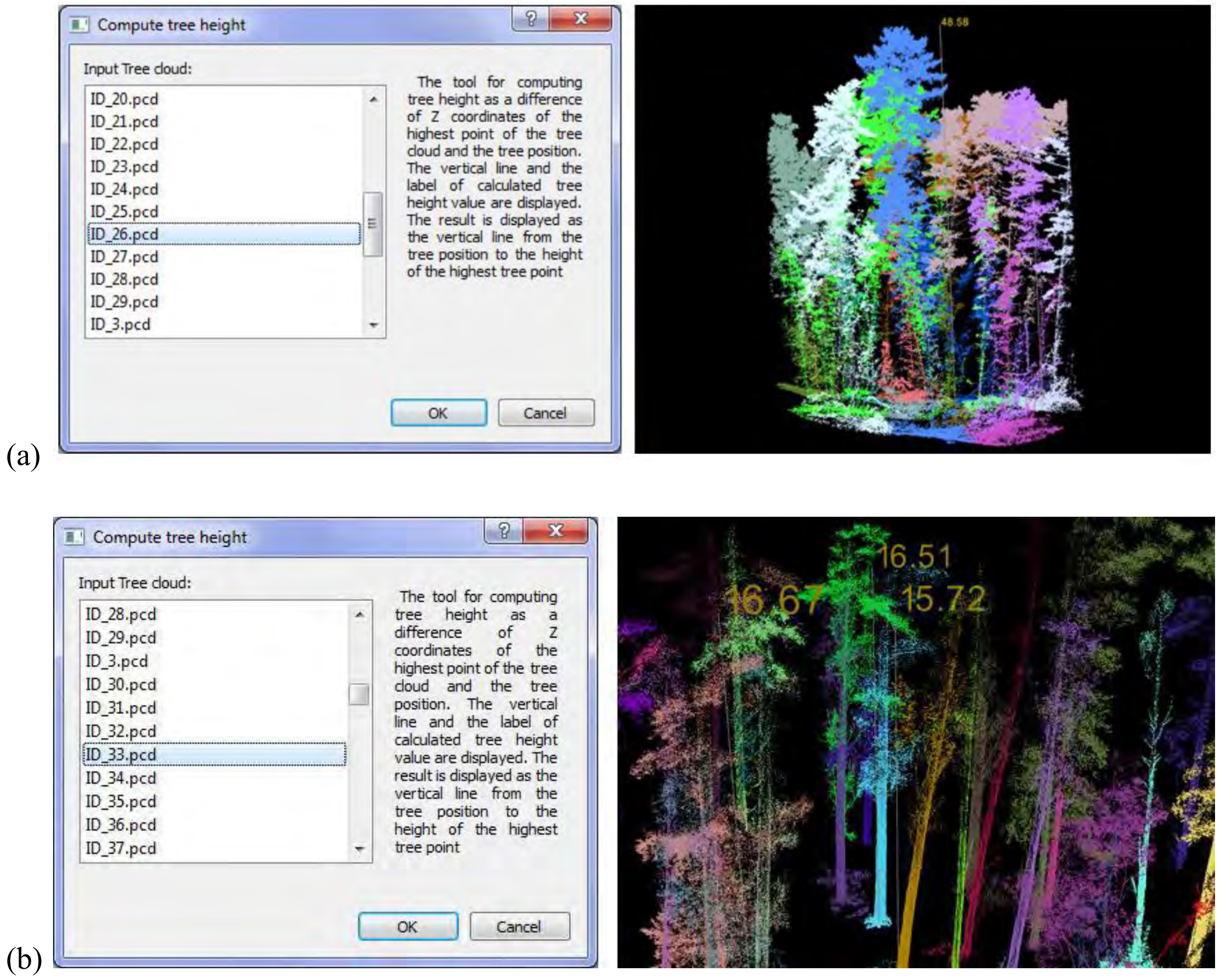

Figure 4: Tree height measurement dialog window and graphical interface, using 3DForest. (a) VUX-1 (Snow217) data; (b) Springfield data.

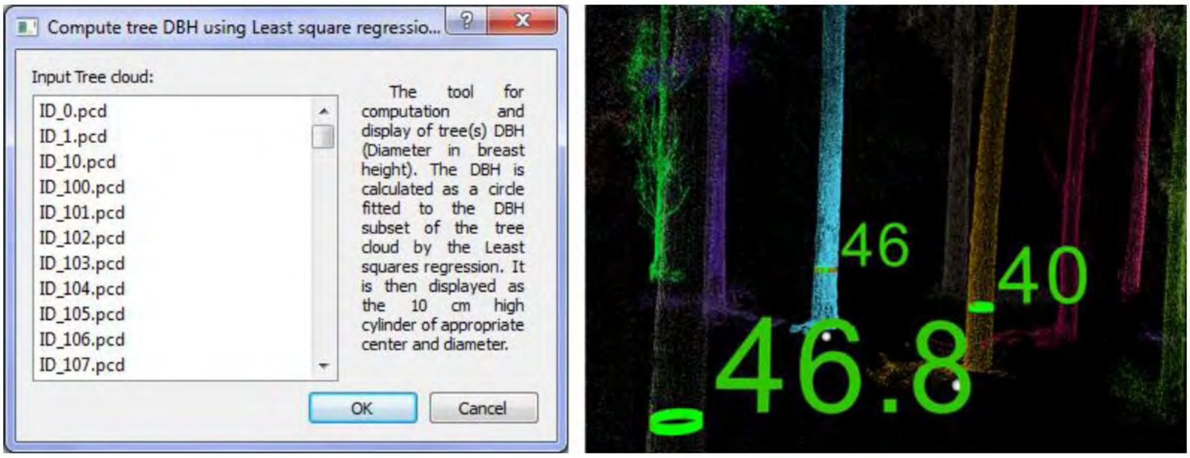

Figure 5: DBH by least squares regression dialog window and graphical interface, Springfield data, using 3DForest:

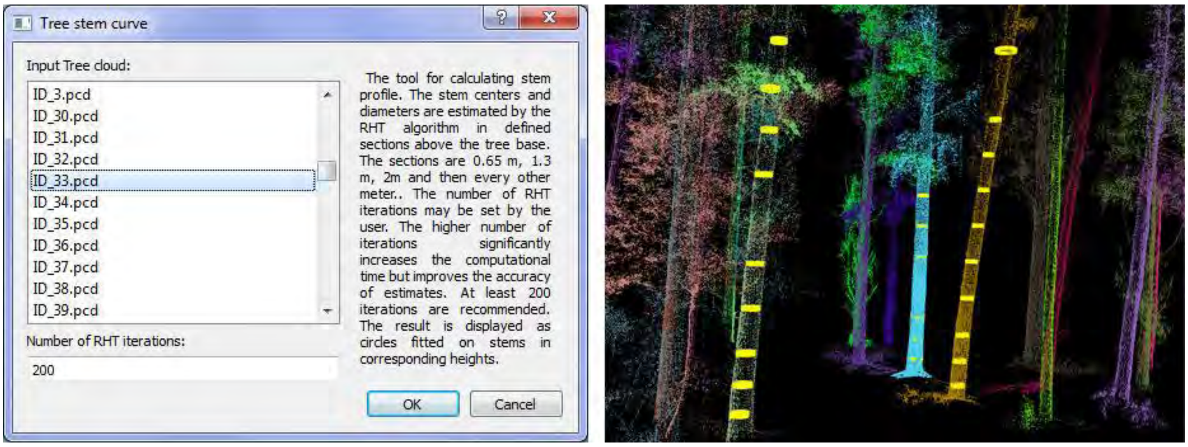

Figure 6: Stem curve measurement dialog window and graphical interface, Springfield data, using 3DForest.

2. Immersive virtual reality technology and methods for interactive cruising[6]

Currently, the choice of software environment for developing immersive VR environments is normally between Unity 3D[7] (Unity Technologies) and Unreal Engine[8] (Epic Games). Both software platforms began as game engines, allowing game developers to develop and export those games to a variety of platforms (such as PC, console or mobile). Since the emergence of advanced display headsets, both software development platforms have responded by positioning their products as software development tools for the new immersive VR hardware devices.

Unity 3D is the more widely used of these game engines and with more assets (plugins) available from Unity 3D's Asset store. Specifically for this research project, there is a point cloud viewer utility asset available on the Unity 3D platform, called "Point Cloud Viewers and Tools"[9]. This utility allows point cloud data to be loaded into the immersive environment. Common point cloud data formats can be loaded, including XYZ, XYZRGB, CGO, ASC,

[6] Components of this section replicate content provided in Chinthammit *et al*. (2017).
[7] https://unity3d.com/
[8] https://www.unrealengine.com/
[9] https://www.assetstore.unity3d.com/en/?_ga=1.242197186.1904995280.1454048114#!/content/16019

CATIA, PLY(ASC), PTS and LAS. For these reasons, the Unity 3D software was adopted as the platform for this research project, and using the LAS data format.

The Unity 3D platform allows customised software programs to be implemented inside the immersive VR environment. This is achieved by coding in either C# or JavaScript languages. The following are key functions:

- **First Person Viewpoint**: This function enables users to view the dense point cloud within an immersive environment from a first person point of view. Users are able to explore a forest point cloud in a manner comparable to walking in a real forest, enhancing the immersion experience. Additionally, the software can make available unique viewpoint options that users would not normally experience, such as fly-through, teleporting from one location to another, or switching in and out of aerial views.
- **Measuring tools**: Two measuring tools have been implemented that allow users to measure (i) a distance between two points and (ii) a stem diameter around a stem within the immersive environment. These are illustrated in Figure 7.

(a) (b)

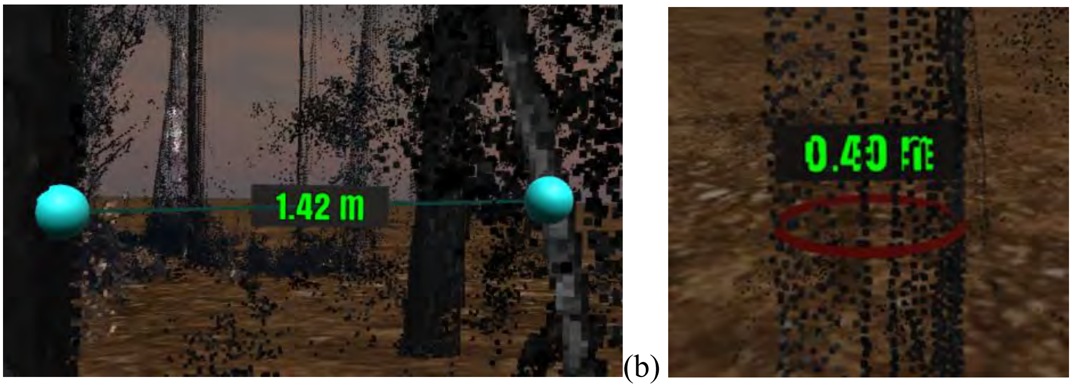

Figure 7: Point cloud data and measurement tools in the pilot-project VR system. Note scalable point dimensions- scaled according to distance from viewer location. (a) Distance tool. (b) stem diameter tool.

Output data from two stem segmentation software were imported into the VR environment. One was 3D Forests; the other was the stem segmentation tools developed by SCION New Zealand (SCION 2017, Pont 2014). These two were selected on the basis of recommendations from the review of segmentation software and in order to lever the stem segmentation tools developed by the SCION team and being further developed and tested in the current research.

The output files from these two software are in pcd format. Using CloudCompare, LAZ (original point cloud data) and pcd (segmentation data) were converted to LAS format (uncompressed). Using the Unity 3D asset "Point Cloud Viewers and Tools", the LAS format data were converted to the asset's own Binary (DX11) format (bin). Within Unity, a "Binary Viewer DX11" script (part of the Point Cloud Viewers and Tools asset) was attached to a game object. Within the "Binary Viewer DX11" script, the previously converted bin file was selected to be rendered in the immersive environment. This process allowed the original point cloud and the segmented stem data to be visualised in an immersive environment. Resulting combined data, displayed on the Unity 3D software's desktop development environment, are shown in Figures 8 and 9 for the SCION and 3DForest segmentations respectively. These are for a pre-harvest inventory stand (thinned and pruned) from the Springfield (NE Tasmania) study site. The data in Figure 8 were collected using a Leica MS50 Multi-station scanner; the data in Figure 9 comprise the same Leica MS50 Multi-station scanner data combined with a dense point cloud derived from UAS photogrammetry.

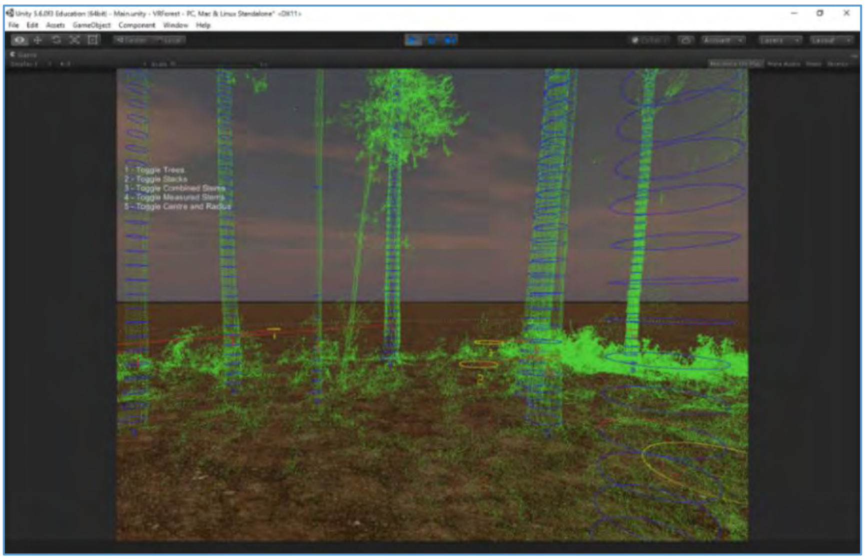

Figure 8: Screen capture of Unity 3D rendering of TLS data acquired in a pre-harvest *Pinus radiata* inventory plot, showing SCION segmentation.

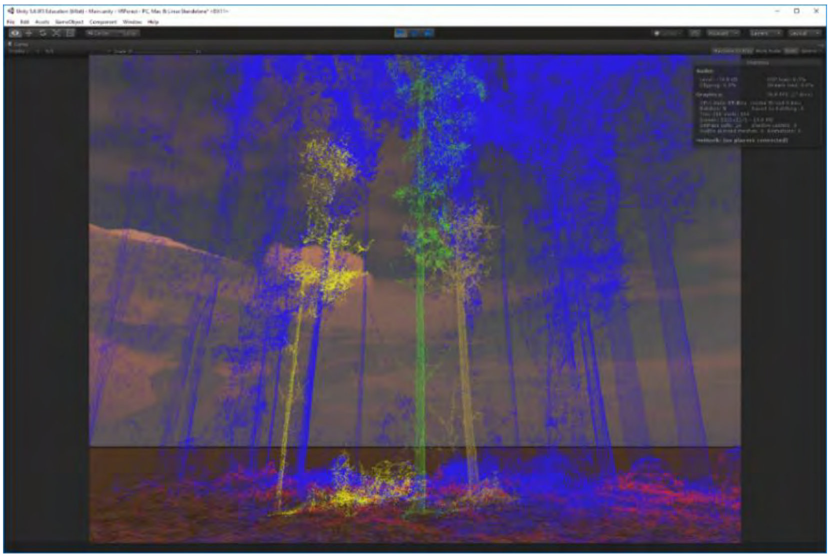

Figure 9: Screen capture of a Unity 3D rendering of combined TLS and UAS photogrammetry data acquired in a pre-harvest *Pinus radiata* inventory plot, showing 3DForest segmentation.

This proto-type VR application has been workshopped at a number of industry events, including ForestTech 2017 in New Zealand and Australia and at workshops associated with current FWPA research projects. It has demonstrated the potential for operational field staff to transfer their skills to within a 3D and 1:1 scaled immersive environment, and to use natural interface functionality such as walking (within limited ranges), 'teleporting' across longer distances (horizontally and vertically) and 'experiencing' the data from within a forest plot.

The findings of this pilot project indicate that the technology to support immersive visualisation and interaction with remotely sensed point clouds is available, that very dense 3D point clouds can be imported into current VR systems, that tools can be developed to allow users to measure stem and tree structure interactively, and that tree architecture segmented from 3D point clouds can be integrated within the same 3D immersive environment.

3. Pathways to operationalising automated extraction of plot metrics using immersive VR technology

The work reported above indicates that:

i. the technology to support immersive visualization of remotely sensed 3D point clouds is available
ii. very dense 3D point clouds can be imported into current VR systems
iii. tree architecture segmented from 3D point clouds using separate software can be integrated within the same immersive environment
iv. tools can be developed to allow users to measure stem and tree structure interactively and to view, quality assure or edit tree architecture data imported into a VR environment.

Our recommendation is that future work should concentrate on:

- further developing tools to allow users to interact with 3D data in order to capture or quality-assure tree metrics
- further investigating both point cloud and alternative data representations in order to optimise the immersive experience

- discovering, describing and evaluating the ways in which users interact with forest point cloud data and measurement tools within a VR environment.
- leveraging maximum returns from the data, in terms of:
    - the data spatial accuracy and resolution required in order for human operators to accurately visualise and measure forest plot measurements, such as DBH, stem diameters and tree height, as well as complex tree metrics such as branching angles and branch diameters
    - the capacity of human operators to undertake quality assurance assessment of tree metrics extracted such as stem circumference, tree height, branching, separately extracted from point clouds using automated software methods
- assessing the performance of VR stem assessments, in terms of both task competency and the operational cost of the VR measurement processes, compared to current field assessments
- transferring to industry a VR software application that can be used by forest managers to build experience and capacity with VR stem assessments and that has sufficient functionality to allow companies to assess and plan their future investments in VR-based methods.

These aims form a current FWPA research grant application, supported by key industry stakeholders and involving current and new research collaborations from the Australian and New Zealand research community. An iterative design approach has been recommended, employing the rich point cloud data already acquired for FWPA projects PNC326-1314 and PNC377-1516, and with the following components:

i. *VR software design and development:* Software development will extend from the current proof-of-concept to include all stem assessment operations that can be supported by the data. Software design and development will be based on an iterative design methodology (design, prototyping, testing, analysing and refining) because, while the required tasks can be determined precisely, the implementation model in a VR environment largely depends on how effectively human operators can perform those task with the VR tools, which is unknown.

ii. *Usability design and testing:* VR usability tests evaluate the effectiveness of interaction tools with respect to a pre-defined set of objectives, such as ease of use, functionality error, misrepresentation of the interaction cues (visual and auditory) and task performance. The development team will work with collaborators to define the objectives of the testing that best capture the important attributes of practical stem assessment operations. The usability testing will measure/extract those attributes from observations of user behaviour and user-extracted data.

References

Bishop, I.D., Ford, R., Loiterton, D. and Williams, K. (2005). Studying the acceptability of forest management practices using visual simulation of forest regrowth. *Visualization in landscape and environmental planning: technology and applications. Taylor & Francis, London*, pp.112-119.

Blaise, F., Saint-André, L., Leban, J.M., Gégout, J.C.& Hervé, J.C. (2004) Connection between forest inventory data and geographic information systems for assessing timber value at the stand level. In *Proceedings of the 4th IUFRO Conference on: Connection between Forest Resources and Wood Quality: Modelling Approaches and Simulation Software, Harrison Hot Springs (BC Canada 2002), INRA, Nancy* (pp. 583-594).

Chinthammit W, Osborn J, Lucieer A, Gordon J, Stone C. (2017) The application of immersive virtual reality technology to remote cruising of *Pinus radiata* using dense point clouds. Section 7.5 pp 234-240, *in* Stone C., Osborn J. (eds) (2017) *Deployment and integration of cost-effective high resolution remotely sensed data for the Australian forest industry.* FWPA. 328pp. December 2017. ISBN: 978-1-925213-66-9

Orland, B. and Uusitalo, J. (2001). Chapter fourteen. *Forests and Landscapes: Linking Ecology, Sustainability, and Aesthetics* **6:** 205.

Pishchugin A., Osborn J., Lucieer A. (2017). Review of automated software for extracting inventory plot metrics. Project Report; FWPA PNC326-1314 and FWPA PNC377-1516. Unpublished report. 66pp.

Pont, D. (2014). Terrestrial LiDAR - Potential for forest inventory using a new hand-held unit. In B. Apthorp (Ed.), ForestTech. Melbourne, Australia: FIEA

SCION (2017). *Cloud2Stem software*, Pont D., Gordon J. SCION New Zealand, 2017

Trochta J, Krůček M, Vrška T, Král K. (2017). 3D Forest: An application for descriptions of three-dimensional forest structures using terrestrial LiDAR. *PLoS ONE* 12(5): e0176871. https://doi.org/10.1371/journal.pone.0176871

Acknowledgement

The research team particularly acknowledge the contribution of the University of Tasmania HIT Lab software engineer, Simon Hogwood, for his contributions to developing the VR application.

3. Specifications and performance of airborne systems for dense point cloud acquisition for *Pinus radiata* inventory

3.1. Determination of optimal data acquisition parameters for UAS LiDAR tree inventory in pre-harvest *Pinus radiata*

Lucieer A., Harwin, S., McCoull C., Sharma, S., and Turner, D.

[1]*Discipline of Geography and Spatial Sciences, School of Technology, Environments and Design, University of Tasmania, Email: Arko.Lucieer@utas.edu.au*

Introduction

In recent years, there have been several major technological advances in unmanned aircraft systems (UAS, also referred to as UAVs, RPAS, or drones) and laser scanning devices. The development of small laser scanners, such as the Velodyne VLP-16 'Puck', for the automotive industry has resulted in major opportunities for UAS-based laser scanning. The Velodyne scanners strike a nice balance between size/weight, accuracy, and cost. In addition, UAS airframe technology has improved to the point where we can reliable fly a 3+ kg laser-scanning payload for ~15 minutes in a systematic survey pattern, facilitating UAS LiDAR surveys at unprecedented point density. The efforts in this project (FWPA PNC377-1516) have built onto a previous FWPA project (PNC326-1314) and a previous collaboration with DPI NSW through Dr Christine Stone. At the start of FWPA PNC377-1516, very few commercial UAS LiDAR systems were available. The systems that were available, such as the RouteScene LiDAR pod, were relatively expensive (AU$130K for LiDAR pod only) and without rigorous scientific testing. The TerraLuma UAS research group at the University of Tasmania has previously developed a UAS LiDAR system in-house, based on the Ibeo LUX laser scanner (2010 – 2014) (Wallace *et al.* 2012, 2016). In 2015-16, we developed a new system based on the Velodyne VLP-16 'Puck' supported by DPI NSW and FWPA PNC326-1314. In the current project (PNC377-1516), the UAS LiDAR system was further optimised for use with a superior UAS multi-rotor platform. The in-house development allowed us to get the highest possible accuracy out of the laser scanner and positioning sensors, and fully understand and calibrate each component of the system. The aim of the UAS LiDAR work package was to identify optimal data UAS LiDAR data acquisition parameters for forest inventory. To achieve this aim, we first developed a calibration workflow and assessed the relative and absolute accuracy that can be achieved with current technology. We collected UAS LiDAR data at three study sites (two in Tasmania and one in New South Wales), and we tested multiple flying heights, flight patterns, and laser scanning angles.

Objectives

Objective 1: Develop an efficient and accurate UAS LiDAR calibration workflow for lever arm determination, boresight calibration, and quantification of IMU drift

Objective 2: Quantify absolute and relative accuracy of a UAS LiDAR point cloud

Objective 3: Collect UAS LiDAR data over pine plantation for dense point cloud input into 'WP2 visualisation' and 'WP3 automated extraction of individual trees and tree metrics'

Objective 4: Identify optimal UAS LiDAR flight parameters (flying height, strip overlap, strip pattern) for optimal data collection in pine plantation

Objective 5: Collect UAS LiDAR data with SCION and UTAS systems over a common site for comparison of UAS systems and verification with plot data

Description of the UAS LiDAR system components

The UAS LiDAR system developed for this project consists of the following components (Figure 1):

- UAS airframe DJI Matrice 600:
    - https://www.dji.com/matrice600
    - Payload capacity ~5 kg
    - Flight duration: 12 – 15 mins (conservative battery use)
    - Survey grids flown with the Autopilot App on a iPad mini
    - Custom-built mounting brackets for LiDAR sensor mount and antennae
- Laser scanner Velodyne VLP-16 'Puck':
    - http://velodynelidar.com/vlp-16.html
    - 16 scan layers with a 30° degree vertical field of view (FOV), which equates to a 15° degree forward and backward distribution of the scan lines in the flight direction (+15° to -15° from nadir with scan lines separated by approximately 2 degrees)
    - 300,000 pulses per second for the full 360° view of the scanner, but only 80° used (40° on either side of nadir) equating to 66,666 pulses per second within the FOV
    - Maximum distance range: 100 m
    - Absolute distance ranging accuracy: 3 cm
    - Beam divergence horizontal: 0.18° (3.0 mrad); vertical: 0.07° (1.2 mrad). Flying at 40 m above ground level (AGL) this beam divergence results in a laser footprint of 12.6 by 4.89 cm.
    - Dual return (strongest and last)
- Global navigation satellite system (GNSS) receiver and inertial measurement unit (IMU) Advanced Navigation Spatial Dual:
    - http://www.advancednavigation.com.au/product/spatial-dual
    - Dual antenna, multi-constellation (GPS, GLONASS), multi-frequency (L1/L2) GNSS receiver
    - Accurate heading (~0.1°) from dual antenna
    - Calibrated MEMS-based IMU: ~0.8° absolute accuracy in pitch, roll, and yaw under typical UAS flight dynamics
    - Custom lightweight dual frequency antennae
- Custom-built sensor frame and electronics for sensor synchronisation
    - Adjustable angle of laser scanner to allow for oblique (forward) scanning angles along the flight direction.
- Machine vision camera: FLIR/Point Grey Chameleon RGB or Mono
    - Not used in this project, but can be used for generation of orthophotos and SfM point clouds.
- Processing routines and scripts developed in-house by TerraLuma group
    - Flight planning calculator (spread sheet)
    - Flight path selection and filtering tool (online) for subsetting of flight lines
    - Production of LiDAR point clouds from raw laser scanner data, GNSS positions, and IMU readings: Python script
    - Boresight calibration: TerraSolid and TerraMatch workflow
    - Leverarm determination: 3D photogrammetric pointcloud of airframe and CAD processing
    - Point cloud noise filtering and classification: lastools script

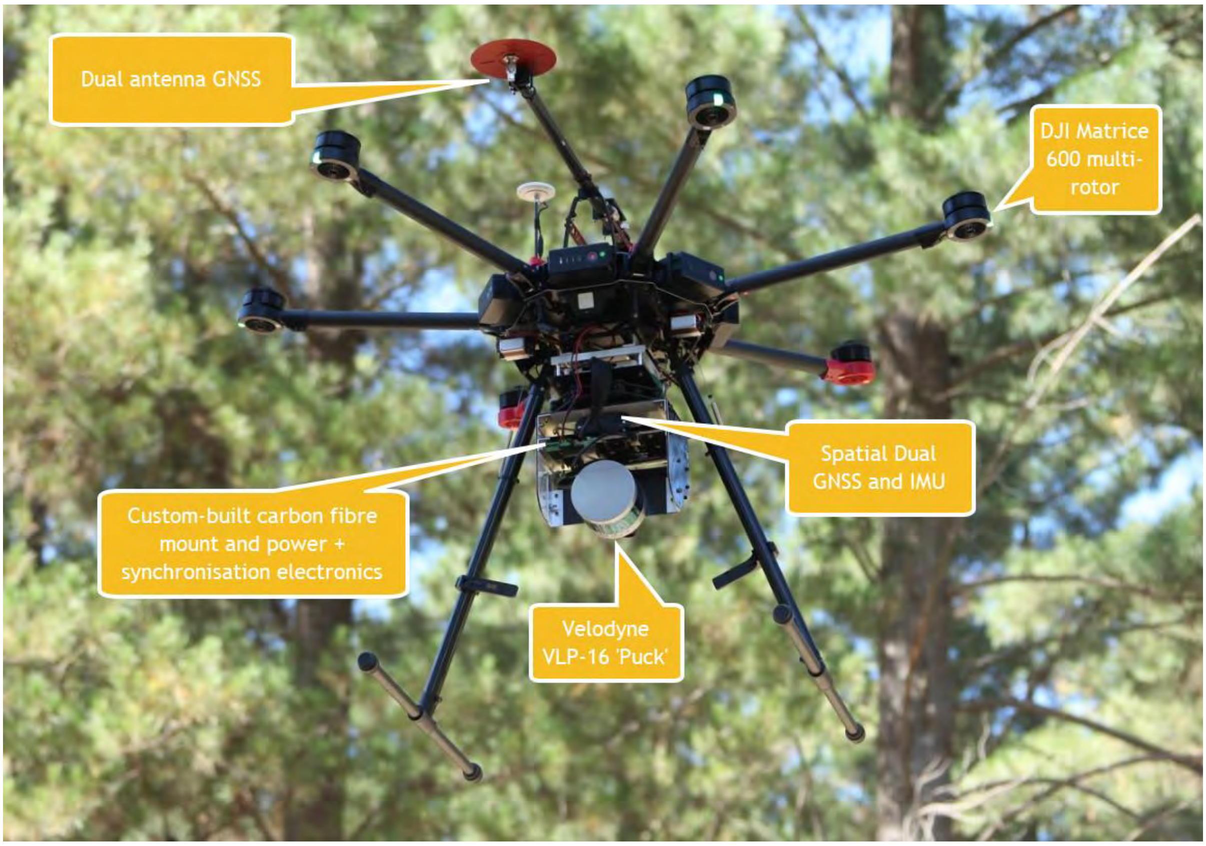

(a)

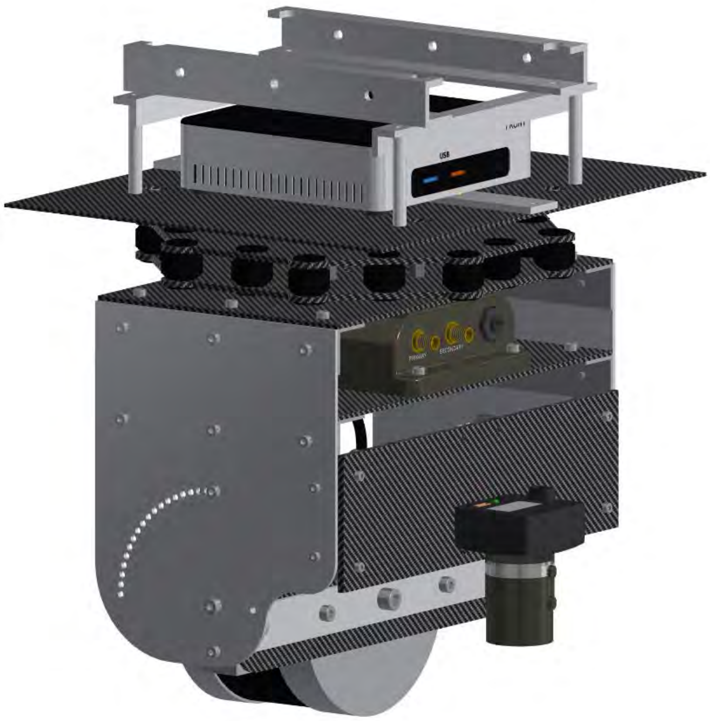

(b)

Figure 1: (a) TerraLuma UAS LiDAR configuration with individual components; (b) CAD drawing of sensor frame showing adjustable angle of laser scanner.

Objective 1: Develop an efficient and accurate UAS LiDAR calibration workflow for lever arm determination, boresight calibration

Tasks

1. Optimise integration of hardware and sensor components on UAS LiDAR system
   i. Mounting position of laser scanner
   ii. Time sync between GNSS and Velodyne
   iii. Mounting of dual antenna
   iv. Modular LiDAR pod for DJI Matrice 600 (M600)
2. Identify most suitable flight planning and navigation app for DJI M600 for reliable and smooth navigation
   i. Test several free and commercial flight planning and navigation apps with a dummy payload in outdoor test. A reliable airframe and smooth navigation is important for the collection of high quality LiDAR data from a multi-rotor platform.
3. Dedicated calibration flight over a field with calibration targets
   i. Targets: light poles, building, 90x90 cm panels on tripods surveyed
   ii. 40 m AGL flying height in overlapping cross strips over the calibration field
   iii. Two flights:
      a. Heading of UAS in direction of flight
      b. Constant heading aligned with direction of flight strips
4. Determination of lever arms of UAS LiDAR system
   i. Generate 3D point cloud based on photogrammetric structure-from-motion (SfM) techniques and export model to CAD for 3D measurements of XYZ offsets between GNSS antenna, IMU, and Velodyne laser scanner
5. Determination of boresight angles
   i. Develop workflow in TerraSolid to derive boresight angles (angular offsets between laser scanner and IMU) from calibration flight
6. Optimise LiDAR processing workflow
   i. Apply lever arm offsets and boresight angles to Python LiDAR processing code (applied to second flight)
   ii. Determine the impact of IMU drift and other residual errors/noise
   iii. Identify most optimal and efficient processing workflow with combination of in-house Python code and TerraSolid software

Overview

The UTAS team has concentrated on the calibration and accuracy assessment of the UAS LiDAR system developed by the TerraLuma research group. Dr Colin McCoull has been working on the determination of leverarm offsets (distances in X, Y, and Z between the primary GNSS antenna and the laser scanner) and boresight angles (angular differences between the laser scanner and inertial measurement unit (IMU)). This calibration procedure is standard for full-size LiDAR systems, but new methods had to be developed to accurately determine the calibration factors for a UAS LiDAR system. The calibration of the UAS LiDAR system is critical for accurate point cloud generation. Colin worked on his Master of Applied Science (MAppSci) thesis during Feb. – Nov. 2016. The findings of his research contributed directly to the current FWPA project.

Lever-arm Offsets

Lever-arm offset is the distance from the measurement system (the laser scanner) to the positioning system. Three possible measurements techniques to determine lever-arm offsets were considered for this study. Offsets could be measured using:

1. direct measurement, i.e. using theodolite and standard surveying techniques (direct measurement);
2. scanning of the UAS with a terrestrial scanner; or
3. photogrammetric techniques based on images of the UAS positioned in a calibration frame.

Due to the complexity and scale of the system, direct measurement was not attempted. Scanning of the UAV frame using a Leica MS50 was attempted, however, the resultant point cloud was very noisy. This was most likely due to the airframe's shiny carbon fibre surfaces causing reflections. We developed a new technique based on photogrammetric 3D point cloud reconstruction of the UAS. The resulting 3D point cloud was exported to a CAD, which allowed direct measurement of X, Y, and Z offsets between the centre of the primary (front) GNSS antenna and the centre of the Velodyne scanner. This was achieved by aligning the UAS over a flat calibration frame consisting of a sheet of wood with small spherical red pins as position targets defining a horizontal grid system to locate all objects in a horizontal X and Y plain. The calibration frame X-axis was aligned as closely as possible to the GNSS antenna pair and IMU x-axis[10]. Twelve reference points were also marked on the UAS. The height and horizontal location of all reference points was determined using a tape measure and a plumb bob (when required) to mark the UAS mark locations on the calibration frame.

Using a DLSR camera (NIKON D5100) 132 photographs of the UAS were taken at between 0.5 m and 1.5 m from the UAS from a range of angles. In Agisoft PhotoScan, a high accuracy image alignment was undertaken, using standard settings with control identified in all images and camera calibration parameters optimised. A dense point cloud reconstruction (with moderate depth filtering) produced the detailed point cloud shown in Figure 2 (a). The error reported for control marker locations following alignment was 0.00097 m or 1.517 pixels indicating a high level of correlation between measured and modelled marker locations. The point cloud was exported in LAS format and converted to a format suitable for opening in Autodesk AutoCAD 2015 using Autodesk ReCap 360. Key features within the point cloud (i.e. the antenna and scanner positions) were then drawn or located (Figure 2(b)) and offset distances between these features were measured (Figure 2(c)). The key offset distance was measured from the centre of the base of the forward GNSS antenna to the centre of the LiDAR scanner unit.

Measured lever-arm vectors were, X = -503.01 mm, Y = 3.15 mm and Z = 503.01 mm (in the Advanced Navigation Spatial DUAL GPS/IMU reference frame). Rotations of these vectors for calculation of the LiDAR unit reference locations were undertaken using the Advanced Navigation Spatial DUAL GPS/IMU Roll, Pitch and Heading values.

[10] https://www.advancednavigation.com.au/sites/advancednavigation.com.au/files/Spatial%20Dual%20Reference%20Manual.pdf

(a)

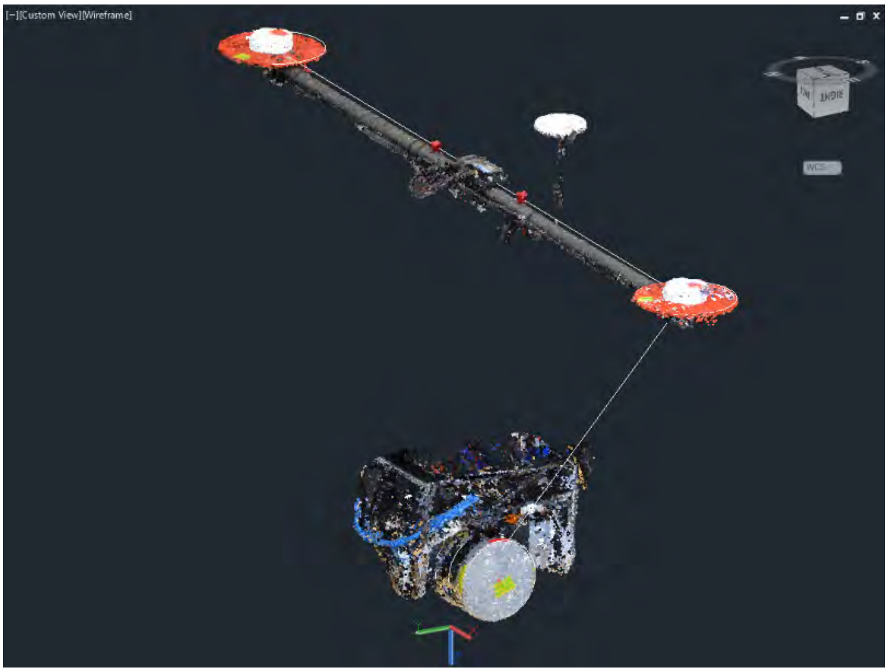

(b)

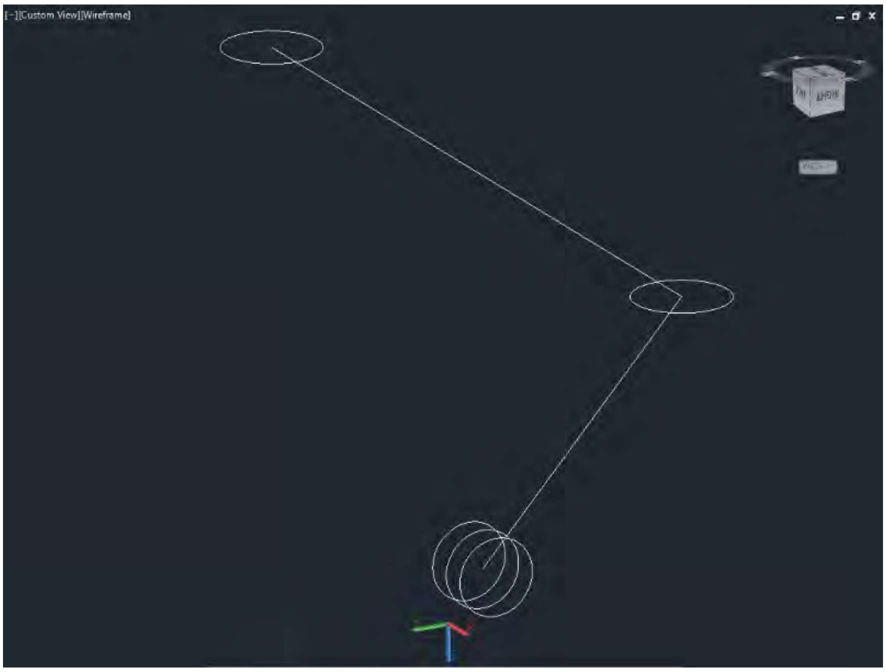

(c)

Figure 2: (a) The coloured point cloud of the UAS derived using Agisoft PhotoScan. (b) The lever-arm offset from the GNSS antenna base to the centre of the LiDAR Scanner (in AUTOCAD2015) with the UAS point cloud. (c) The lever-arm offset from the GNSS antenna base to the centre of the LiDAR Scanner (in AUTOCAD2015) without the UAS point cloud.

Boresight Experiment

Boresight offsets are the physical angular mounting offsets (in roll, pitch and heading) between the IMU and the laser scanner. Measurement of boresight angles is only possible through experimental data collection. The UAS LiDAR unit had to be flown at a suitable, accurately surveyed, calibration site. Calibrations undertaken previously (in 2016) indicated that the optimal calibration field should include flat surfaces and vertical features. The vertical poles allow for precise alignment between flight strips, e.g. a pole should appear in the same location in each flight strip. For this work a suitable site on Mt Nelson (Hobart) was selected (Figure 4). The site is located at the Olinda Grove University of Tasmania Soccer Fields (Figures 3 & 4). The site provides several vertical light poles, a building with multiple roof surfaces and two open areas of short grass. The calibration field was set up with ten raised target pads (0.9 x 0.6 m) and seven evenly distributed ground control points (GCP). The 0.3 x 0.3 m GCPs were constructed of highly reflective material ensuring they stand out in the lidar dataset to aid in GCP identification in the LiDAR point clouds (Wallace *et. al.* (2012). Raising flat targets on tripods provided the ability to physically identify targets as separate features to ground. These raised targets and GCPs were measured with a rapid static GNSS survey (absolute accuracy ~2 cm) on February 7, 2017.

Figure 3: Olinda Grove calibration site.

Figure 4: Tripod mounted calibration targets.

LiDAR data was collected over the calibration site on February 7, 2017 (Figure 5). Two flights were undertaken in a grid pattern flight path. During both flights a Leica GNSS (Leica Viva GS14) collected static data at the base station established nearby for later post-processing of flight trajectories. Raw flight position and orientation information as well as ranging information collected by the UAS carrying the Velodyne VLP-16 LiDAR 'Puck' were stored on the on-board the Intel NUC data logging computer during flights. Flying height during the survey was approximately 45 m and flight velocity was approximately 3 m/s to simulate typical forest flight conditions. Both flights were undertaken under automated control (Figure 6). Wind conditions during the flights were generally mild.

Figure 5: UAS Lidar in flight.

Figure 6: Calibration flight autopiloted by Hangar Autopilot App[11].

[11] http://autoflight.hangar.com/

Processing of UAS LiDAR Data

After collection, the raw data from the on-board GNSS and base station, the IMU and the scanner were extracted. The on-board GNSS data was post-processed against base station data with RTKLIB[12] software. This step produced a trajectory file with accurate UAS locations at 10 – 20 Hz. In addition, the IMU outputs pitch, roll and heading angles at 100 Hz, and the Velodyne data are stored in one large binary file with laser fire packets. The GNSS, IMU, and laser data streams need to be combined to produce a georeferenced point cloud, which involves interpolation of the position and orientation of the laser scanner based on GNSS and IMU data respectively, and application of the LiDAR equation to compute the 3D coordinate of each laser return. Software code implementing the LiDAR equation was initially developed in MATLAB for earlier PhD research by Wallace *et al.* (2012). This code was rewritten in Python and further refined by Stephen Harwin, Arko Lucieer between 2016 and 2018. The code was optimised to work with the Velodyne laser scanner and Spatial Dual IMU. In addition, the LiDAR equation was optimised for lever-arm and boresight adjustments (with input from Deepak Guatam). Alexander Pishchugin was employed to implement an online data upload and visualisation tool to allow subsetting and selection of flight lines for processing (Figure 7 -9).

Figure 7: Lidar processing web interface - main screen.

[12] http://www.rtklib.com/

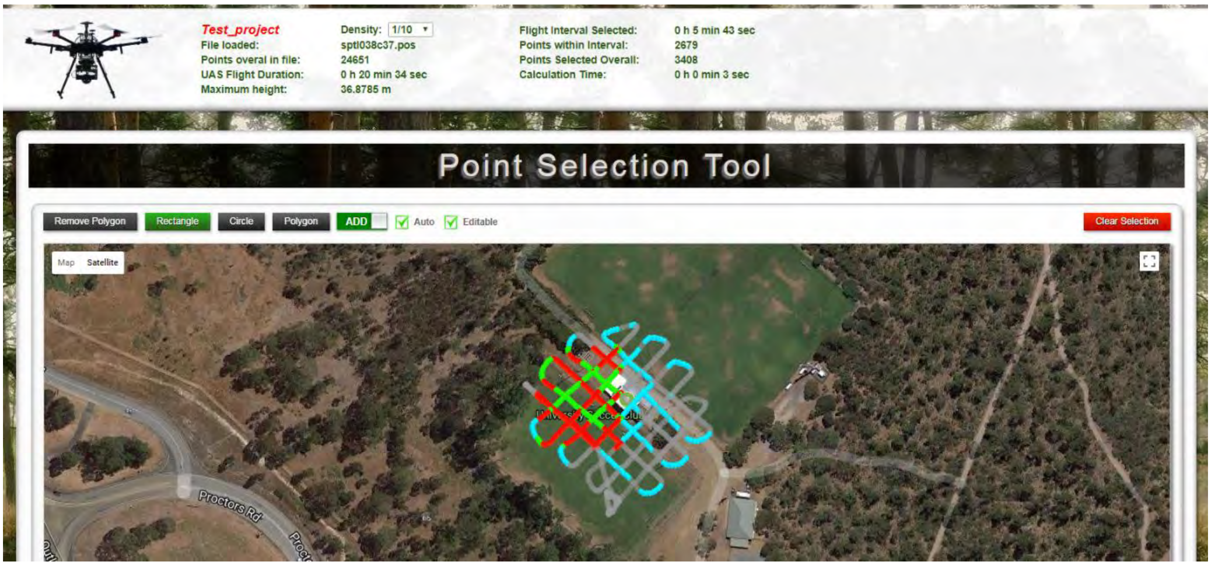

Figure 8: LiDAR processing web interface - Selection tool map view.

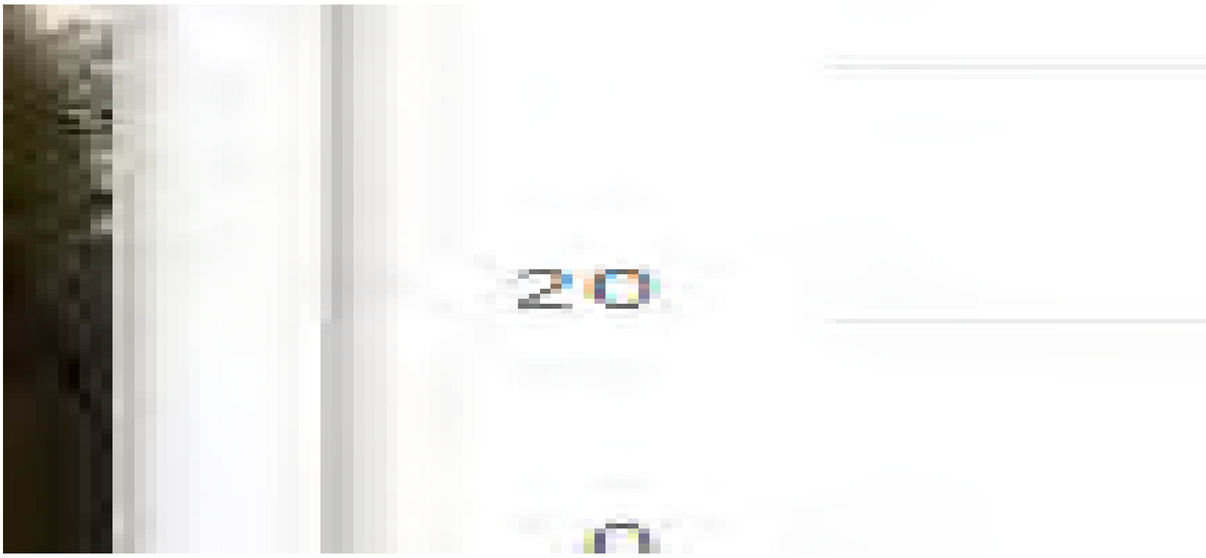

Figure 9: LiDAR processing web interface - Selection tool data views.

Boresight Calibration

Following the preparation of the data for boresight offset determination, a quasi-rigorous boresight calibration of the UAV LiDAR unit was undertaken using the un-calibrated (for boresight) LAS files and exported .csv trajectory information using TerraScan and TerraMatch (© TerraSolid).

The first calibration stage involved a manual calibration of the flight lines using the TerraMatch “Apply Corrections” tool. Corrections were only applied to heading shift, roll shift and pitch shift. Figure 10 show a cross section of uncalibrated points. Determination of initial approximate correction values focused on rotating flight strips to produce well-matched overlaps of all flight strips. The light poles were used in this stage as they allow for quick assessment of the initial offset correction estimates as can be seen in the before and after cross sections (Figure 11). Initial calibration values identified using this method were heading shift 0.2 degrees, roll shift -0.1 degrees and pitch shift 0.3 degrees.

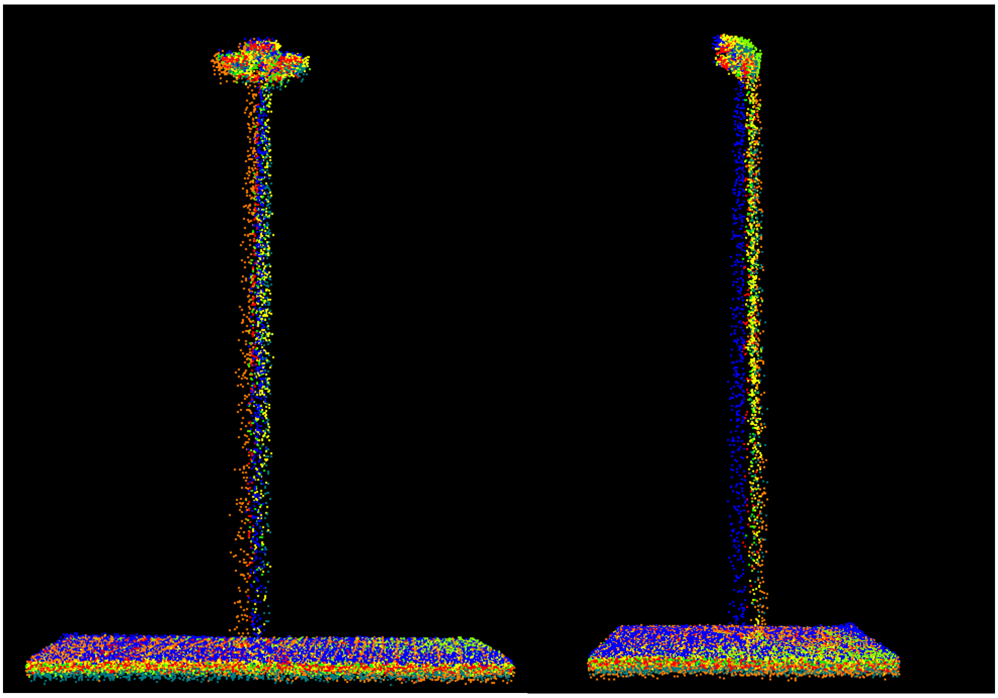

Figure 10: Uncalibrated light pole. Flight lines 1 to 7 are depicted in cross section prior to boresight calibration.

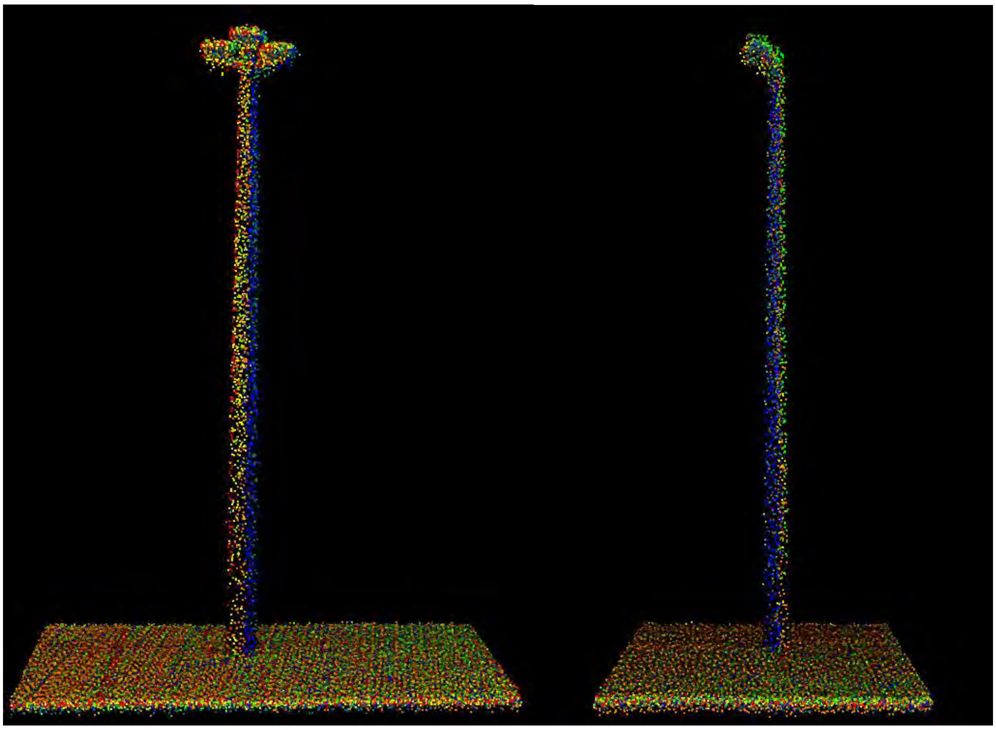

Figure 11: Calibrated light pole. Flight lines 1 to 7 are depicted in cross section following boresight calibration.

Following identification of approximate correction values, the "Find Match" tool was applied such that a more exact solution for correction parameters could be found. In this step, corrections for heading shift, roll shift and pitch shift were identified least squares adjustment between the seven overlapping flight strips. The LiDAR datasets were cleaned of all points that were not raised targets (0.9 x 0.6m) (see Figure 4 and Figure 12). This provided a set of small flat, low noise point cloud features that were well distributed to achieve an accurate match across the set of flight line point clouds.

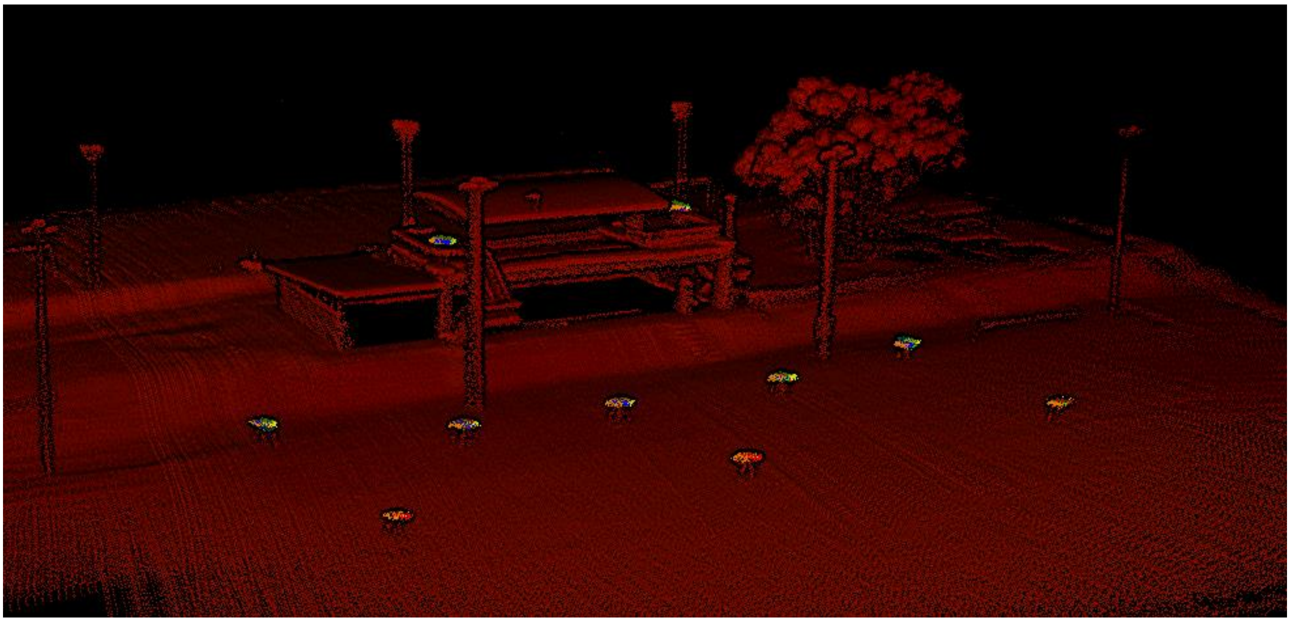

Figure 12: Location of raised targets (0.9x0.6 m pads on tripods) used for accurate calibration.

This further refinement in boresight calibration identified a further heading shift of 0.0491 degrees, roll shift of -0.0185 degrees and pitch shift of -0.0359 degrees. Final RMS errors improved from dz RMS 0.066 m to 0.063 m. Given these results, the additional calibration step appeared to slightly improve the result.. Figure 13 - Figure **20** show cross sections of the datasets before and after calibration.

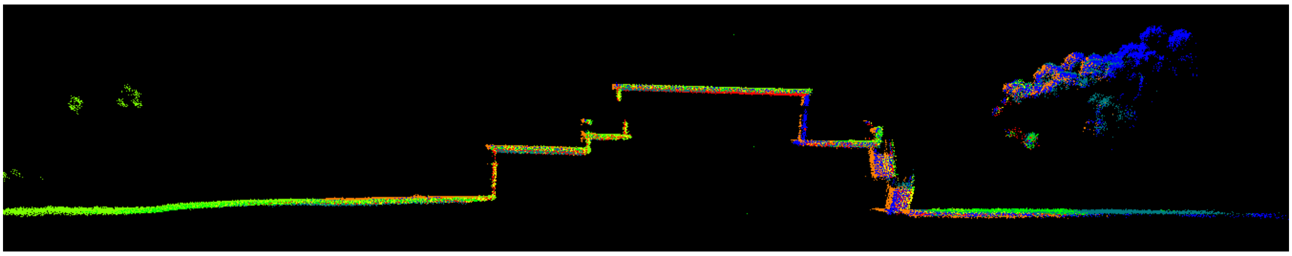

Figure 13: Uncalibrated scan lines. Flight lines 1 to 7 are depicted in cross section prior to bore sight calibration.

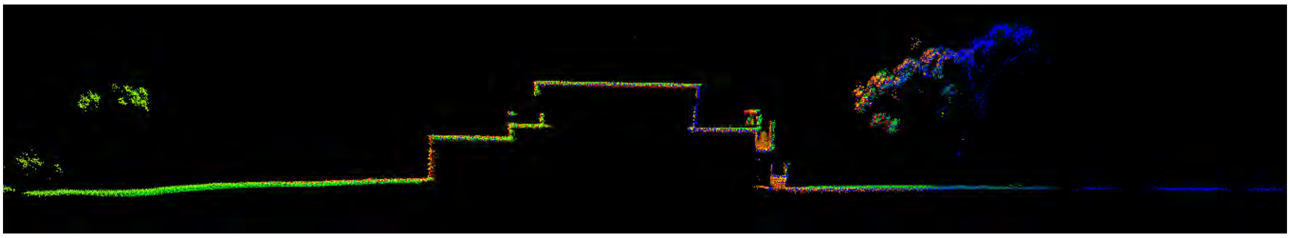

Figure 14: Calibrated scan lines. Flight lines 1 to 7 are depicted in cross section following accurate bore sight calibration.

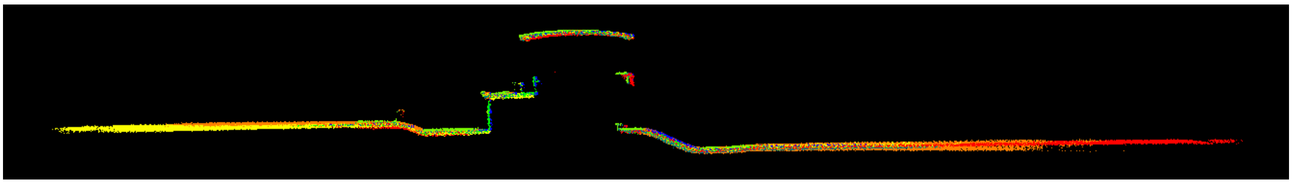

Figure 15: Uncalibrated scan lines. Flight lines 1 to 7 are depicted in cross section prior to bore sight calibration.

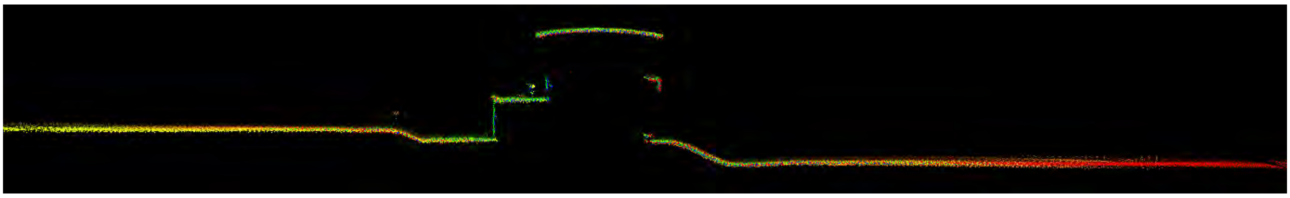

Figure 16: Calibrated scan lines. Flight lines 1 to 7 are depicted in cross section following accurate bore sight calibration.

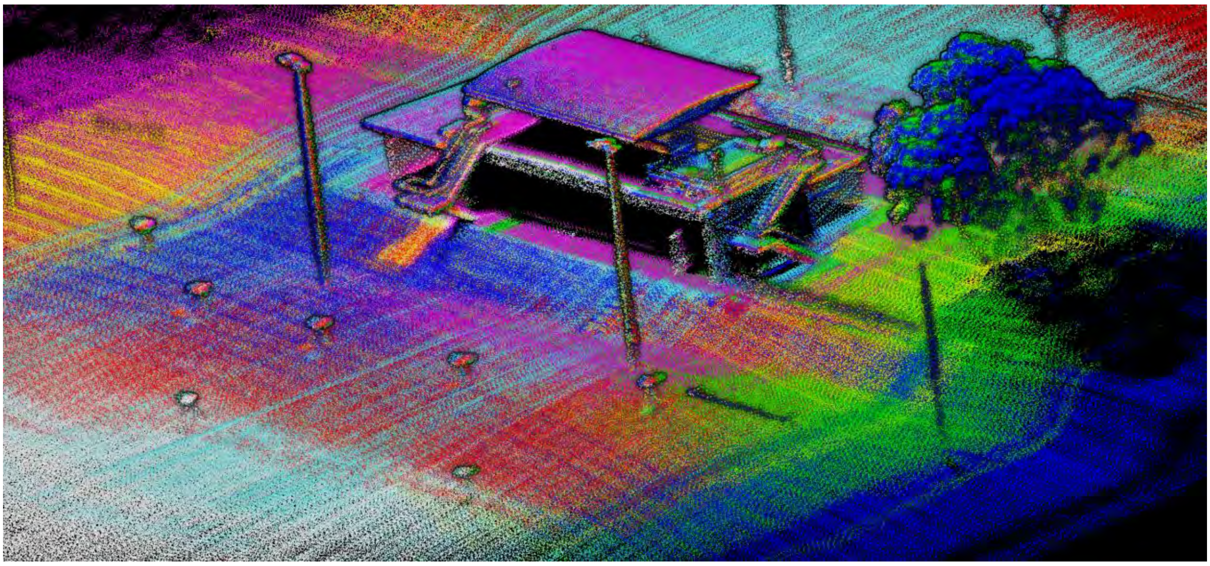

Figure 17: Uncalibrated LiDAR data points from flight lines 1 to 7.

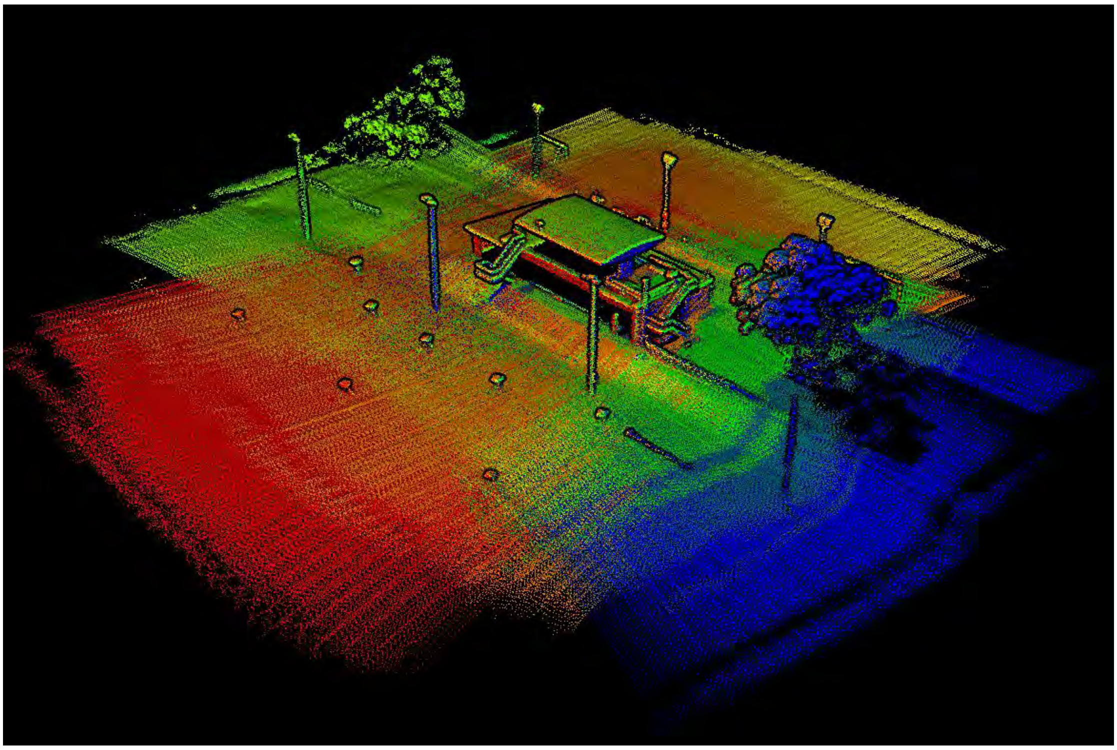

Figure 18: Calibrated LiDAR data points from flight lines 1 to 7.

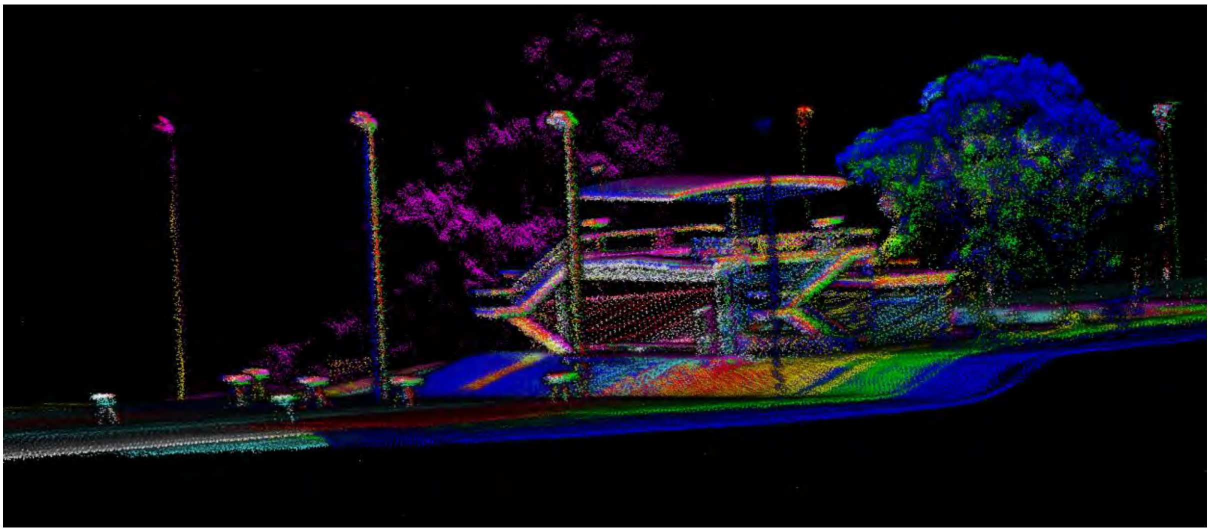

Figure 19: Side view of uncalibrated LiDAR data points from flight lines 1 to 7.

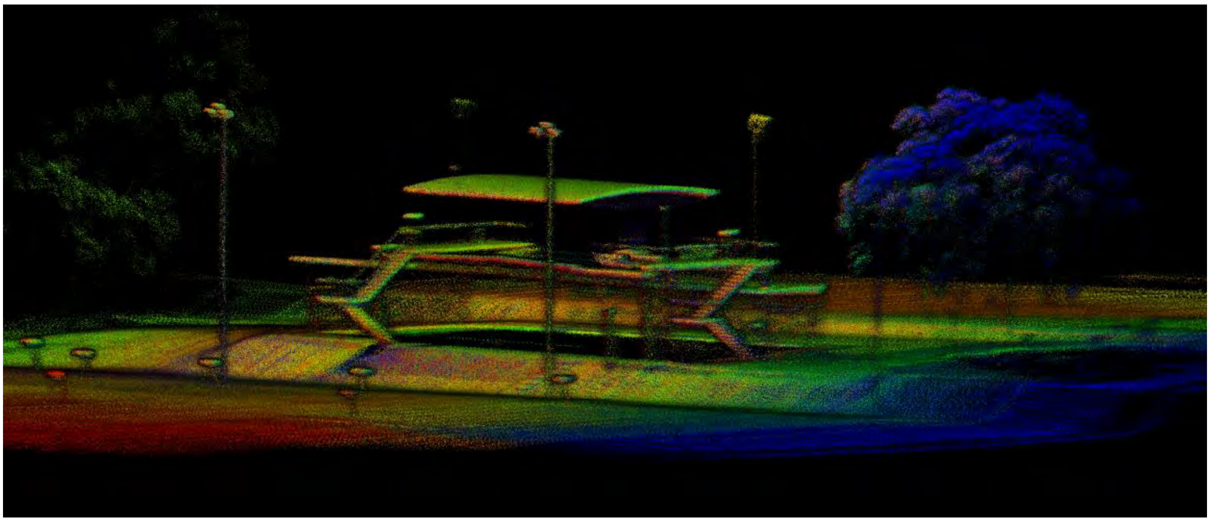

Figure 20: Side view of uncalibrated LiDAR data points from flight lines 1 to 7.

Identification of heading drift, roll drift and pitch drift was also undertaken using TerraMatch. All flight flight lines were corrected for heading shift, roll shift and pitch shift based on the final boresight angles. Observation of these data indicated drift was not present in the dataset.

Final LiDAR Point Cloud Properties

Table 1 shows the point cloud properties including point density and point spacing for all flight lines used in this assessment. Point densities range from 270 points per m^2 to 360 points per m^2 for individual flight strips. The total point density of the final combined point cloud was 1122 points per m^2 and the average spacing of points was 0.03 m. Last return only density for this point cloud was 559 points per m^2.

Table 1: Point densities and point spacing of flight strips for all strips used in the calibration process.

Scan Line	**number of returns**	**number of last returns**	**covered area in square metres per length**	**point density: all returns (per m2)**	**spacing: all returns (m)**	**point density: last returns (per m2)**	**spacing: last returns (m)**
1	1130984	563733	4184	270.31	0.06	134.74	0.09
2	1155468	576019	4068	284.04	0.06	141.60	0.08
3	1278485	637249	4104	311.52	0.06	155.28	0.08
4	1049900	523746	3816	275.13	0.06	137.25	0.09
5	1850543	921884	5228	353.97	0.05	176.34	0.08
6	1680408	837378	5096	329.75	0.06	164.32	0.08
7	1845481	919450	5128	359.88	0.05	179.30	0.07
All Flights Combined	**9,991,269**	**4,979,459**	**8908**	**1121.61**	**0.03**	**558.99**	**0.04**

UAS LiDAR Flight Planning and LiDAR Configuration Tool

To assist in UAS flight planning, we have developed a spreadsheet that calculates point spacing, flight strip overlap, beam size on the ground, etc., which allows for more informed flight planning and laser scanner configuration. This spreadsheet was adapted for the Interpine Riegl VUX-1 helicopter survey at Carabost, and helped to plan flying heights and speeds to achieve the desired point density. The spreadsheet is available from Arko.Lucieer@utas.edu.au on request.

LiDAR scanning acquisition parameters (26/08/2017)

Arko Lucieer (Arko.Lucieer@utas.edu.au),Deepak Gautam (Deepak.Gautam@utas.edu.au)

Fields	Value	Unit	Remark		
Velodyne variables					User input
Forward tilt angle	0.00	Deg	No impact		Flight parameters
Cross-track FOV	45.00	Deg		**Bold**	**Important**
Along-track FOV	30.00	Deg			
Cross-track beam divergence	0.18	Deg			
Along-track beam divergence	0.07	Deg			
LiDAR strike frequency	21700.00	Hz	= 21700*16 laser points per second.		
Rotation rate	5.00	Hz	Range from 5 to 20 HZ		
Lidar scan line spacing	2.00	deg			
UAS variables					
Speed	5.00	m/s			
Flying height	70.00	m			
Canopy height	30.00	m			
AGL height	40.00				
Side overlap	60.00%				
Width of site (Cross-track)	100.00	m	Width of survey area		
Length of site (Alon-track)	100.00	m	Length of survey area		
Max flight time	12.00	min			
Flight plan specific					
Along-track swath length	21.44	m			
Cross-track swath width	33.14	m			
Flight line spacing	13.26	m			
Number of cross-track flight lines	8.00		Number of flight strips for the survey area		
Number of along-track flight lines	8.00		Number of flight strips for the survey area		
Total flight distance	949.00	m			
Flight duration	**3.16**	min	does not take into account take-off and landing		
Pointcloud specific					
Scan line spacing	1.40	m			
Cross-track average points spacing	**6.11**	cm	Side overlap ignored. Divide point spacing by 2 for 60% side overlap.		
Along-track average point spacing	**6.52**	cm	Overlap considered		
Cross-track footprint spot size	12.57	cm	Size of the footprint on ground		
Along-track footprint spot size	4.89	cm	Size of the footprint on ground		
Changelog					
AL	30/04/2017	First version create. Beam divergence and point spacing to be added			
DG	26/08/2017	Beam divergence and point spacing added			

Flight Planning Apps

We tested a range of Apps for flight planning and automated UAS navigation

- Drones made easy (Map Pilot)
- Drone deploy
- Precision Flight
- Pix4D capture
- DJI ground station Pro
- Auto Pilot
- Litchi

At the time of testing and writing (Jan - June 2018), we found Hangar AutoPilot to be the best App for UAS LiDAR purposes.

Objective 2: Quantify absolute and relative accuracy of a UAS LiDAR point cloud

Tasks

1. Dedicated accuracy assessment flight over a field with surveyed targets
    i. Targets: light poles, building, 90x90 cm panels on tripods surveyed
    ii. 40 m AGL flying height in overlapping cross strips over the calibration field
2. Relative accuracy assessment
    i. TerraMatch: translation and rotation to match overlapping flight strips
    ii. CloudCompare: rigid-body transformation on ground points to match ground points of photogrammetric model (used as a reference). Assessment of accuracy through:
        a) Rotation angles required for optimal match
        b) Point-to-point distance
3. Absolute accuracy assessment
    i. Comparison of known distances in LiDAR point cloud
    ii. Comparison of absolute location of targets

Overview

The aim of this section is to determine the relative and absolute on-ground LiDAR point accuracy and internal noise of the LiDAR model through comparison of the scanned output to known control points / surfaces at the test site.

Strip adjustment is a commonly used technique to assess the separation between overlapping flights strips as a measure for data quality. However, strip adjustment is primarily undertaken to correct systematic error in overlapping strips. In this study, the "Find Match" in TerraSolid/TerraMatch was the strip adjustment method used to determine the boresight angles and, therefore, this approach was not used to examine the final relative and absolute accuracy of the LiDAR datasets.

Relative Accuracy Assessment

Relative accuracy assessment is concerned with determining the degree of consistency between LiDAR points in overlapping strips and with determining the internal quality of individual strips. In this case, relative accuracy was quantified as the elevation difference between overlapping strips.

The "Measure Match" tool in TerraMatch measures how well different strips match each other vertically. It computes the elevation difference between surfaces from individual strips and a mean surface. In this case, it was applied to filtered LiDAR flights strip containing only points representing areas of open ground (sports field) and roof areas.

Table 2 shows the results for the relative accuracy assessment where the magnitude represents the absolute value of the elevation difference between a strip and the mean surface, and Dz is the mean value of the elevation difference between a strip and the mean surface. The average magnitude (average absolute value of the elevation difference) of all strips is 0.075m.

Table 2: Vertical strip agreement assessed using TerraMatch (Measure Match tool).

Flight	Scan Line	Points	Magnitude (m)	Dz (m)
1	1	3350089	0.06	0.0079
1	2	3965812	0.0858	0.0350
1	3	3950225	0.0753	0.0128
1	4	3526028	0.0727	-0.0287
1	5	4035226	0.0686	-0.0107
1	6	3923924	0.0904	-0.0262
1	7	3761887	0.0687	0.0083
Average magnitude (m): **0.07488**				

Absolute Accuracy Assessment

For the absolute accuracy assessment, an independent point cloud dataset was created using photogrammetric/structure-from-motion (SfM) techniques. To construct this accurate site model, a DJI Phantom 3 Advanced UAV was flown at 40 m to capture 80% side and forward overlap photography and derive a high-density point cloud using Agisoft Photoscan (Figures 21 and 22). The 3D model was controlled with the established GCPs resulting in an error of 0.0367 m. In addition, the site was also surveyed using a total station (Leica MS50 MultiStation) on February 7, 2017. During this survey, additional control was collected and verification observations were made.

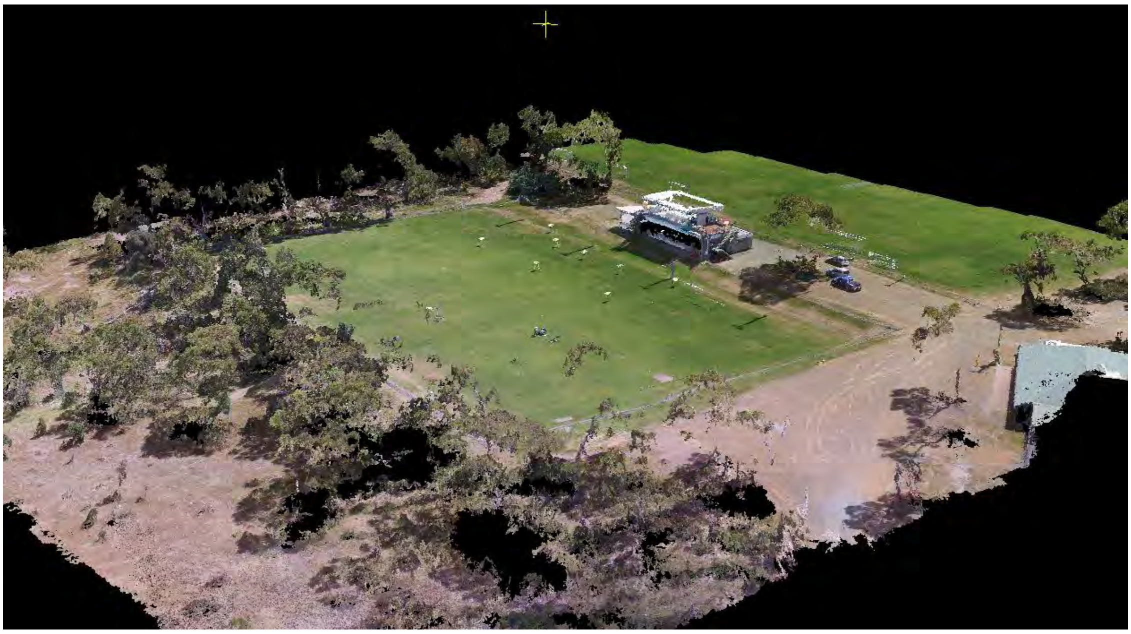

Figure 21: A photogrammetric point cloud of the main building and surrounding land at the Calibration Site (point cloud constructed using Agisoft Photoscan from Phantom 3 photography flown at 45 m).

Figure 22: Orthophoto of the Olinda Grove calibration site (created using a Phantom 3 UAV and Agisoft PhotoScan).

Both LiDAR and photogrammetric datasets were filtered such that only points representing areas of open ground (sport field) and the main roof were used. A mean distance and standard deviation between each data point of the LiDAR strips and its nearest neighbour in the photogrammetric reference cloud was determined using the "Cloud to Cloud Distance Tool" in CloudCompare[13]. The average distance between the LiDAR and photogrammetric point cloud quantifies the absolute accuracy of the LiDAR data. Furthermore, the Iterative Closest Point (ICP) algorithm was used to co-register the LiDAR point cloud to the photogrammetric point cloud to minimise the difference between the two dataset. After the ICP adjustment, the mean distance was measured again to determine the absolute accuracy in an optimally adjusted dataset. Table 3 show that the average distance between the seven flight strips and the reference dataset was 7.8 cm. After adjustment, the absolute accuracy improved to 4.6 cm.

Table 3: Cloud/Cloud Distance analysis results for individual scan lines from flight 1 as calculated in Cloud Compare using the photogrammetric point cloud as the model surface. Results are for calibrated LAS data and for ICP co-registered data.

Scan Line	Raw calibrated flight lines		Flight lines following ICP matching	
	Mean Distance (m)	Std. Deviation	Mean Distance (m)	Std. Deviation
1	0.050553	0.039166	0.039751	0.032319
2	0.092047	0.065437	0.048697	0.036939
3	0.067794	0.054592	0.045506	0.033921
4	0.084768	0.071107	0.045793	0.046860
5	0.086105	0.048865	0.042694	0.030046
6	0.116523	0.084335	0.057836	0.044512
7	0.047065	0.035280	0.041502	0.030762
Combined	**0.0778**		**0.0459**	

13 http://www.danielgm.net/cc/

Reference Distances Between Objects

Distances were measured between objects in the field using direct traditional surveying. The distance between reference points (raised markers) on tripods was determined by undertaking a survey using the Leica MS50 MultiStation. In each flight strip the distance between identifiable objects was measured and compared to the surveyed values. The location of targets on tripods was identified by locating the average position of points on the tripod in CloudCompare. Distances between targets are presented in Table 4. Generally, agreement between distances measurements is better than 10 cm.

Table 4: Differences between the distance between measured targets (on tripods) from point cloud measurements (per scan line) and "known" distances from the site survey. TL = Building target to west, TL = Building target to east, GL = Central western ground target in front row (row next to building), GR = Central eastern ground target in front row (row next to building)

Flight	Scan Line	Measurement and Surveyed Distance (m) between Targets				
		TL to TR	GL to GR	Tl to GR	TR to GL	TL to TR
		19.452m	11.004m	22.615m	26.245m	19.452m
1	1	-0.12	0.001	-0.018	-0.007	-0.12
1	2	0.015	-0.006	0.052	-0.007	0.015
1	3	-0.021	0.016	0.019	-0.032	-0.021
1	4	0.033	-0.015	-0.045	-0.054	0.033
1	5	0.008	0.024	-0.001	0.04	0.008
1	6	0.017	0.001	-0.054	0.096	0.017
1	7	0.019	-0.001	-0.007	0.074	0.019
Average		-0.007	0.003	-0.007	0.016	-0.007
Combined Average		0.001m (Range -0.12m to 0.096m)				

Objective 3: Collect UAS LiDAR data over pine plantation for dense point cloud input into 'WP2 visualisation' and 'WP3 automated extraction of individual trees and tree metrics'

Tasks

1. Collect UAS LiDAR over a pre-harvest *Pinus radiata* sites
   i. UAS LiDAR flight at two to three flying heights, e.g. 5 – 10 m above 23 m tall trees (~30 m AGL), 20 – 30 m above trees (~45 m AGL), 40 – 50 m above trees (~70 m AGL) at high overlap (>50%) to allow selection of flight strips at two perpendicular flight directions.
2. Process LiDAR flight strips and check boresight calibration derived in Objective 1.1.
3. Verify accuracy of point clouds against ground targets.
4. Point cloud to be delivered to project partners via CloudStor

Overview

To achieve the objectives of the UAS LiDAR work package we performed four major field campaigns:

1. Olinda Grove UTAS soccer field: calibration experiment (7 February 2017), described in Objective 1.1.
2. Uxbridge, southern Tasmania, 15-year old *Pinus radiata* plantation managed by Norske Skog (thinned, unpruned): experiment to assess impacts of flying height and flight strip overlap on point density and canopy penetration (15 May 2017)
3. Payanna, northeast Tasmania, 26-year old *Pinus radiata* plantation managed by Timberlands (thinned and pruned): experiment to assess optimal UAS flight parameters (17 – 21 September 2017)
4. Carabost SF, New South Wales: collaborative field campaign for data comparison (18 – 23 February 2018), described in Objective 1.5.

Uxbridge, Tasmania (May 2017)

We identified a mature (15 years' old) pine stand at Uxbridge, one hour out of Hobart, to allow for efficient testing of the system (Figures 23 – 25). After calibration and accuracy assessment, a thorough UAS LiDAR survey was undertaken over this test site at flying heights of 50 m and 70 m above ground level (AGL). The maximum tree height was 25 m. We flew high overlapping crossed flight strips to determine the impact of flight direction, flight strip overlap, and flying height (Figure 26). This survey was flown on 15 May 2017. The data was processed and calibrated and flight strips for both flying heights were made available on the shared online CloudStor project drive (Figures 27 and 28).

Figure 23: UAS LiDAR platform ready for take-off at the Uxbridge study site (15-year old thinned unpruned plot).

Figure 24: Aerial view of the Uxbridge test site.

Figure 25: Photo taken inside the plot showing thin, unpruned stems.

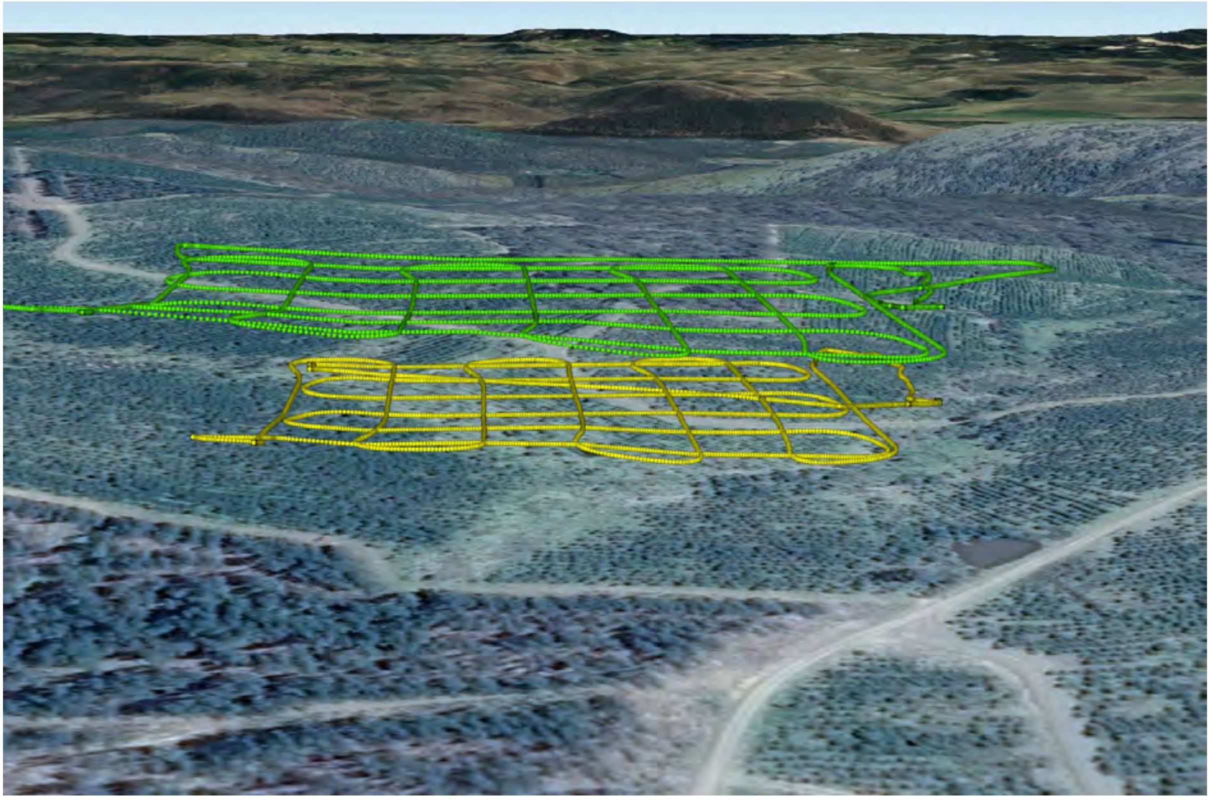

Figure 26: Crossed flight strips at 50% side overlap flown at 50 m and 70 m above ground level.

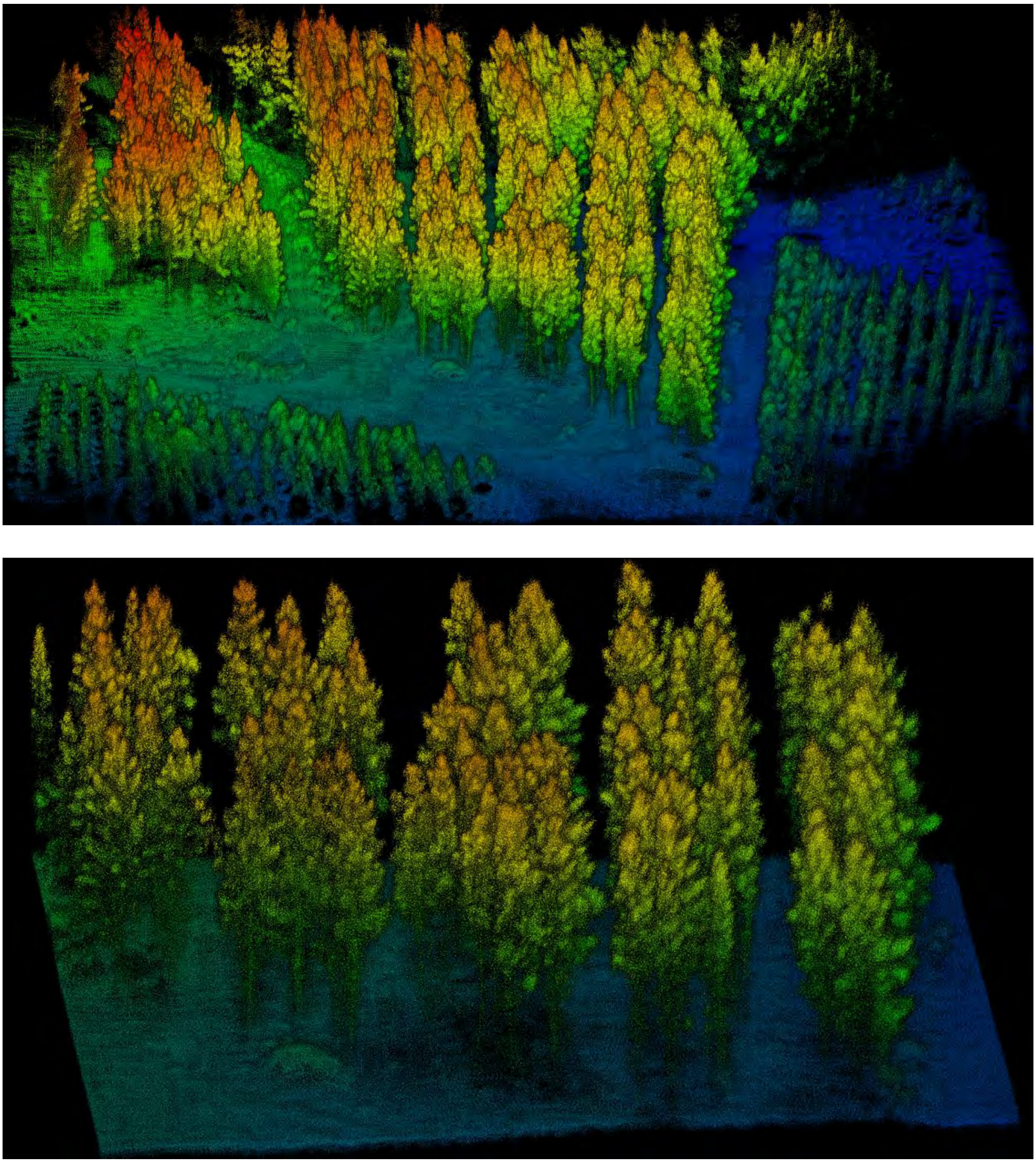

Figure 27: UAS LiDAR point cloud, combined flight strips from 50 m flight.

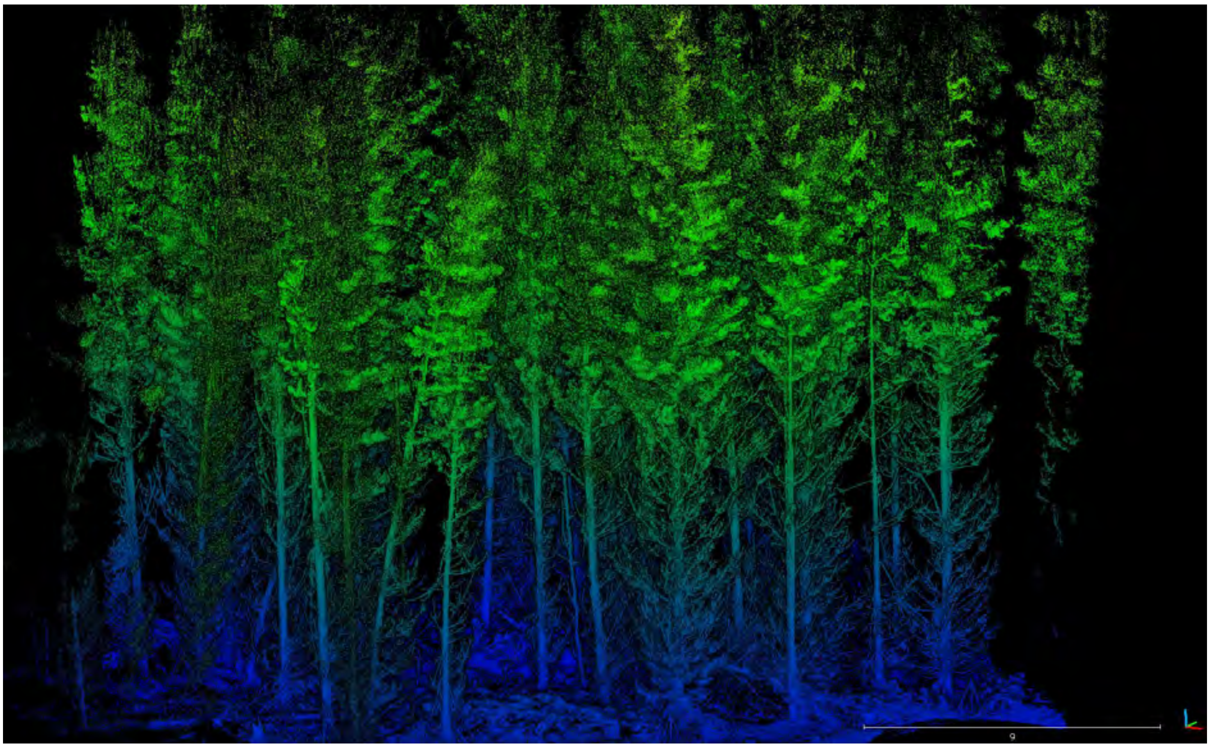

Figure 28: A terrestrial laser scan (TLS) was carried out by Robert Anders (UTAS) for a student project and comparison purposes.

The data showed that we can achieve very high point densities of 1200 pts/m2 for the 50 m flight (all returns, 3 cm point spacing) and 388 pts/m2 for the 70m flight (all returns, point spacing 5 cm). Feedback from project members at the Parramatta workshop (May 2017) indicated that this study site is not ideal for demonstrating the ability of UAS LiDAR to capture tree stems in a pre-harvest and thinned stand. The trees at the Uxbridge site are 15 years' old and unpruned, which makes for a complex environment and a very challenging task for automated stem extraction. Nevertheless, this dataset provided an early indication of the point densities that can be achieved with a low-cost UAS LiDAR system, and the data characteristics for different flying heights. These flights showed that we should aim to fly as close to the top of the canopy as feasible to optimise the number of stem strikes.

Payanna, Northeast Tasmania (September 2017)

Based on the Uxbridge UAS LiDAR datasets it was decided that an additional UAS LiDAR survey was required to demonstrate the potential for this technology to derive stem strikes. In addition, an additional survey was needed to test more flight parameters, such as oblique scanning angles. In consultation with Timberlands Pacific and with input from the FWPA project group, we selected a 26-year old site in northeast Tasmania (Payanna). The coupe had been thinned twice and pruned resulting in 375 stems per hectare with very few branches up to 6 metres (Figure 29). The main argument for selecting this site was that it offered the most mature trees in the area, and offered the lowest stocking density, thereby optimising our chances of LiDAR stem strikes.

We organised a field campaign from 17 to 21 September, and focused on a site of 200 by 150 m. We were able to complete 8 UAS LiDAR flights under different flight configurations. The team consisted of a field crew of three (Dr Steve Harwin, Deepak Gautam, and Saroj Sharma), and a UAS team of two (A/Prof Arko Lucieer and Dr Darren Turner). Don Aurik and Gareth

Tempest from Timberlands Pacific visited on the 18th of September. The field team focused on terrestrial laser scanning (TLS) and accurate measurement of tree location (Figure 29).

Figure 29: One of the field plots at the Payanna site.

An overview of the data collected is provided below:

UAS LiDAR Flights

- 18 & 19 September: 10 flights
- Size of survey area 200 by 150 m
- 35 – 60 m flying height above take-off point (most flights at 35 – 40 m)
- 3 m/s flight speed for 12 mins per flight
- Five flights at 30 degree oblique (changing direction) (Figure 30)
- Crossed overlapping flight strips at 50% overlap (Figure 31)
- Summary of flights:
    - 2x flights nadir @ 40 m flying height, crossed flights strips
    - 1x flight 30° oblique, constant heading, descending from 40 to 35 m flying height
    - 4x flight 30° oblique, changing heading in flight direction (scanning trees from multiple sides) @ 35 m flying height, crossed flight strips (two flights out of four can be used for analysis)
    - 1x flight nadir @ 60 m flying height (larger area)
    - 1x DJI Phantom 4 Pro photogrammetric flight
    - 1x 3DR Solo with 4-band multispectral Sequoia

On the evening of the first UAS flight day (18 September), preliminary processing was carried out to assess the impact of the flying height. We established that stem strikes and ground strikes were relatively sparse, which resulted in the decision to limit the number of flying height scenarios, and focus on low flights. In the end, we flew at 35, 40, and 60 m above ground level (from take-off point) with the tallest tree near the take-off point at 28 m. We flew crossed strip flight paths, which meant approximately 10 parallel flight lines for each flight, changing 90 degree in flight direction between flights (e.g. flight 1 east-west, flight 2 north-south). On average we flew 15 m above the canopy (any closer would have been too risky). We were able to maintain visual line of sight from a clearing above the stand.

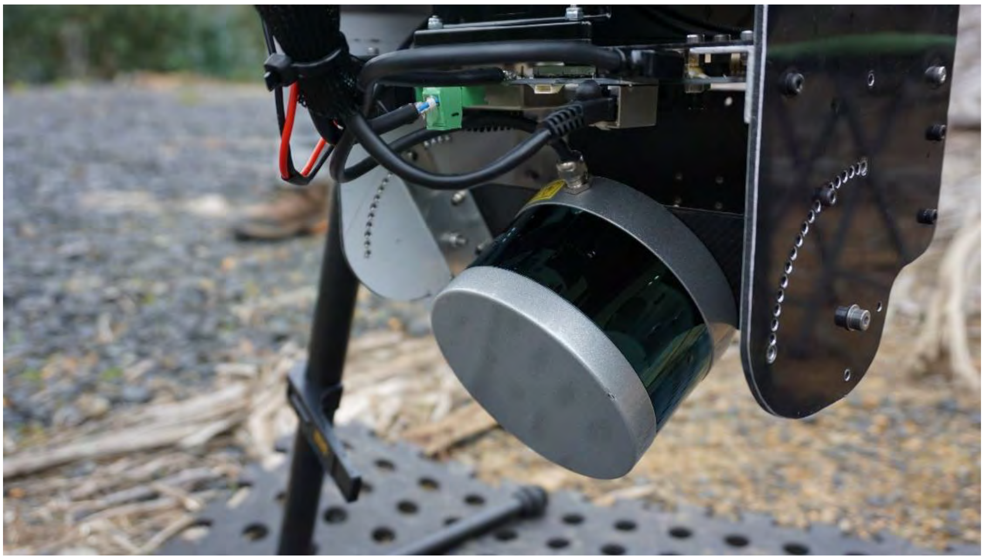

Figure 30: Velodyne scanner mounted at a 30 degree oblique angle.

Figure 31: Flight path patterns.

Inventory and TLS Plots

A total of five circular plots (two 15 m radius plots and three 25 m radius plots) were established randomly throughout the site. For uniformity in the plot size, four 15 m radius plots were considered. Plots were positioned in the field by establishing a traversed network using a combination of total station and GNSS surveyed control. For each plot, each of the trees were uniquely numbered, and the stems were positioned by measuring radiation distance and bearing using a total station. The plots were relatively dense with an average of 396 trees per hectare (range was 325-438 trees per hectare, see Table 5 and Figure 32). The survey team survey and marked the following TLS plots (Figure 34 and Figure 35):

Single dome scans:

- I01 - Radiations to 25 trees within approx. 15 m
- I02 - Radiations to 18 trees within approx. 15 m

- I04 - Radiations to 77 trees within approx.25 m

Four Scans (one dome scan and three inward-looking side scans):

- I03 - Radiations to 84 trees within approx. 25 m
  - I03S01, I03S02/I05S02, I03S03
- I05 - Radiations to 76 trees within approx. 25 m
  - I05S01, I05S02/I03S02, I03S03

From each inventory point (e.g. I01) each tree was given a number (painted) and a radiation distance and bearing taken (e.g. I01T01 is the first tree in the plot)

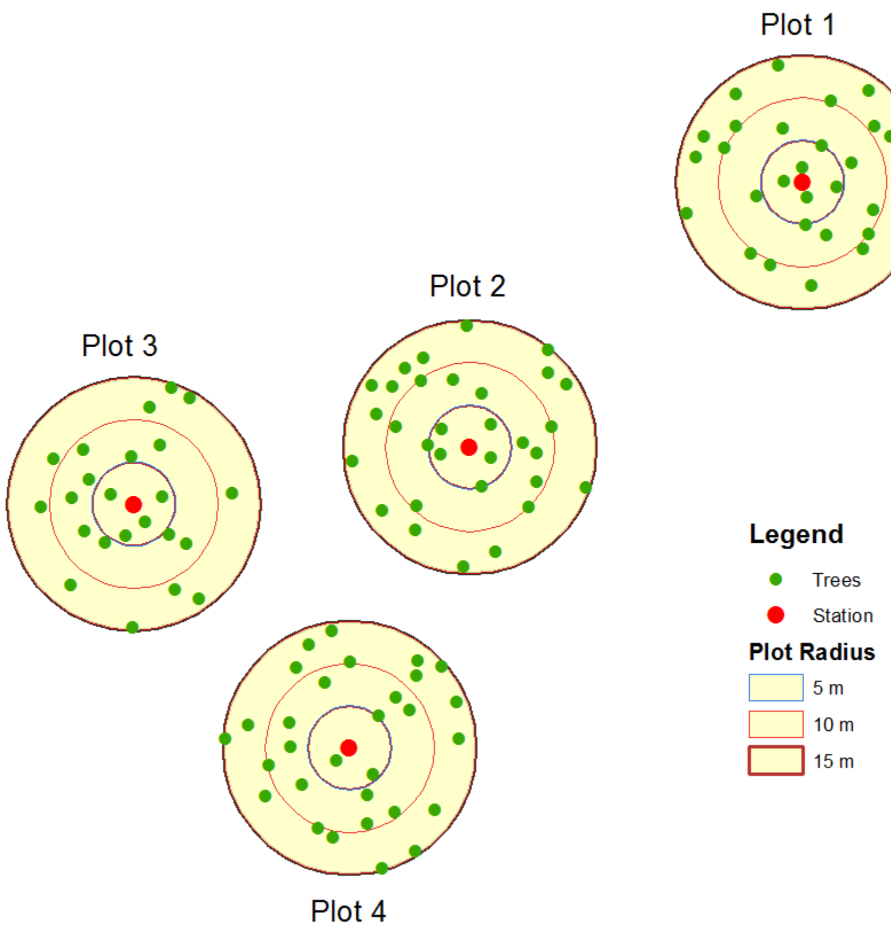

Figure 32: The distribution of trees in different field sample plots.

Table 5: Summary statistics of trees in different plots.

Plot ID	< 5m	5m -10m	10m -15m	Total	Density
1	5	7	16	**28**	396
2	6	8	17	**31**	438
3	4	9	10	**23**	325
4	2	11	17	**30**	424
Total	**17**	**35**	**60**	**112**	**396**

Post-processing and Technical Developments

After the field campaign, all UAS LiDAR, TLS, and Total Station survey data had to be post-processed to produce georeferenced point clouds). All data were referenced against a local base station (setup over a star picket and processed through the national AUSPOS processing service to obtain a sub-decimetre accurate coordinate for the base station) (Figures 34 -35).

Figure 33 provides an example for one of the resulting datasets, where we combined two nadir flights (20 crossed flight strips), containing ~94 million points over 6.5 hectares, 1500 pts/m2, 3 cm point spacing. A lastools workflow was developed for noise removal and ground classification (tuning of lastools filtering parameters required).

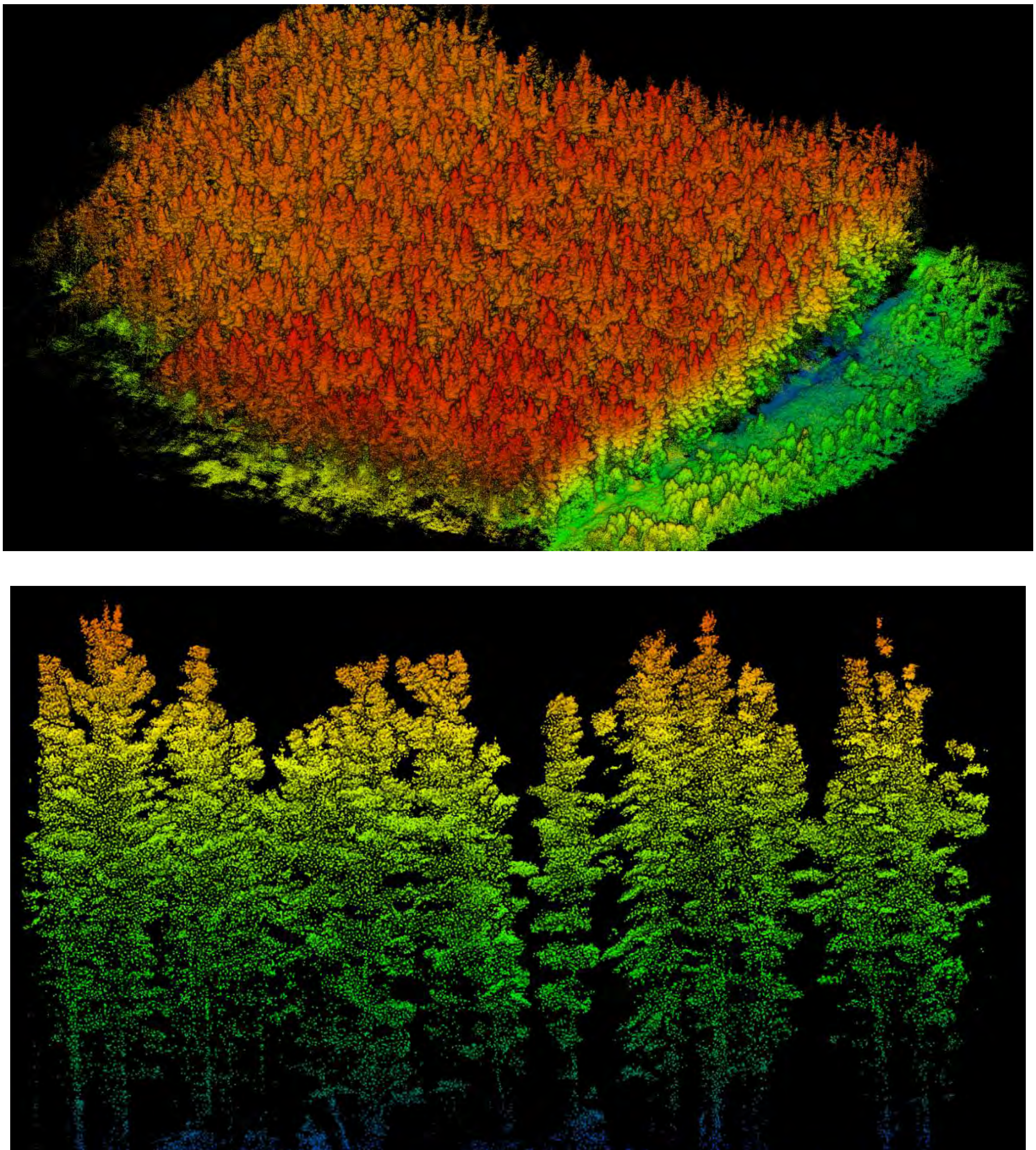

Figure 33: UAS LiDAR point cloud of 20 nadir crossed flight strips flown at 40 m AGL.

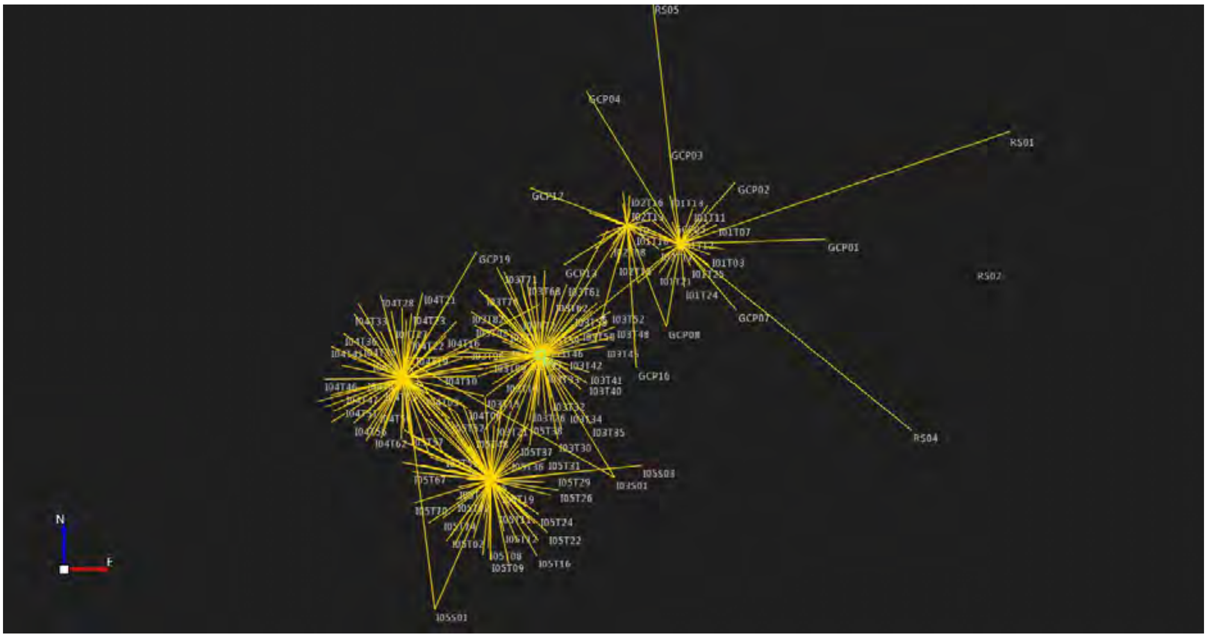

Figure 34: Top-down view of all radiations to individual stems (five plots).

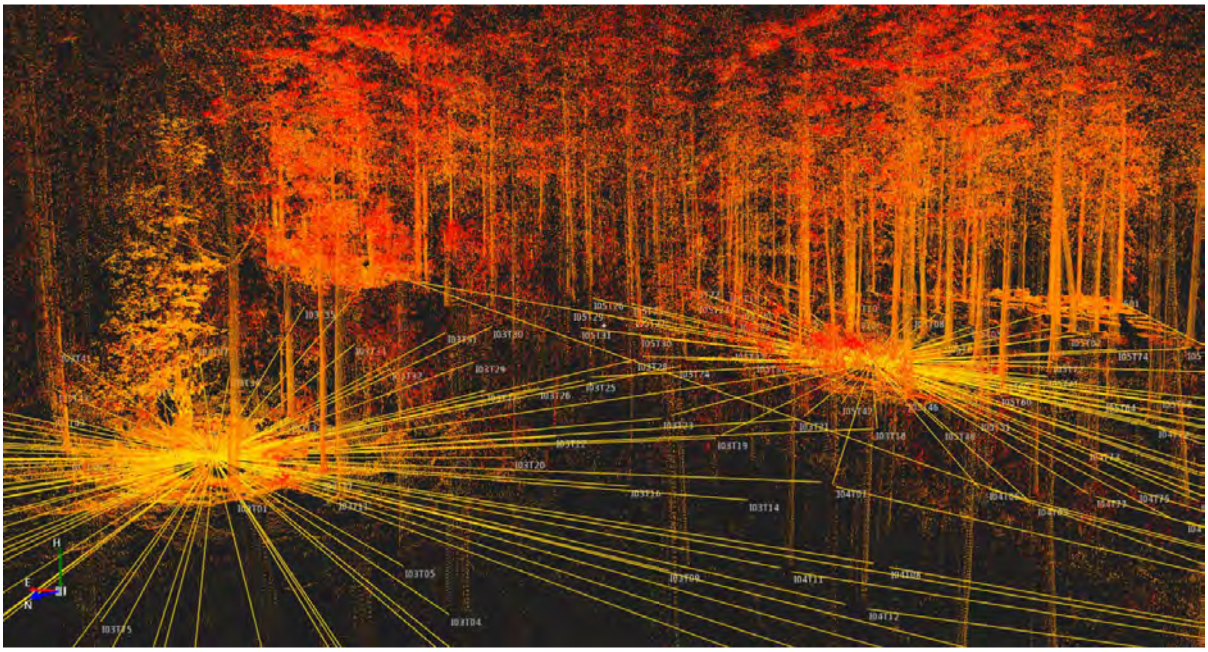

Figure 35: Oblique view of two TLS dome scans and two TLS side scans including radiations to trees.

Objective 4: Identify optimal UAS LiDAR flight parameters (flying height, strip overlap, strip pattern) for optimal data collection in pine plantation

Tasks

1. Quantify point density for
    i. Single flight strips at different heights
    ii. Different overlap (side overlap and crossed overlap)
2. Quantify percentage of ground strikes and vertical point distribution for
    i. Single flight strips at different heights
    ii. Different overlap (side overlap and crossed overlap)
3. Assess impact of mounting angle of laser scanner on canopy penetration
    i. Nadir
    ii. 30 degrees oblique

Overview

This section is based on Saroj Sharma's Masters research, which compared UAS LiDAR flight parameters against TLS data to determine optimal UAS LiDAR acquisition parameters for forest inventory. Plot level forestry metrics including height metrics and quantile based metrics, point cloud density, density of stem strikes and vertical profile of percentage strikes were generated, analysed and compared among 4 plots and between all UAS data collection scenarios. In summary, results indicate that UAS LiDAR is an ideal tool for capturing data for the estimation of forest metrics of upper canopy, however, TLS can provide the most accurate estimation of ground, stem and lower canopy areas. The drawback of TLS is that is a much more time-consuming process. The UAS results also indicate that LiDAR data point density is inversely related to flying height. Interestingly, despite more complex mechanical and data processing requirements, oblique UAS LiDAR flights may not result in higher density stem strikes than nadir flights of equivalent flying height.

Flight Configurations and Data Analysis Scenarios

We focused our analyses on eleven datasets. Separating these datasets allowed us to test the impact of flight overlap, flying height, flight direction, and oblique scanning (Table 6).

Table 6: Summary description of the eleven Velodyne-UAS datasets

ID	Point cloud name	Description
F1_1Strip40m	filtF140ms3singlenewnorm	Nadir flight 1, 40 m AGL, single strip
F1_10Strips40m	filtF140ms0to9comb_lgnewnorm	Nadir flight 1, 40 m AGL, 10 strips combined, 50% overlap

F2_1Strip40m	filtF240ms3singlenewnorm	Nadir flight 2, 40 m AGL, single strip
F2_9Strips40m	filtF240ms0to8combnewnorm	Nadir flight 2, 40 m AGL, 9 strips combined, 50% overlap
F1_F2_Grid40m	filtF1_1Strip40mnd240mcombnewnorm	Nadir flight 1 + 2, 40 m AGL all perpendicular strips combined
F3_1Strip60m	filtF560ms3singlenewnorm	Nadir flight 3, 60 m AGL, single strip
F3_6Strips60m	filtF560ms0to6combnewnorm	Nadir flight 3, 60 m AGL, all strips combined, 50% overlap
O1_10Strips35m	filtF135m0to10oblqnorm	Oblique flight 1, 35 m AGL, 10 strips combined, 50% overlap
O2_10Strips35m	filtF135m10to20oblqnorm	Oblique flight 2, 35 m AGL, 10 strips combined, 50% overlap
O1_O2_Grid35m	filtF135m0to20oblqnorm	Oblique flight 1 +2, 35 m AGL, 20 perpendicular strips combined
TLS	filtTLSnewnorm	TLS plot scans

All point clouds were filtered for noise and ground points classified (Table 7). In all data collection scenarios, accurate identification of noise points above the canopy and below the ground surface was a major challenge. However, we developed a novel multi-step lastools workflow (Figure 36 - 38-). All combined datasets (F1_F2_Grid40m, O1_O2_Grid35m, and TLS) were made available on CloudStor for use and testing by project partners, these combined datasets are the focus of the following analysis.

For each point cloud, we quantified the following metrics:

- Height
    - maximum height, average height and standard deviation in height
- Quantile-based metrics
    - point cloud density (total point strikes per unit plot area) and ground strike percentage
- Vertical profiles
    - percentage of point strikes in different height bins (using bincentiles, (sometimes also referred to as decile) gives the percentage or fraction of points between the specified height and the maximum height which can be further analysed to quantify and interpret the point distribution in defined height bins.)
- Stem strike density
    - stem strikes per square metre

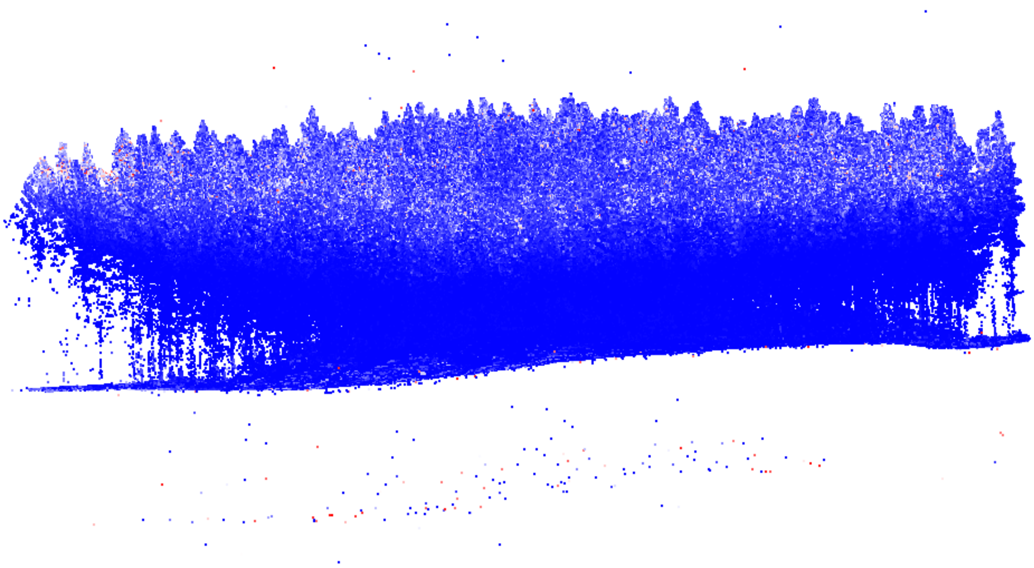

Figure 36: Raw LiDAR point cloud data with positive outliers (noise points above the canopy) and negative outliers (noise points below the ground). Different colours represent laser pulse intensity gradient.

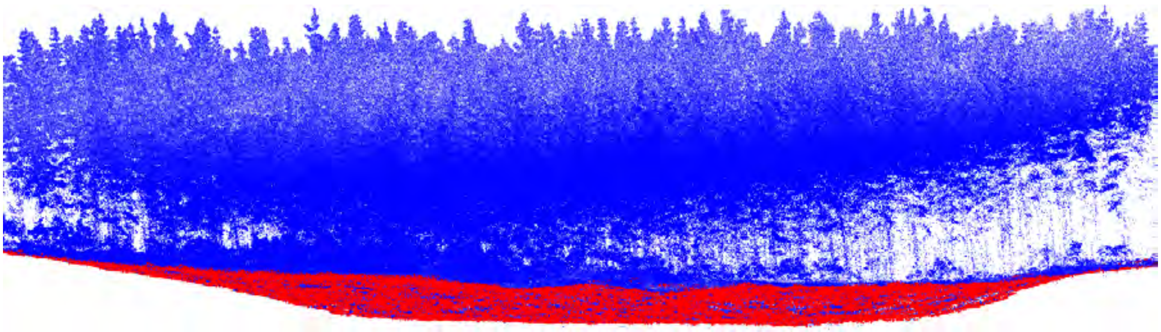

Figure 37: An example of classified ground (red) and non-ground (blue) points after removing outliers.

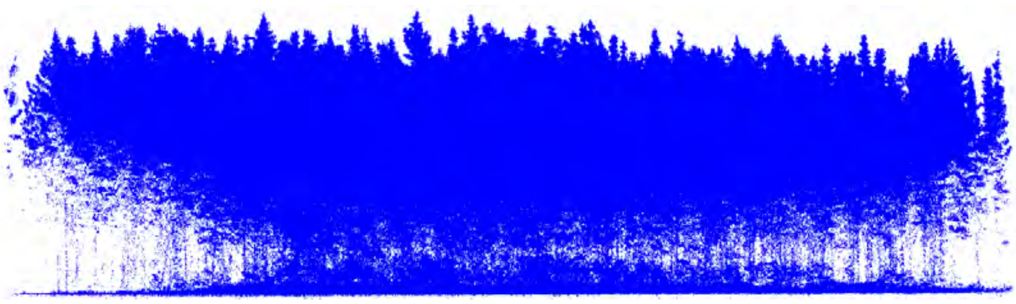

Figure 38: An example of normalized point cloud.

Table 7: Summary statistics of classified ground points, non-ground points and noise points in different data collection scenarios.

Scenario	number of points			% of noise	ground non-
	non-ground	ground	noise	filtered	ground ratio
O1_10Strips35m	21821424	130292	1063	0.005	0.0060
O2_10Strips35m	21957785	127346	759	0.003	0.0058
O1_O2_Grid35m	43915570	254692	1518	0.003	0.0058
F1_1Strip40m	2269252	31840	744	0.032	0.0140
F2_1Strip40m	2994119	47801	873	0.029	0.0160
F3_1Strip60m	1269159	22954	7038	0.542	0.0181
F1_10Strips40m	14997397	132729	525	0.003	0.0089
F2_9Strips40m	19303415	164356	556	0.003	0.0085
F3_6Strips60m	4461779	58045	11205	0.247	0.0130
F1_F2_Grid40m	34399736	198662	580	0.002	0.0058
TLS	2004097	624623	7738	0.293	0.3117

Height Metrics

For each scenario, height metrics including maximum height, average height and standard deviation in height were calculated. With respect to maximum and average height, the UAS based data showed similar height metrics across the scenarios. In particular, the 40 m nadir and 35 m oblique UAS scenarios were very similar, highlighting that oblique mounting does not seem to have a significant impact on tree height derivation. Comparison of height metrics between TLS and UAS based point cloud data showed that the maximum height detected by TLS was significantly lower than other scenarios. Also, the TLS data had the highest standard deviation in observed height among all data collection scenarios. A comparison of UAS based data with TLS data showed a difference of 1.5 m to 4 m in the maximum detected height (Figure 39) and even larger differences of 13 m to 16 m in observed average heights in different plots.

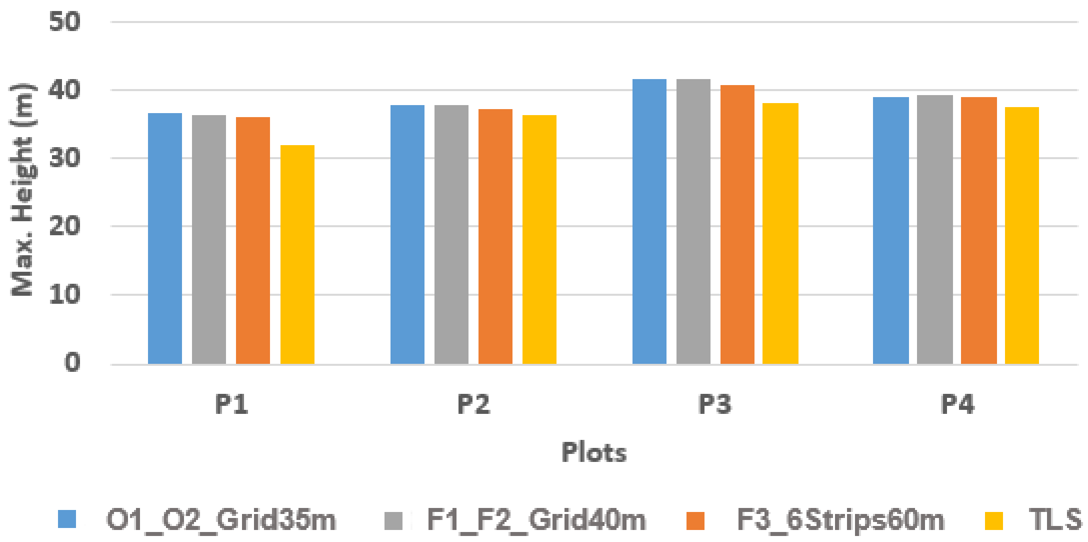

Figure 39: Plot level summary of maximum height in different data collection scenarios – two combined 35 m oblique flights (O1_O2_Grid35m), two combined nadir flights of 40 m flying height (F1_F2_Grid40m), combined strips of a nadir flight of 60 m flying height (F3_6Strips60m) and ground-based terrestrial laser scanning (TLS).

Quantile-based Forestry Metrics

To facilitate the description of specific vertical structure of canopy, two sets of strata specific quantile-based forestry metrics were created (Tables 8 – 9):

1) major height bincentiles (1st, 4th, 10th, 15th, 20th, 30th, 40th, 50th, 60th, 70th, 80th, 85th, 90th, 95th and 99th represented as b01, b04, b10, b15, etcs) and;

2) height percentiles (1st, 5th, 10th, 25th, 50th, 75th, 90th, 95th and 99th represented as p01, p05, p10, p25 and so on respectively).

Table 8: Height bincentile metrics of Plot 2 in different data collection scenarios. Values represent percentage of points below respective height bins (b01, b04, … b99).

Scenario	b01	b04	b10	b15	b20	b30	b40	b50	b60	b70	b80	b85	b90	b95	b99
O1_10Strips35m	1.7	2.2	2.5	2.6	2.7	3.2	4.2	8.7	26.5	56.8	84.5	92.4	96.9	99.2	100
O2_10Strips35m	2.1	2.7	3.1	3.2	3.4	3.8	5.1	10.7	30.1	60.4	87.2	94.1	97.9	99.6	100
O1_O2_Grid35m	1.8	2.5	2.8	3	3.1	3.6	4.6	9.6	28.3	58.5	85.8	93.2	97.4	99.4	100
F1_10Strips40m	3.9	5.2	5.8	6	6.2	6.9	8.2	13.7	33.2	61.6	85.9	93.1	97.1	99.2	100
F2_9Strips40m	4.1	5.4	5.9	6.2	6.3	7	8.3	14.5	35	63.1	87.2	93.9	97.5	99.4	100
F3_6Strips60m	4.4	5.1	5.4	5.5	5.6	5.8	6.4	10	24.7	53.8	83	91.8	96.6	99.1	100
F1_F2_Grid40m	3.7	5.4	5.9	6.2	6.4	7	8.3	14.1	34.2	62.6	86.7	93.6	97.3	99.3	100
TLS	38.4	44.6	56.2	64.3	71.7	82.4	89.8	95.2	98.4	99.4	99.9	100	100	100	100

The calculated bincentile metrics for plot 2 (see Table 9) showed that in all height strata, O2_10Strips35m (across plantation rows) had a higher percentage of points than O1_10Strips35m (parallel to plantation rows). The TLS data recorded more than 38% of the non-ground points below 40 cm and less than 5% of points from the upper half of the canopy. Only 0.6% points in top 30% were recorded with negligible points for the top one-fifth portion of the canopy. Hence, TLS data, although exceptionally good for detecting ground and stem points, was very poor for precisely detecting the upper half of the canopy.

Table 9: Height percentile metrics of plot 2 with specified height cut-off of 1.37 m for different data collection scenarios.

Scenario	p01	p05	p10	p25	p50	p75	p90	p95	p99
O1_10Strips35m	10.9	18.1	19.9	22.6	25.7	28.6	31.3	32.9	35.5
O2_10Strips35m	10.2	17.6	19.4	22.2	25.4	28.3	30.9	32.5	35.2
O1_O2_Grid35m	10.6	17.9	19.7	22.4	25.6	28.5	31.2	32.8	35.4
F1_10Strips40m	6.47	16.9	19.1	21.8	25.3	28.4	31.1	32.8	35.4
F2_9Strips40m	6.68	17.1	19	21.7	25.2	28.3	31	32.7	35.4
F3_6Strips60m	12.9	18.6	20.5	23.1	26	28.9	31.4	33	35.4
F1_F2_Grid40m	5.91	17	19.1	21.8	25.3	28.4	31	32.8	35.4
TLS	1.5	1.94	2.41	4	7.39	12.7	17.3	19.9	25.4

The findings relating to TLS data are corroborated by the height percentile metrics (see Table 9). The TLS had very low percentile height values compared to the corresponding UAS based data. Data showed that more than 50% of the points were recorded below 7.5 m, and more than 99% of points were recorded below 25.5 m. This means that the TLS data can produce exceptionally good point density for the lower half of the canopy including stems but is very poor for analysing upper canopy.

Point Cloud Density

Point cloud density describes the proportion of points in all height strata relative to plot area. Hence, point cloud density was calculated as a total number of point strikes (ground and non-ground) per unit area of the plot (706.9 m^2). Table 10 shows the point cloud density of different data collection scenarios over different plots.

Table 10: Point cloud density of different data collection scenarios in different plots.

Scenario	Plot 1	Plot 2	Plot 3	Plot 4
F2_9Strips40m	1591.0	1520.3	1240.8	1270.5
F3_6Strips60m	284.1	290.5	275.5	358.5
F1_F2_Grid40m	3049.6	3010.2	1409.6	2888.3
O1_10Strips35m	1606.8	1596.5	1485.7	1566.9
O2_10Strips35m	1596.0	1612.3	1717.4	1483.1
O1_O2_Grid35m	3202.9	3208.8	3203.1	3050.0
TLS	546.7	488.2	750.4	431.0

In terms of the point density seen in the different scenarios, Table 10 indicates that the point cloud density resulting from oblique flights is higher than that of nadir flights of equivalent flying height and that flying higher significantly reduces point density. The point cloud density has an inverse proportional relationship to flying height. i.e., increase in flying height sees a significant decrease in the point cloud density. For instance, the point density for the 60 m nadir flight was four times lower than the point density of the 40 m nadir flight. In regard to the TLS scenario, point density for the lower canopy including stems was very high, however, the overall density was approximately 1.5 to 3 times lower than that of the 40 m nadir and 35 m oblique UAS flight scenarios. Interestingly, in all cases, the TLS scenario had higher point densities (ranging from 431 points/m^2 to 750 points/m^2) than the point density from the 60 m nadir flight. These densities imply that the optimal flying height for achieving high point densities is just above the canopy. Unfortunately, this is also the most challenging and high-risk areas for UAS operations.

Percentage of Ground Strikes

Extracting the ground surface is an important step in the point cloud processing workflow. Table 11 show the ground strike percentage for eight key scenarios. Unsurprisingly, the TLS data had a high percentage of ground strikes, in all plots, more than 30% of the total points were ground strikes. In contrast, the UAS based data collection scenarios resulted far fewer ground strikes below 1.5%).

Table 11: Percentage of ground strikes in key data collection scenarios in each plot.

Scenario	Plot 1	Plot 2	Plot 3	Plot 4
F1_10Strips40m	0.92	0.70	2.62	0.79
F2_9Strips40m	0.87	0.79	1.00	1.02
F3_6Strips60m	1.46	1.30	0.99	1.09
F1_F2_Grid40m	0.51	0.47	0.91	0.56
O1_10Strips35m	0.70	0.33	0.57	0.69
O2_10Strips35m	0.81	0.42	0.56	0.86
O1_O2_Grid35m	0.49	0.28	0.41	0.54
TLS	33.36	30.87	32.81	33.00

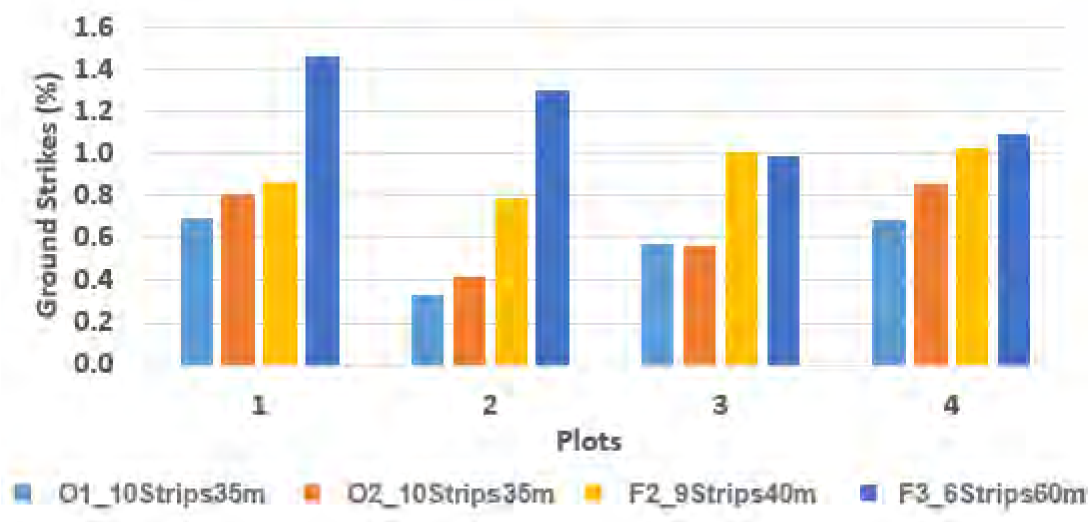

Figure 40: Plot level summary of percentage of ground strikes in four data collection scenarios – oblique flight along the row (O1_10Strips35m), oblique flight across the row (O2_10Strips35m), 40 m nadir flight (F2_9Strips40m) and 60 m nadir flight (F3_6Strips60m).

As seen in the point density comparison above (Table 10), of the two oblique flights, O2_10Strips35m (across plantation rows) recorded a higher percentage of ground strikes than O1_10Strips35m (parallel to plantation rows) in three of the four plots. Surprisingly, for the nadir flight scenarios, in 3 out of 4 plots, the 60 m nadir flight recorded the highest percentage of ground strikes. The greater flying height causes less shadowing of laser pulses by the tree canopy resulting in a higher percentage of ground strikes, however, the total number of ground points is still higher for lower flying heights.

Vertical Profile

The vertical profiles for key flight scenarios in Plot 2 (Figure 41) show significant differences in point distribution percentages relating to height. As seen in the previous metrics, TLS results in the highest percentage of points in the lower half of the canopy and the UAS data captured most points in the upper half of the canopy. As expected, TLS is obstructed by the dense lower canopy resulting in less penetration to the upper canopy.

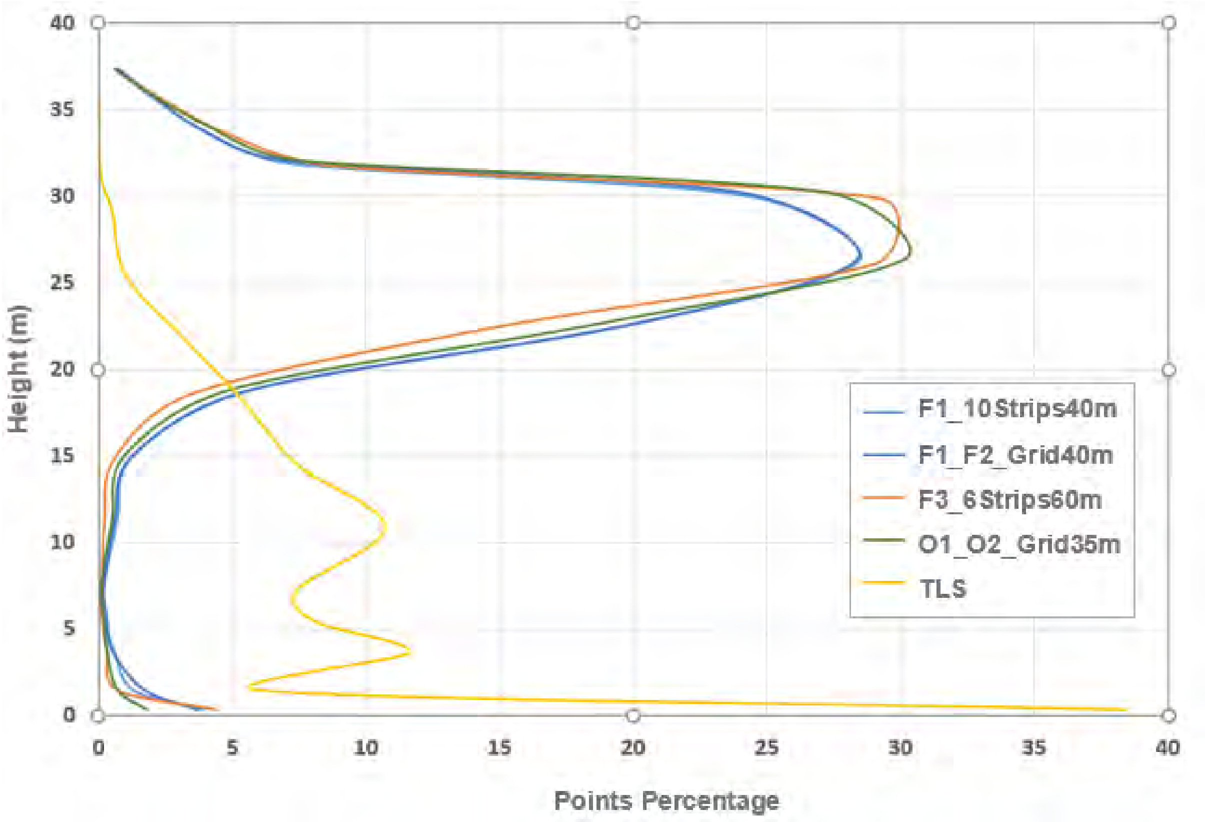

Figure 41: Vertical profile diagram for plot 2 summarizing percentage of points in each height bin for key data collection scenarios – 40 m nadir flight (F1_10Strips40m), two combined 40 m nadir flights (F1_F2_Grid40m), combined 60 m nadir flight (F3_6Strips60m), two combined 35 m oblique flights (O1_O2_Grid35m) and terrestrial laser scanning (TLS).

The UAS based data collection scenarios resulted in very similar point cloud structures with the highest percentage of points recorded in the 25 m to 30 m height ranges and the lowest percentage of points recorded for stem areas. The combined oblique flights scenario (O1_O2_Grid35m) had the highest percentage of points for 25 m to 28 m of tree height. Below 25 m, the percentage of points for the oblique scenario was higher than seen for the F3_6Strips60m scenario and fewer than captured in the 40 m nadir flights. This similarity of results implies that flying oblique may not result in a significant increase in stem strikes or strikes in the canopy. It is important to understand that while the higher percentage of low strikes is seen in the 40 m nadir scenarios, this does not necessarily mean that they have a greater number of stem strikes. Since, the 40 m nadir flight recorded a lower percentage of points for canopy areas above 25 m, this might have resulted in higher percentage of points below 25 m. To assess this further we can investigate the density of stem strikes in the key scenarios.

Density of Stem Strikes

Calculation of plot based stem point density (stem strikes per square metre) was done for all data collection scenarios by analysing stem points from 3 m to 7 m on the normalised point cloud. The plantation was pruned and thinned so there were no significant branches present between 3 m and 7 m, however significant understory vegetation was present below 3 m.

Table 12: Plot level density (points/m^2) of stem strikes (3 m to 7 m) in different data collection scenarios.

Scenario	Plot 1	Plot 2	Plot 3	Plot 4
F1_10Strips40m	9.70	9.22	0.33	7.32
F2_9Strips40m	7.98	8.81	1.78	7.90
F3_6Strips60m	0.92	0.88	0.11	1.39
F1_F2_Grid40m	17.93	18.15	2.08	15.41
O1_10Strips35m	5.87	4.85	1.64	7.14
O2_10Strips35m	6.92	6.75	1.78	5.85
O1_O2_Grid35m	12.77	11.79	3.45	12.84
TLS	50.68	84.38	58.27	31.26

As shown in Table 12 stem strike density was highest for the TLS scenario and lowest for the 60 m nadir flight scenario. The oblique flight across the plantation rows (O2_10Strips35m) had higher stem strike density than the oblique flight parallel to the plantation rows (O1_10Strips35m) in three out of four plots. In general, the 40 m nadir flights had the highest density of stem strikes. When comparing the 40 m nadir flights with the 35 m oblique flights. The nadir flights resulted in a higher density of stem strikes than the oblique scenarios.

In comparison to UAS data, TLS is a more effective method for characterising stems due to the very high density of stem strikes. As seen above, UAS based 40 m nadir flights just above the canopy can record a higher density of stem points than when flying higher (60 m). Furthermore, the multiple cross strip flights at same flying height nearly double the number of stem strikes (and ground strikes) when the perpendicular flight datasets are combined. When comparing the oblique flight scenarios to the nadir flight scenarios the stem strike density is not significantly improved by flying with the scanner mounted obliquely. This was not expected, however the laser scanner fire lasers at a range of angles both in nadir and oblique mounting configurations and this in combination with flying a grid pattern results in higher stem strike densities for the 40 m nadir scenario (F1_F2_Grid40m). This may improve in the result of stem detection and precise ground point delineation.

Summary of findings

In this project, the quality of the stem strikes has not been assessed. The density of the stem strikes quantified here can only be used to compare different UAS LiDAR acquisition scenarios. The absolute density and accuracy achieved on stem strikes is still highly dependent on the footprint size of the laser pulse, the error in the laser distance measurement, and all errors associated with pose determination. The stem retrieval algorithms developed in this FWPA project were primarily developed (Joel Gordon, SCION and Mitch Bryson ACFR) for TLS and high density VUX1 data collected by helicopter. Their algorithms were briefly tested on UAS LiDAR data collected at Uxbridge and Payanna, however, more rigorous testing needs to be carried out to identify the full potential for UAS LiDAR data to quantify stem properties. Based on the analysis presented here, we conclude that with the current Velodyne system it is best to fly low (closer to the canopy the better, within practical reason), e.g. 35 – 40 m AGL for 25 m canopy. We also conclude that an oblique mounting angle of the laser scanner does not improve penetration to the stems and the ground. A nadir scanning angle is optimal. A high side overlap between adjacent scan lines (30 – 50% at the tops of the trees) and overlapping flight paths at perpendicular flight angles ensure a regular and dense distribution of points, thereby maximising the number of stem strikes.

Objective 5: Collect UAS LiDAR data with SCION and UTAS systems over a common site for comparison of UAS systems and verification with plot data

Tasks

1. Capture UAS LiDAR data with UTAS and SCION system over inventory plot(s) at optimal flying height and flight line configuration.
    i. Capture inventory data at the same time
    ii. Collect TLS data at the same time

Summary of Carabost SF Campaign

Between 18 and 23 February 2018 a large multi-disciplinary team came together at Carabost, NSW (near Tumut) to collect the penultimate datasets for this FWPA project. Staff from Forestry Corporation New South Wales, Department of Primary Industry New South Wales, Interpine, and the University of Tasmania joined the field campaign. The TerraLuma team from UTAS was represented by Arko Lucieer, Darren Turner, and Stephen Harwin. Darren and Arko performed 35 UAS flights, including12 hours of air time with 3 UAV platforms (multi-rotor), collecting LiDAR, RGB/SfM, Multispectral (4-band Sequoia), and thermal data with the key focus on LiDAR collection. Over 1 billion points of LiDAR data was collected over five sites (200 by 200 m for each site). All flights were flown at 40 m AGL in nadir configuration, apart from site 9, which has to be flown at 50 – 60 m AGL due to sloping terrain. Sites 4 and 8 were the focus sites (because of their low stocking density and absence of undergrowth), and both sites were flown in an overlapping cross pattern. We selected these flight parameters based on previously identified optimal acquisition parameters. Operationally, it was challenging to maintain line of sight of the UAS LiDAR airframe. We surveyed all sites with RGB UAS imagery for future SfM studies. We surveyed two sites with UAS thermal imagery and three sites with MicaSense Sequoia multispectral imagery to test these alternative sensing technologies for detection of blackberries and understory growth. Also, Professor Anthony Finn (Adelaide) reported that SfM based on thermal imaging can potentially be used to identify stems. We wanted to collect data to test this approach. Steve focused on collected TLS scans at site 4 and 8. He collected two dome scans, each with overlapping three side scans. An overview of the UTAS data collection efforts is presented in Table 13 and examples of the types of acquired data illustrated in Figures 42 – 45.

Table 13: Overview of UTAS data collection in Carabost SF, NSW.

			TLS	UAV				
Site	**GCP**	**Plot**	**TLS**	**Under canopy**	**LiDAR**	**RGB**	**Thermal**	**Multispec**
2A	5	0 1		x	X Single 40 m	x		
3	2	-				x	x	x (blackberry trial)
4	5	4 5 6	x	x	X Double/cross 40 m	x	x	x
5	5	7 8			X Single 40 m	x		
6	5	9		x				
8	5	15 16	x	x	X Double/cross 40 m	x		x
9	5	16 17			X Double/cross 50-60 m	x		

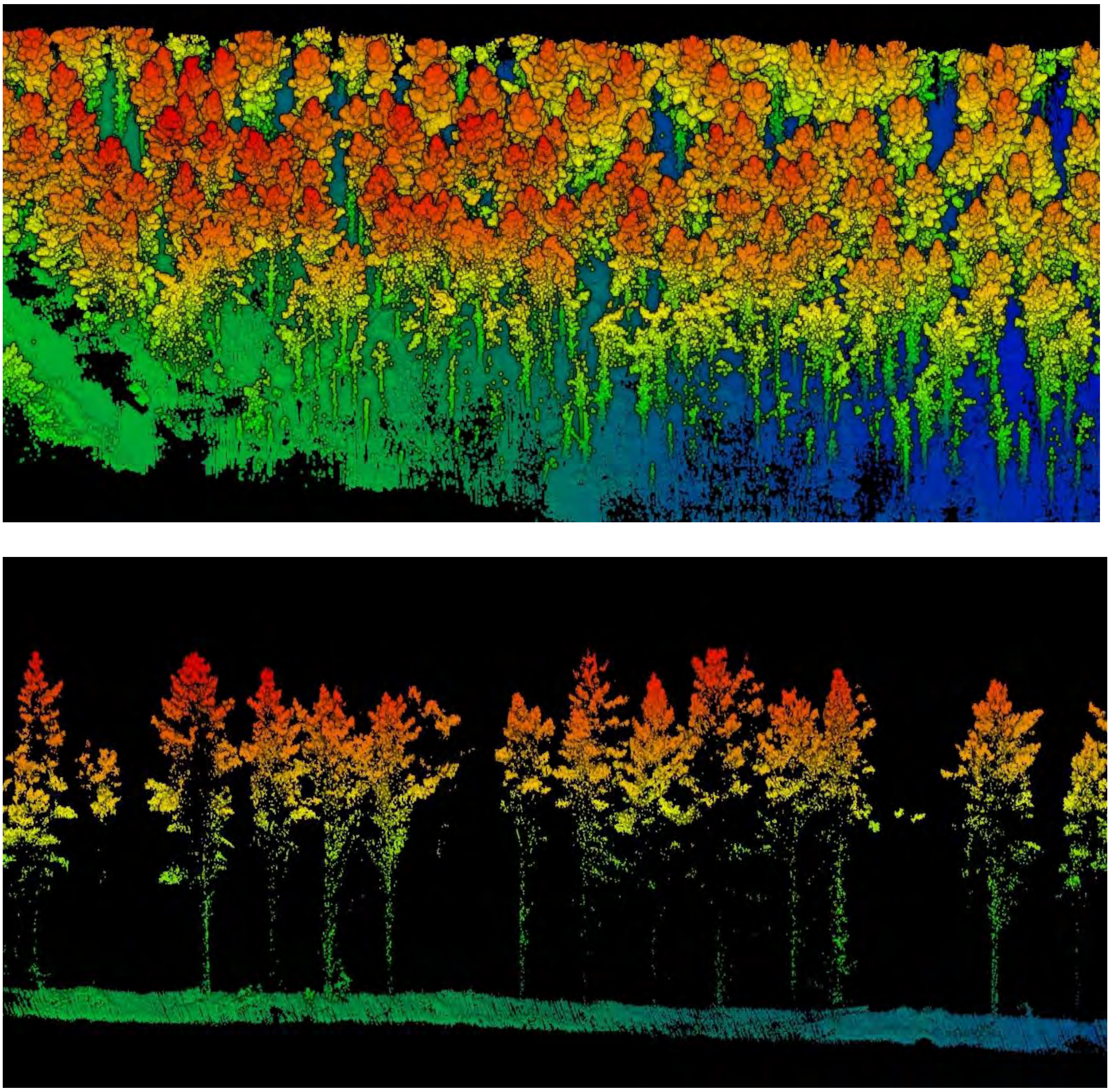

Figure 42: Overview of UAS LiDAR scans at site 8.

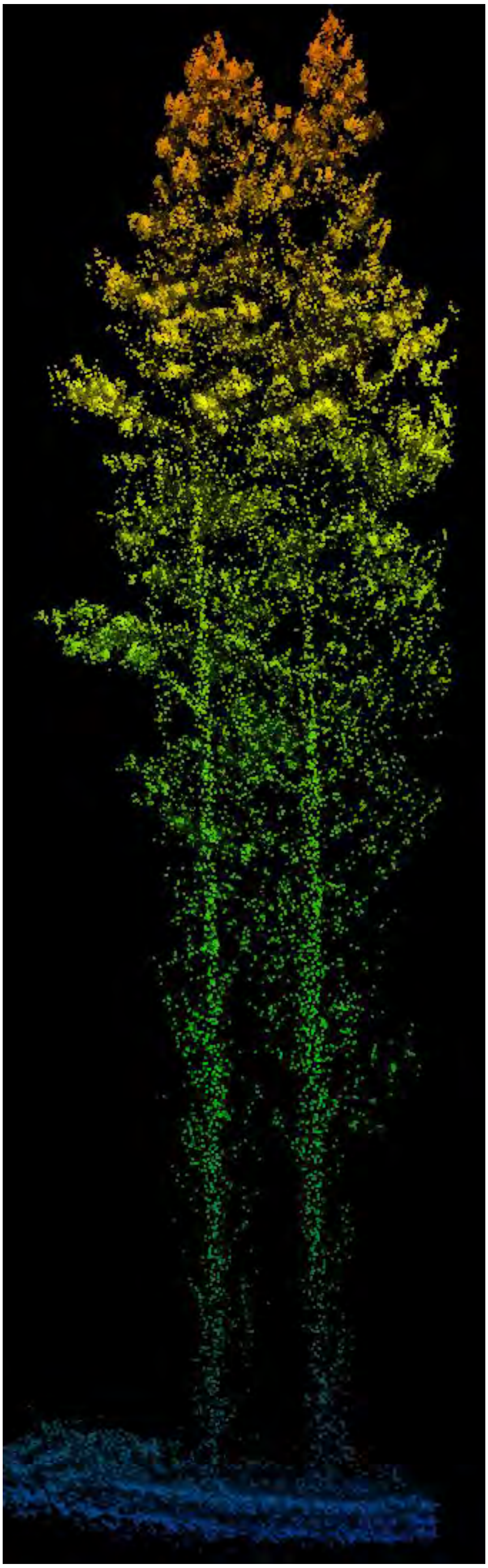

Figure 43: Subset from UAS LiDAR dataset (two combined flights) of two trees at site 8.

Figure 44: Multispectral orthomosaic acquired at site 4 (Micasense Sequoia flown on 3DR Solo).

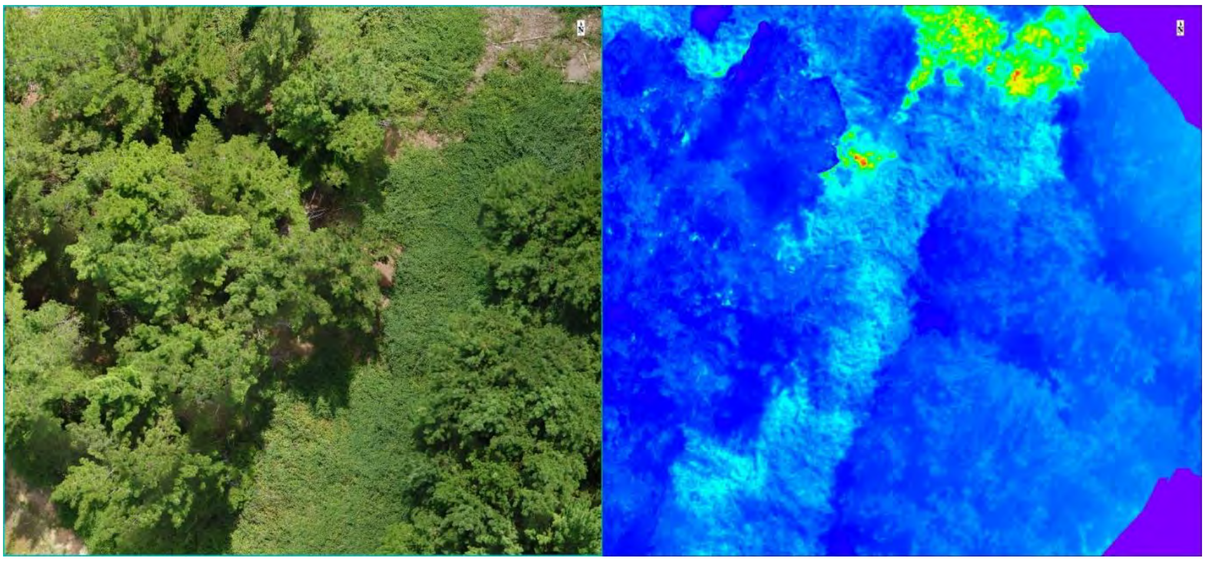

Figure 45: Example of blackberry patch/carpet at site 3. Left: RGB Phantom4 Pro imagery, Right: thermal imagery (FLIR Vue Pro R, yellow/red is hot and blue is cool). Blackberries appear to be warmer than the tree canopy.

Key findings

Sensors

The Velodyne 'family' of laser scanners provides a ground-breaking combination of low cost, high density, and high accuracy sensing, compared to the previous generation of laser scanners (Ibeo LUX, SICK, and Hokuyo). The point density that can be achieved with the Velodyne scanners is in the order of 200 – 1200 points/m^2, which is sufficient for very dense reconstruction of individual trees. Velodyne scanners, however, are primarily designed for the automotive industry, e.g. self-driving cars, so they are not specifically designed for aerial surveying and mapping. The accuracy requirements for forest inventory surveys at the individual tree level demand a very high level of absolute accuracy (< 3 cm), especially when stem reconstruction is required. The absolute ranging accuracy of the Velodyne scanners is 3 cm at best. However, when taking into account the positioning accuracy of the GNSS (3 – 5 cm), orientation accuracy of the IMU (0.1° IMU orientation accuracy equates to a 7 cm positional uncertainty at 40 m flying height), and the laser footprint size of ~10 cm (at ground level for a flying height of 40 m), we come to the conclusion that sub-decimetre absolute accuracy is very difficult to achieve with these systems.

A laser scanner with a narrower beam divergence and a higher ranging accuracy is required for stem extraction and characterisation. Also, an IMU with a higher absolute accuracy is required. These sensor improvements add a significant amount to the overall budget of a UAS LiDAR system. Current commercial UAS LiDAR systems based on Velodyne scanners cost between $80K and $150K. Newer high-accuracy UAS LiDAR systems based on Riegl scanners, such as the VUX1-UAV and miniVUX, cost between $230K and $600K.

UAS Operations

UAS operations in a forested environment are challenging. An open space of at least 10 x 10 m needs to be found for safe take-off and landing. One of the key challenges is the current CASA regulation that requires the UAS to be within visual line of sight (VLOS) from the operator. Flying the UAS at 40 – 60 m above the ground over a plantation with ~25 m tall trees results in loss of sight within tens of metres from the take-off point. Indirect line of sight can be achieved with a spotter flying a DJI Phantom (or similar) UAS with a live camera view of the UAS LiDAR platform. The smaller UAS effectively acts like a "camera on a pole". This setup can help to keep the UAS LiDAR platform in sight, and potentially guide the pilot in case of an emergency (e.g. eagle attack), however, this solution does not strictly conform to current CASA regulations as it is an indirect line of sight.

Auto-piloted operation of the UAS platform is required to achieve the desired flying speed and overlap between flight strips, and ensures consistency in flight dynamics. Many Apps exist for DJI autopilot navigation, but we found Autopilot (http://autoflight.hangar.com/) to be most suitable in terms of customisation and reliability. In auto-navigation mode, the UAS tends to speed up through the turns when moving between flight lines. The increase in speed causes some instability that can affect the accuracy of the LiDAR point cloud. We have taken the approach to cut out the flight line sections where the UAS turns. This has an impact on the total size of the survey area that can be covered. In flight planning, the UAS has to 'overshoot' the edge of the survey area.

Typical flying heights were between 35 m and 70 m with 40 m flying height typical (for 25 – 30 m canopy height). At flying height >50 m the laser penetration to the ground and resulting point density at ground level are very low.

Processing

Lever-arm and boresight calibrations are essential for high-accuracy 3D point clouds from UAS LiDAR. New calibration techniques were developed in this project for both lever-arm and boresight calibration. The use of 3D photogrammetric models for lever-arm determination, and the use of large poles for boresight calibration were found to perform well. We have demonstrated the importance of lever-arm and boresight calibration for the final accuracy of the data product. UAS LiDAR system calibration is essential for future systems and projects.

GNSS data processing is an important aspect of the LiDAR processing workflow. We deployed a local GNSS base station, recording raw data at 10 – 20 Hz. We post-processed the GNSS data recorded on the UAS against the base station data. This can be a time-consuming process, and requires expertise in GNSS processing. A real-time kinematic (RTK) radio link between the base station and the GNSS receiver on the UAS can help to achieve high-accuracy coordinates in real-time without the need for post-processing. The radio link relies on visual line of sight. While this approach can reduce the GNSS processing time, the performance of RTK GNSS in a forested environment still needs to be tested.

We developed an online flight line sub-setting tool, which was valuable and important to split the raw data into individual flight lines before processing. All LiDAR data processing was carried out with Python code developed by the TerraLuma group. We also developed a lastools script for noise removal and ground classification.

Data Characteristics

In our calibration and accuracy assessment experiment, we achieved an absolute accuracy of 7 cm for a direct georeferencing solution. This was further improved to 4.6 cm after strip adjustment and fine-tuning. The overall point densities varied from 300 points per m^2 for single flight strips to 1200 points per m^2 for combined flight strips (50% overlap between adjacent flights lines and two crossed strip flights).

Based on the analysis from the Payanna dataset, we conclude that with the current Velodyne system it is best to fly low (closer to the canopy the better, within practical reason), e.g. 35 – 40 m AGL for 25 m canopy. We also conclude that an oblique mounting angle of the laser scanner does not improve penetration to the stems and the ground. A nadir scanning angle is optimal. A high side overlap between adjacent scan lines (30 – 50% at the tops of the trees) and overlapping flight paths at perpendicular flight angles ensure a regular and dense distribution of points, thereby maximising the number of stem strikes. At best, we achieved 17 points per m^2 on stems between 3 and 7 m above ground level. The absolute accuracy of these stem strikes and the suitability of these points for quantitative and automated stem retrieval needs to be further tested.

The absolute density and accuracy achieved on stem strikes is still highly dependent on the footprint size of the laser pulse (>10 cm for Velodyne at typical flying heights), the error in the laser distance measurement, and all errors associated with pose determination (~7 cm at best for direct georeferencing). The VUX1 data collected at Carabost appears to show a much higher point density on stems. The Riegl VUX1 is a survey-grade instrument that was coupled with a survey-grade GNSS/IMU sensor capable of achieving sub-5cm absolute accuracy. Our recommendation is that this level of absolute accuracy is further pursued in future forest LiDAR project if the focus is on stem characterisation.

Recommendations for Future Work

1. To test the SCION and Interpine voxel approach to plot-based forest inventory on UAS LiDAR data for the Carabost site. To expand the plot-based voxel approach to a tree based approach.
2. To test new machine learning techniques on UAS LiDAR datasets to predict tree-level inventory metrics.
3. To test if advanced crown metrics can be developed based on dense UAS LiDAR data for prediction of stem characteristics.
4. To test Mitch Bryson's (ACFR) and Joel Gordon's (SCION) stem fitting algorithms on Carabost UAS LiDAR data.
5. To compare and optimise individual tree and crown detection (ITCD) algorithms optimised for UAS LiDAR point clouds. ITCD algorithms for UAS data should focus on methods that can segment points from the point cloud (as opposed to a CHM approach).
6. To pursue future UAS LiDAR studies based on survey-grade sensors. The new UAS LiDAR kit that was recently by CR Kennedy in Australia (late May 2018) appears to meet the desired specifications. The UAS LiDAR unit is based on the DJI Matrice 600, but it carries a Riegl miniVUX-UAV laser scanner and is coupled with a high-end IMU sensor. An early price indication is AU$230K for the full system. A rigorous accuracy assessment (and system calibration) would have to be undertaken to verify the absolute accuracy and suitability for individual tree characterisation.
7. We recommend that the commercial UAS industry and the forest industry continue to lobby CASA and CAA for beyond visual line of sight (BVLOS) operations. BVLOS operations within a short range (1 – 2 km) could be developed as a separate class of operation (without the need to cover systems that can fly for hundreds of kilometres and need multiple redundant communication links). This would meet the need of the forest industry for future UAS operations.

Acknowledgments

The authors thank Richard Ballard for the design and construction of the UAS LiDAR system. Dr Luke Wallace (RMIT) is acknowledged for making available the original MATLAB code for LiDAR processing. Deepak Gautam is acknowledged for improving the LiDAR equation in the Python code and testing boresight and lever-arm corrections, and for assisting in the Payanna field campaign. Alexander Pishchugin is acknowledged for the development of the LiDAR flight trajectory selection tool. Peter McLoughlin from Boyer – Norske Skog is acknowledged for providing access to the Uxbridge site. We thank Don Aurik and Gareth Tempest from Timberlands Pacific for providing access to the Payanna site and for providing us with plot inventory data. Robert Anders and Andrea Hendrey, Spatial Sciences Group, School of Land and Food, University of Tasmania for his assistance with fieldwork surveying and associated data processing for the Uxbridge Tasmania study site. Dr Jon Osborn is greatly acknowledged for assistance with the project. We thank Dr Christine Stone (DPI NSW) for her earlier support to the UAS LiDAR prototype development. We thank industry partners for their support (Interpine, SCION, Timberlands Pacific, and ForestCorp NSW). All contributors to the Carabost field campaign are greatly acknowledged for their hard work in the field.

References

Wallace, L, Lucieer, A, Malenovský, Z, Turner, D & Vopěnka, P 2016, 'Assessment of Forest Structure Using Two UAV Techniques: A Comparison of Airborne Laser Scanning and Structure from Motion (SfM) Point Clouds', *Forests*, vol. 7, no. 3, p. 62, accessed from <http://www.mdpi.com/1999-4907/7/3/62>.

Wallace, L, Lucieer, A, Watson, C & Turner, D 2012, 'Development of a UAV-LiDAR System with Application to Forest Inventory', *Remote Sensing*, vol. 4, no. 6, pp. 1519–1543, accessed May 28, 2012, from <http://www.mdpi.com/2072-4292/4/6/1519/>.

3.2 Optimal acquisition specifications for the Riegl VUX-1LR over a *Pinus radiata* plantation

Barbara Del Perugia[1], Susana Gonzalez Aracil[2], David Herries[2]

[1]University of Florence; barbara.delperugia@unifi.it
[2]Interpine Group Ltd; susana.gonzalez@interpine.nz , david.herries@interpine.nz

1. Introduction

Recently, Light Detection and Ranging (LiDAR) has been widely applied in forest inventory to improve precision**.** The tendency is to use Airborne Laser Scanning (ALS) data as standard practice for inventory surveying, in New Zealand and Australia (Watt *et a*l, 2013 a & b) as in the rest of the world (Næsset, 2004 & 1997; He *et al,* 2017, Magnussen, 2018). Current technology can collect more dense point clouds than in the past, and at a more reasonable price than older sensors. These denser point cloud datasets are being evaluated for their suitability for tree-level on screen visual assessments and 3D reconstruction modelling.

There are several tasks currently performed manually in inventory assessments, including diameter and height measurements, branch size estimation, sweep estimation and stem quality assessments. Virtual Reality (VR) technology offers an opportunity to replace these in forest measurements for which human skills are required (Widjojo, 2017). VR is a 3D human computer interface technology that enables users to be immersed in a computer generated virtual environment. 3D point clouds can be imported into a VR system and tools developed that will allow users to interactively measure stem and tree structure.

The Riegl VUX-1LR datasets were acquired as part of a FWPA Trans-Tasman project that links forest inventory, data processing and VR. Data was also collected by several different sensors mounted on unmanned aerial vehicles flown over the same stands. The helicopter mounted Riegl VUX-1LR used in this study is an example of new light-weight, survey-grade laser scanners

In this report, we compare the VUX-1LR point cloud datasets that were acquired at three different altitudes and four different flight path directions in order to identify optimal acquisition specifications for the acquisition of ultra-dense point clouds that may be suitable for application in a virtual reality environment.

2. Materials and Methods

2.1 Study Area

The Carabost State Forest (SF) is a *Pinus radiata* plantation, near Tumut, in southern New South Wales, Australia, managed by Forestry Corporation of NSW.

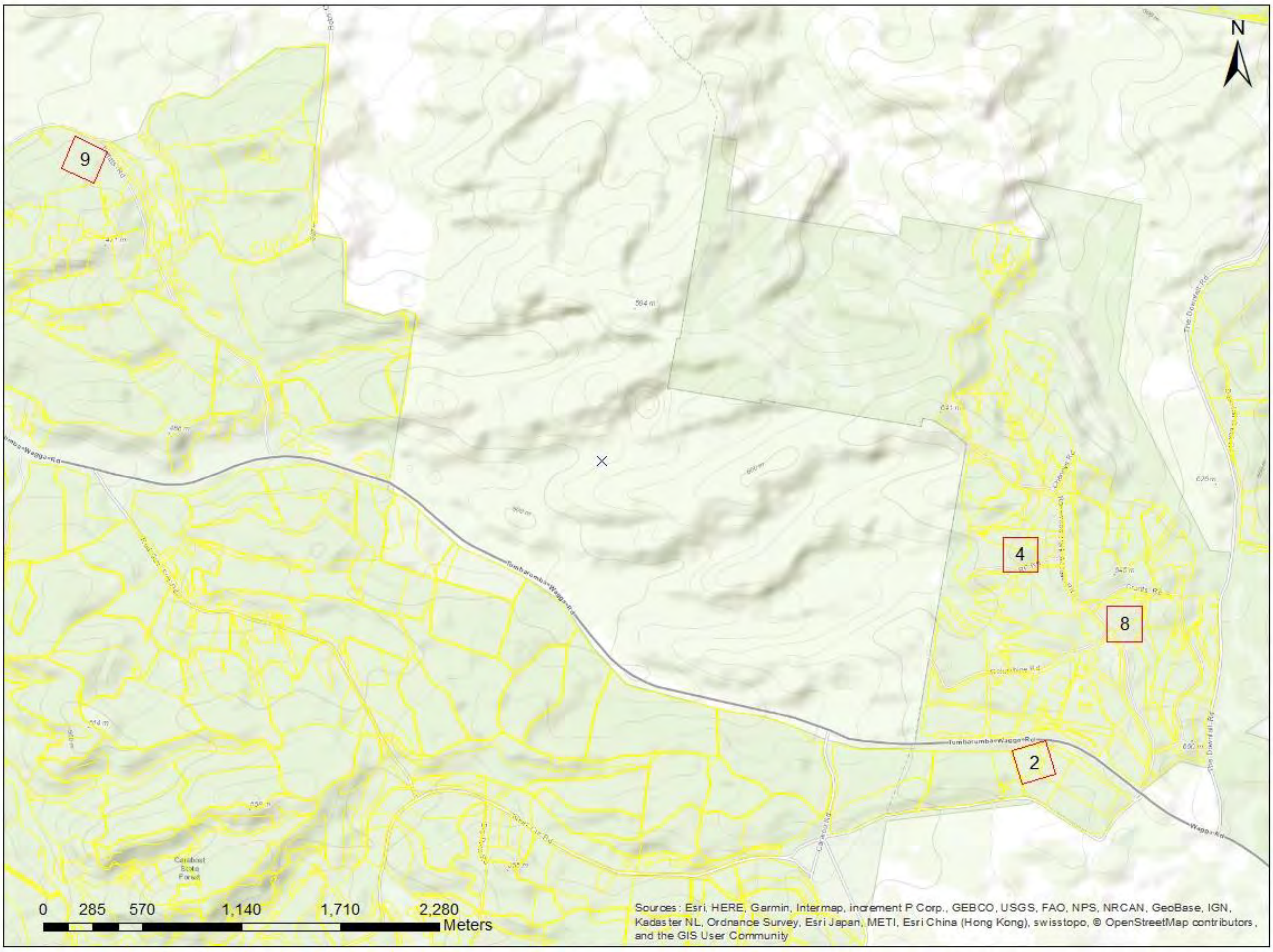

Figure 1: Detailed map presenting the relative location of each study area.

Four stand areas were selected targeting a diverse range of *Pinus radiata* structures, including unthinned, single thinned and multi-thinned as well as stands varying in tree age and form (Figure 1, Figure 1).

Table 1: Description of the seven *P. radiata* stands measured for reference data as part of the Carabost SF acquisition campaign.

Site	Age	Cpt/Stand	Thinning	Stocked Area	Pruned
2	1987	1/1	Delayed thinning (2009)	19.65	1999
4	1995	455/1	T2 (2017)	61.51	2004
8	1995	454/1	T2 (2017)	33.97	2004
9	1989	383/1	T2 (2013)	53.00	1998

2.2 Data

2.2.1 Remotely sensed data from helicopter

On the 22nd of February 2018 a flight was carried out by Geomatics Technologies (Melbourne, Victoria) using a helicopter equipped with a Riegl VUX-1 long range LiDAR sensor (specification of the sensor reported in Table 2) and a Nikon D810. A full-waveform ALS data was registered and discretized to a point density of over 8,000 points/m^2 (the emission was between 5,000 and 9,000 points/m^2). Digital orthophotos with 1cm spatial resolution were taken with the Nikon D810 RGB camera in the blue (400-540 nm), green (480-600 nm) and red (580-600 nm) wavelengths.

Table 2: VUX-1LR standard specifications.

VUX1-LR	
Eye Safety Class	Laser Class 1
Max. Range @ Target Reflectivity 60%	1,350 m
Max. Range @ Target Reflectivity 20%	820 m
Minimum Range	5 m
Accuracy/Precision	15 mm / 10 mm
Max. Effective Measurement Rate	750,000 meas./sec
Max. Scan Speed	200 scans/sec
Field of View (FOV)	330°
Max. Operating Flight Altitude AGL	530 m / 1,740 ft
Inertial Measurement Unit (IMU)	Trimble Applanix AP20

The LiDAR survey consisted of three flights by Site (200 x 200 m), the flight altitudes were selected to be as close to the canopy as possible, approximately 30 m, then at 60 m and 90m. The flight speed was set around 5m/s or 10 knots. The trajectory has been set 15 m apart with 14 flight lines per flight altitude. Flight lines were done from east to west and from north to south, in two sites the same pattern was done also at a 45 angle from northeast to southwest and from northwest to southeast (a summary of the flight directions is reported in Table 3, while an example of the flight lines is reported in Figure 2).

Figure 2: Flight plan.

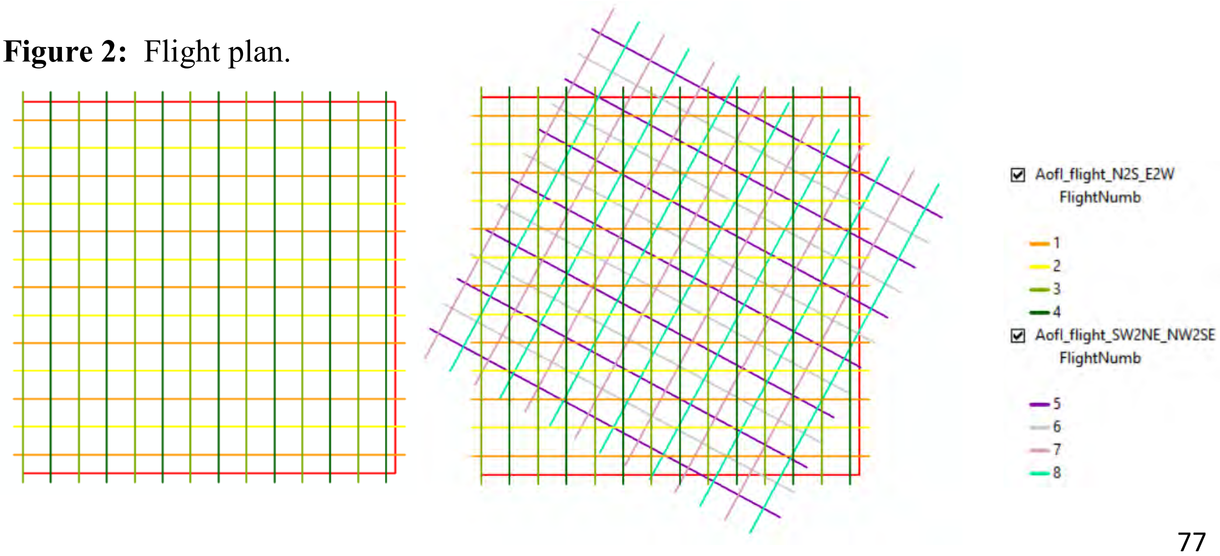

Table 3: Summary of acquisition specifications for each study site.

			VUX-1LR			
			400Mhz			600Mhz
Site	**GCP**	**Field plot**	**30 m**	**60 m**	**90 m**	**60m**
2	5	0 1	NWSE SWNE	NWSE SWNE		
4	5	4 5 6	NS EW	NWSE SWNE	NS EW	
8	5	15 16	NS EW	NS EW	NS EW	NS
9	5	16 17		NWSE SWNE		

2.2.2 Ground-based data

A local forest inventory was carried out in the study area the same week of the helicopter acquisition. The nine plots were established with a radius of 13.82m (=0.06 ha). At each site at least two plots were collected (Table 4). A wooden pole with a reflective poly ball on top was positioned in the centre of each inventory plot. The x,y coordinates of the plot centre were collected using a Trimble® Geo 7X receiver connected to an external high quality GNSS antenna, with a positional error of 5-50 cm (see Attachment 1). For each tree, distance and magnetic bearing of the tree stem and tree top from the plot centre (CP), were collected. For each tree the species was noted, the diameter was measured using a DBH tape, the height was measured with a Haglof VL5 Vertex and the tree was cruised using the PlotSafe Overlapping Feature Dictionary (PLOTSAFE, 2007) (example of PlotSafe collected data reported in Figure 3). In each plot five photographs were also captured (i.e. N, E, S, W facing to the plot centre and crown cover from the plot centre).

Table 4: Summary of field data collection.

Plot Establishment	Location Plot Centre Coordinates Size and type Slope adjustment Hazardous
Tree Measurement	Species Bearing and distance Marginal tree checks Tree marking Diameters Pruned Heights Tree Heights
Tree Cruising	Forks / reductions / top outs Features - (spike knots, rot, fluting, etc.) Tree quality assessment- Sweep & Branching

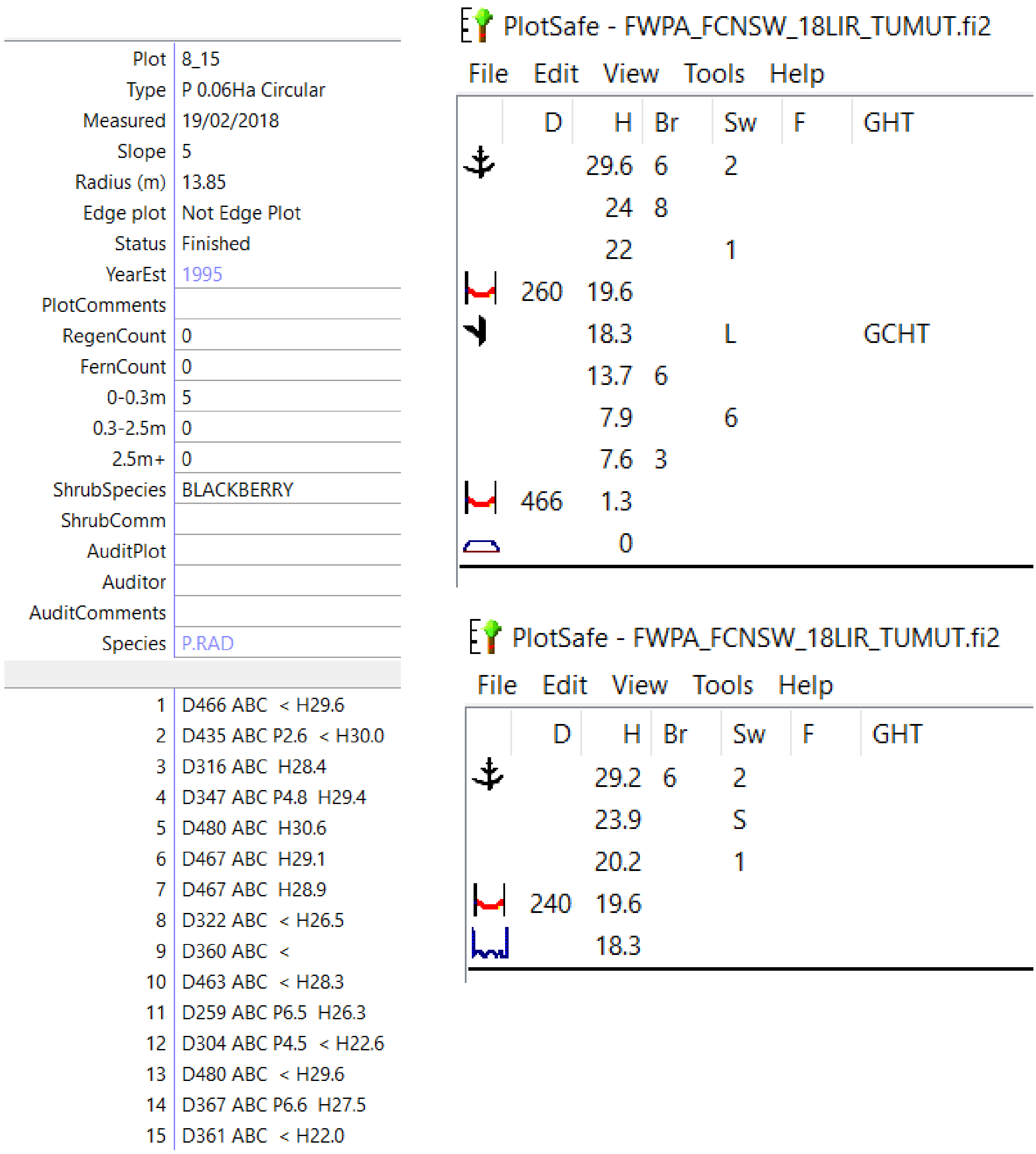

Figure 3: Example of PlotSafe collection Site 18 Plot 15 and details of tree number 1.

The collected field data was then processed and used as references for the validation of the VUX-1LR datasets. Through an application written in the statistical program R software (version 3.4.1), stem maps were produced for each plot using both the stem and crown top positions.

An example of the derived plot stem maps is illustrated in Figure 4.

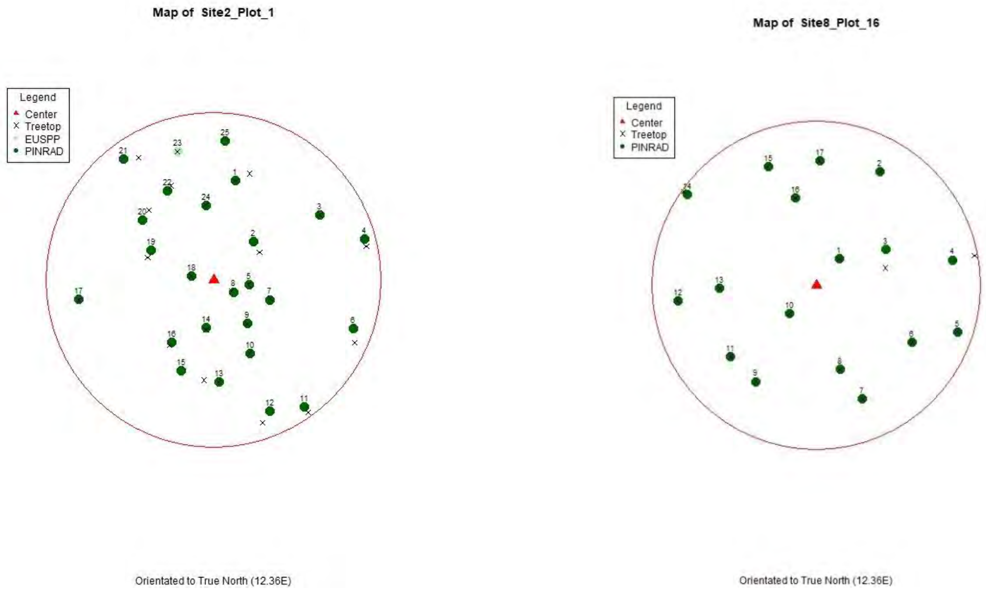

Figure 4: Example of Stem and tree top map, Site2 Plot1 and Site8 Plot16.

2.2.3 Ground Control Point

Before the flights, to match the point cloud with the field data, 20 high reflective Ground Control Points (GCP) (five for each site) were positioned on the ground in open spaces (Brede et al., 2017) and geo-located with a high grade GPS (Trimble® Geo 7X with the same antenna used for the plot centre collection).

The GCP consisting of two equally sized closed cell foam panes (50 cm x 50 cm with a base of 80 cm), covered with high retro-reflective tape, connected via piano hinges. When set up the panes form a 110° angle between them, which makes them look like tents (Figure 5).

The GNSS fixing location report (see Attachment 1 in this Section) was computed to measure the positioning error of the GPS, necessary for the subsequent LiDAR analysis.

Figures 6 and 7 show the actual LiDAR locations vs GNSS measured locations of GCP and CP for each site and a close example for Site4 Plot4.

Figure 5: Ground Control Point.

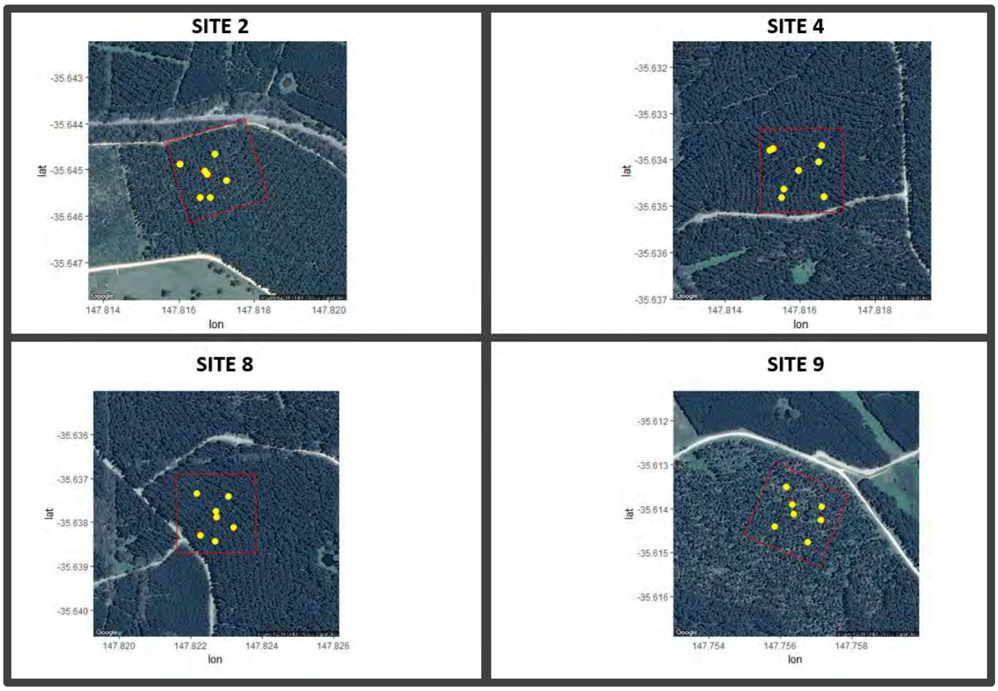

Figure 6: GNSS Centre Plot and Ground Control Points locations measured (yellow) and the actual LiDAR location (red) for each Site.

Figure 7: Detail of measured GNSS location of PC (yellow dot) and GCP (blue square) with the actual LiDAR location shown with a black circle for Site4 Plot4.

2.3 Processing VUX-1LR Data

The raw LiDAR dataset acquired by Geomatics was divided by site, height and direction of acquisition.

The trajectory lines were generated, and we used a procedure to transform the point cloud in shapefile line with the information of the flights as the swaths were not ordered chronologically due to the helicopter different fly path. The User data field on the LiDAR data was used to define the flight altitude. The Point source id field on the LiDAR data was updated with the corresponding flight line.

The raw LAZ data points were then classified, with LAStools (version 14 September 2017- rapidlasso GmbH) as ground and non-ground, then de-noised and clipped by site and by plot and finally separated by User Data. QTModeler (8.0.7 - Quick Terrain Modeler, Applied Imagery) was used mainly to visualize the point cloud and to generate 1m resolution Digital Terrain Model (DTM) by each site. Five meters contours from the DTM were derived with ArcMap (version 10.5.1 - Esri).

The quality of the VUX-1LR datasets and the derived products were checked using QTModeler software. A formal list of all the complete data checks is provided at the end of the QA-QC Report (see Attachment 2).

For each site, the specifications of the LiDAR data (such as intensity, scan angle, classification) were summarized. The overlap of flights and the difference with the ground (if there is offset) were also checked. This process measured the relative accuracy between flight lines, or how well one flight line fits an overlapping flight line vertically. Some noise points were misclassified as ground, but this problem was fixed.
Due to the high point density of the data, the LAZ file was divided in tiles of 30 m x 30 m. After the pre-process steps, the coverage was checked, and all the tiles supplied were found to be uncorrupted and readable.

The pulse and point density were very high: between 5,000 and 9,000 points/m^2 and over 8,000 points/m^2 respectively (Table 5). Nominal Point Spacing was checked and confirmed that the constant down track and cross track point spacing meet the LiDAR specifications (i.e. the spacing of all returns and the last return is 0.01m). No issues were found during this step.

Table 5: Pulse and point density by Site.

Variables	Site 2	Site 4	Site 8	Site 9
Pulses/m^2	9,234	6,824.6	7,955	5,322.1
Returns/m^2	16,830	11,947	14,064	8,734.1

Therefore, based on the procedures and quality assurance checks, we confirmed that the data classification conformed with the project specifications set by the scope of work. All issues found during the qualitative QC were fixed. In addition, the datasets conformed to project specifications for format and header values.

The pre-processed 3D laser point cloud classified datasets were then subjected to a normalization process. The first step was to define a tile size. Since this database is characterized by a high dense point cloud, several tests were made to find the working specifications. Then the height of each point above the ground was computed. After that the normalized dataset were clipped by plot and separated by User Data.

The RGB images collected were processed with Pix4D (version 4.1.24) software to create orthoimages.

The point clouds were coloured with the RGB imagine. At this stage there was an offset between the LiDAR data and the images, solving this issue remains a subject for future research.

3. Results

3.1 Height Analysis

A 0.3 m resolution Canopy Height Model (CHM) raster for each flight height was also produced using a pit free algorithm developed by Khosravipour (2015). Due to the high dense point cloud duplicate points were found and removed, and the point cloud was thinned and rasterized by height-layers.

The percentile p95 metric raster was derived to check the validity of CHM.

The potential tree tops, peaks, were computed with the CanopyMaxima method using the free software FUSION (version 3.42 - USDA Forest Service), the duplicated peaks were cleaned as well as the overlapping (distance <30cm) ones.
The images reported in Figures 8 and 9 are an example of the different CHM computed by User Data.

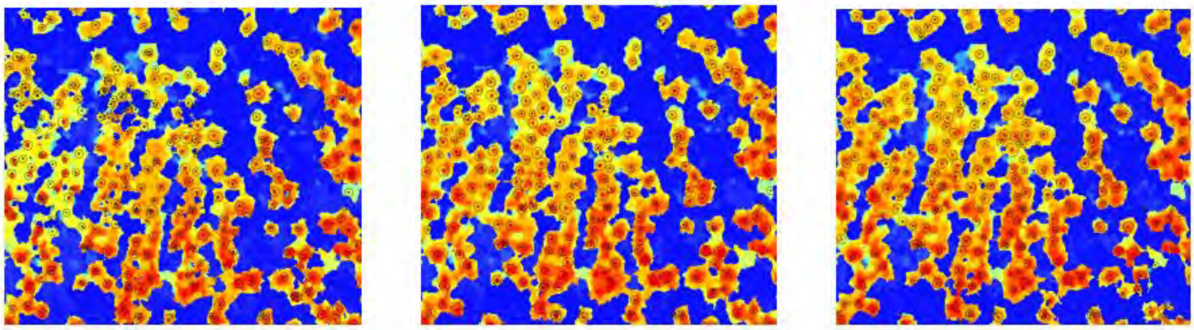

Figure 8: PEAKS (points) detected at 30m, 60m and 90m with potential crown estimation (circles) - Scale at 1:400 - Site4.

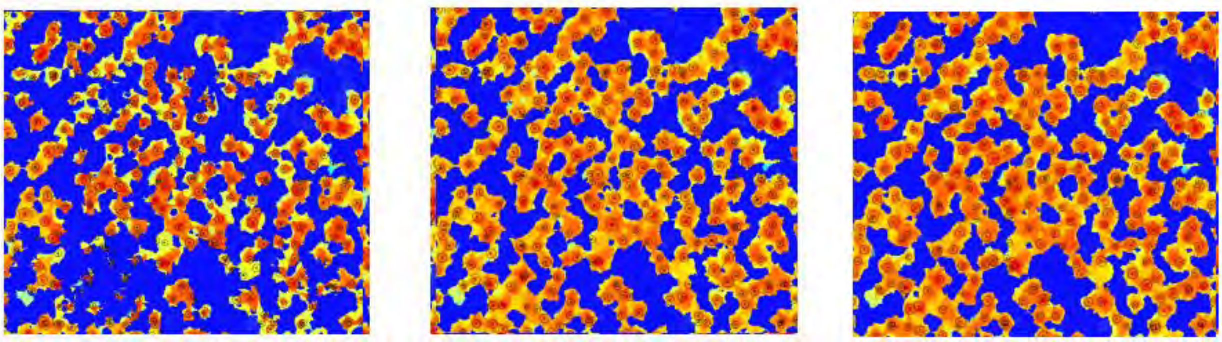

Figure 9: PEAKS (points) detected at 30m, 60m and 90m with potential crown estimation (circles) - Scale at 1:400 – Site9.

The CHM at 30 m presented several canopy misclassifications in comparison with the other two altitudes. As shown in Figures 8 and 9 the differences between the 3 altitudes can be appreciated.

An automatic procedure was developed by Interpine with R software (version 3.4.1 - CRAN-R) to understand which flight altitude returns the closest peaks to the field measurement. The inputs were peaks and the field tree top, the process is based on Euclidean distance and difference of height. The results are reported in Table 6. On a total of 74 trees, the 30m CHM produced the best match between peaks and tree tops on 31 occasions, the 60m CHM produces the best match on 28 occasions and the 90m CHM produces the best match on 15 occasions.

Table 6: Best match between peaks and tree tops at different AGL flights.

AGL	Count TreeID
30	31
60	28
90	15
Total	**74**

The maximum height detected at different flight heights was compared with the field data. All flight altitudes produced acceptable results for height deviation (Figure 10): the field data = 31.00 m, 30 m AGL (height above ground level) = 30.60 m, 60m AGL = 30.70 m and 90 m AGL = 30.65 m. The mean for the field data was 27.31 m, while the mean for the 30, 60 and 90m is respectively 27.17 m, 27.15 m and 27.40 m. The R^2 and RMSE show that the best result is achieved with the 60 m flight (Table 7).

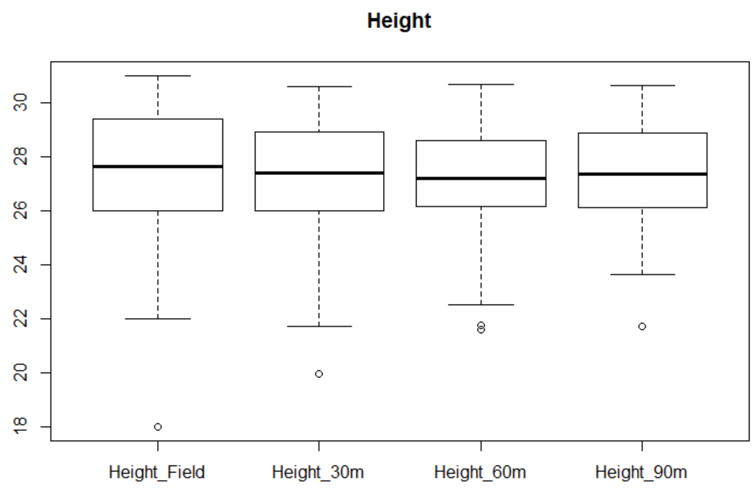

Figure 10: Distribution for maximum height.

Table 7: Results of maximum height analysis at different AGL flights.

AGL	R^2	RMSE
30	0.5303	1.73
60	**0.5867**	**1.61**
90	0.5808	1.62

3.2 Stem Detection

Because of the survey-grade instrumentation used to acquire the point cloud dataset, this aspect of the work it is assumed to be very precise, while the field measurements are affected by a double positioning error: a random error due to the bearing collecting and a GPS error (see Attachment 1). These factors were considered when the point cloud was compared with the field data. For these reasons a buffer of two meters was applied to the field tree tops and with the best peaks detected previously.

The points cloud was sliced between 1 m and 2 m at different AGL and intersected with the 2 m buffer generated from the Tree Top field position (TT) and the selected Peaks position (P). In Figure 11 there is an example of the stem detection at different AGL, the green one is at 30 m, the red one is at 60m and the yellow one is at 90m. The 90 m AGL was found to unacceptable at capturing DBH accurately so it was discarded.

The results of the intersection between TT and P buffers with the point cloud, for the five plots were considered, are reported in Table 8. The best combination is Tree Top location buffer with the 60m AGL point cloud. Only 6 trees out of 74 weren't detected (with a percentage accuracy of 91.9%). With this intersection the point cloud of the stems was identified with the field TreeID, using R software. After the intersection an automatic clean-up was done based on the distance of point from the xmean and ymean of the stem centre. An example is reported below in Figure 13. The threshold for the automatic clean-up was chosen as the quantile three; this number is still error affected but produces a first approximation of the real DBH (the error of overestimation is 3-15%) (Table 9).

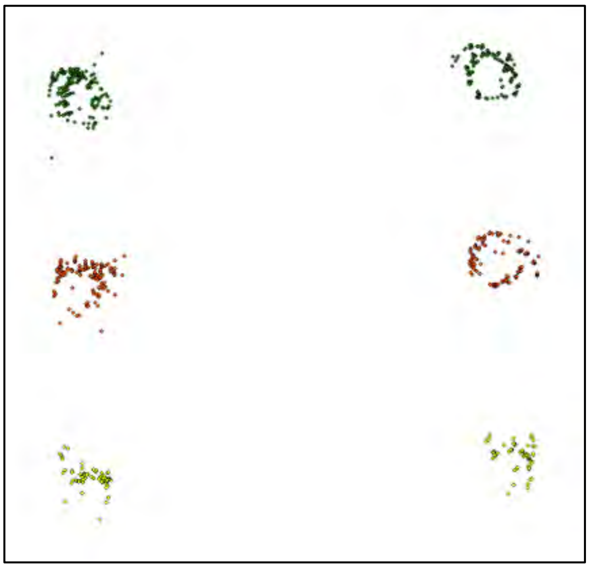

Figure 11: Example of stem detection at different AGL (green=30 m, red=60 m, yellow=90 m).

Table 8: Stem detection: intersection between Point cloud and Tree Top field position (TT) and the selected Peaks position (P).

		30m PointCloud		60m PointCloud	
Plot #	**Field count**	**Buffer TT**	**Buffer P**	**Buffer TT**	**Buffer P**
4	15	14	15	13	15
5	15	8	6	11	10
6	12	12	11	12	11
15	15	8	15	15	15
16	17	8	11	17	13
Tot	**74**	50	58	**68**	64
% accuracy	100%	67.6%	78.4%	**91.9%**	86.5%

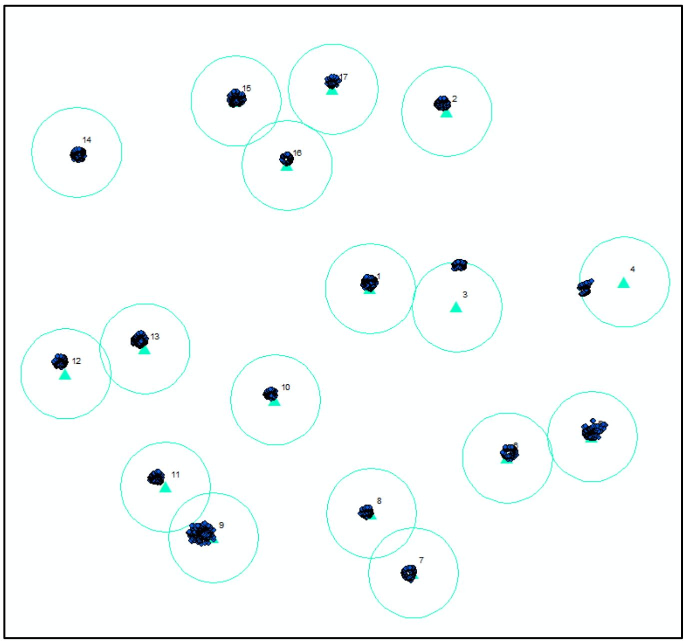

Figure 12: Plot 16 stem detection of Point Cloud at 60m (blue dots) and field Tree top (triangles) and the corresponding buffer of two meters.

Site 4 Plot 4 Tree 11

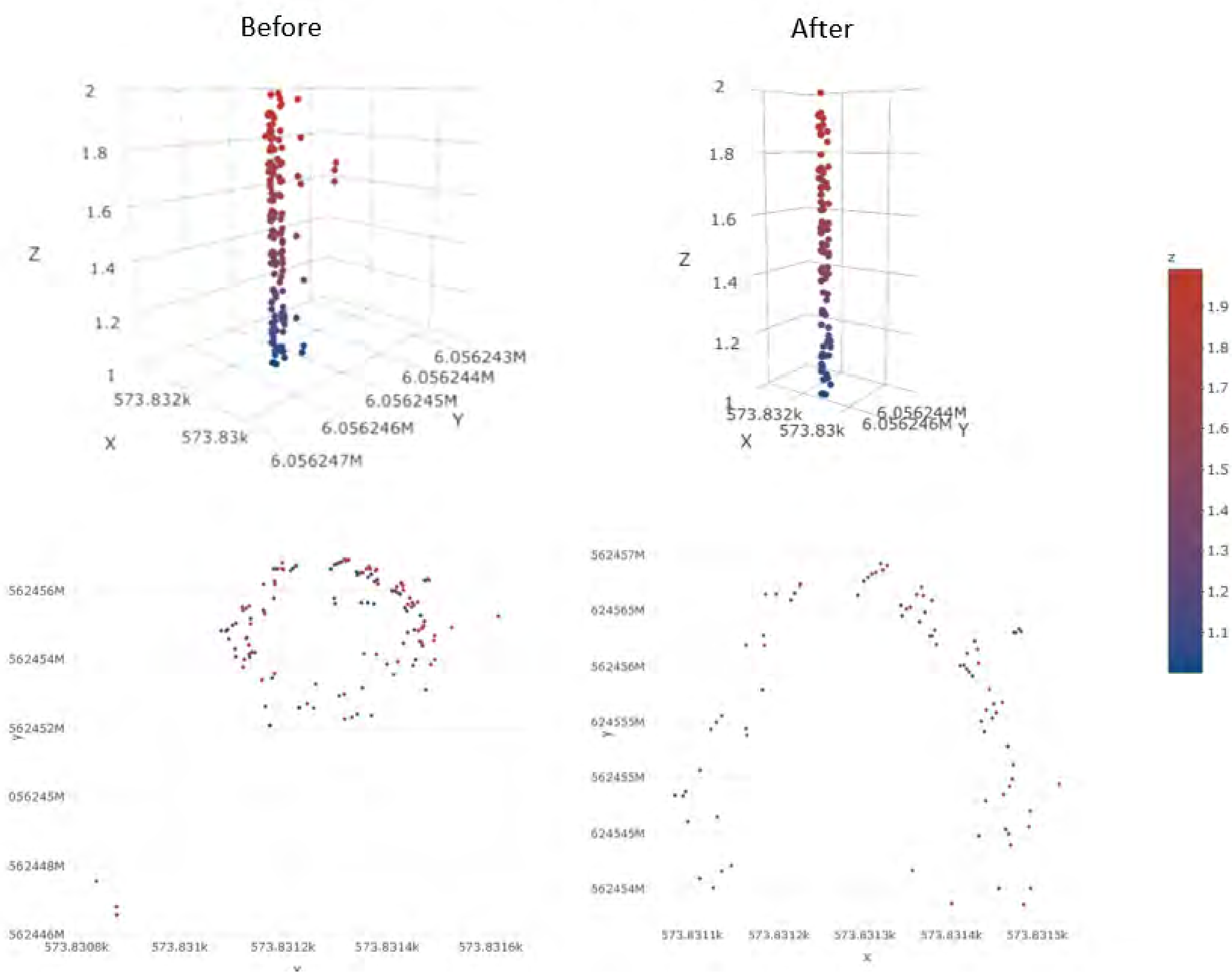

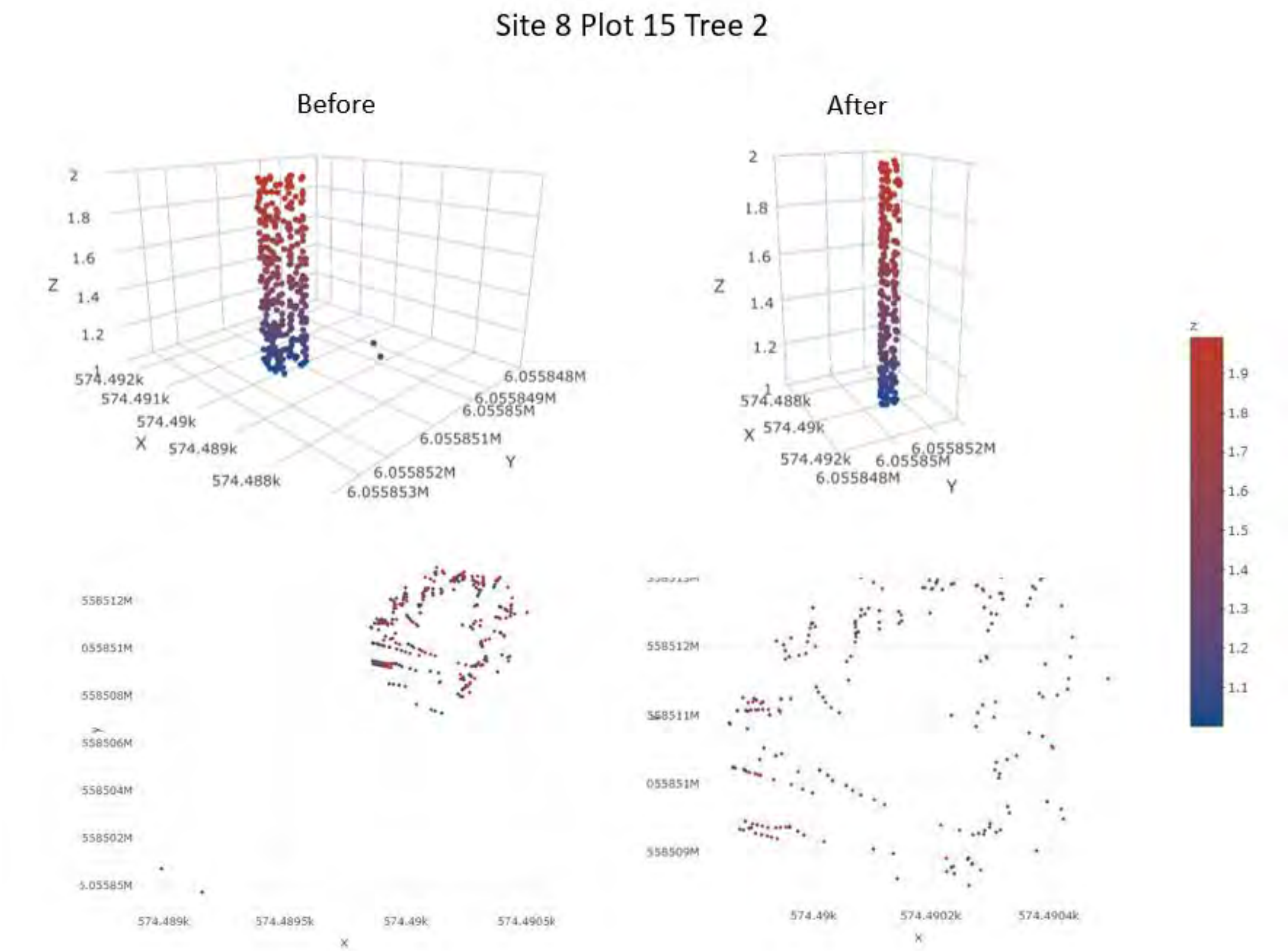

Figure 13: Plot 4, tree number 11 and Plot 15, tree number 2. The top left graphic represents the stem before the automatic clean-up. The top right graphic represents the stem after the automatic clean-up without outliers. The bottom graphics represent the same in 2D.

Table 9: Example of automatic diameter detection from the outliers cleaned stems.

	Site 4 Plot 4	Site 8 Plot 15
ID Tree	11	2
Field DBH (mm)	358	435
Automatic Diameter DBH (mm)	403	537
RMSE	0.04	0.10

4. Discussion and Conclusion

The study was conducted to find the optimal parameters of the VUX-1LR to obtain an ultra-dense point cloud suitable for a virtual reality environment. Four sites of 200 m square were flown, a total of nine field plots (radius 13.82 m) were measured. Two sites, number 4 and 8, were flown at 30, 60 and 90 m AGL. This study is a comparison on the five plots inside those two sites. The analysis investigates which point cloud from three different flight altitude produces the height and the diameter closest to the field measurements.

The pulse and return density of this LiDAR dataset was very high: between 5,000 and 9,000 pulses/m^2 and over 8,000 pulses/m^2. Meanwhile the field measurements are affected by a double positioning error: a random error due to the bearing collecting and a GPS error (<50 cm). This discrepancy is a weakness for making an acceptable comparison. Nevertheless, with the automatic procedure developed in this study the point cloud trees were successfully assigned to the Field Tree Id.

For the height analysis the 0.3 m resolution CHM was compared at different altitudes. The 90 m height and the 60 m height gave a positive result, while the 30 m height presented an inaccurate canopy representation. The analysis of potential tree tops is based on the peaks at different height, peaks computed from the CHM, showing that the best flight altitude is 60 m, with an R^2 and an RMSE respectively of 0.5867 and 1.61. This analysis provides a comparison of the influence of the sensor altitude.

This study computed the peaks using a 0.3m canopy height model resolution raster to identify the local maxima in the canopy. Since numerous Individual Tree Detection (ITD) algorithms now exist including a software application 'PointcloudITD', developed by Mitch Bryson (Australian Centre of Field Robotics) further work can be done in this area, knowing that the peak detection base on point could improve significantly the peak detection accuracies (Kaartinen *et al*., 2012).

The stem detection, with a 91.9% accuracy, confirmed that the optimal flight altitude is 60m. The stem detection analysis is at the first stage, further analysis will be made in the near future comparing different algorithms, some of them based on a machine learning approach. At the same time this dataset will be tested in a virtual reality environment.

Future Work

These results present a preliminary analysis of the Carabost SF point cloud dataset. With a large group of researchers, the possibilities for analysing this dataset are enormous. The VUX-1LR data is available for any researchers or organizations interested in analysing a high density point cloud. Feel free to contact Interpine Group or FWPA to request a copy.

Under the next FWPA project, it is anticipated that researchers will analyse the data using the Cloud2Stem software developed by Joel Gordon at Scion. Additionally, the data will be interrogated by Mitch Bryson at the Australian Centre for Field Robotics using stem segmentation algorithms developed in the current FWPA project. Both approaches together will produce automatic tree detection, stem reconstruction and estimation of stem-level diameters, volumes, taper and log products.

A new FWPA grant application has been successfully accepted giving the opportunity to the Human Interface Technology Laboratory (HIT Lab), University of Tasmania, to carry on with the project *VR in Tree Cruising*, under the supervision of Winyu Chinthammit and the assistance of the Interpine team.

Attachment 1

FWPA Carabost SF study site - GNSS Plot And Ground Control Location Fixing - April 2018

Overview

Interpine established the location of 9 Plot Centers (CP) and 5 Ground Control Points (GCP) for each Site in the Carabost study area (Figure 1) using a survey grade decimeter GNSS (Trimble® Geo 7X). This was for the purposes of fixing CP and GCP pegs for subsequent LiDAR analysis.

Figure 1 shows the area of interest with all Sites covered during the field inventory.

Figure 2, 3, 4, 5 shows the actual LiDAR locations vs GNSS measured locations of GCP and CP for each Sites.

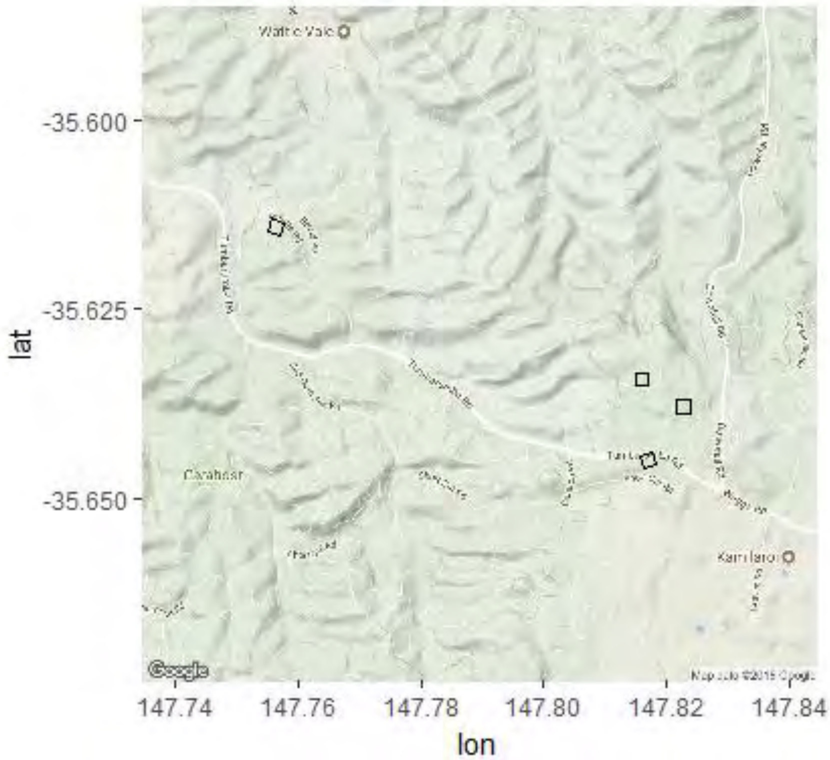

Figure 1: Operational area where inventory was completed.

SITE 2

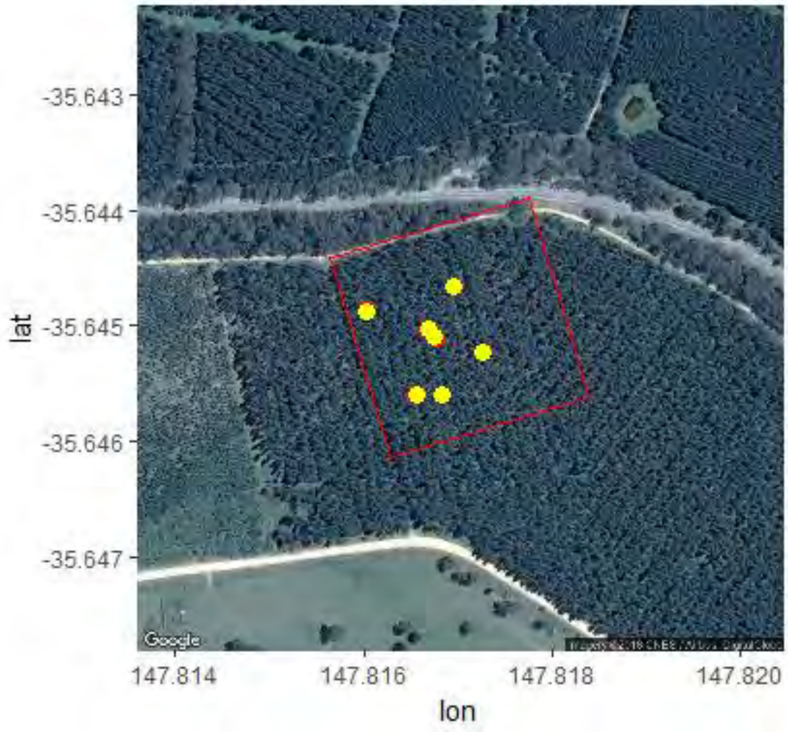

Figure 2: GNSS CP and GCP location measured (yellow) and the actual LiDAR location (red) for Site2.

SITE 4

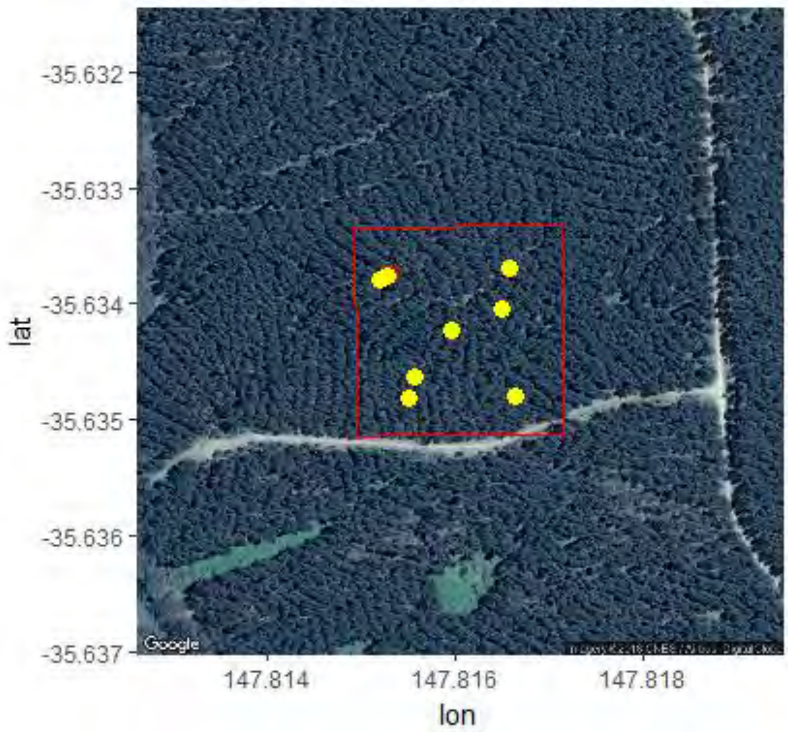

Figure 3: GNSS CP and GCP location measured (yellow) and the actual LiDAR location (red) for Site4.

SITE 8

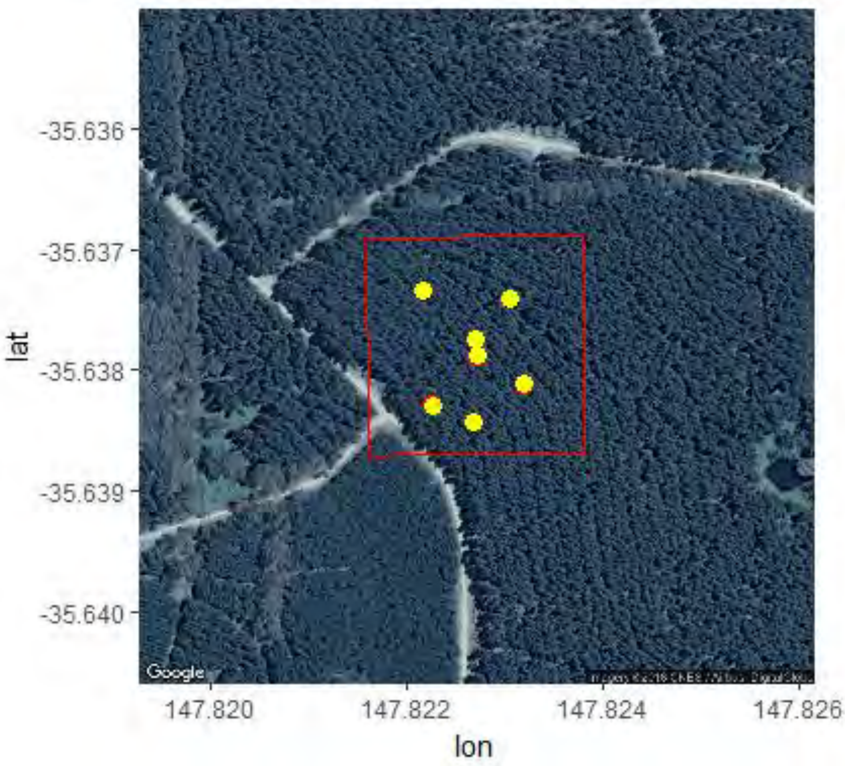

Figure 4: GNSS CP and GCP location measured (yellow) and the actual LiDAR location (red) for Site8.

SITE 9

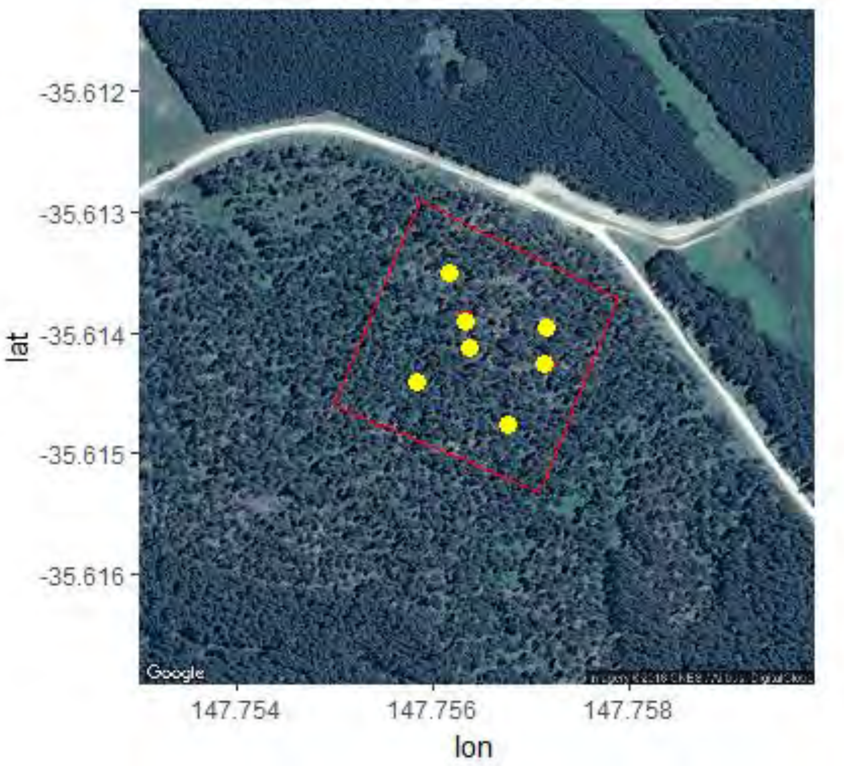

Figure 5: GNSS CP and GCP location measured (yellow) and the actual LiDAR location

(red) for Site9.

Figure 6: Example of measured GNSS location of CP (yellow dot) and GCP (blue square) with the actual LiDAR location shown with a black circle for Site4.

Equipment and Methodology

Extracted from: Herries *et al,* 2014 Interpine Guide to PlotSafe Data Collection - Capture of LiDAR Field Reference Inventory. Locating Plot Centre in the field, To establish a new plot follow these steps:

1. Calibrate your compass on your Garmin GPS unit prior to each day's field inventory.
2. Using a Garmin 62s or 64s (or equivalent unit with GPS / GNSS with digital active compass and barometer) should be used to navigate to within 15-20 m of the plot centre. At this point use the magnetic compass bearing and horizontal distance provided by the GPS, to navigate to the plot centre.
3. While crew member 1 remains where the GPS reading is taken, crew member 2 navigates to the approximate plot centre using the distance and compass bearing taken from the GPS.
4. Crew member 1 uses the Vertex to confirm horizontal distance and re-checks the compass bearing to confirm the plot centre.
5. Confirm that the location of the plot on the ground matches the map provided.

Technical Note:

An unbiased location is very important. The purpose of this procedure is to ensure the inaccuracies of navigation with the GPS do not influence the plot location in a bias manner.

For slopes > 5 degrees the Vertex function for slope distance must be used in conjunction with slope to provide a horizontal distance.

Fixing the Plot Centre and Ground Control Points with High Grade GPS:

Record the location using a high grade GPS such as the Trimble® Geo 7X with Floodlight Technology connected to an external high quality GNSS antenna.

1. Position the high grade GPS unit exactly over the plot centre or the ground control point.
2. Open TerraSync software, and select Data menu screen.
3. Create New Datafile for each plot using the Dictionary LiDAR.
4. Set the antenna height to 0m if placed on the ground.
5. Record high grade GPS data for the full measurement time at the plot (as a guide a minimum of 500 data collection points should be collected if time is limited).

Technical Note:
This fix is one of the most important characteristics aside from crop tree measurements. This will be used to extract the matching aerial LiDAR survey data for this plot area.

Post Processing

Data was post-processed using Trimble Pathfinder Office V5. Trimble® Geo 7X GNSS units deployed were H-star enabled and three base stations closest to the survey site were selected for processing.

Base Provider: Trimble Positioning Services – Holbrook, Tumbarumba and Walwa.
Differential Correction Summary Ground Control Point:
3.12% of positions were code corrected by post-processing against three base providers
96.88% of positions were carrier corrected by post-processing against three base providers
Differential Correction Summary Plot Centre:
28.12% of positions were code corrected by post-processing against three base providers
71.88% of positions were carrier corrected by post-processing against three base providers

Estimated accuracies GCP during processing for corrected positions are as follows:

Range	Percentage (%)
0-5cm	0.00
5-15cm	34.38
15-30cm	28.12
30-50cm	28.12
0.5-1m	9.38
1-2m	0.00

Estimated accuracies CP during processing for corrected positions are as follows:

Range	Percentage (%)
0-5cm	0.00
5-15cm	50.00
15-30cm	41.67
30-50cm	8.33
0.5-1m	0.00
1-2m	0.00

Precision Fixes:

Figures 7 and 8 shows precision estimates at 68% and a 99% confidence interval (CI) of the dataset for GCP and CP respectively.

Estimated mean precision during processing ground control point positions were:

CI	Mean (m)
68%	0.29
99%	0.72

Estimated mean precision during processing plot centre positions were:

CI	Mean (m)
68%	0.18
99%	0.56

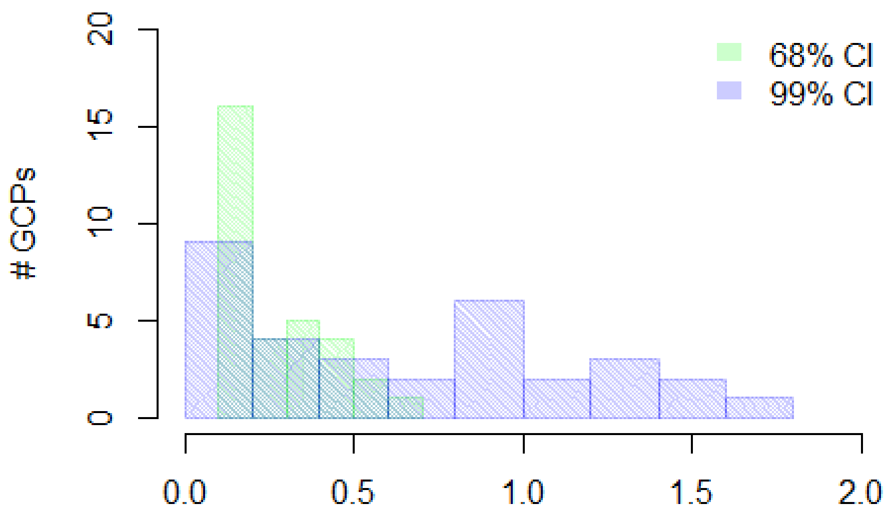

Figure 7: GNSS Horizontal Precision GCP (m).

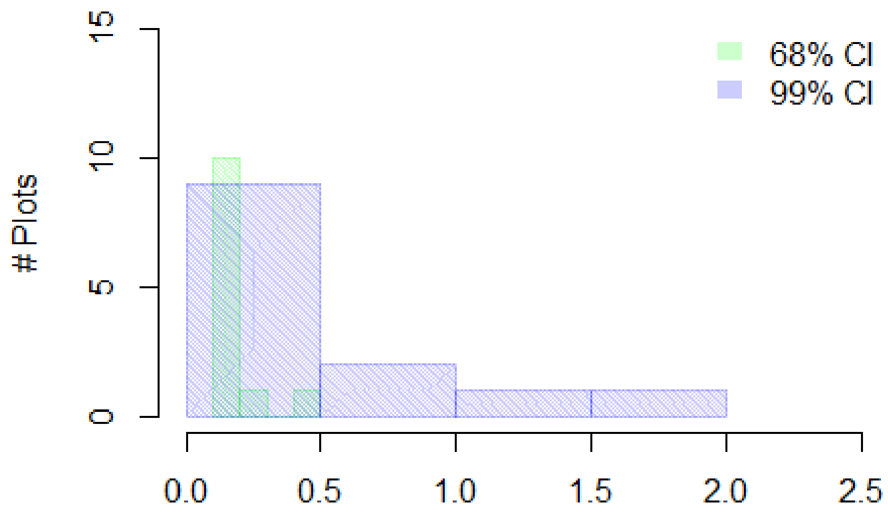

Figure 8: GNSS Horizontal Precision CP (m).

Technical Note:

A recreational style GPS/GNSS typically displays its precision to the user at a 50% confidence interval or less. Survey grade GPS/GNSS usually represent precision at a 68% CI. For the purposes of this work Interpine also display a precision interval of 99%.

Variation to GNSS Locations:

Figures 9 and 10 displays the distribution of LiDAR plots locations vs GNSS measured locations.

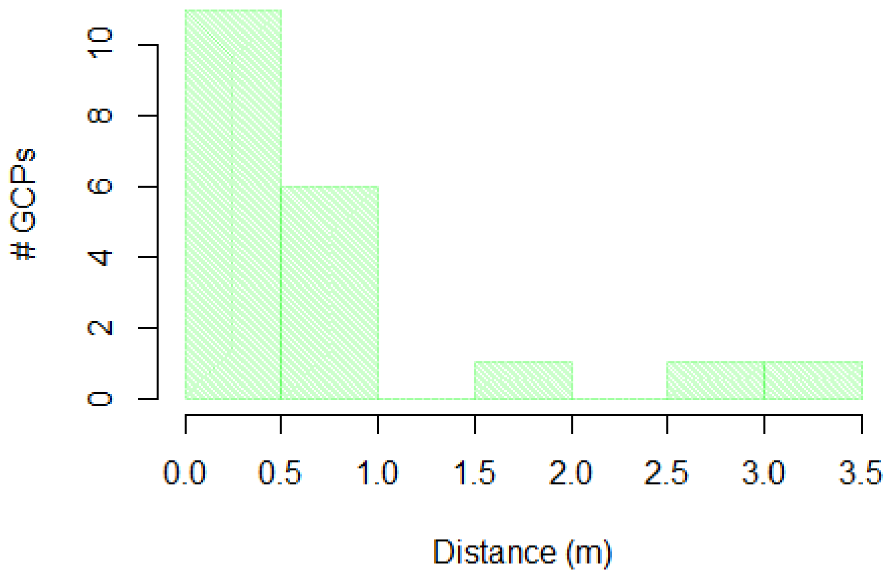

Figure 9: Measured GNSS Ground Control Point location vs actual LiDAR location.

The following GCPs are the outliers in Figure 7, being greater than 2 m from their intended location:

GCP 16
GCP 39

The following is the RMSE mean and distance for the plots from their GNSS locations vs actual LiDAR locations.

Mean Distance: 0.72
RMSE: 1.09
Max Distance: 3.01

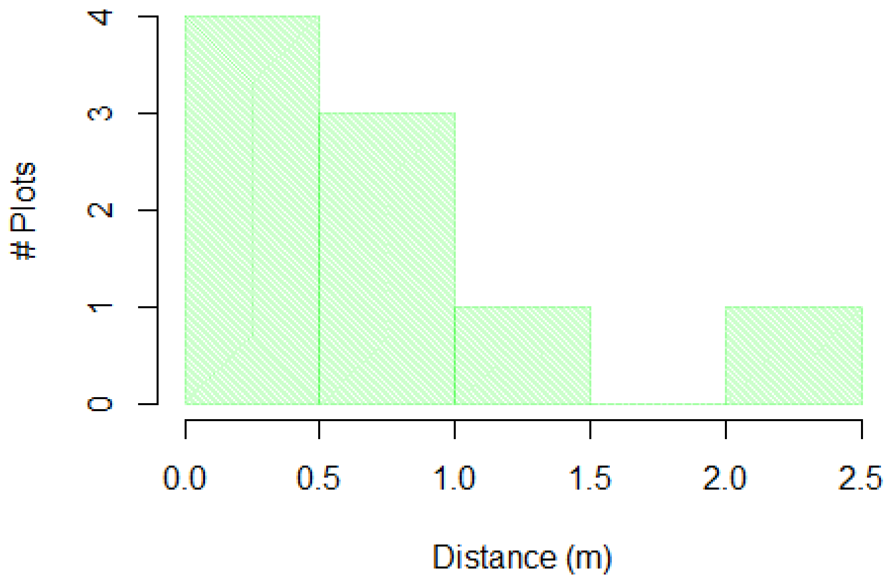

Figure 10: Measured GNSS Centre Plots location vs actual LiDAR location.

The following plots are the outliers in Figure 8, being greater than 2 m from their GNSS location:

PLOT 1

The following is the RMSE mean and distance for the plots from their GNSS locations vs actual LiDAR locations.

Mean Distance: 0.73
RMSE: 0.9
Max Distance: 2.03

Outputs

Post processed plot and ground control location shapefiles can be provided by request to Interpine or FWPA. The attribute table of the shapefiles includes details on the quality of the location fix and collection parameters. The file contains the Inventory Population Name and Plot/Ground Control No. for linking to original plot/ground control locations.

Attachment 2

Carabost SF Study Site – LIDAR VUX-1LR QA-QC Review

Interpine undertook the review of the VUX-1LR LiDAR data captured over the Carabost SF study site, near Tumut, N SW, on 22nd February 2018. This attached document discusses some of the key points of the LiDAR quality assurance and quality control.

1. Introduction

1.1 Project Overview

This report includes attributes of the quality review across the extended Area of Interest (AOI) (Figire 11) for representation purposes only.

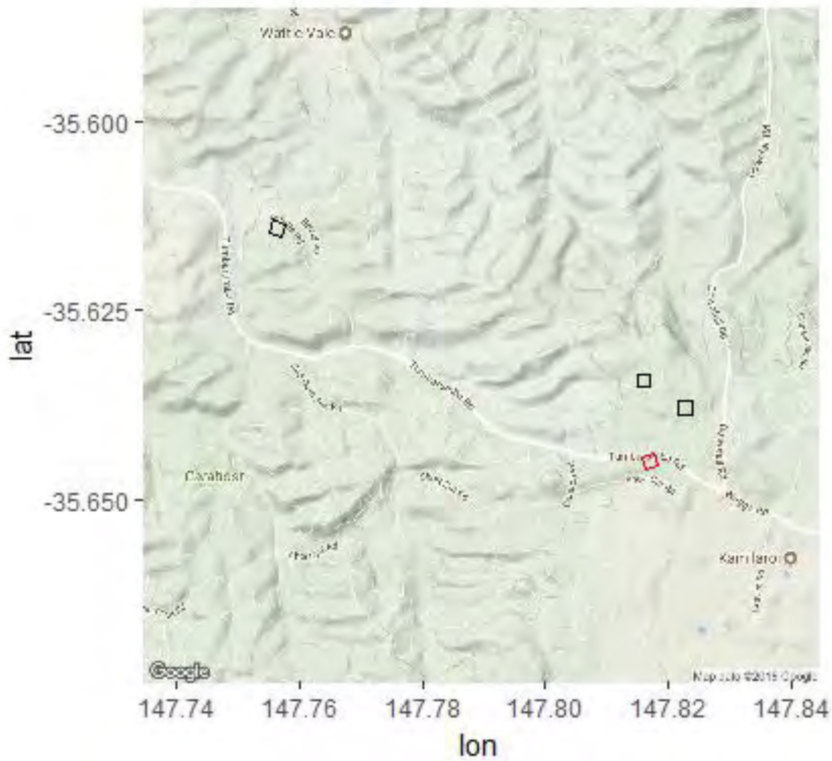

Figure 11: Operational area where LiDAR data was collected.

1.2 Purpose of this Report

Interpine conducted a number of quality assurance workflows across the VUX-1LR datasets acquired as part of the FWPA Carabost SF data acquisition campaign in February 2018. This report shows the quality of the VUX-1LR LiDAR dataset and the derived products. It aims to provide a high level overview of the dataset quality and its contents. A formal list of all the complete data checks is provided at the conclusion of this Attachment.

1.3 LiDAR Metadata

SUPPLIER: Geomatics Technologies

LiDAR SENSOR: Riegl VUX-1LR

LiDAR FORMAT: 1.4 LAZ Point Format 6

DATUM: D_GDA_1994

MAP PROJECTION: GDA94/MGA zone 55

TILE SIZE: 30m x 30m

1.4 Software Used in Analysis and Processing

The raw LiDAR point cloud was processed for this delivery using:

- LASTools (14 September 2017)
- Quick Terrain Modeler (8.0.7)
- ArcMap (10.5.1)
-

2. Objective

Ensure LiDAR data products meet project standards.

3.Terminology

ACCURACY: The statistical comparison between known (surveyed) points and measured laser points. Typically measured as the standard deviation (R^2) and root mean square error (RMSE).

BEAM FOOTPRINT: The size (radius) of the laser pulse once it starts interacting with objects.
DATA VOIDS: Considered as areas greater than four times the post-spacing of data (for the purposes of QA/QC this excludes dropouts caused by normal water bodies, or low near infra-red (NIR) reflectivity such as asphalt or composition roofing).
EFFECTIVE FIELD OF VIEW (FOV): When flight lines are merged, excessive scan angles are often trimmed / reclassified as overage or withheld points to suit the required scan angle specification. This is especially relevant for scanners with a fixed FOV. This results in an effective scan swath width.
FIELD OF VIEW (FOV): The total opening view of the sensor or "sensor scan window" i.e. scan angle of 80° = 160° FOV. Rotating polygon mirror scanners will often have a fixed FOV, oscillating mirror scanners can be varied.
FLIGHT LINE ALIGNMENT: The flight of horizontal and vertical flight line swath overlap merging.
NADIR: A single point or locus of points on the surface of the Earth directly below a sensor as it progresses along its line of flight.
NOMINAL POST SPACING: A measure of LiDAR resolution, measured as the average distance between laser footprints.
POINT DENSITY: A measure of LiDAR resolution, measured as total returns per square meter. This will include all returns from a single pulse.
PULSE DENSITY: A measure of LiDAR resolution, measured as total pulses reaching the

surface per square meter. For post capture analysis this is often considered as the last return point density.
OVERAGE (OVERLAP): A survey AOI which gets covered by more than a single swath flight line. This is also known as overlap during flight specification.
SCAN ANGLE: The angle from nadir to the edge of the scan, measured in degrees.
SCAN WIDTH: Width of the FOV as projected on the ground along the flight line. Can also be considered as Effective Swath Width when considering effective FOV.
SURVEY AREA OF INTEREST (AOI): Total survey area covered that is specified by contract as the focal area of interest.

4. Pre Processing Supplied Data Products

Prior to review Interpine undertook the following activities on the RAW dataset supplied:

- Set up project level file structure
- Validate that files are readable and uncorrupted
- Check all data geo-referencing: GDA_1994_MGA_Zone_55
- Spatial indexing built into LAZ: index files for fast search and use, this is incorporated into the LAZ file.

5. File Summary

All parameters have been checked and are within acceptable limits (Tables 1 and 2).

Table 1: File summaries for Sites 2 and 4.

	Site 2		Site 4	
FEATURE	MinValue	MaxValue	MinValue	MaxValue
X	313,899	1,887,646	547,503	1,347,689
Y	399,539	1,892,019	690,295	1,490,482
Z	-748,513	175,926	-772,479	179,994
Intensity	0	65,535	0	65,535
return number	1	7	1	7
number of returns	1	7	1	7
edge of flight line	0	1	0	1
scan direction flag	0	0	0	0
Classification	1	7	1	7
scan angle rank	-89	84	-88	86
user data	3	6	3	9
point source ID	201	254	401	476
gps time	361,396	367,639	341,971	350,278

Table 2: File summaries for sites 8 and 9.

FEATURE	Site 8 MinValue	Site 8 MaxValue	Site 9 MinValue	Site 9 MaxValue
X	330,123	1,130,313	313,636	1,363,403
Y	-350,486	449,705	-334,743	739,253
Z	-746,780	127,966	-276,293	171,787
Intensity	0	65,535	0	65,535
return number	1	7	1	7
number of returns	1	7	1	7
edge of flight line	0	1	0	1
scan direction flag	0	0	0	0
Classification	1	7	1	7
scan angle rank	-85	85	-86	83
user data	3	9	6	6
point source ID	801	879	901	931
gps time	350,477	361,194	367,922	369,545

6. Coverage and Overlap

6.1 Coverage Review

The number of tiles is 239 (30m x 30m). All tiles supplied are uncorrupted and readable (Figures 12 – 15).

SITE 2

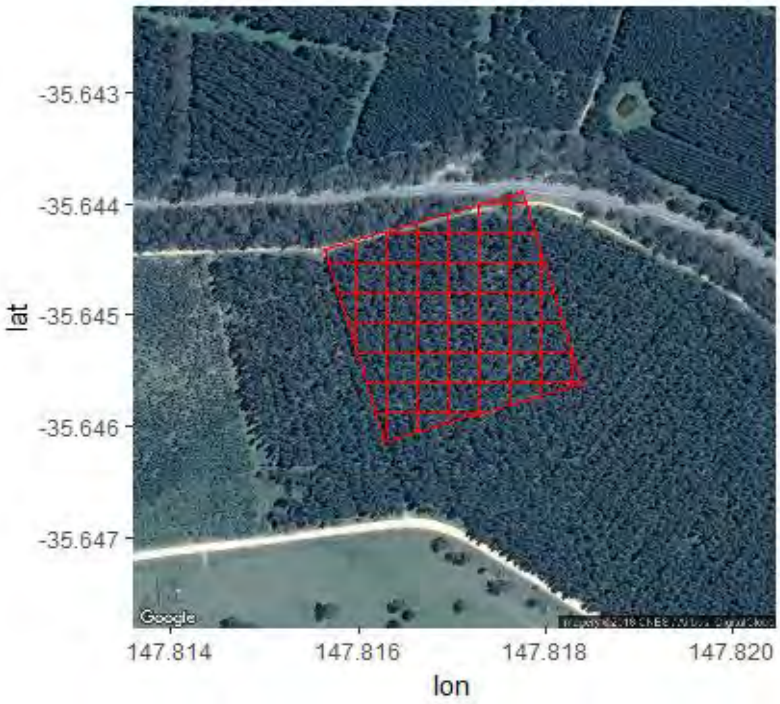

Figure 12: LiDAR tiles overview.

SITE 4

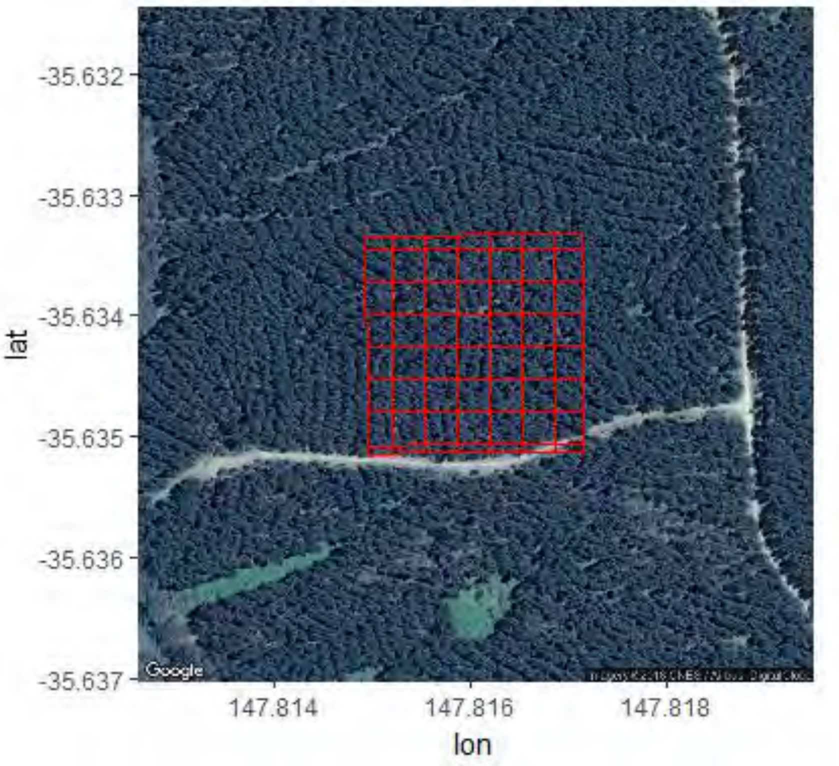

Figure 13: LiDAR tiles overview.

SITE 8

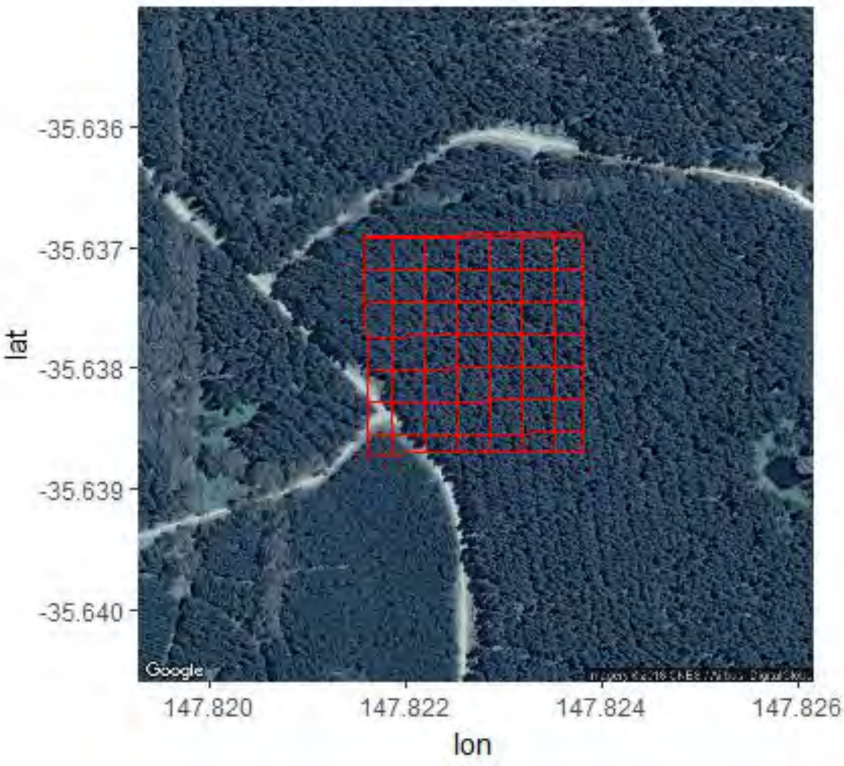

Figure 14: LiDAR tiles overview.

SITE 9

Figure 15: LiDAR tiles overview.

6.2 Flight Lines Review

The LiDAR survey consisted of several flights; the flight altitudes have been selected as close to the canopy as possible or a maximum of 30 m, then at 60 m and 90 m. The flight speed was set around 5m/s or 10 knots. The trajectory has been set 15m apart with 14 flight lines per flight altitude. Flight lines were done from east to west and from north to south, in two sites the same pattern was done also at a 45 angle so from northeast to southwest and from northwest to southeast (Figures 16 – 27).

SITE 2

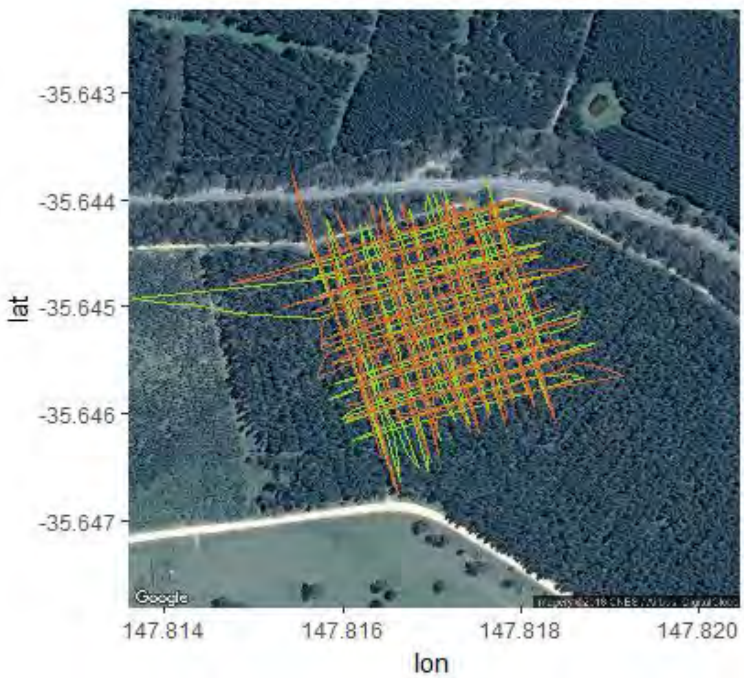

Figure 16: All trajectories coloured by height Site 2.

Figure 17: Trajectories 30m height Site 2.

Figure 18: Trajectories 60m height Site 2.

SITE 4

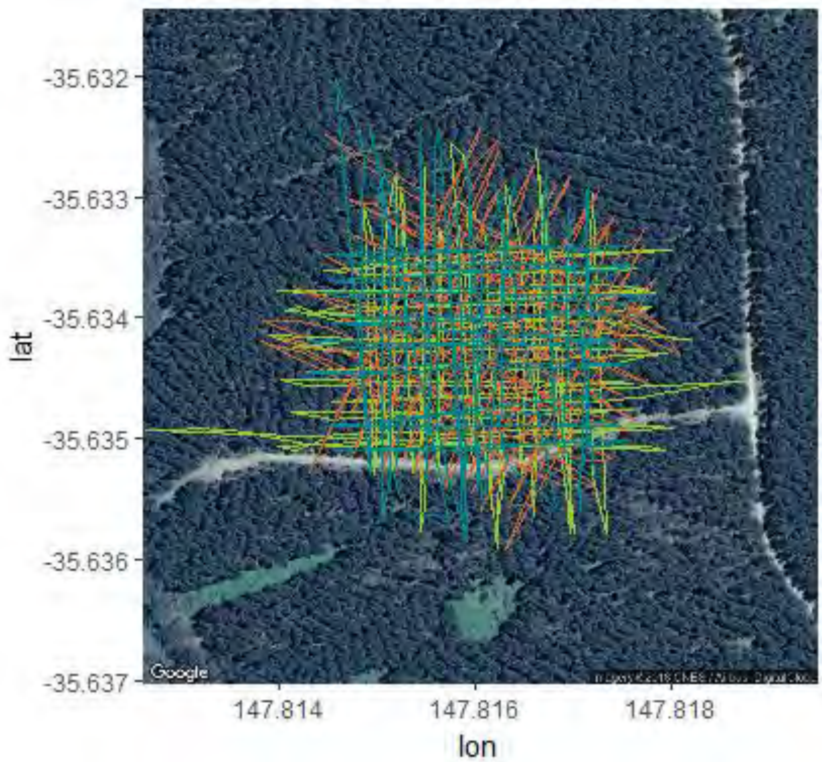

Figure 19: All trajectories coloured by height Site 4.

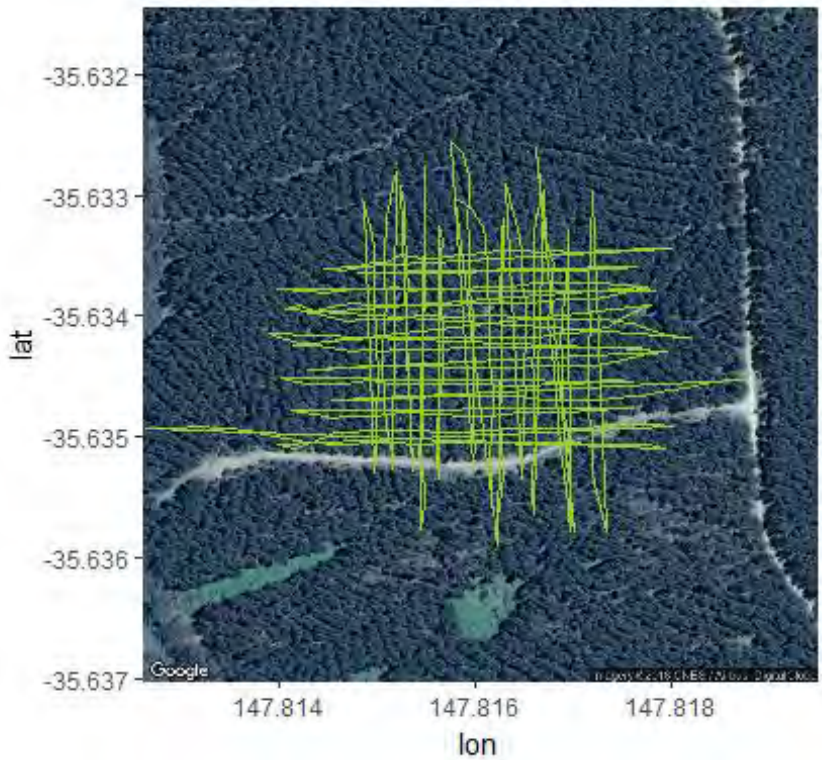

Figure 20: Trajectories 30m height Site 4.

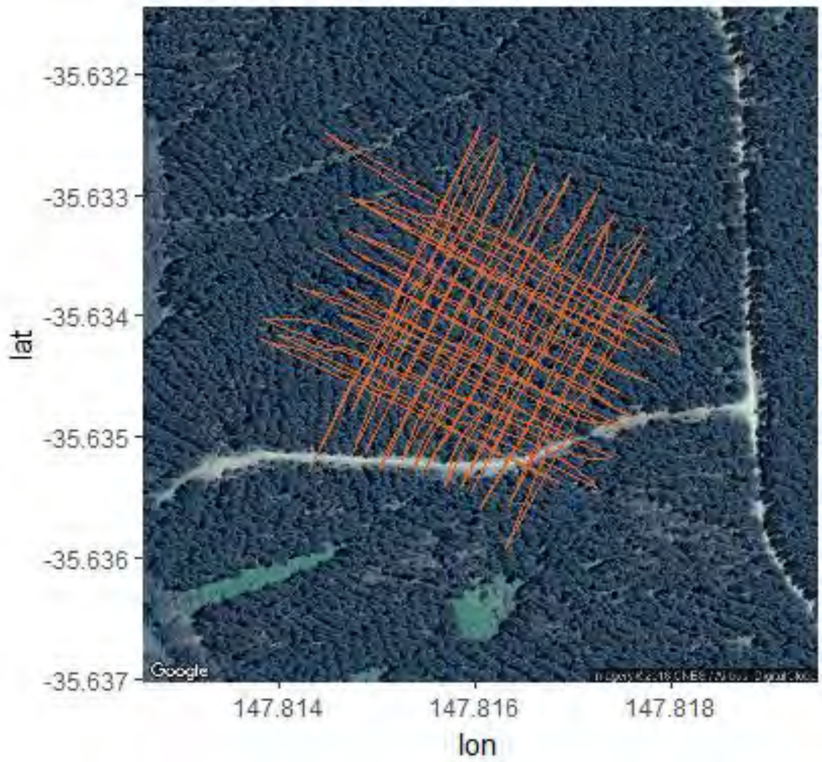

Figure 21: Trajectories 60m height Site 4.

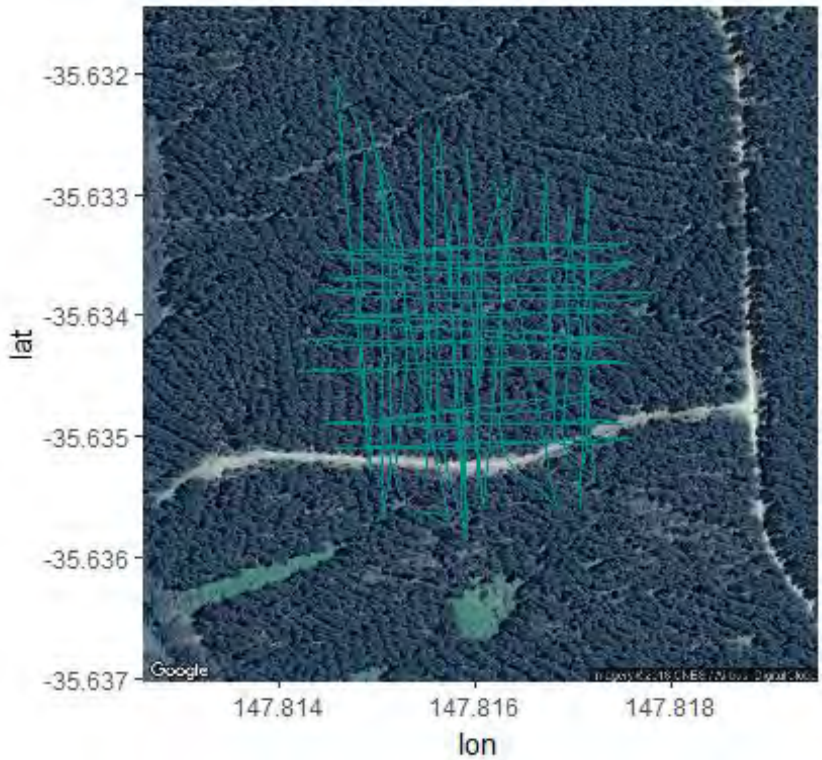

Figure 22: Trajectories 90m height Site 4.

SITE 8

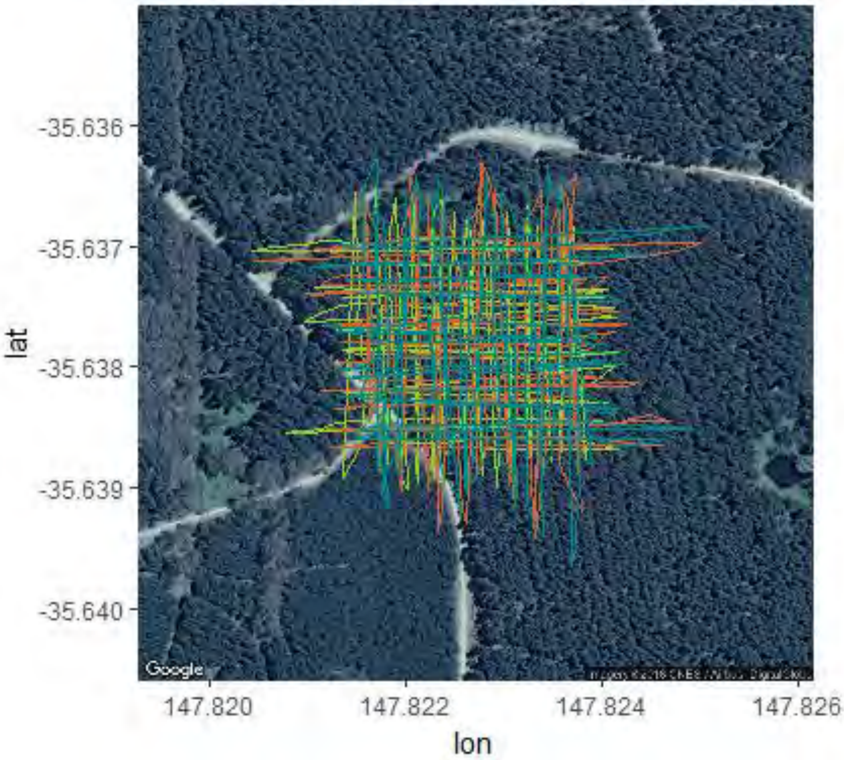

Figure 23: All trajectories coloured by height Site 8.

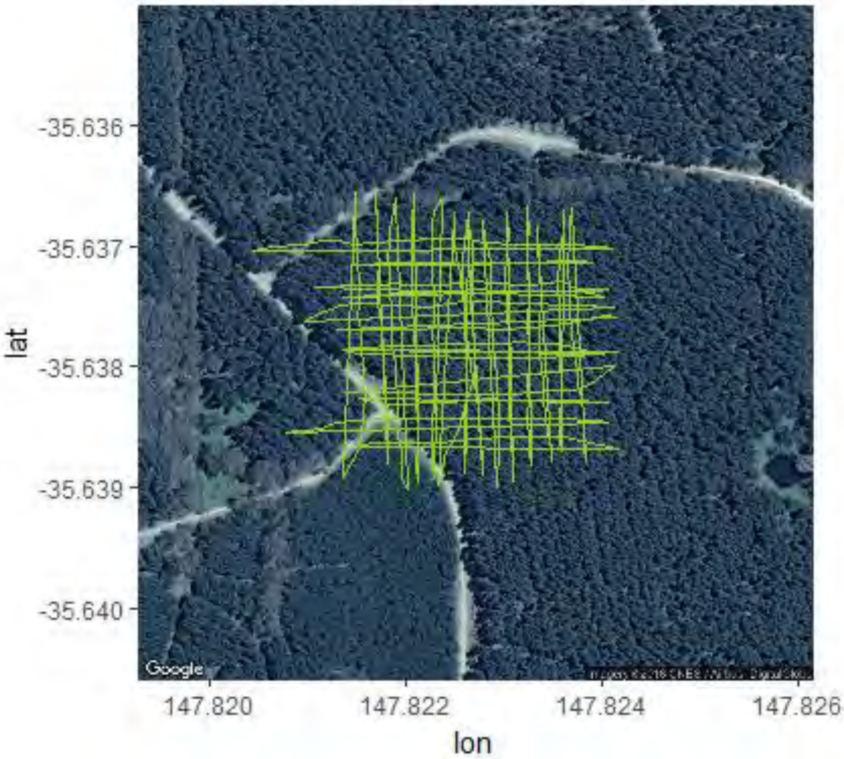

Figure 24: Trajectories 30m height Site 8.

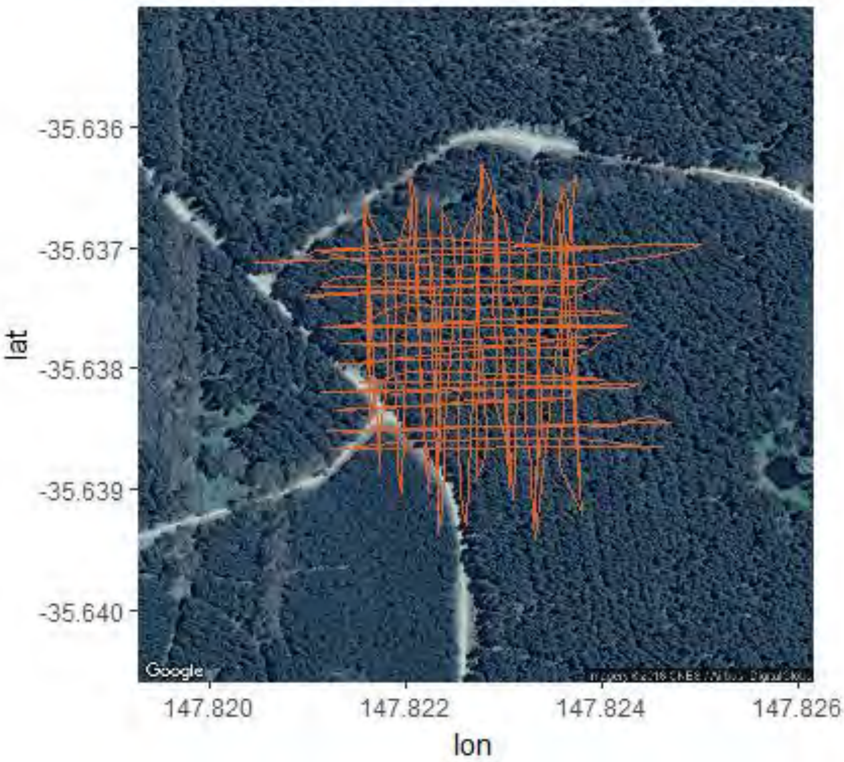

Figure 25: Trajectories 60m height Site 8.

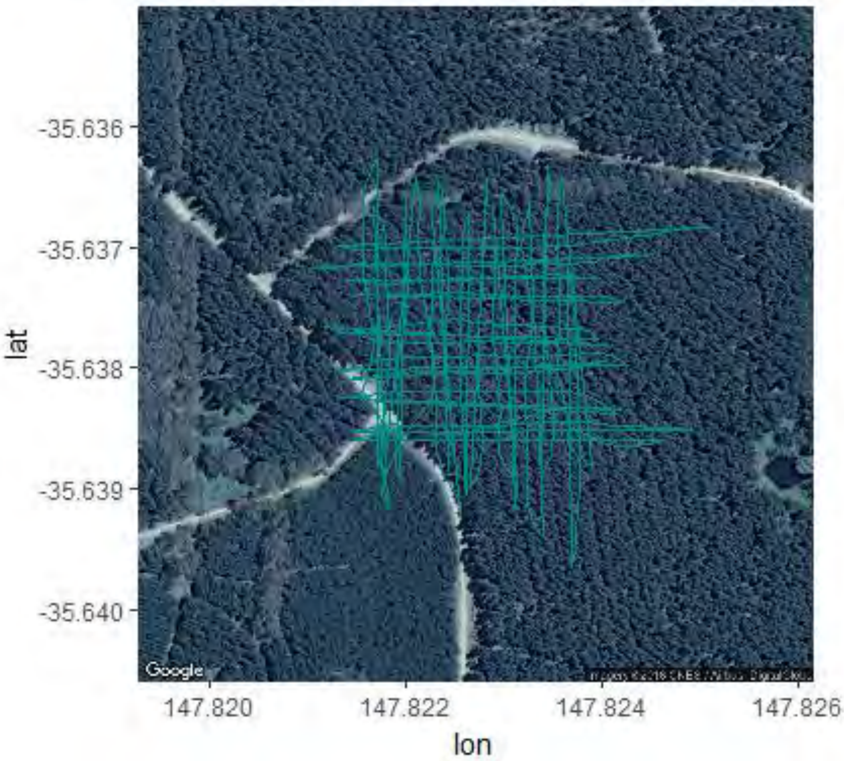

Figure 26: Trajectories 90m height Site 8.

SITE 9

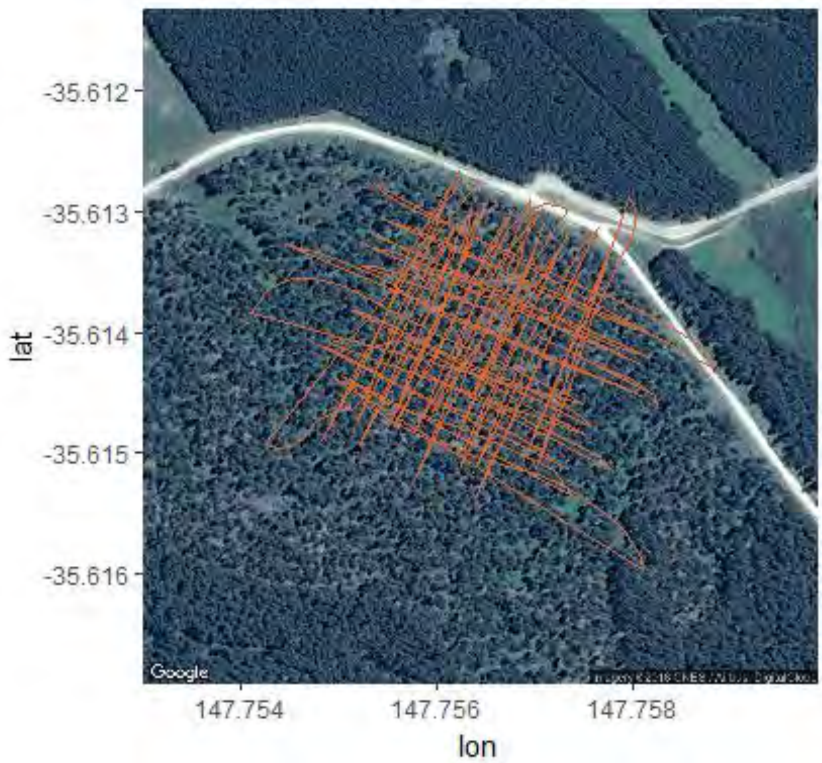

Figure 27: Trajectories 60m height Site 9.

6.3 Flight Coverage Review

Survey area covered by at least 5 flights (Figures 28 – 31).

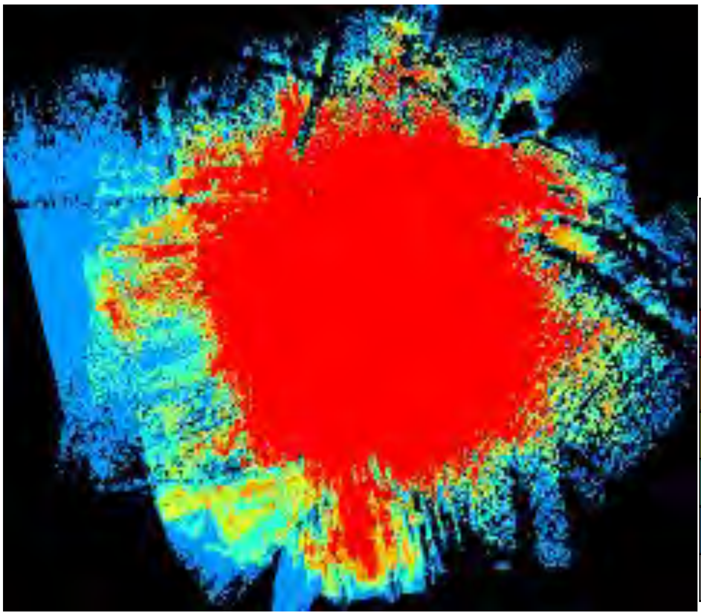

Colour	Number of Flights Lines
red	5
orange	4
yellow	3
green	2
blue	1
white	None

Figure 28: Flight Coverage Site 2.

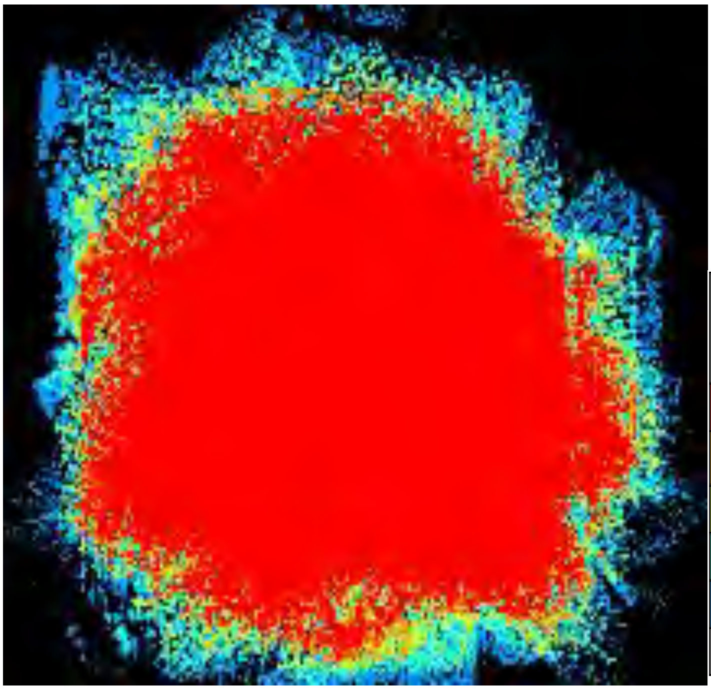

Colour	Number of Flights Lines
red	5
orange	4
yellow	3
green	2
blue	1
white	None

Figure 29: Flight Coverage Site 4.

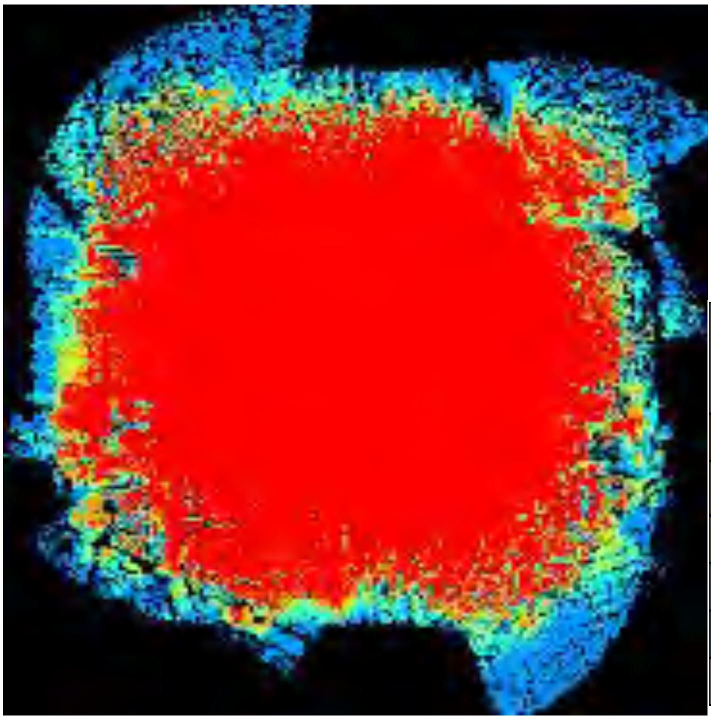

Colour	Number of Flights Lines
red	5
orange	4
yellow	3
green	2
blue	1
white	None

Figure 30: Flight Coverage Site 8.

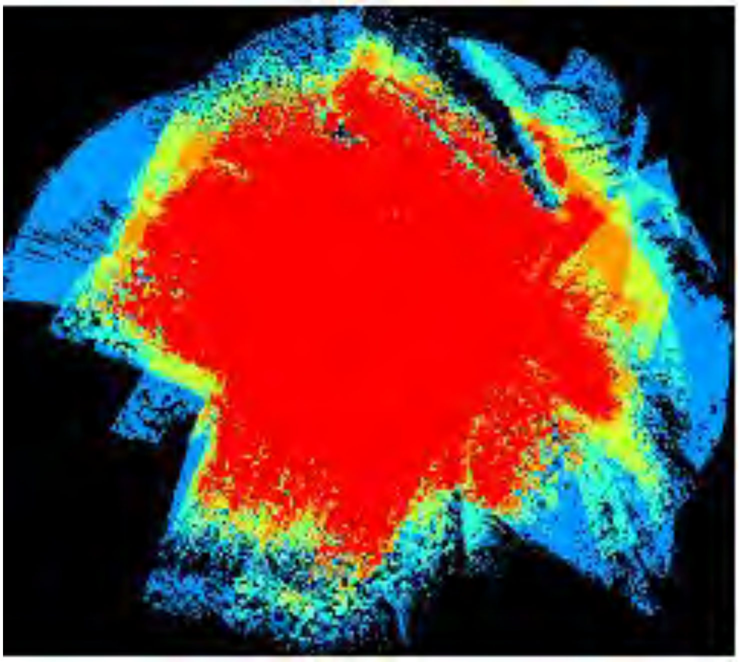

Colour	Number of Flights Lines
red	5
orange	4
yellow	3
green	2
blue	1
white	None

Figure 31: Flight Coverage Site 9.

6.4 Flight Alignment Review

No significant flight line misalignment (Figures 32 – 35)

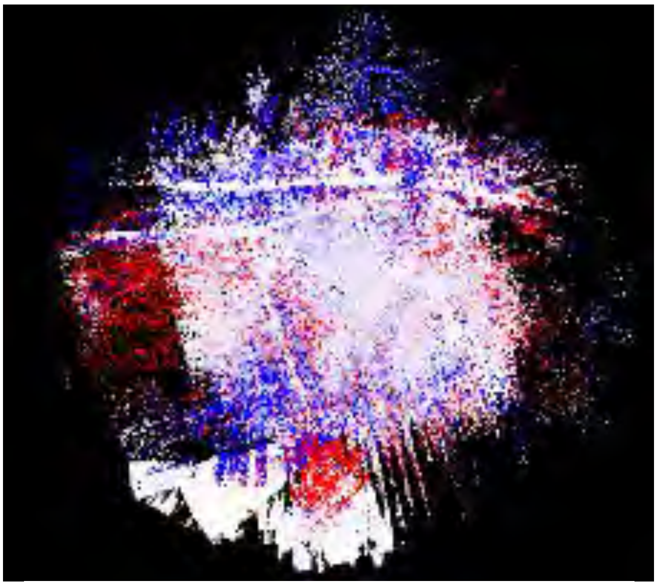

Colour	Flight align
White	Flights match
Blue	Flights Alignment Error <2.5m
Red	Flight Alignment Error > 2.5m

Figure 32: Flight alignment Site 2.

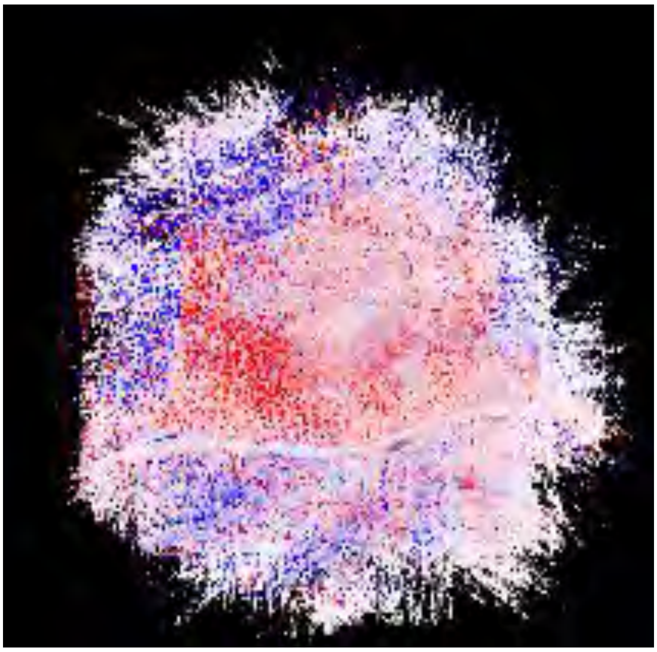

Colour	Flight align
White	Flights match
Blue	Flights Alignment Error <2.5m
Red	Flight Alignment Error > 2.5m

Figure33: Flight alignment Site 4.

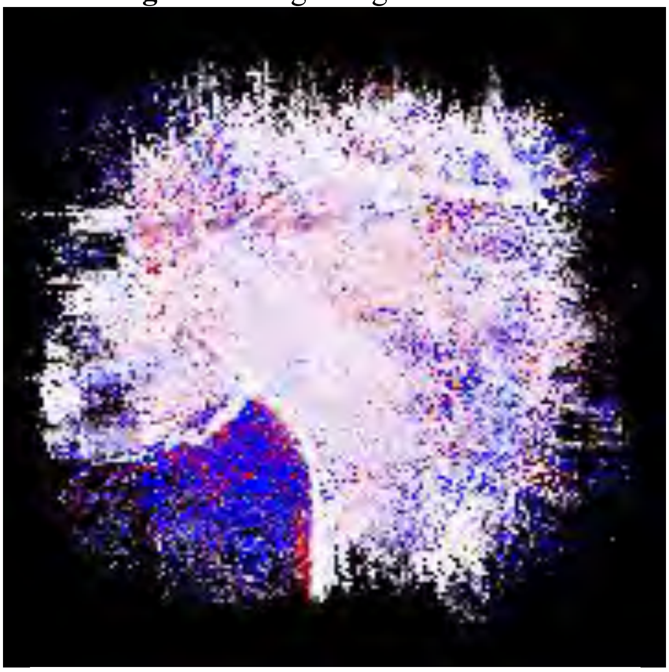

Colour	Flight align
White	Flights match
Blue	Flights Alignment Error <2.5m
Red	Flight Alignment Error > 2.5m

Figure 34: Flight alignment Site 8.

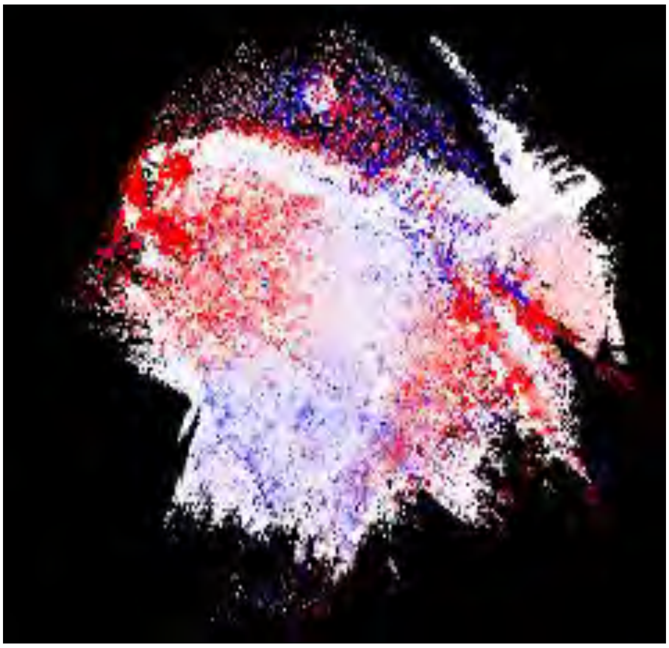

Colour	Flight align
White	Flights match
Blue	Flights Alignment Error <2.5m
Red	Flight Alignment Error > 2.5m

Figure 35: Flight alignment Site 9.

7. Pulse and Point Density

Nominal Point Spacing was checked, there is a constant down track and cross track point spacing that meets the LiDAR specifications (Tables 3 -6 , Figures 36 – 43)

SITE 2

Table 3: Pulse and point density.

Variables	Value
Pulses/m2	9,233.99
Returns/m2	16,829.95
Spacing: all returns(m)	0.01
Spacing: last returns(m)	0.01

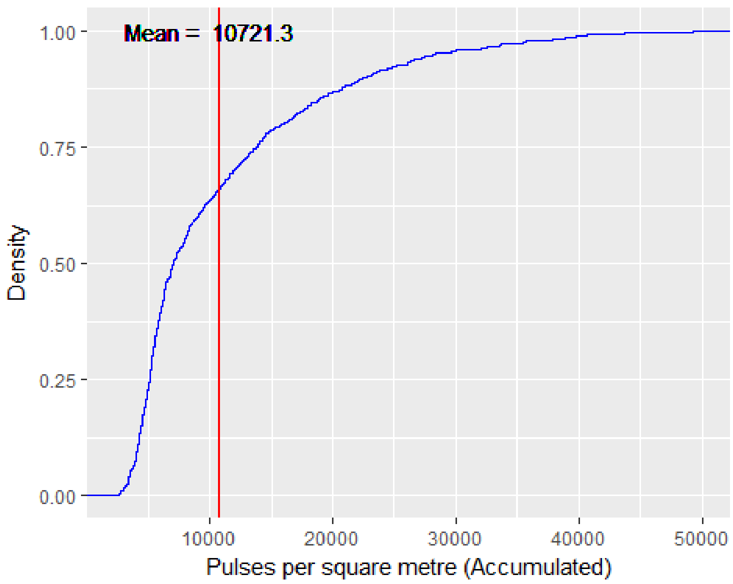

Figure 36: Accumulated pulses.

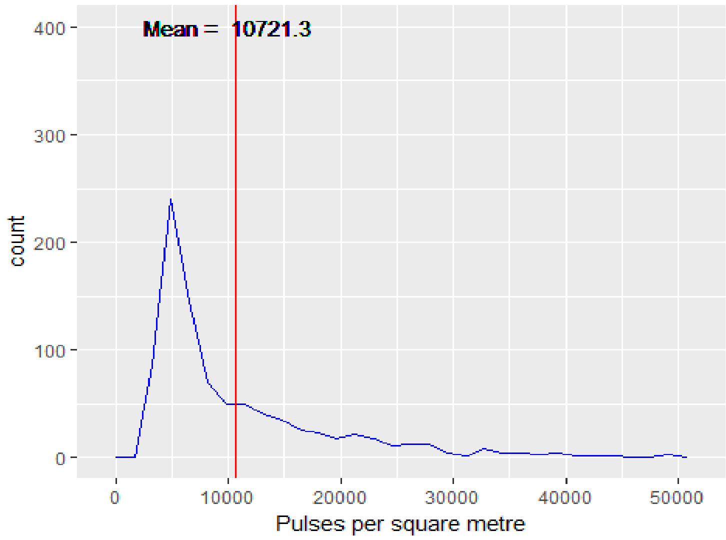

Figure 37: Counted pulses.

0.1% of area covered by < 2500 pulses/m2

92.1% of area covered by > 4000 pulses/m2

SITE 4

Table 4: Pulse and point density.

Variables	Value
Pulses/m2	6,824.55
Returns/m2	11,946.81
Spacing: all returns(m)	0.01
Spacing: last returns(m)	0.01

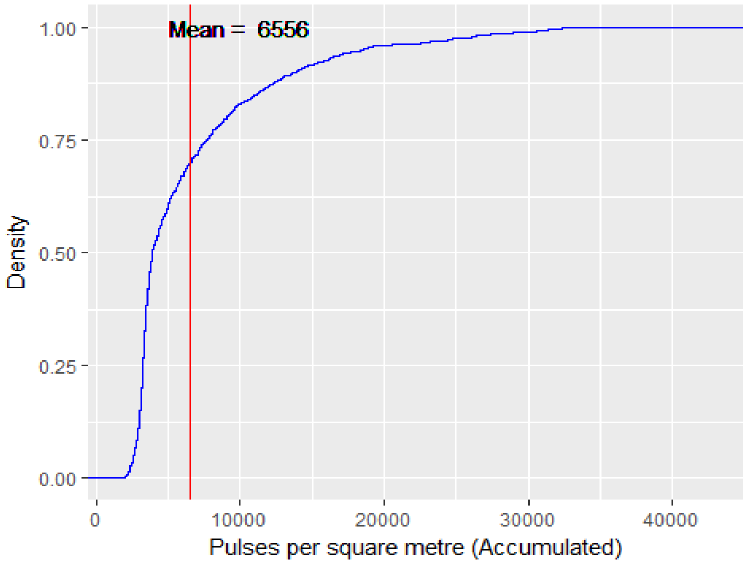

Figure 38: Accumulated pulses.

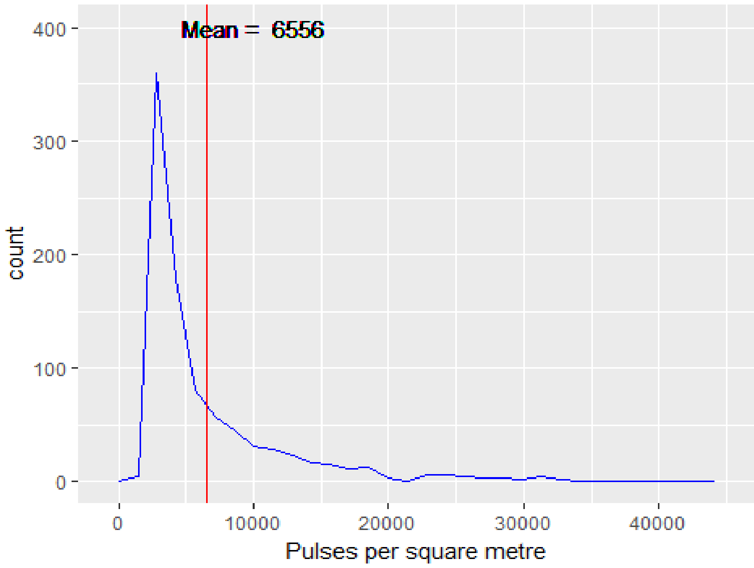

Figure 39: Counted pulses.

3.6% of area covered by < 2500 pulses/m2

49% of area covered by > 4000 pulses/m2

SITE 8

Table 5: Pulse and point density.

Variables	Value
Pulses/m2	7,954.95
Returns/m2	14,063.74
Spacing: all returns(m)	0.01
Spacing: last returns(m)	0.01

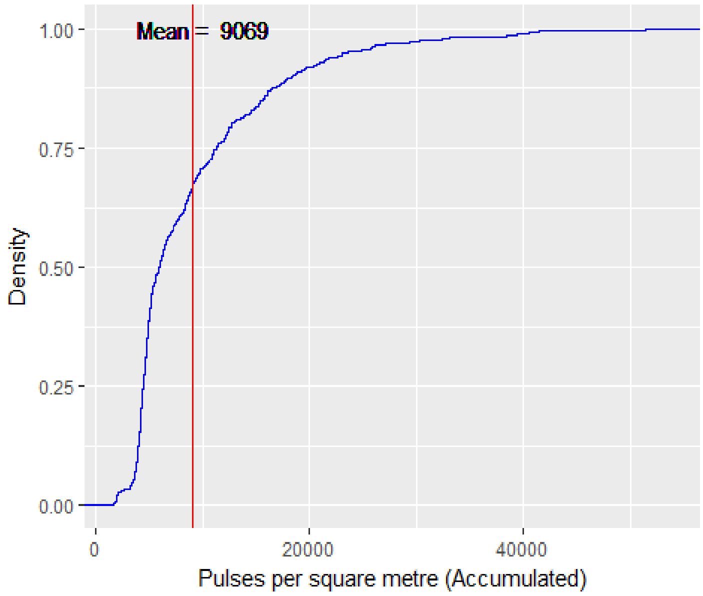

Figure 40: Accumulated pulses.

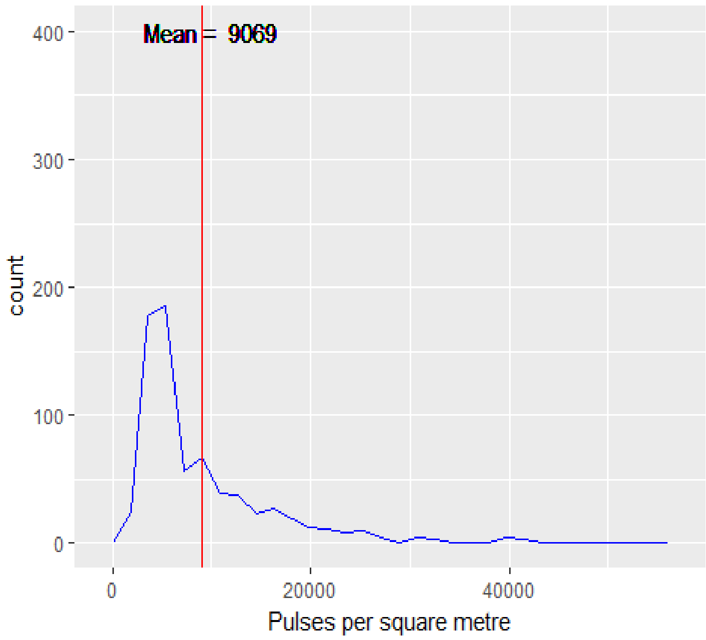

Figure 41: Counted pulses.

3.1% of area covered by < 2500 pulses/m2

86.2% of area covered by > 4000 pulses/m2

SITE 9

Table 6: Pulse and point density.

Variables	Value
Pulses/m2	5,322.1
Returns/m2	8,734.05
Spacing: all returns(m)	0.01
Spacing: last returns(m)	0.01

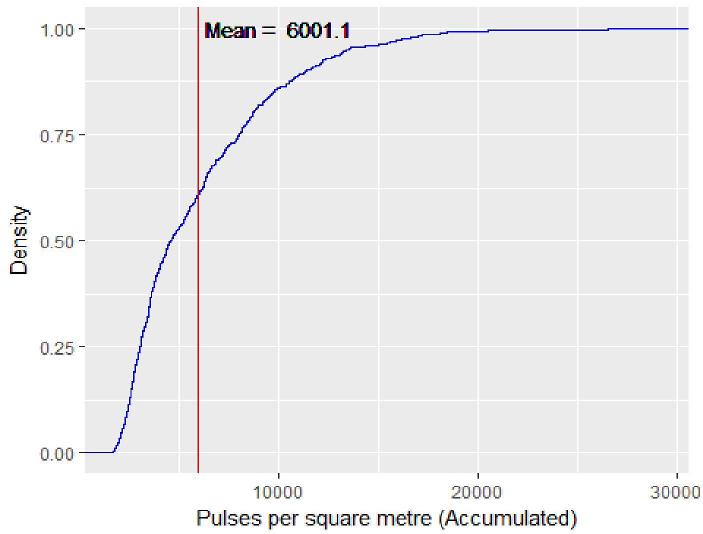

Figure 42: Accumulated pulses.

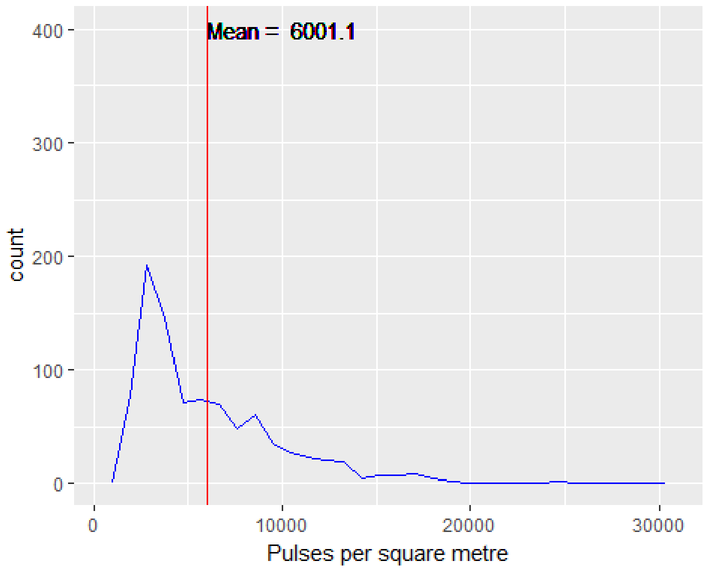

Figure 43: Counted pulses.

11.3% of area covered by < 2500 pulses/m2

57.2% of area covered by > 4000 pulses/m2

8. Return Intensity

All points have valid intensity values Range 0 – 65535 (Figures 44 – 47).

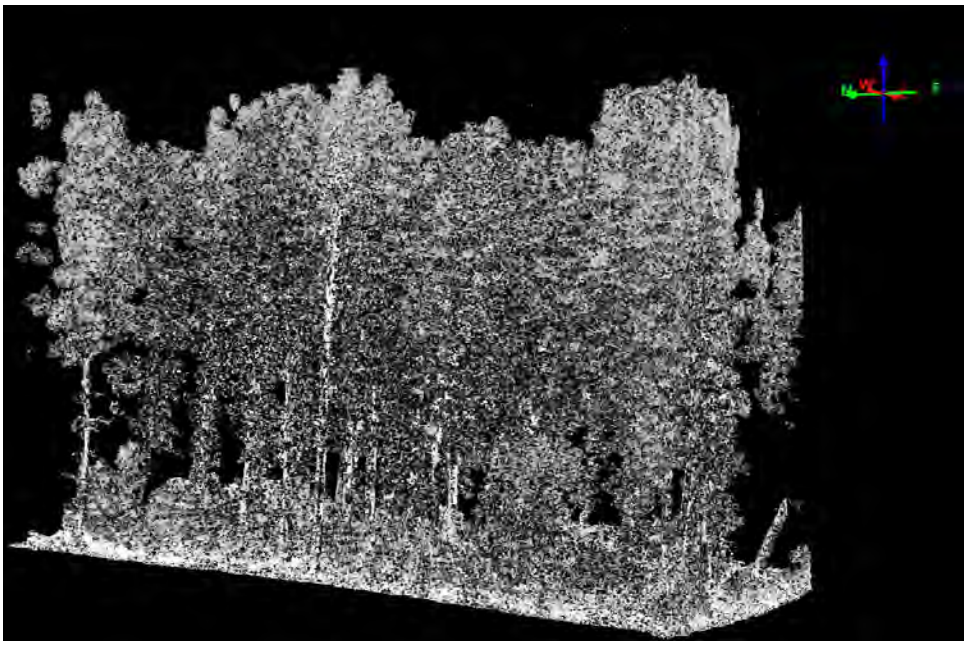

Figure44: Intensity example Site 2.

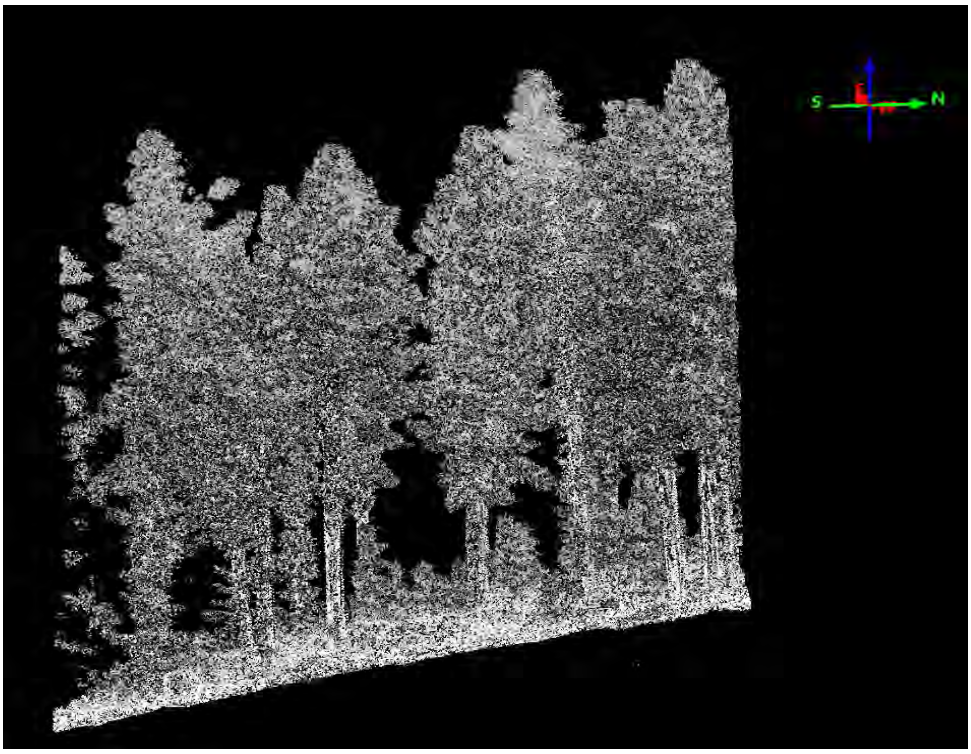

Figure 45: Intensity example Site 4.

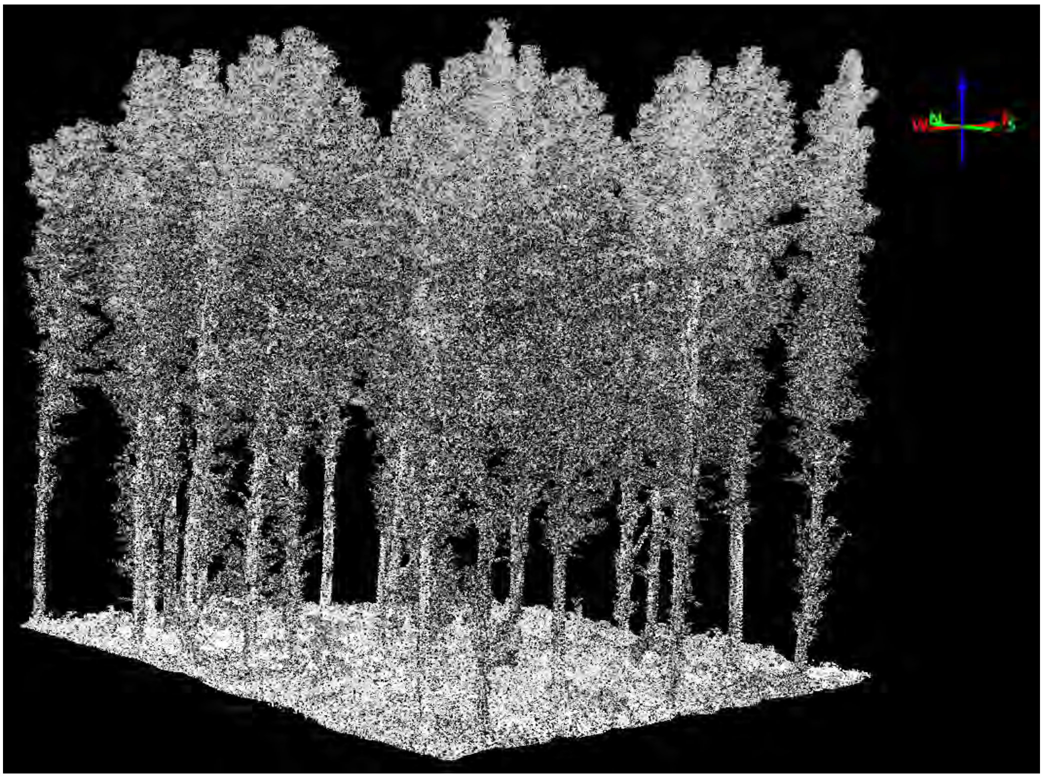

Figure 46: Intensity example Site 8.

Figure 47: Intensity example Site9.

9. Point Classification

SITE 2

Table 7: LiDAR classification.

Class	Description	# returns
1	unclassified	601,374,882
2	ground	87,260,622
7	noise	988,481

Figure 48: Classification example.

Example of the point classification provided in Figure 48

SITE 4

Table 8: LiDAR classification.

Class	Description	# returns
1	unclassified	412,027,232
2	ground	73,962,506
7	noise	1,487,745

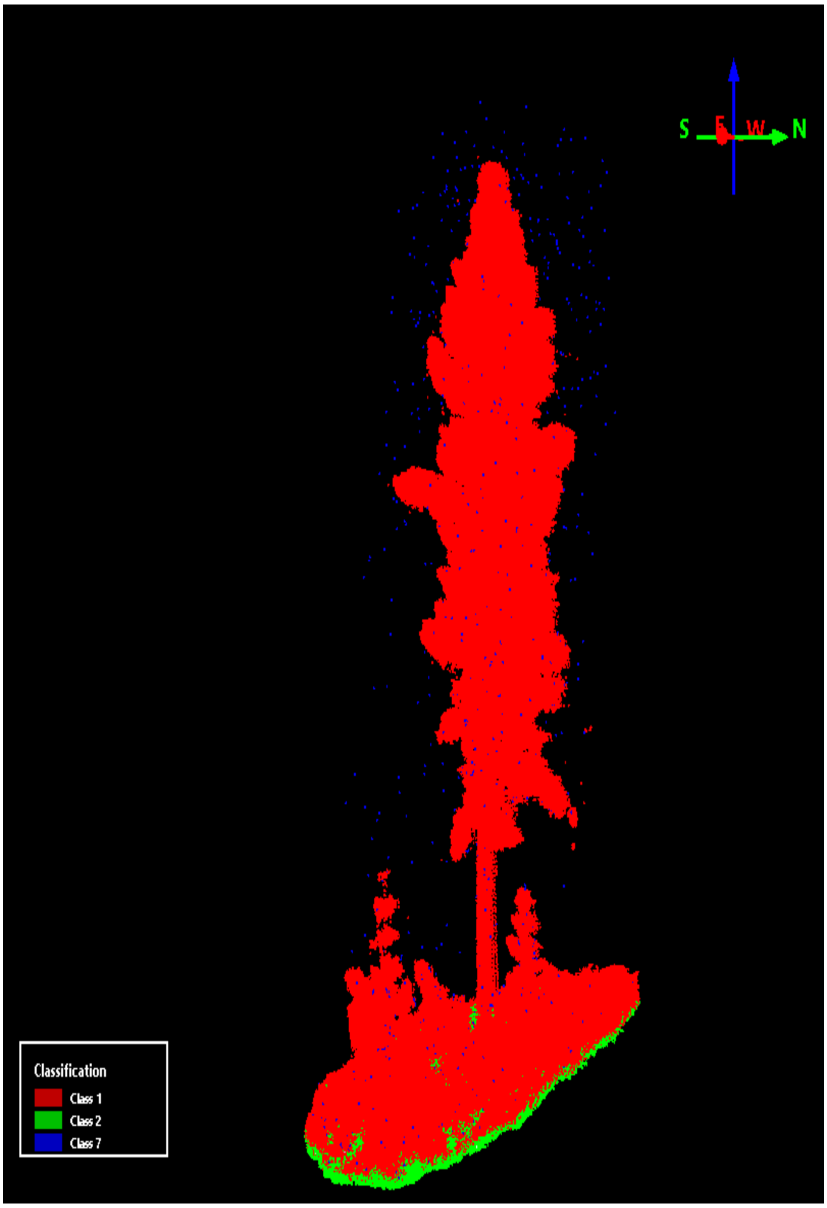

Figure 49: Classification example.

Example of the point classification provided in Figure 49

SITE 8

Table 9: LiDAR classification.

Class	Description	# returns
1	unclassified	477,318,962
2	ground	94,912,945
7	noise	1,624,835

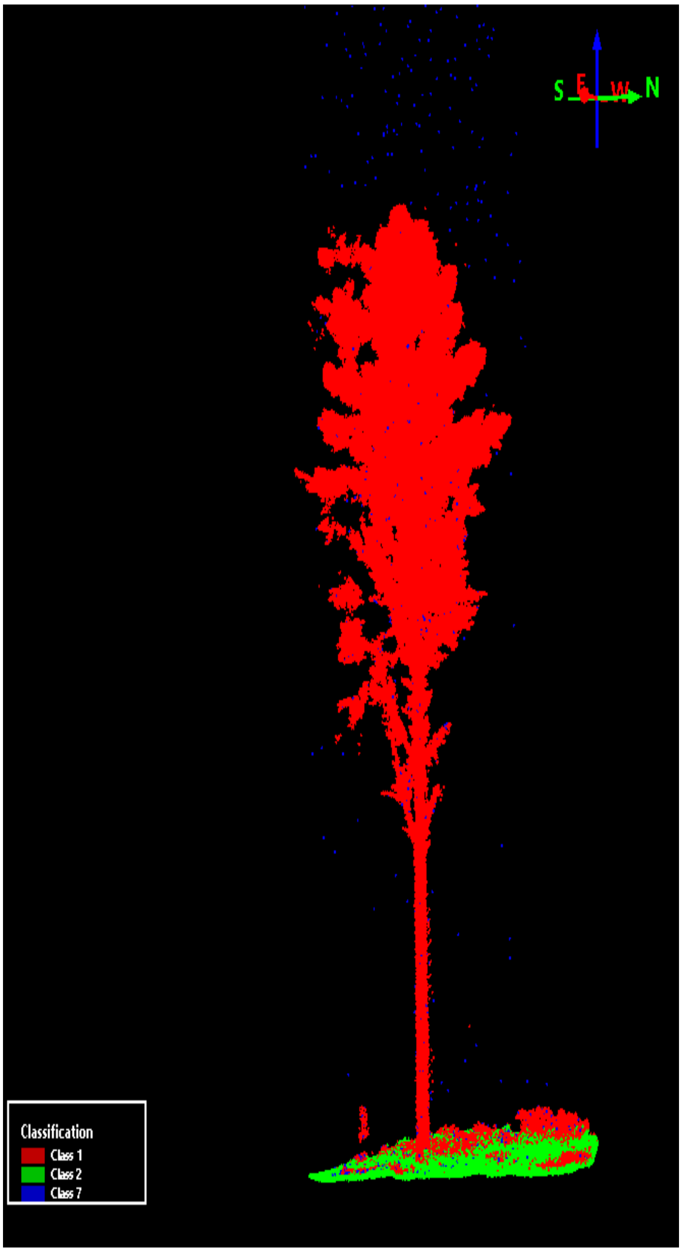

Figure 50: Classification example.

Example of the point classification provided in Figure 50.

SITE 9

Table 10: LiDAR classification.

Class	Description	# returns
1	unclassified	299,983,331
2	ground	62,625,293
7	noise	378,371

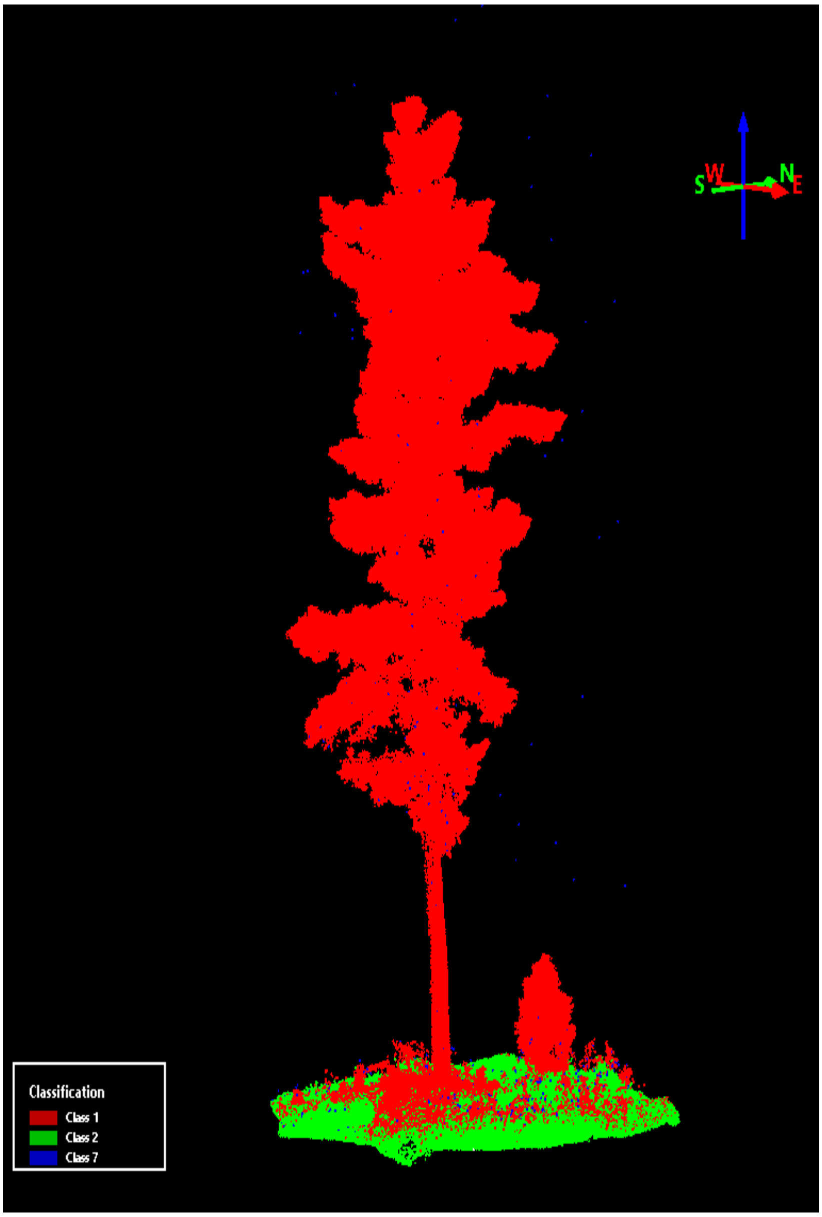

Figure 51: Classification example.

Example of the point classification provided in Figure 51.

9.1 Class 1

Class 1, unclassified data, corresponds mainly to the vegetation class in this project. This class is acceptable as per requirements (Figures 52 – 55).

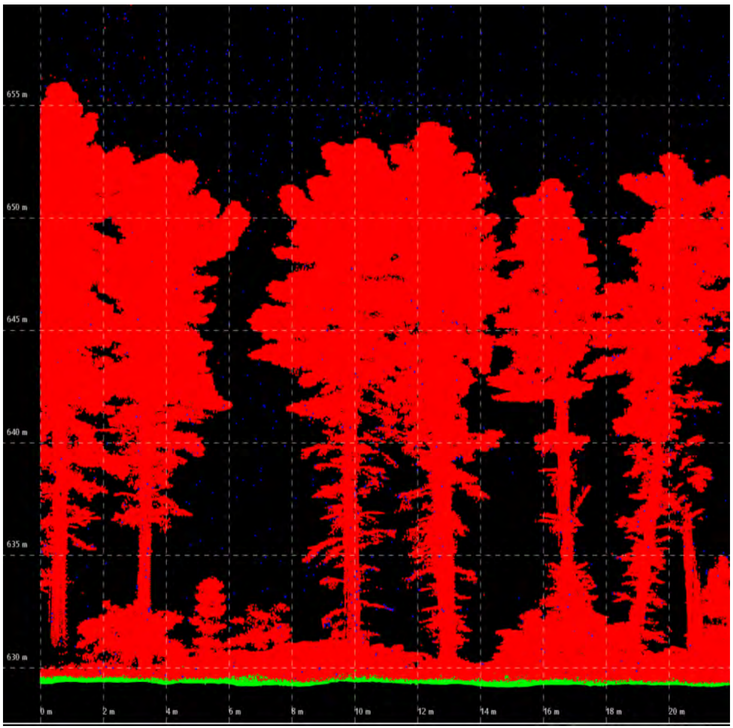

Figure 52: Site 8, 3m width, Classification Profile.

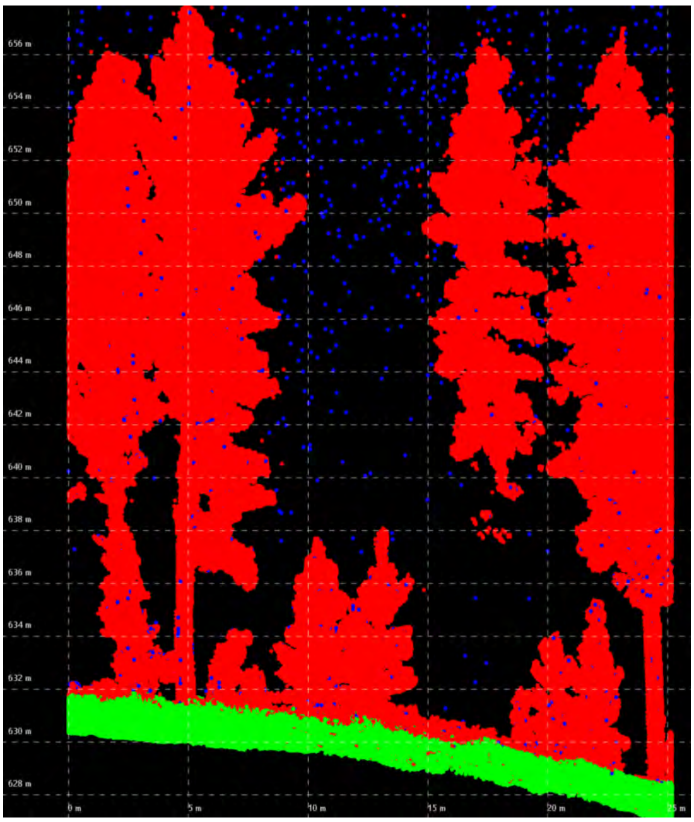

Figure 53: Site 4, 3m width, Classification Profile.

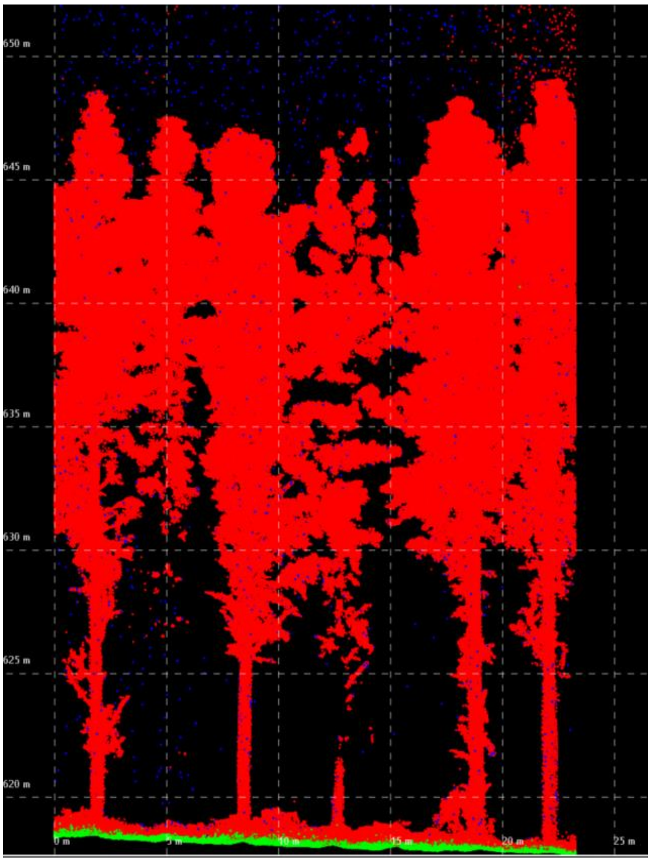

Figure 54: Site 8, 3m width, Classification Profile.

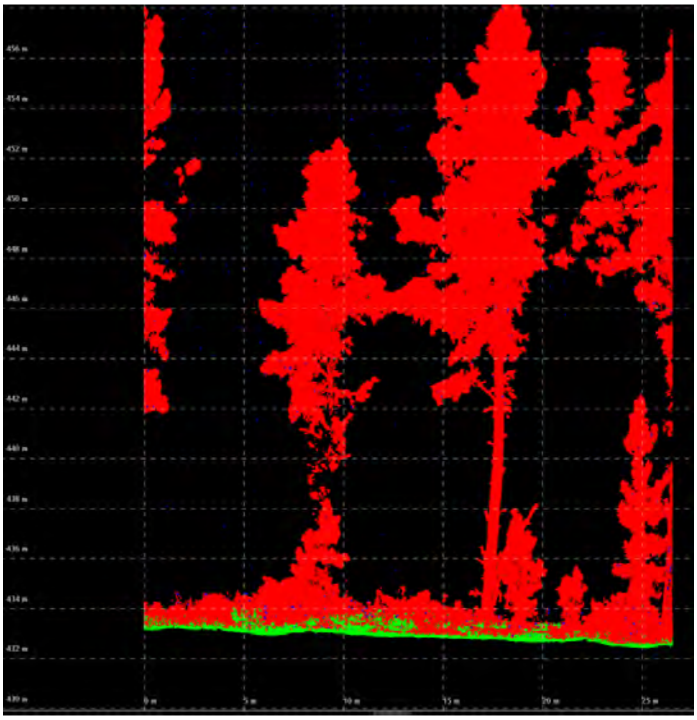

Figure 55: Site 9, 3m width, Classification Profile.

9.2 Class 2

All the tiles contain Class 2 (ground), acceptable as per requirements (Figures 56 – 59)

Figure 56: Ground coverage Site 2

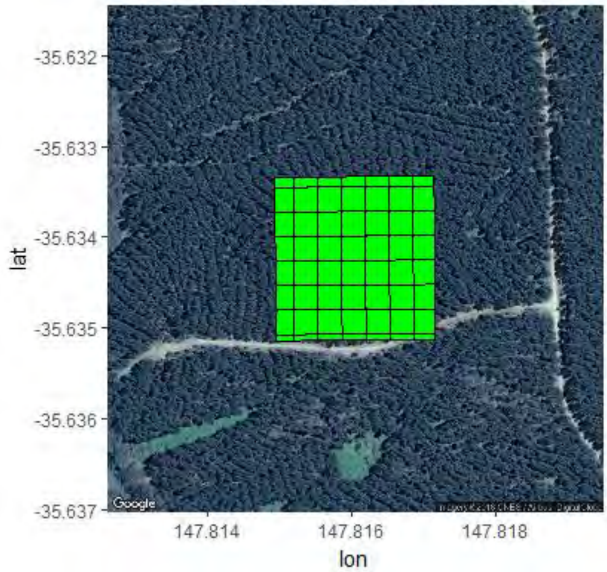

Figure 57: Ground coverage Site 4.

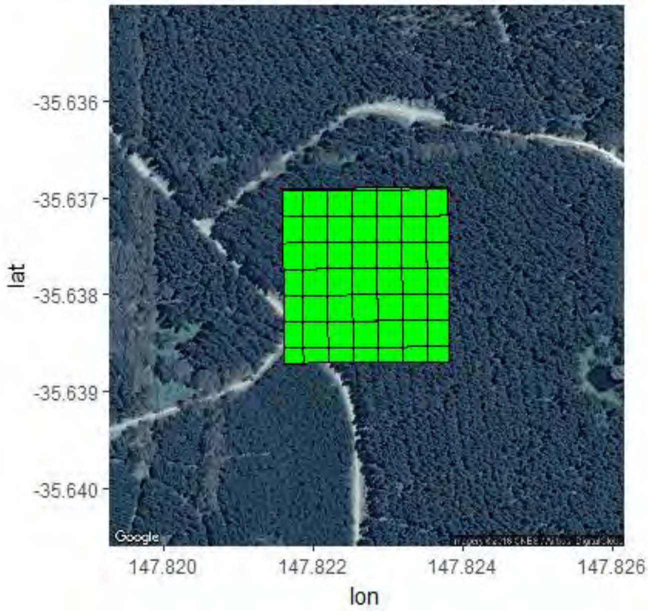

Figure 58: Ground coverage Site 8.

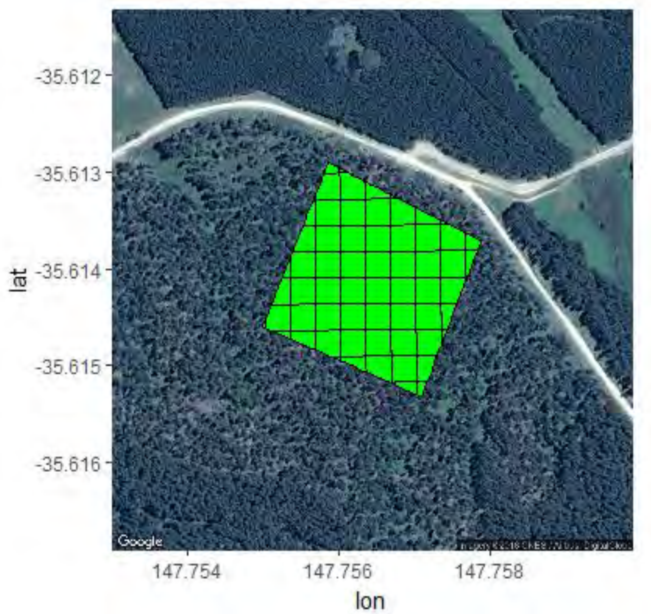

Figure 59: Ground coverage Site 9.

9.3 Class 7

Areas of concentrated noise were investigated for outliers or misclassification Figures 60 – 63).

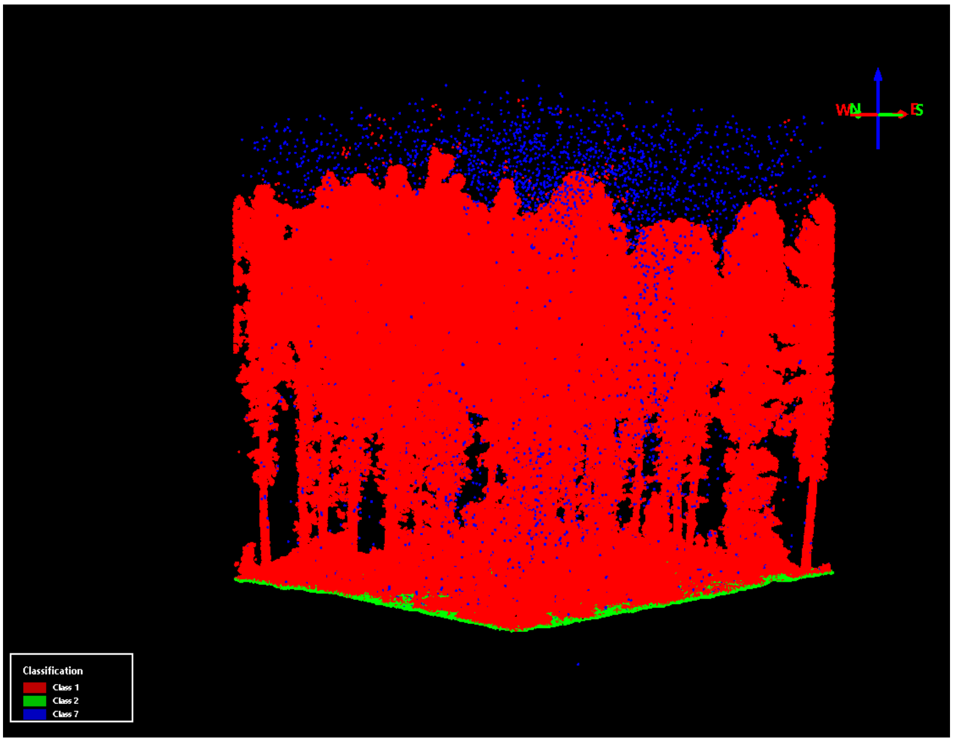

Figure 60: Noise Site 2.

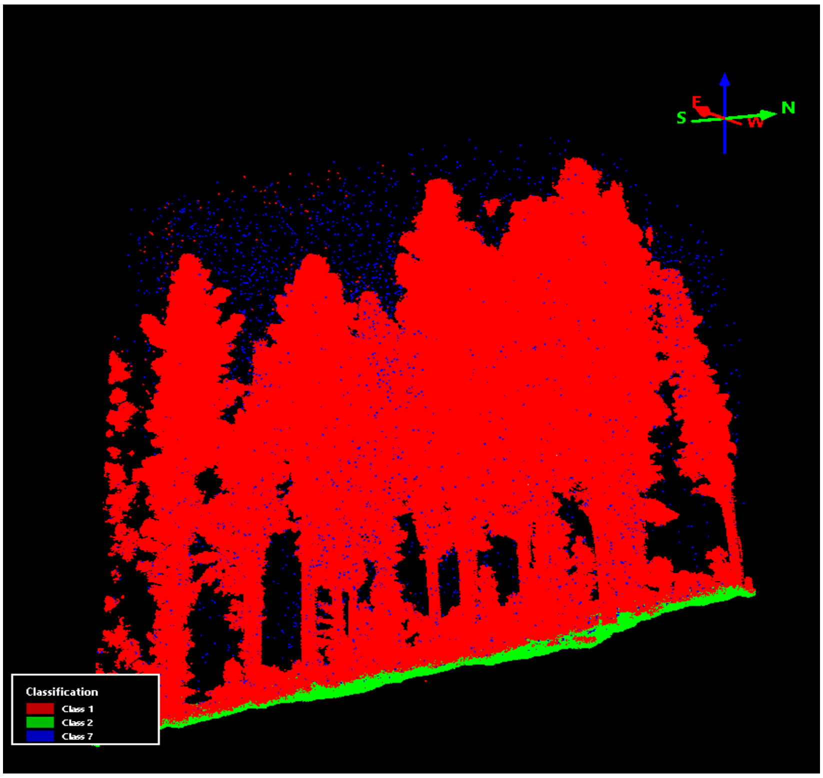

Figure 61: Noise Site 4.

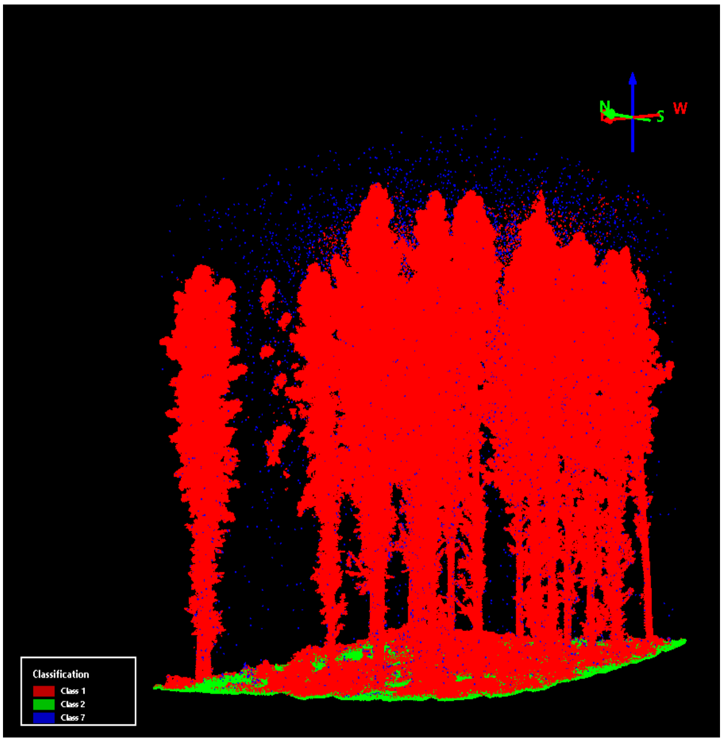

Figure 62: Noise Site 8.

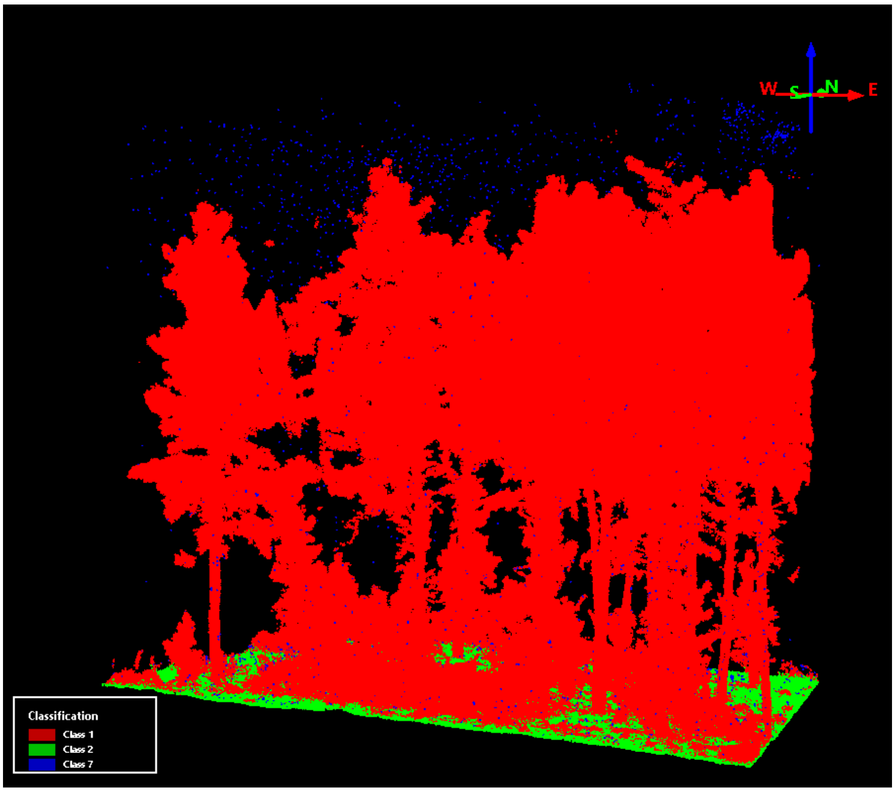

Figure 63: Noise Site 9.

10. Noise and Data Errors

All noise was correctly classified as noise. All errors found in the dataset were corrected.

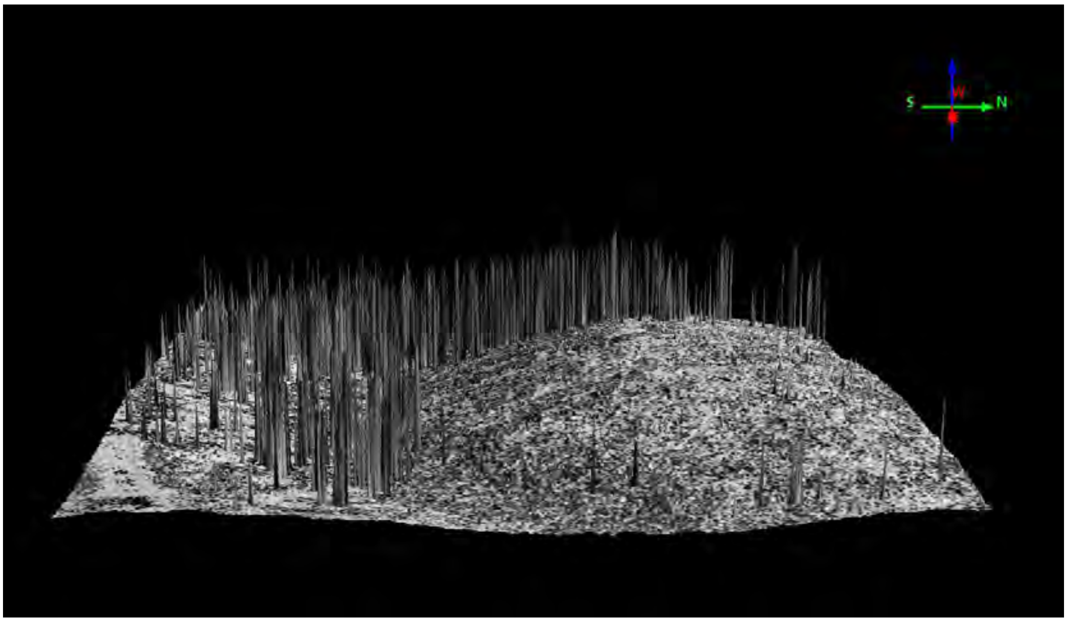

Figure 64: Digital Terrain Model (DTM) Error.

11. Spatial Products

Interpine have derived a number of additional spatial products from the raw LiDAR data provided by the supplier (Figures 65 – 68).

- DTM

  1m digital terrain model derived through triangulated mesh.

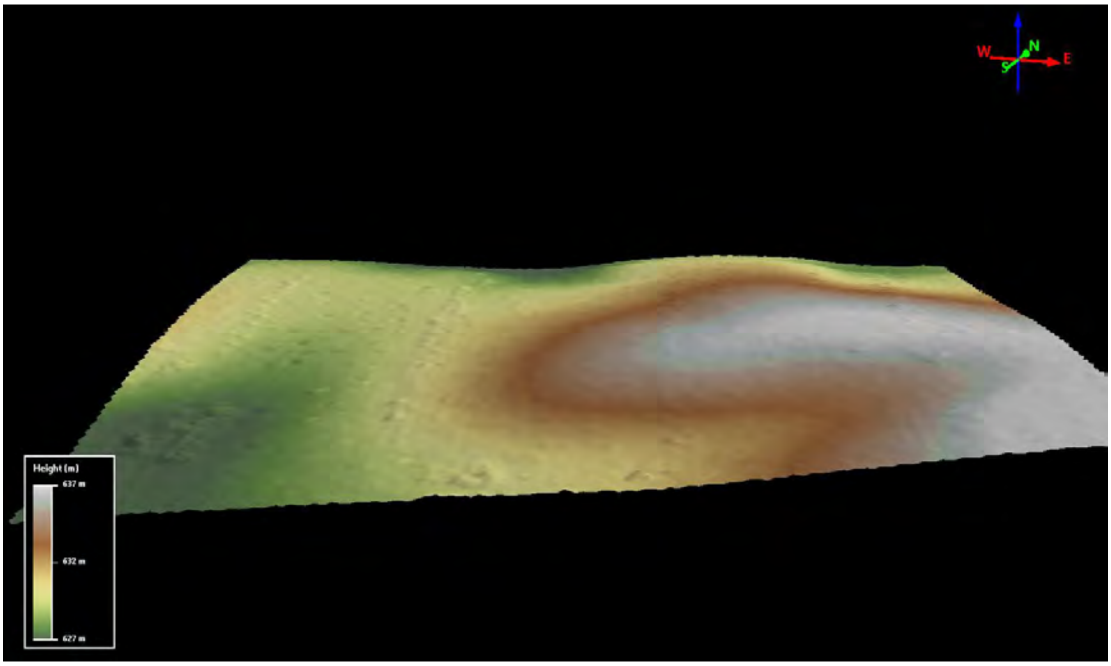

Figure 65: DTM Site 2.

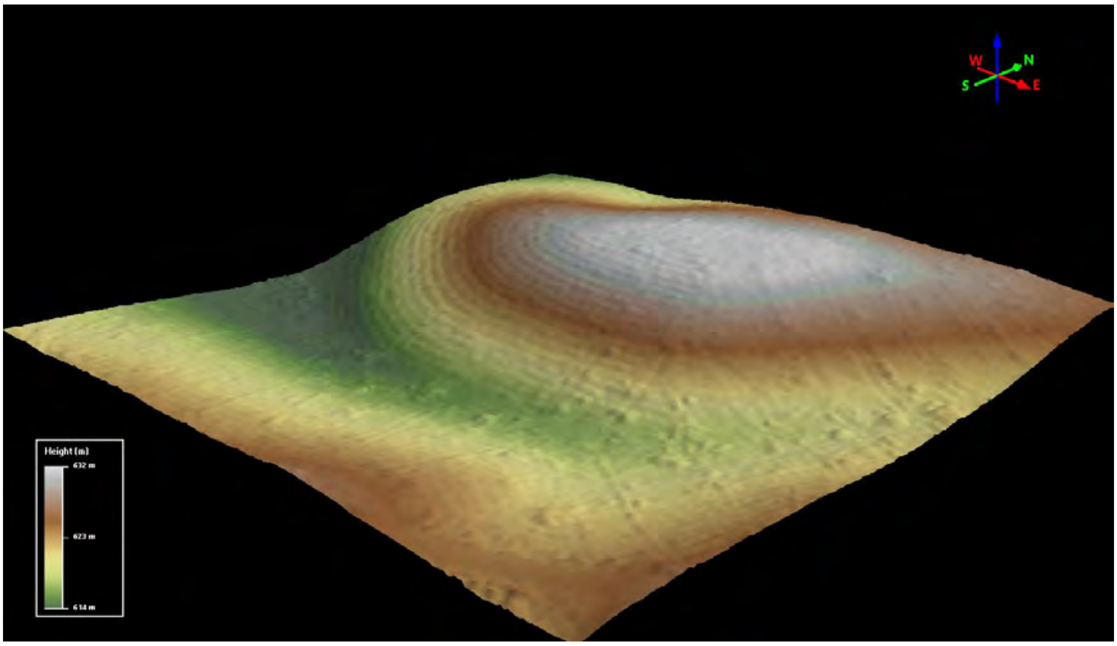

Figure 66: DTM Site 4.

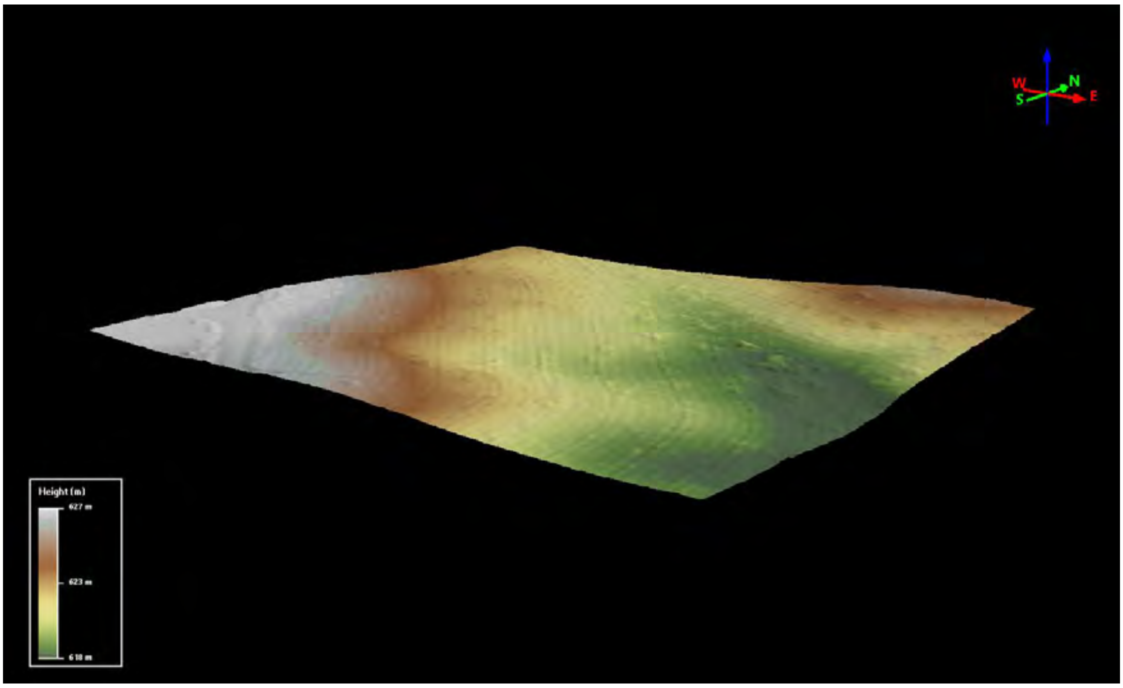

Figure 67: DTM Site 8.

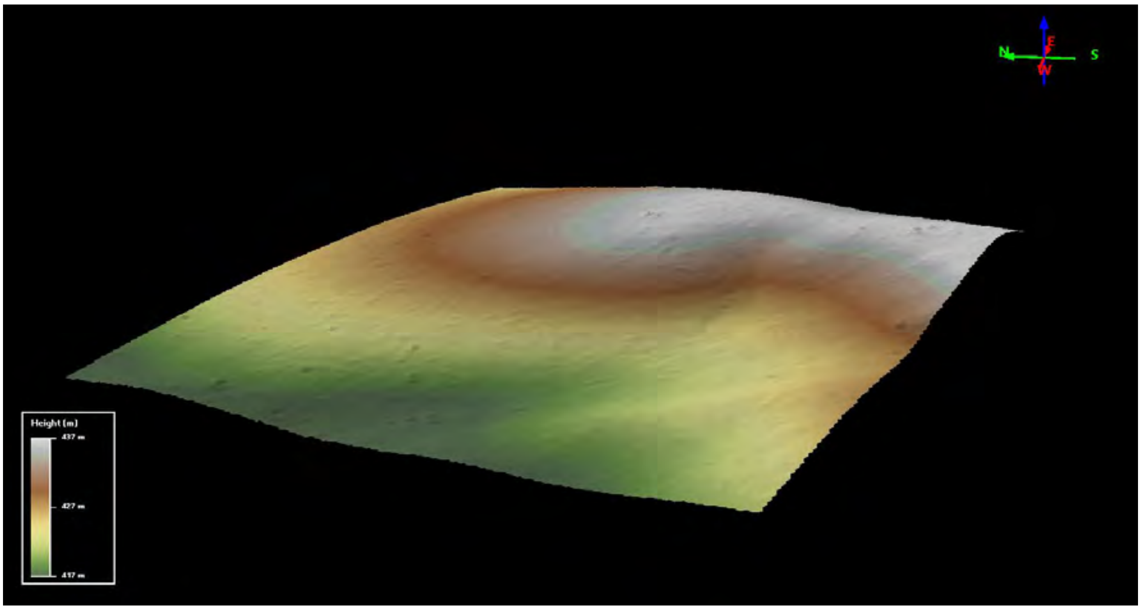

Figure 68: DTM Site 9.

- HILLSHADE

  This raster is derived from the DTM for 2D representation (Figures 69 – 72).

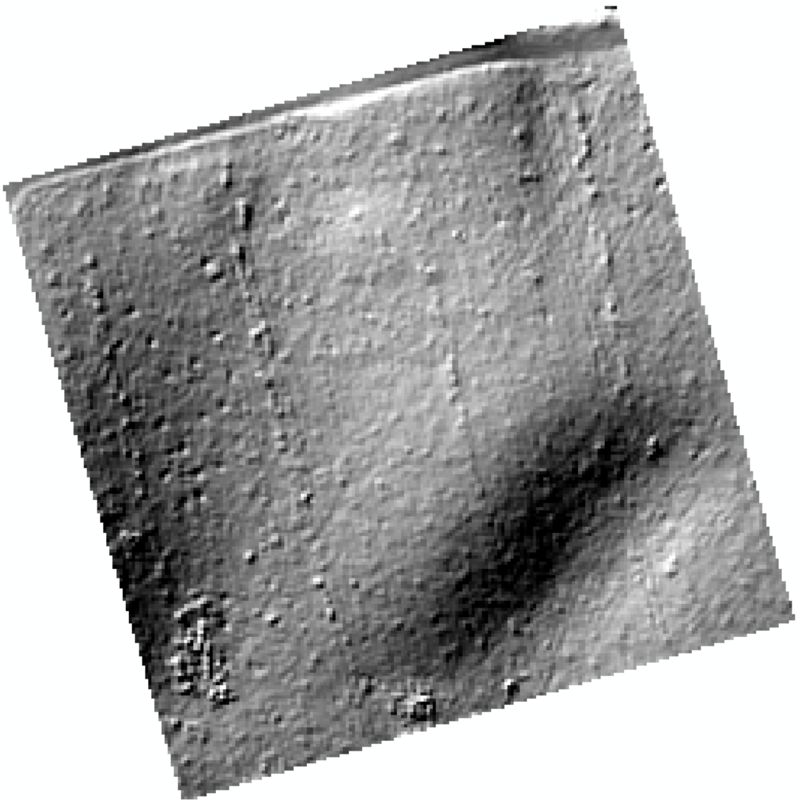

Figure 69: Hillshade Site 2.

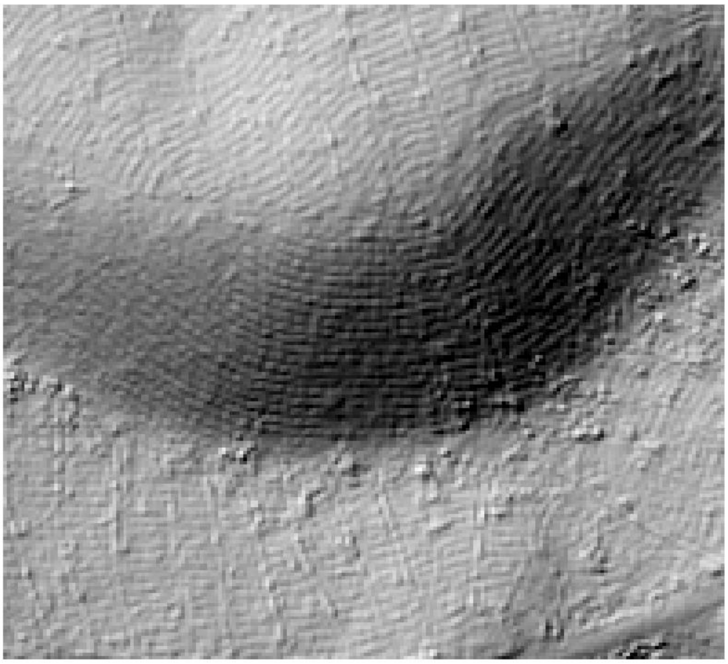

Figure 70: Hillshade Site 4.

Figure 71: Hillshade Site 8.

Figure 72: Hillshade Site 9.

- CONTOURS

  5m contours derived from the DTM were computed (Figures 73 – 76).

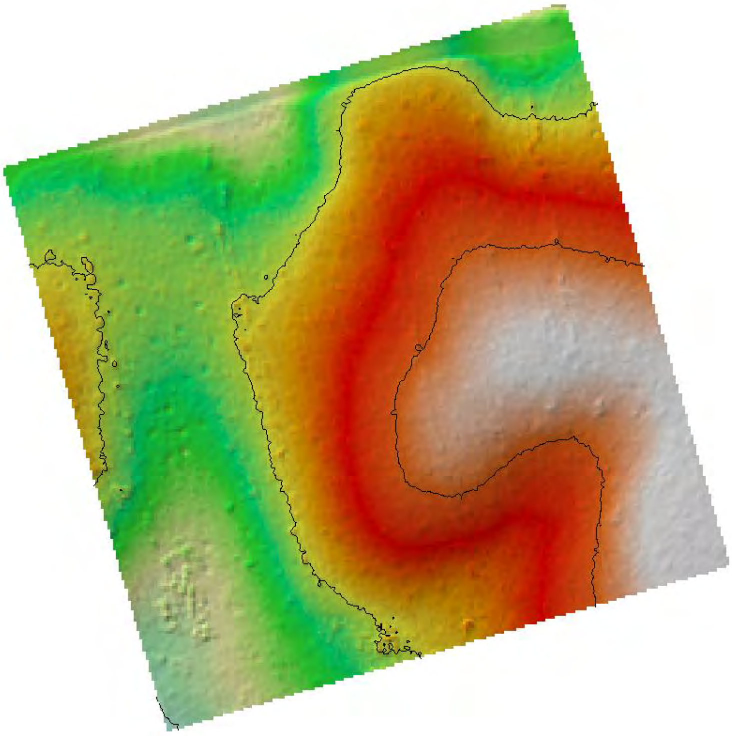

Figure 73: Contours Site 2.

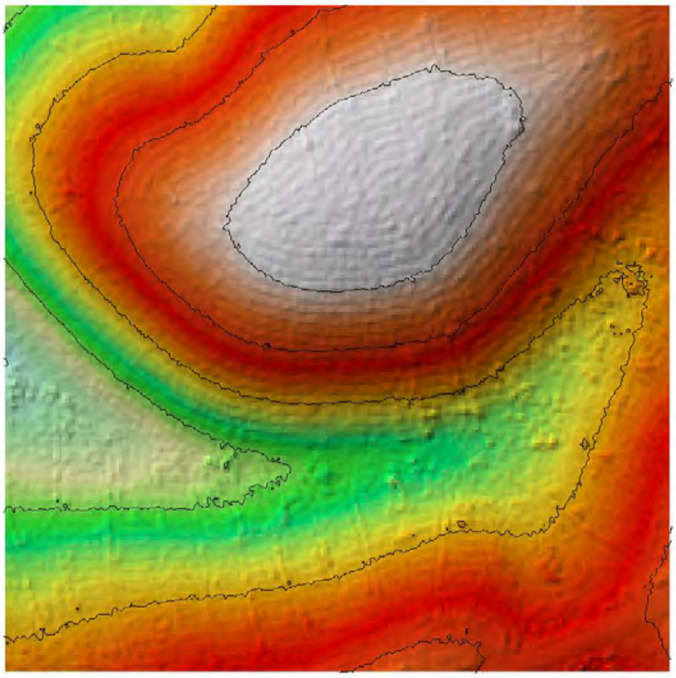

Figure 74: Contours Site 4.

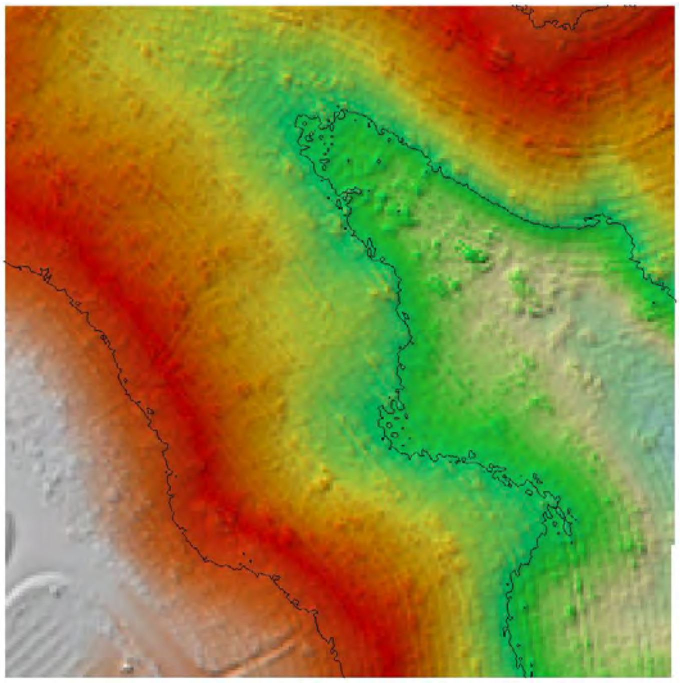

Figure 75: Contours Site 8.

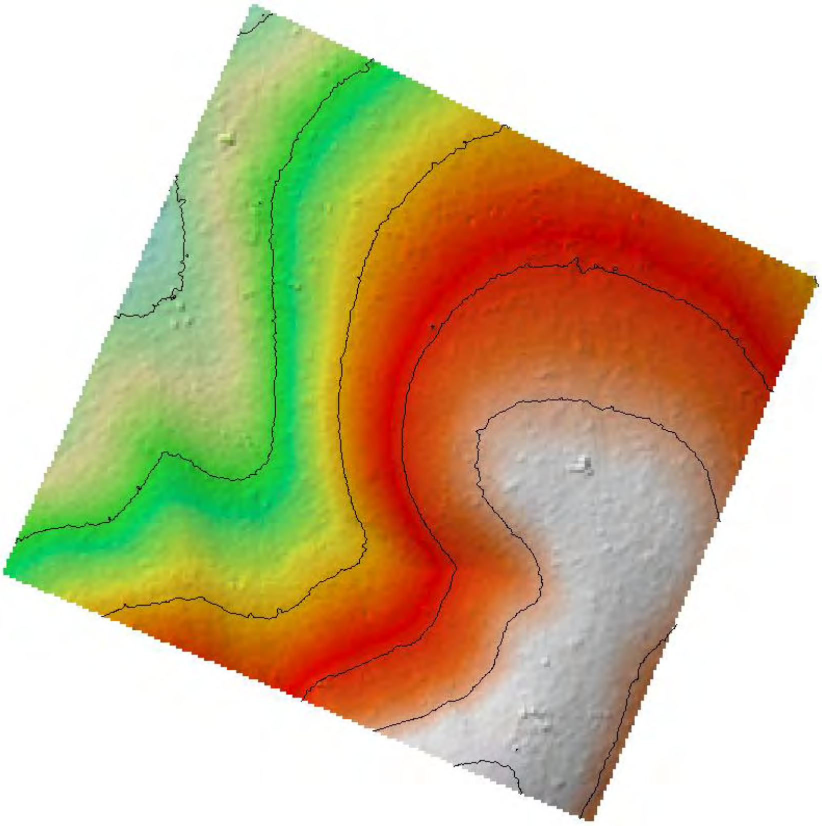

Figure 76: Contours Site 9.

- Canopy Height Model (CHM)

  The Canopy Height Model is a type of DSM (digital surface model) specific to the vegetation canopy. This is derived using a pit-free algorithm at 0.3m resolution (Figures 77 – 80).

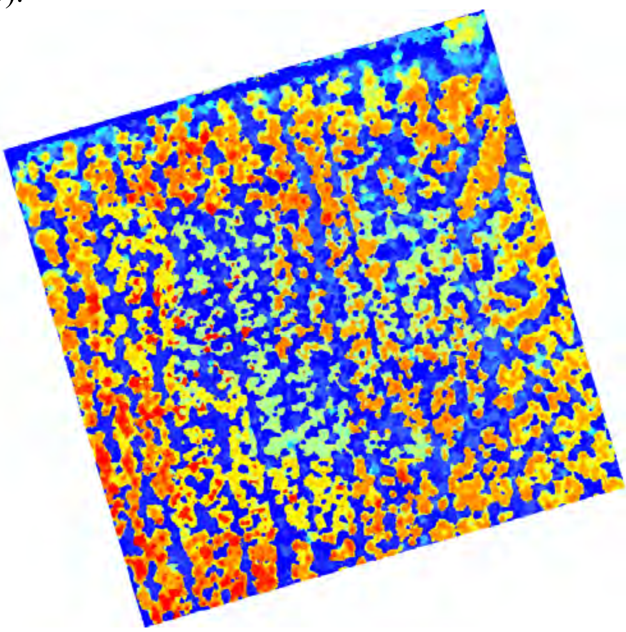

Figure 77: CHM at 60m with 0.3m resolution Site 2.

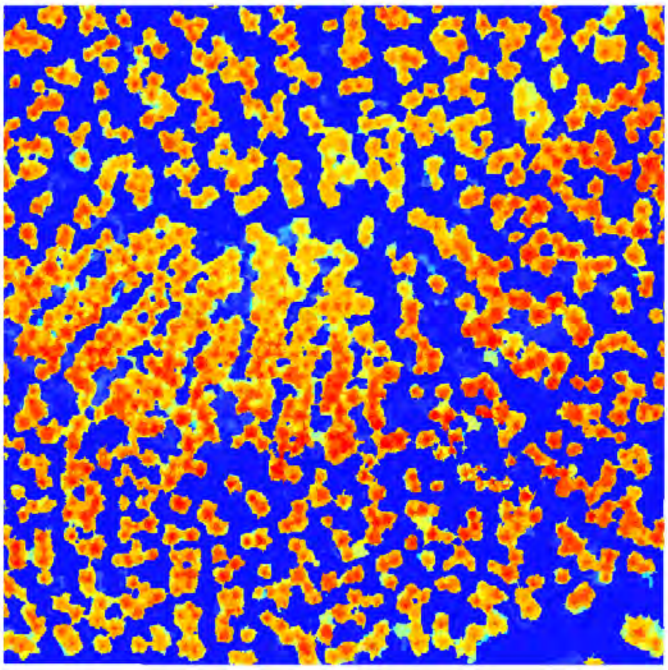

Figure 78: CHM at 60m with 0.3m resolution Site 4.

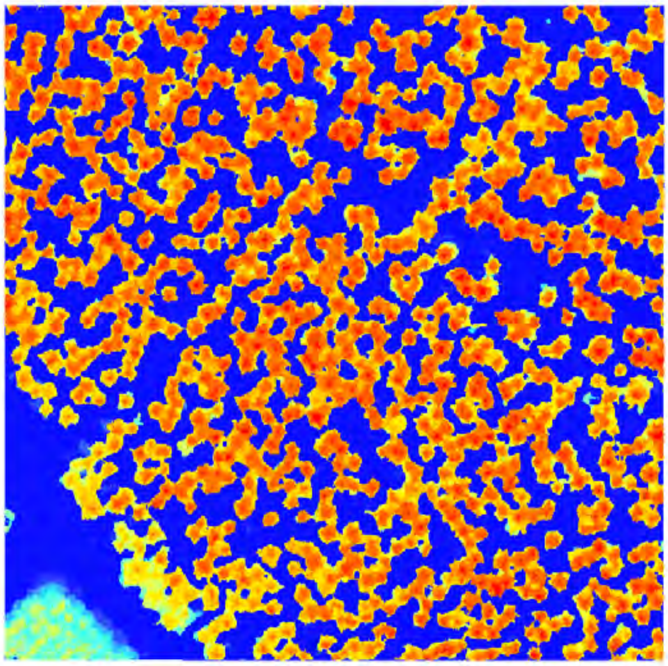

Figure 79: CHM at 60m with 0.3m resolution Site 8.

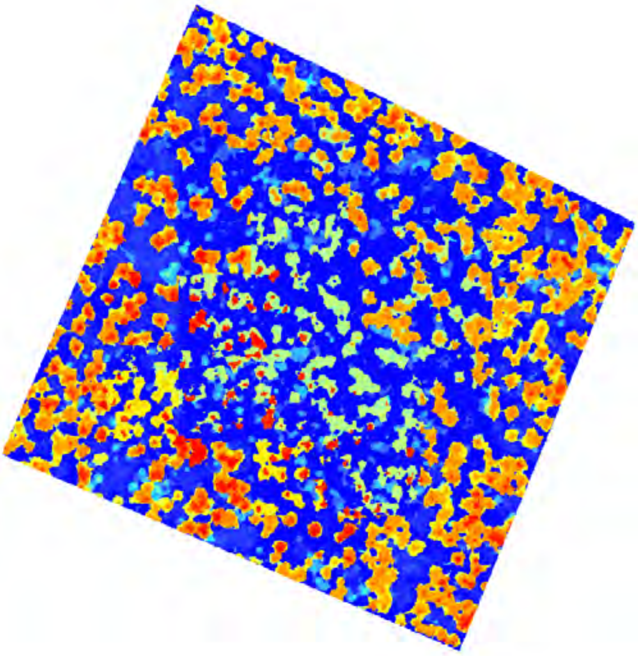

Figure 80: CHM at 60m with 0.3m resolution Site 9.

- PEAKS

Potential tree tops and crown detection (Figures 81 - .

SITE 2

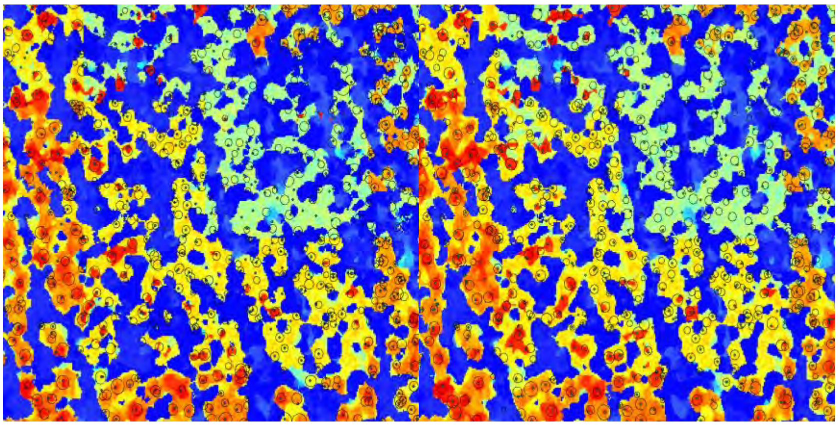

Figure 81 – 84: Peaks detected at 30m (left) and 60m (right) with potential crown estimation - Scale at 1:400.

SITE 4

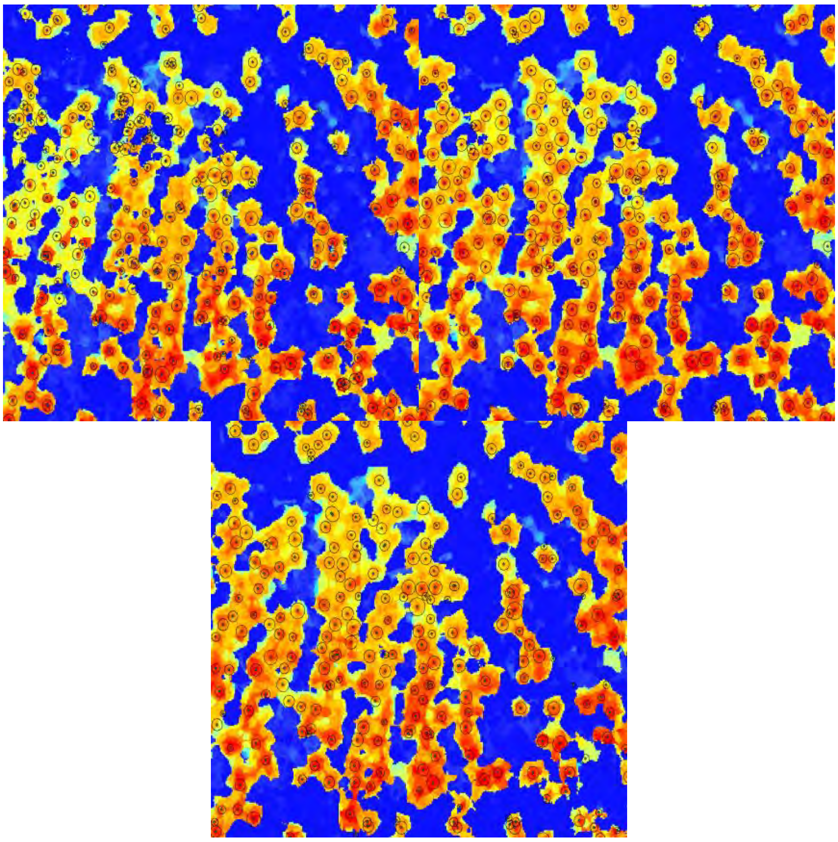

Figure 82: Peaks detected at 30m (left), 60m (central) and 90m (right) with potential crown estimation - Scale at 1:400.

SITE 8

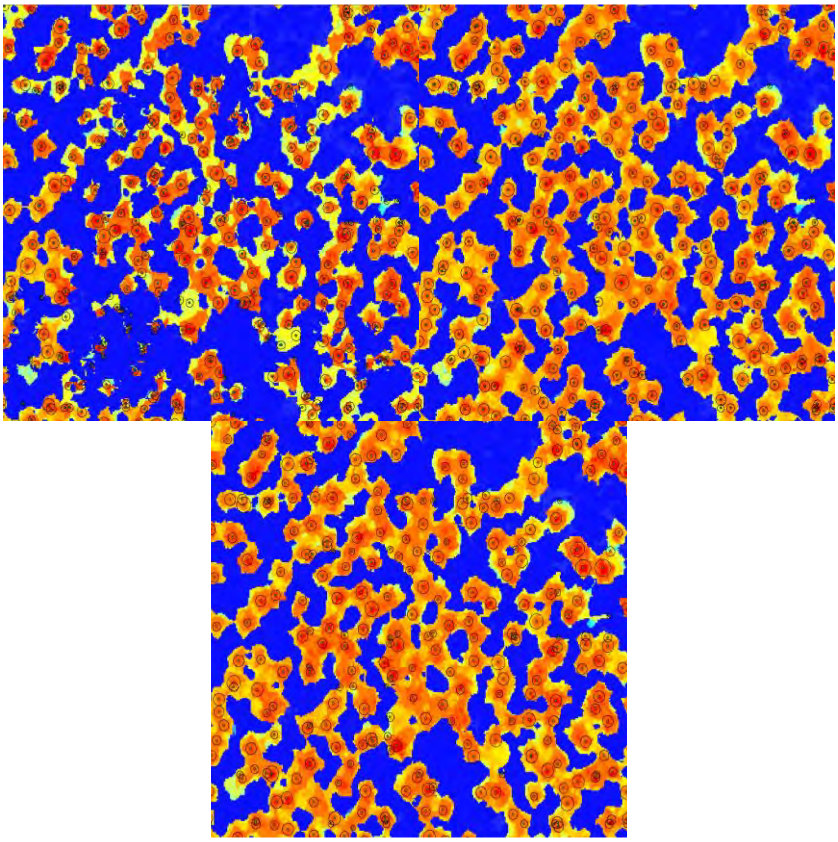

Figure 83: Peaks detected at 30m (left), 60m (central) and 90m (right) with potential crown estimation - Scale at 1:400.

SITE 9

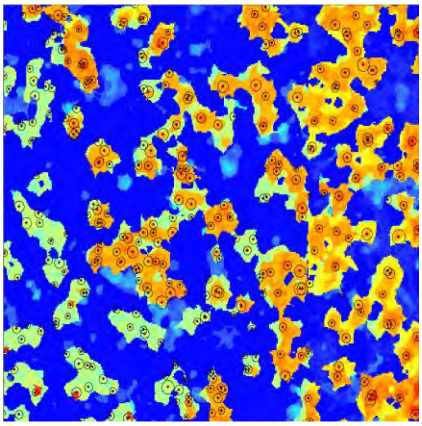

Figure 84: Peaks detected at 60m with potential crown estimation - Scale at 1:400.

13. Summary and Next Steps

Table 11: Check list

QC CHECKED	CHECKED BY	CHECKED ON	PASS/FAIL	COMMENT
Lidar Sensor Scan Set	SG	Feb/March 2018	Pass	VUX-1LR
Footprint	SG	Feb/March 2018	Pass	
Laz files	SG	Feb/March 2018	Fail	Conversion from LAS to LAZ
Correct Header Information	SG	Feb/March 2018	Pass	
Contains Gps Times	SG	Feb/March 2018	Pass	
Contains Intensity Values	SG	Feb/March 2018	Pass	
Contains Easting	SG	Feb/March 2018	Pass	
Contains Northing	SG	Feb/March 2018	Pass	
Contains Elevation	SG	Feb/March 2018	Pass	
Tile To 30 m X 30 m Tile Grid	SG	Feb/March 2018	Pass	Tiles were generated
Classified with Class 1 – Unclassified	SG	Feb/March 2018	Pass	
Classified with Class 2 – Bare-Earth Ground	SG	Feb/March 2018	Pass	
Classified with Class 7 – Noise	SG	Feb/March 2018	Pass	
Classified With User Class	SG	Feb/March 2018	Fail	User data was defined as 3, 6 and 9
Check For Any Misclassification	SG	Feb/March 2018	Fail	Full dataset was reclassified
Check for False Low and High Points That Are Wrongly Classified to Ground Class.	SG	Feb/March 2018	Pass	
Check for Abnormal Spikes in Data.	SG	Feb/March 2018	Warning	Reviewed rasters: DTM and P95
All Files Contains First Return Lidar Data	SG	Feb/March 2018	Pass	
All Files Contains Last Return Lidar Data	SG	Feb/March 2018	Pass	
Files Contain Multiple Returns (Minimum First, Last, And One Intermediate)	SG	Feb/March 2018	Pass	
Files Contain Single Returns	SG	Feb/March 2018	Pass	
Number Of Returns	SG	Feb/March 2018	Pass	
At Least 90% Of the Tiles Contain At Least 3 Points	SG	Feb/March 2018	Pass	
Shapefile of Area of Interest	SG	Feb/March	Fail	Shapefile created

		2018		
Shapefile of Planned Flight Lines	SG	Feb/March 2018	Fail	Shapefile created
Index Project Boundary Delivered as Shapefile	SG	Feb/March 2018	Fail	Shapefile created
Project Area Coverage – Buffered by A Minimum of X Meters	SG	Feb/March 2018	Pass	
Tile Named According with Shapefile	SG	Feb/March 2018	Pass	Tiles were naming according with the project name
Non-Overlapped Tiling Scheme	SG	Feb/March 2018	Pass	
Projection Information, Datum and Units	SG	Feb/March 2018	Pass	
Control Points - Gps Checkpoints	SG	Feb/March 2018	Pass	GPS report generated
Vertical Accuracy / Vertical Offset	SG	Feb/March 2018	Pass	
Horizontal Accuracy	SG	Feb/March 2018	Pass	
Scan Angle Rank	SG	Feb/March 2018	Pass	
Correct Number of Files Delivered and All Files Adhere to Project Format Specifications	SG	Feb/March 2018	Pass	Data supply check
Las Statistics Are Run to Check for Inconsistencies	SG	Feb/March 2018	Pass	Created P95 raster and compared with plot height and plot metrics
Density Raster	SG	Feb/March 2018	Pass	dns rasted created
Excessive Noise	SG	Feb/March 2018	Fail	Data was corrected
Elevation Steps	SG	Feb/March 2018	Pass	
Other Anomalies Present in The Point Cloud	SG	Feb/March 2018	Pass	
Deliverable Tiles Checked for Significant Gaps Not Covered By Aerial Acquisition Checks And/Or Caused By Data Post-Processing/Filtering	SG	Feb/March 2018	Pass	
Duplicated Points	SG	Feb/March 2018	Pass	Duplicated points were removed

- Some misclassification in class 7 (noise), but within the tolerance allowed for contract, this was fixed.
- Interpine recommends acceptance of the supplied data.
- The VUX-1LR LiDAR dataset meets specifications.

References

Brede, B., Lau, A., Bartholomeus, H. and Kooistra, L. (2017). Comparing RIEGL RiCOPTER UAV LiDAR Derived Canopy Height and DBH with Terrestrial LiDAR. Sensors, 17(10), p.2371.

He, Yi & Song, Ziqi & Liu, Zhaocai. (2017). Updating Highway Asset Inventory Using Airborne LiDAR. Measurement. 104. 132-141. 10.1016/j.measurement.2017.03.026.

Hu, B., Li, J., Jing, L., Judah, A.,(2014). Improving the efficiency and accuracy of individual tree crown delineation from high-density LiDAR data. Int. J. Appl. Earth Observ. Geoinf. 26, 145–215. http://dx.doi.org/10.1016/j.jag.2013.06.003.

Kaartinen, H., Hyyppä, J., Yu, X., Vastaranta, M., Hyyppä, H. et al. (2012) An international comparison of individual tree detection and extraction using airborne laser scanning. Remote Sensing 4, pp. 950-974.

Khosravipour, A., Skidmore, A.K., Isenburg, M. and Wang, T.J. (2015) Development of an algorithm to generate pit-free Digital Surface Models from LiDAR, Proceedings of SilviLaser 2015, pp. 247-249, September 2015.

Magnussen, S. Nord-Larsen, T., Riis-Nielsen, T. (2018). Lidar supported estimators of wood volume and aboveground biomass from the Danish national forest inventory (2012–2016). Remote Sensing of Environment 211, pp. 146–153. DOI: 10.1016/j.rse.2018.04.015

Næsset, E. (2004). Practical large-scale forest stand inventory using a small-footprint airborne scanning laser. Scandinavian Journal of Forest Research, 19(2), 164-179, doi:Doi 10.1080/02827580310019257.

Naesset, E. (1997). Estimating timber volume of forest stands using airborne laser scanner data. Remote sensing of environment, 61(2), 246-253.

PLOTSAFE Overlapping Feature Cruising Forest Inventory Procedures – Feb 2007

SCION (2017). Cloud2Stem software, Pont D., Gordon J. SCION New Zealand, 2017

Watt, M. S., Adams, T., Aracil, S. G., Marshall, H., & Watt, P. (2013a). The influence of LiDAR pulse density and plot size on the accuracy of New Zealand plantation stand volume equations. New Zealand Journal of Forestry Science, 43(1), 15.

Watt, P., & Watt, M. S. (2013b). Development of a national model of *Pinus radiata* stand volume from LiDAR metrics for New Zealand. International Journal of Remote Sensing.

Widjojo, Elisabeth Adelia & Chinthammit, Winyu & Engelke, Ulrich. (2017). Virtual Reality-Based Human-Data Interaction. 1-6. 10.1109/BDVA.2017.8114627.

Yu, X., Hyyppä, J., Kaartinen, H., & Maltamo, M. (2004). Automatic detection of harvested trees and determination of forest growth using airborne laser scanning. Remote sensing of environment, 90(4), 451-462

Contact

Susana Gonzalez

Email: susana.gonzalez@interpine.co.nz

Telephone: 07 350 3209

About Interpine Group Ltd

This report was prepared by Interpine Innovation (Interpine Group Ltd). Interpine Innovation is an industry leading organisation providing technical and consulting services for a wide range of forestry-related companies. Interpine's success is underpinned by a committed management team of professional foresters backed by qualified field technicians and data analysts.

Interpine has three main divisions: Forestry Services, IT & Research, and Consulting. Its key services relate to forest mensuration, value chain improvement, value recovery auditing, log scaling, and carbon accounting.

Since 1980 Interpine has been providing New Zealand forestry with innovative ideas and solutions for an ever-changing forest industry. Today, Interpine's head office in Rotorua is nestled in the hub of New Zealand forestry working with a wide range of companies from large corporate entities to generalist farm foresters. Whatever the needs of the client, Interpine will always strive to find quality solutions at a competitive price. If you would like to know more about Interpine and its dedicated team please contact us on the details provided. Further information about Interpine can also be found by visiting www.interpine.com.

Disclaimer

The information in this document has been prepared and approved by Interpine Group Limited (Interpine). Access to the information in this document is being given by Interpine specifically to the person(s) to which it was intended. The information contained in this document remains the intellectual property of Interpine and may not be reproduced, distributed or published by any recipient for any purpose without the prior written consent of Interpine.

Although all reasonable care has been taken to ensure that the information contained in this document is accurate, neither Interpine nor its respective officers, advisers or agents makes any representation or warranty, express or implied as to the accuracy, completeness, currency or reliability of such information or any other information provided whether in writing or orally to any recipient or its officers, advisers or agents.

Interpine and its respective officers, advisers, or agents do not accept: any responsibility arising in any way for any errors in or omissions from any information contained in this document or for any lack of accuracy, completeness, currency or reliability of any information made available to any recipient, its officers, advisers, or agents; or any liability for any director or consequential loss, damage or injury suffered or incurred by the recipient, or any other person as a result of or arising out of that person placing any reliance on the information or its accuracy, completeness, currency or reliability.

Interpine Group Ltd
P.O. Box 1209, Rotorua
Telephone. . +64 7 350 3209
Email. info@interpine.co.nz
Website. www.interpine.com

3.3. A Comparison of Helicopter-based VUX-1LR LiDAR with Below-canopy UAV Photogrammetry and Manual Measurements

*Sean Krisanski[1,2**], Mohammad Sadegh Taskhiri[1], Paul Turner[1]*

1 University of Tasmania, eLogistics Research Group
2 Australian Research Council – Centre for Forest Value
*** Presenting Author: sean.krisanski@utas.edu.au*

Aim

This study aims to determine which sensing approach captured the greatest detail in the sub-canopy, and to provide an initial recommendation for the flying height of the VUX-1LR sensor to capture this information.

Introduction

UAV Photogrammetry is typically performed from above the forest canopy, however it suffers from poor penetration when compared to LIDAR systems such as the VUX-1LR. One way to capture sub-canopy information using photogrammetry, is to avoid the need to penetrate the canopy entirely. Close-range photogrammetry (CRP), a technique typically performed by walking through a plot taking still photos, has been demonstrated as an effective method of capturing sub-canopy information by Mikita *et al.* (2016). In their study, they achieved a root mean square error (RMSE) of less than 1 cm for their diameter measurements. In this study, CRP was performed using a UAV, allowing flight over challenging terrain (such as areas with a dense blackberry understorey) as well as the ability to capture images from a variety of heights within the forest.

Method

The sub-canopy data captured by the VUX-1LR LiDAR was compared in performance to the first trial of a below-canopy UAV photogrammetry system. The baseline used for comparison was the manual measurement of the diameter at breast height for each tree in the plot. These were collected with a measuring tape at 1.3 m above the highest side of the tree base. Note that if the tree had significant branching or bulges at 1.3 m, the tape was moved up or down to the nearest representative location. The plots used for this study were selected because there was data from each sensing method for them. The below-canopy UAV system was also tested in plots of higher tree density (where airborne laser scanning was not applied) as this is the intended use case for such a system.

The purpose of using this approach is to develop an efficient alternative to taking manual measurements. This system is most practical in areas where canopy density prevents above canopy techniques from providing useful information from the understorey. With this system, a 13m radius plot can be mapped in a little over 20 minutes by flying the plot manually and taking a single, identifiable distance measurement and bearing for scaling and orientation purposes. The improvements in data acquisition time over manual measurements are more apparent in denser forest than the plots used for this analysis. The plots used for this study had a density of approximately 283 stems/hectare. Another plot which is not considered in this study, had a density closer to 717 stems/hectare with 38 trees in the plot and was still flown in approximately 20 minutes. An example point cloud generated using this approach can be seen in Figure 1.

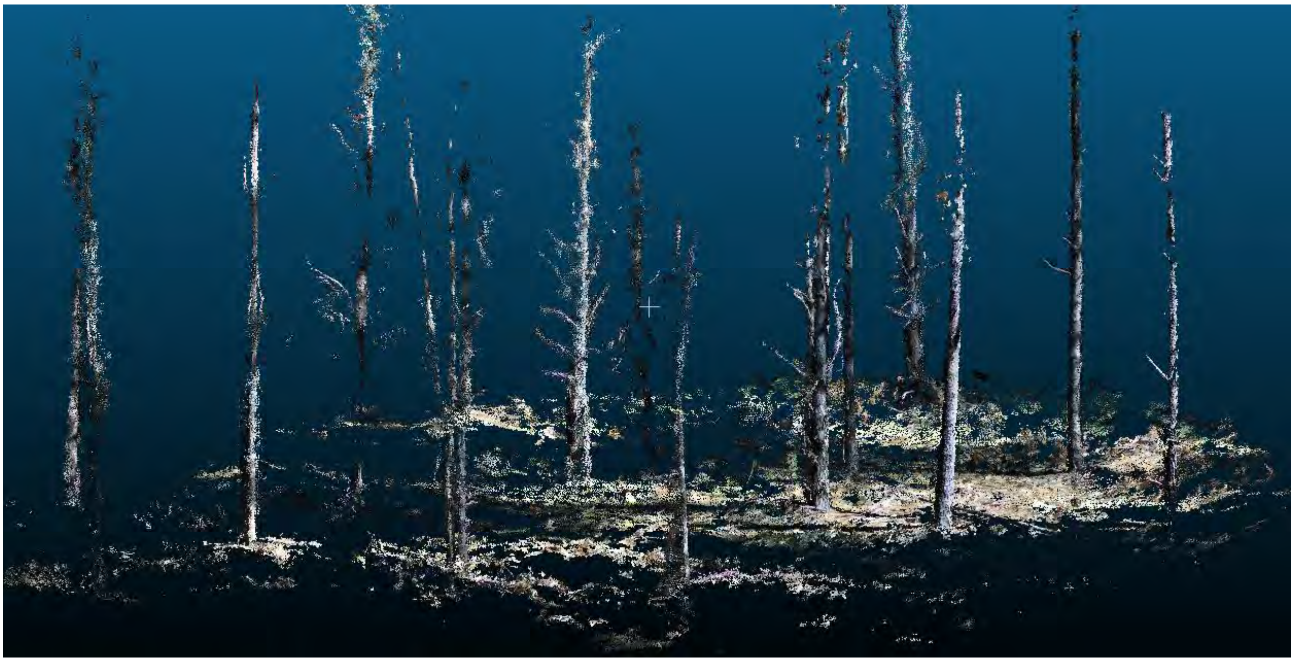

Figure 1: Below-canopy UAV-based photogrammetric point cloud of Site 8, Plot 15 shown in CloudCompare (2018)

The below-canopy UAV point cloud was created using the photogrammetry software MicMac (Rupnik *et al.*, 2017). The scale of this point cloud was initially arbitrary and so was scaled using a single known measurement between the centre marker and a given tree for each point cloud.

The various point clouds were trimmed to a 15-metre radius from the plot centres and were aligned using CloudCompare (2018).These point clouds were exported to .LAS format, then imported into DendroCloud (Koreň, 2018).

A digital terrain model (DTM) was generated in DendroCloud using a 2D grid with a spacing of 1.5m. This spacing was chosen to deal with gaps in the ground point data in some samples. The minimum point option was used to generate this DTM.

The DTM was visually inspected to ensure that the model was appropriate for the point cloud

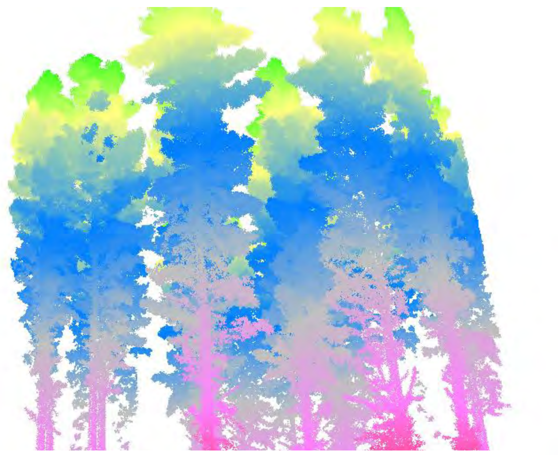

Figure 2: Example VUX-1LR point cloud with 1.5m DTM grid at the base. DTM created in DendroCloud.

and that the slices of the trees would be generated appropriately in the next step. An example DTM can be seen in Figure 2. Using the point cloud and the DTM as inputs, the surface cross-section tool is used to extract a slice of the trees at breast height (1.3 m). With the below-canopy UAV data, this slice could be thin (5-10 cm) due to the high point density, however due to the sparser points from the VUX-1LR LIDAR, the slice was taken between 1.15 m and 1.45m so that there were sufficient points for circle fitting.

As this slice contained points from branches, small bushes and noise, cleaning of the point cloud was necessary. Many filtering approaches were tested to perform this automatically on the analysed data sets, however this is a highly complex problem with imperfect data, and there is no explicit definition of how a stem should look in a point cloud. Humans can easily identify a stem from branches and noise, so this was the approach taken for this study. This problem may be a suitable application for the use of artificial neural networks, however this was beyond the scope of this project.

The slices were exported to a .CSV file and imported into CloudCompare for manual cleaning. Where the stem circles were clear, the surrounding points from branches and other objects were removed. Any clusters without a clear stem circle were only minimally cleaned using the unsliced point cloud for clarification. This was to avoid misinterpretation of the stem shape where the points were sparse. Figure 3 shows a VUX-1LR slice from Site 4, Plot 4, with the original (LEFT) and the cleaned slice (RIGHT).

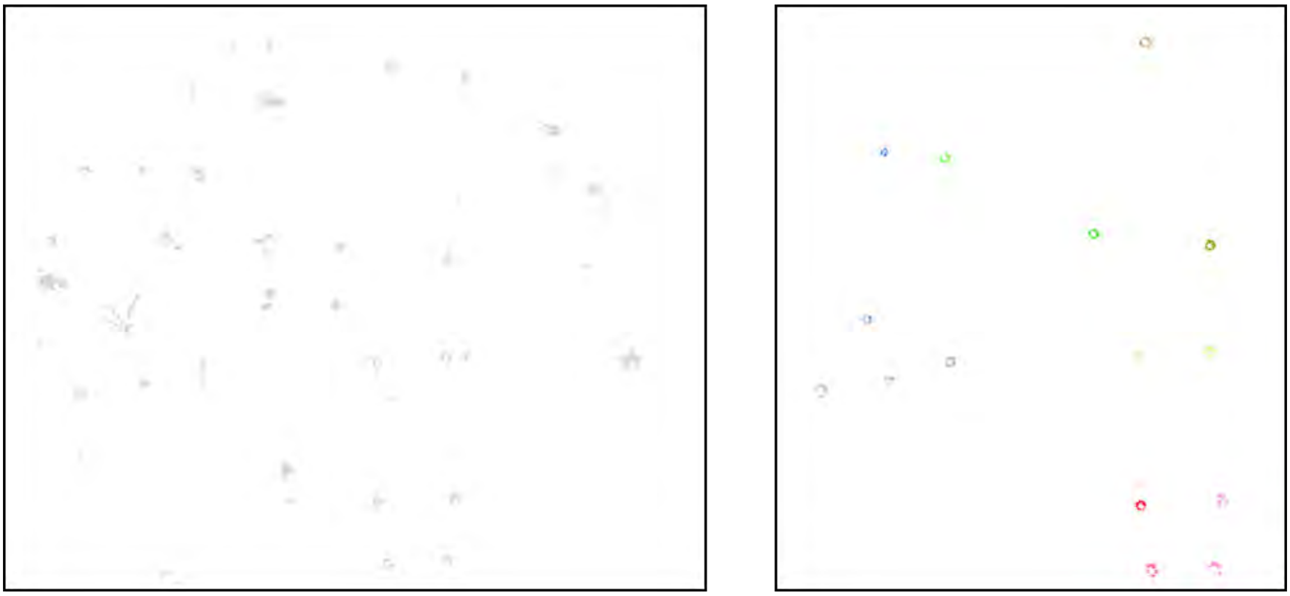

Figure 3: LEFT: Raw slice 1.15m to 1.45m above DTM. RIGHT: Cleaned and grouped slice ready for circle fitting.

The cleaned slice was exported to a .LAS file and imported back into DendroCloud. The group-by-distance function was used to group the clusters of points belonging each tree. The maximum distance between points belonging to the same group was set to 1m, and each cluster was required to have greater than 10 points.

The clusters were inspected in the cross-section analyst tool to ensure that the circle fitting appeared appropriate for each cluster. Figure 4 shows an example circle fitting from this tool of the same tree from two different data sets. Once inspected, the automated circle fitting tool was used with the Optimal Circle function (Koreň *et al*., 2017), with the Monte Carlo option selected, a count limit of 10,000, and a root mean square limit of 0.001. The positions and diameters of the clusters were then saved to a .CSV file for analysis.

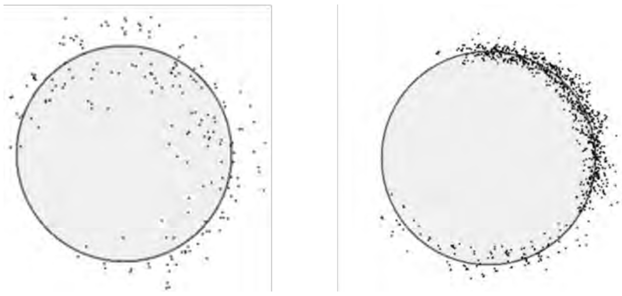

Figure 46: Examples of fitted stem circles created in DendroCloud. LEFT: VUX-1LR, RIGHT: Below Canopy UAV Photogrammetry.

Results

The below results are from combining the measurements from Site 4, Plot 4 and Site 8, Plot 15. Each plot contained 15 trees within a 13m radius of the plot centre, giving a plot density of approximately 280 trees per hectare. Figure 5 shows the difference between the DBH measured from the point clouds, and the manually measured DBH on an individual tree basis (rather than a plot level comparison). The statistical analysis was performed using “R: A Language and Environment for Statistical Computing” (R Core Team, 2018).

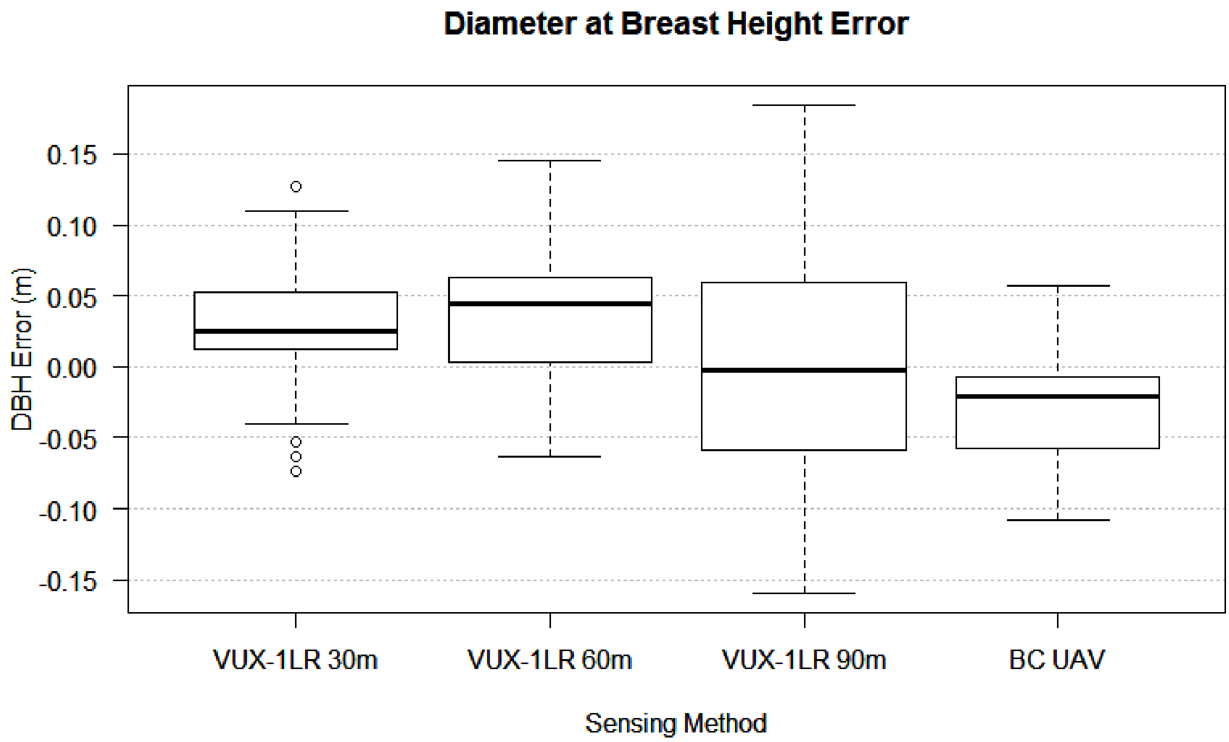

	VUX1LR 30m	VUX1LR 60m	VUX1LR 90m	BCUAV
Min. (m)	-0.07300	-0.06300	-0.15900	-0.1080
1st Quartile (m)	0.01300	0.00350	-0.05750	-0.0575
Median (m)	0.02550	0.04500	-0.00300	-0.0210
Mean (m)	0.02620	0.03467	0.00817	-0.0305
3rd Quartile (m)	0.05025	0.06275	0.05825	-0.0070
Max. (m)	0.12700	0.14500	0.18400	0.0570
RMSE (m)	0.05600	0.05700	0.08200	0.0500

Figure 5: A boxplot comparing the differences between the DBH measurements made with sensed methods, with the DBH measurements taken manually using a measuring tape in the field.

As seen in Figure 6, linear model analysis was performed on the DBH data to explore how accurate each sensing method was relative to the manually measured DBH.

The below-canopy UAV data most closely matched the manually measured tree diameters with an R^2 value of 0.698 and a p-value of 9.1e-09 showing a very high confidence in the fitted model. The VUX-1LR data captured from 60m altitude gave the second closest DBH estimates with an R^2 of 0.563 and a p-value of 1.8e-06. The 30m flying height was close behind with an R^2 of 0.447 and a p-value of 5.3e-05. The 90m flying height was found to be poor at capturing the DBH accurately as no statistically significant correlation (p-value = 0.5) was observed with the manually measured DBH for this data set and method.

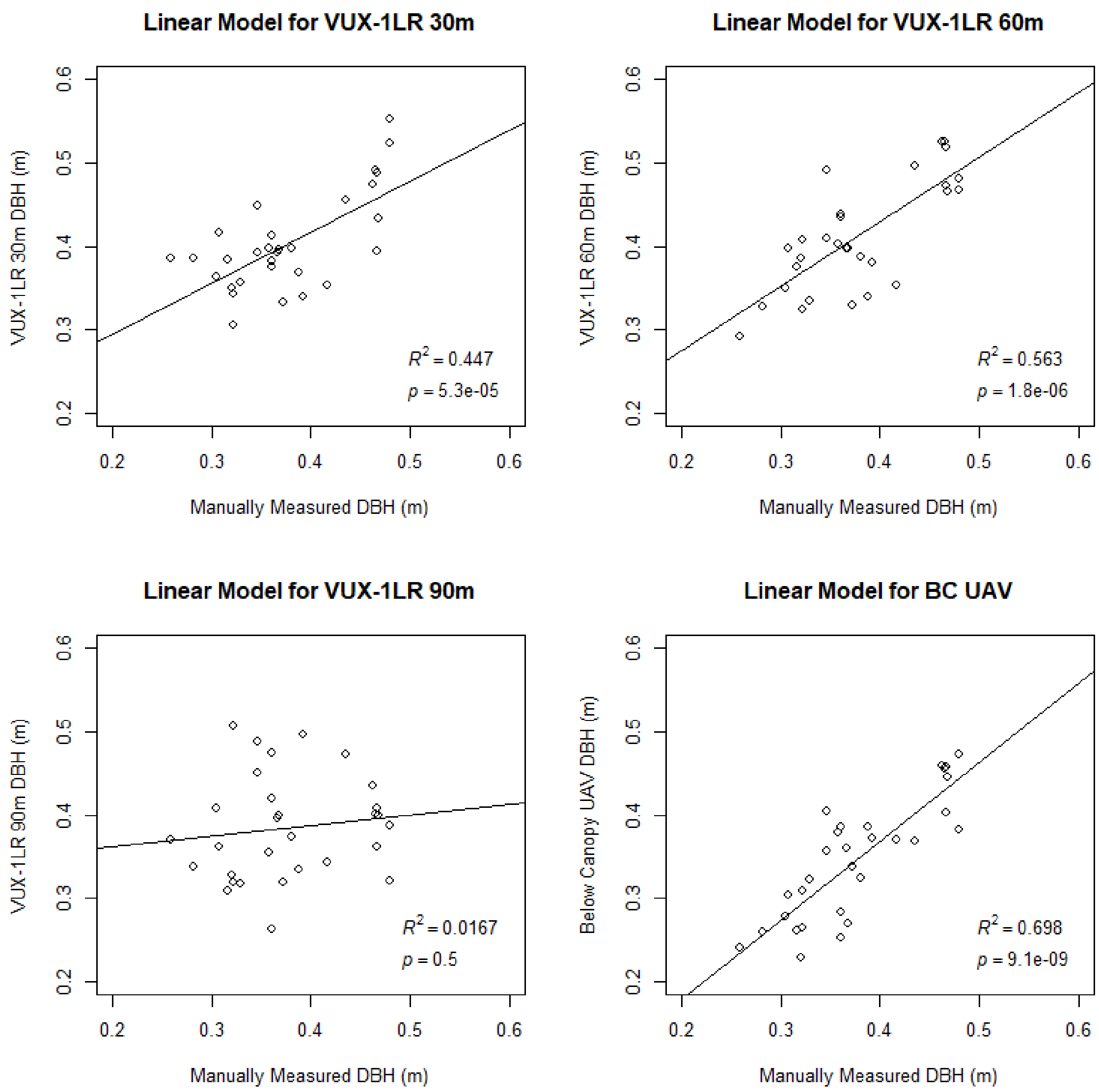

Figure 6: Linear Model Analysis comparing the DBH estimates from the sensing systems with the manually measured DBH.

Limitations of This Study

It is important to acknowledge that with all the presented data sets, accuracy may be improved with a DBH measurement technique that accounts for a larger section of the stem. The technique used in this report only makes use of the region within ±15cm of 1.3m above the DTM.

This comparison assumes that the manually measured DBH were perfect measurements and were taken at 1.3m. Each measurement may have been shifted vertically due to branching or bulges in the tree. The measured diameter will have also been affected by the shape of the stem not being a perfect circle.

The manual cleaning of the point clouds is subject to misinterpretation of the points and may experience bias depending on the person cleaning the point clouds. To combat this, a single person performed all the cleaning and where there was doubt about a point, minimal or no cleaning was performed.

Conclusion

The helicopter-based VUX-1LR LIDAR and a sub-canopy UAV photogrammetry system were compared based on their accuracy for providing diameters at breast height in an openly-spaced radiata pine forest. A consistent method was used to extract the measurements from the point clouds and these were compared with the manually measured diameters at breast height. Based on a sample size of 30 trees from 2 plots, the 60m flying height gave the most consistent data from the VUX-1LR LIDAR. When considering the height measurement performance in the previous section, a flying height of 60m appears to be an appropriate choice for capturing useful data from both the canopy and the sub-canopy in openly-spaced forests. When high tree density prevents airborne laser scanning from effectively capturing sub-canopy data and/or greater accuracy is required, below-canopy UAV photogrammetry presents an interesting solution. With further development, sub-canopy UAV inventories are expected to become largely automated and approach the accuracy of manual tree measurements.

Acknowledgements

- Future Forest Research for allowing us to be a part of this project.
- Interpine Group Ltd for providing field measurements, LiDAR data and to Susana Gonzalez for designing the flight path for the LiDAR acquisition.
- Barbara Del Perugia (University of Florence) for reviewing the LiDAR dataset and pre-processing the raw data.
- Maciej Matuszak (University of Tasmania) for his incredibly valuable help with setting up the UAV's on-board computer and teaching me how to control the sensors in a very short time-frame.
- Australian Research Council - Centre for Forest Value for providing my PhD scholarship.

References

Girardeau-Montaut, D. 2018. CloudCompare. v2.10.alpha ed.

Koreň, M. 2018. DendroCloud. 1.47 ed.: Technical University in Zvolen.

Koreň, M., Mokroš, M. & Bucha, T. 2017. Accuracy of tree diameter estimation from terrestrial laser scanning by circle-fitting methods. *International Journal of Applied Earth Observation and Geoinformation,* 63**,** 122-128.

Mikita, T., Janata, P. & Surový, P. 2016. Forest Stand Inventory Based on Combined Aerial and Terrestrial Close-Range Photogrammetry. *Forests,* 7**,** 165.

R Core Team 2018. R: A Language and Environment for Statistical Computing. R Foundation for Statistical Computing.

Rupnik, E., Daakir, M. & Pierrot Deseilligny, M. 2017. MicMac – a free, open-source solution for photogrammetry. *Open Geospatial Data, Software and Standards,* 2**,** 14.

4. Individual tree detection, 3D reconstruction and extraction of forest inventory metrics

4.1 Algorithms and 3D modelling techniques for tree detection and tree-level volume estimates

M. Bryson[1] *and J. Gordon*[2]

[1] Australian Centre for Field Robotics, The University of Sydney, NSW, Australia
[2] SCION, Rotorua, New Zealand

Introduction

Individual Tree Detection (ITD) involves the detection, segmentation, counting and quantification of structural parameters (such as height, shape) of trees from remotely sensed data over potentially large areas of a forest. Traditionally, ITD methods have used imagery sources such as from aerial photography or satellite remote sensing. Commonly used approaches include valley-finding algorithms (Gougeon, 1995; Leckie *et al*., 2005) or local-maxima finding algorithms (Dralle & Rudemo, 1997; Wulder *et al.,* 2000) that search for local peaks in the image intensity data that correspond to the shading of well-delineated tree crowns. (Pollock, 1996) presented an approach to tree detection based on template matching of using a crown shape to create a shaded appearance model, which is used to detect tree crowns. (Olofsson *et al.,* 2006) use a similar template based approach and use the unshaded sections of canopy to additionally classify tree species based on spectral bands.

With the increased use of LiDAR in forestry applications, more recent approaches to ITD based on pointcloud data have appeared. Algorithms that have been adapted to locate trees in rasterised canopy height models generated from airborne LiDAR include pouring algorithms (Weinacker *et al.,* 2004), adapted watershed (Ziegler et al., 2000) and region-growing approaches (Hyyppa *et al.,* 2001). These algorithms detect and segment trees based on the shape and structure of the canopy surface height, while ignoring sub-canopy LiDAR returns. More recently, with the advent of high-resolution airborne scanners, techniques have emerged that exploit structural data below the canopy; (Reitberger *et. al*., 2009) develop a tree segmentation approach based on the normalised cut algorithms that segments 3D pointclouds directly in 3D while (Ayrey *et. al.,* 2017) develop an approach to segmenting trees that find local density maxima in multiple vertical slices of sub-canopy LiDAR points. Approaches have also been developed that detect trees based on stem strikes; (Lamprecht *et al.,* 2015) describe a ITD method based on the detection of trunk points in LiDAR below the canopy.

In contrast to ITD methods using airborne LiDAR, tree/trunk detection and segmentation algorithm using Terrestrial Laser Scanning (TLS) are mature: for example, (Raumonen *et. al*., 2013; Wang *et. al*., 2017) and (Bienert *et. al*., 2007) all present examples of tree trunk segmentation using TLS datasets with greater than 5000 points per m^2 and algorithms that can exploit these densities to segment/measure tree trunks. These existing TLS algorithms are designed to work with near perfect data and do not scale to datasets beyond the size of a small plot (tens of meters and tens of trees), due to the computational complexity of the algorithms involved. Recently acquired UAV-borne LiDAR pointcloud datasets such as (Wallace *et al*., 2014) and from the Reigl VUX-1 used in this project exhibit point densities of approximately

200-700 points per m^2 that lie in between traditional ALS and TLS datasets. The aim of this work was therefore to develop new approaches adapted to the medium density pointclouds gathered using UAV-borne sensors such as the VUX-1, while exploring the potential of existing approaches designed for either low resolution airborne pointclouds or high-resolution TLS pointclouds.

This chapter discusses work performed towards individual tree detection, 3D reconstruction, segmentation and measuring stems using dense airborne LiDAR pointcloud data. Two separate sets of algorithms/workflows have been developed in parallel: a "top-down" approach to tree detection and stem-fitting and a "bottom-up" approach to tree detection and stem profile measurements. The aim of the "top-down" approach is to extend existing algorithms and methods used for individual tree detection using conventional, lower resolution (5-30 points/m^2) pointclouds to work with dense pointclouds and detect and reconstruct stems below the canopy. The "bottom-up" approach builds upon existing algorithms and a SCION-developed software package "Cloud2Stem" used for measuring trees in Terrestrial Laser Scanning (TLS) datasets, extending the approach to deal with lower-resolution scans and scans presenting occlusions. Both approaches use a combination of different stem-fitting strategies (circles and vertical linear sections) that are robust to noise to detect trees and model the shape (sweep and lean) and diameter profiles along the stem. Results of the two approaches are shown using TLS LiDAR and VUX-1 LiDAR pointclouds over relatively low-density stands (~400 stems per hectare), for which stem maps and tree-level measurements of DBH, sweep and taper profile are shown and compared to measurements made in the field.

A workflow that includes the two different algorithms is described that would allow for efficient processing of dense pointclouds for providing tree stem maps and basic inventory attributes over both plot-scale and larger areas as part of future work. The overall idea of the workflow is to initially perform tree detection based canopy-based peak models and the RANSAC-based model fitting algorithms, which are potentially fast and scalable to larger LiDAR datasets. These detections could then provide refined candidate search regions in the pointcloud data that could be passed to Cloud2Stem for a more accurate and computationally-intense search for tree stems from which basic stem attributes could be extracted.

Methodology

Tree Detection and Segmentation Algorithms using a "Top-down" Approach

Algorithms were developed that use a combination of crown peak detection and fitting to circular stem sections and vertical curve segments to detect trees and fit tree stem models to LiDAR pointclouds. The algorithms and processes were developed keeping in mind the resolutions of points observed in typical pointclouds from the VUX-1 datasets available and the types of occlusion structures (partial circumferential coverage, missing sections of stem etc.) observed in this data (i.e. see Figure 1). Rather than use point segmentation strategies sometimes used in TLS-based tree detection algorithms (for example (Raumonen *et. al.*, 2013)), the approach used a robust modelling-fitting approach (based on RANdom SAmple Concensus (RANSAC) (Fischler & Bolles, 1981)) which is designed to fit models in a computationally-efficient manner, with partial data and in the presence of noise.

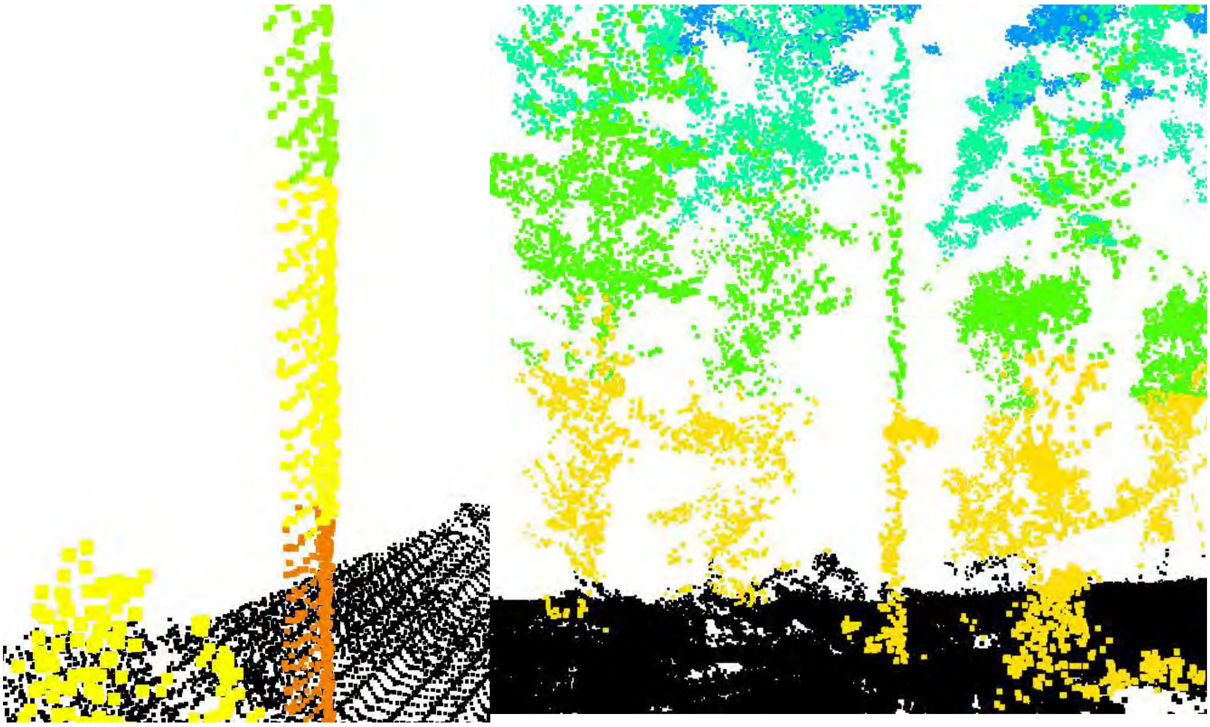

Figure 1: Examples of LiDAR stem hits using aerially-acquired data (VUX-1): the density of stem hits is typically lower than that of Terrestrial Laser Scanning (TLS) and occlusions through the canopy mean that stems sometimes only contain visible hits along one side of the stem.

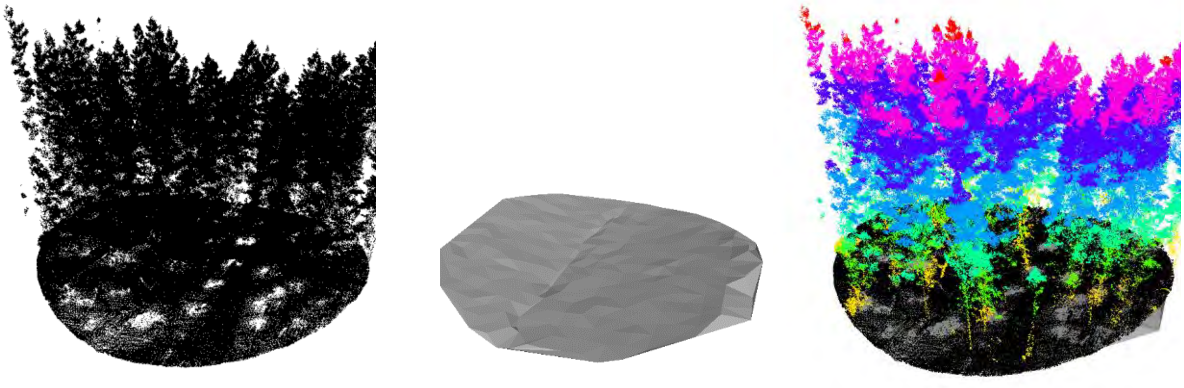

(a) (b) (c)

Figure 2: (a) Original/raw LiDAR pointcloud, (b) extracted ground plane and (c) tree/canopy points coloured by height above ground (ground shown in black). These points are maintained in their original global coordinate system for further processing

The approach takes raw LiDAR pointclouds and produces a stem map which contains the location data of detected trees in the area and reconstructed segments of the tree stem. The algorithm proceeds with the following steps:

1. **Ground plane estimation:** The algorithm creates a digital terrain model of the ground by finding local minima points within a search radius of 2m. These points are then

converted into a triangulated surface model (using Delaunay triangulation) (see Figure 2 (a) and (b)).

2. **LiDAR point height above ground:** Using the ground plane, the height above ground for each point is calculated and recorded by interpolating the ground height at the point's horizontal location. Points below 1m are classified as ground and discarded from further processing (see Figure 2 (c)). Unlike in traditional ALS pointcloud processing, points are maintained in global (un-normalised) coordinates for further processing (stem fitting). The reason for this is to prevent further measurements of the stem (i.e. diameters, sweep etc.) from being skewed by the shape of the terrain.
3. **Canopy Peak Detection:** Canopy peak points are detected in the non-ground points by finding local maximas (based on height above ground) within a radius of 2m. These points are used to guide a stem finding strategy discussed in step 5 below.
4. **Stem Circle Fitting:** The above ground LiDAR points are separated into a number of 1m vertical bins, starting from the lowest non-ground point in the data and moving up to the top of the canopy. For each bin, the points are flattened into a horizontal pointcloud and a RANSAC algorithm is used to detect and fit circles to the data (see details in subsection below). This stage of the processing can reconstruct circles from partial data (i.e. stems hits that have a limited circumferential coverage) and produces circles that correspond to tree stems and other parts of the canopy that are fortuitously "circular" in shape.
5. **Stem Vertical Profile Fitting:** In order to extract circles that correspond to real tree stems and turn these into coherent stem profiles in 3D space, a second RANSAC algorithm is used to fit a cubic spline curve through the centers of detected circles (see details in Section 2.3 below). A cubic spline is a curve in space defined by three points, and when oriented in a vertical direction, provides a simple model of the centreline of a tree stem that can account for sweep and lean in a way not possible by using a straight-line segment. This process begins by defining the top point of each spline based on the detected peak points described in step 3 above.
6. **Final Stem Output:** A final stage of processing is used to merge overlapping stems into a single model (by selecting the model with the best fit) and provide a finalised list of stems.

Further details of the circle-fitting and cubic spline fitting steps in the process are discussed in more detail in the sections below.

Detection of Stem Circles From Points Using a RANSAC-based Algorithm

During step 4 of the detection procedure, the above-ground points are separated into a number of 1m thick vertical bins, and for each bin, horizontal circles are detected in the points using a RANSAC procedure. The procedure consists of the following steps:

1. Randomly select three nearby points: At first one point is selected at random. A further two points are selected at random from all points within a 1m radius.
2. The parameters of a circle (x-y position and radius) are calculated that fit exactly through the three points.

3. The remaining points are tested to determine their distance from the boundary of the circle. The number of points that "fit" the circle (lie within 5cm of the circle boundary) are counted (fitting points). The number of points that lie inside the circle, including a 5cm inner buffer are also counted (inner points). If the number of inner points is zero and the number of fitting points is greater than a threshold (currently 10 points), then the circle is maintained as a potential candidate. The presence of inner points indicates that the circle is not likely to come from a stem as the LiDAR is not expected to penetrate into stems.
4. If maintained as a potential candidate, the stem is compared to any other existing circles that overlap, and in this case only the circle with the maximum number of fitting points is maintained.
5. The process is repeated from step 1 by selecting another random point. The process is repeated a large number of times (currently 200 times for each 1x1m horizontal grid in the data).

Once the algorithm has finished computing circles within one bin, it repeats the whole procedure for each remaining vertical bin of points and assigns a height to each circle based on the average height of the fitting points. The idea of the RANSAC algorithm is to repeatedly try to fit a randomised circle to the data, while only maintaining fits that meet the above-mentioned criteria. The greater the number of times that the process is repeated, the greater the probability that all "real" circles have been detected in the data (i.e. probability that at least once for each stem, three points have been selected together that lie on the stem). The number of required samples depends on the density of points and ratio of actual stem points to other "clutter/noise" points, and was determined experimentally from the datasets examined.

Figure 3 illustrates the resulting detected circles overlaid with the non-ground LiDAR points. The process detects multiple circles that correspond to both stems and other "circular-looking" arrangements of points.

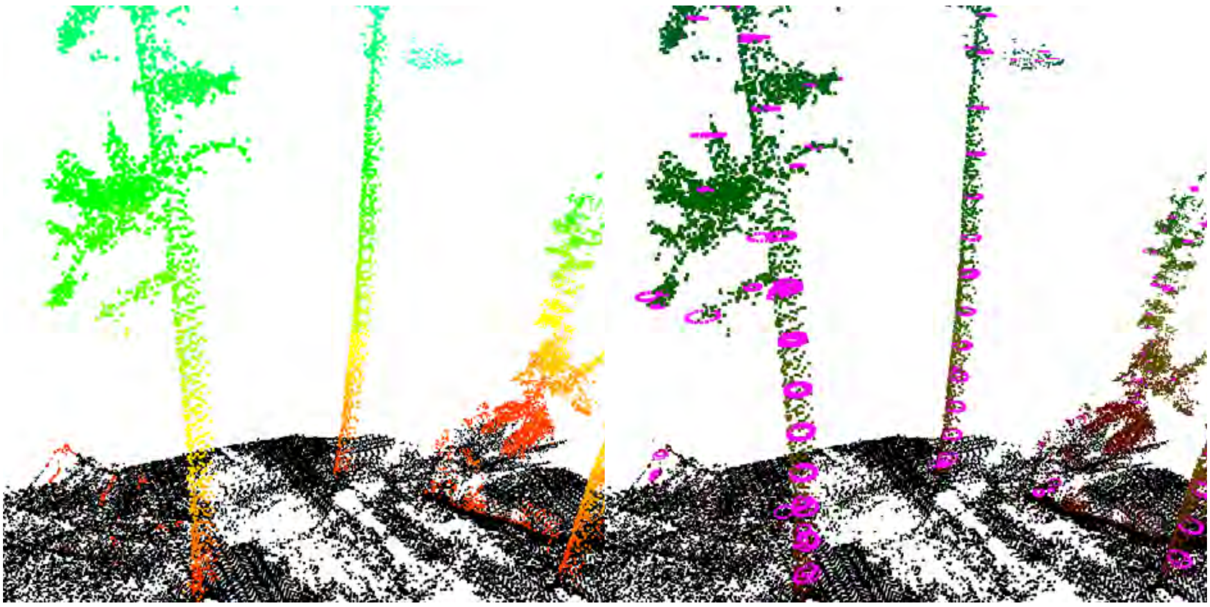

(a) (b)

Figure 3: (a) Original LiDAR pointcloud (coloured by height above ground), (b) pointcloud overlaid with detected circles at 1m height intervals

Detection of Tree Stem Arcs From Points Using a Cubic Spline RANSAC-based Algorithm

Once circles have been detected, a second processing stage is used to detect vertically coherent tree stems using the circles. The procedure consists of the following steps:

1. A crown point is selected at random and two circles are selected at random from all circles within a 4m horizontal distance of the selected crown. Circles are selected from different vertical bins.
2. A cubic spline is computed that runs through the three points (crown points and circle centers). A cubic spline is a curve that passes through all three points and minimises the maximum bending (curvature) between the three points.
3. LiDAR points are tested for fit with the generated cubic spline. The distance of each point from the centreline of the spline is measured and, similarly to the case with circles, we measure the number of points that are at a distance to the line that is equal to the radius of the corresponding fitted circles (fitting points), and also measure the number of points closer to the line than the fitted circle radius (inner points). The candidate stem is kept if the number of fitted points is above a threshold of 10 in at least three different vertical bins and if the number of inner points is zero.
4. The process is repeated from step 1 by starting from another random crown point. The process is repeated a large number of times (currently 200 times for each 4x4m horizontal grid in the data).

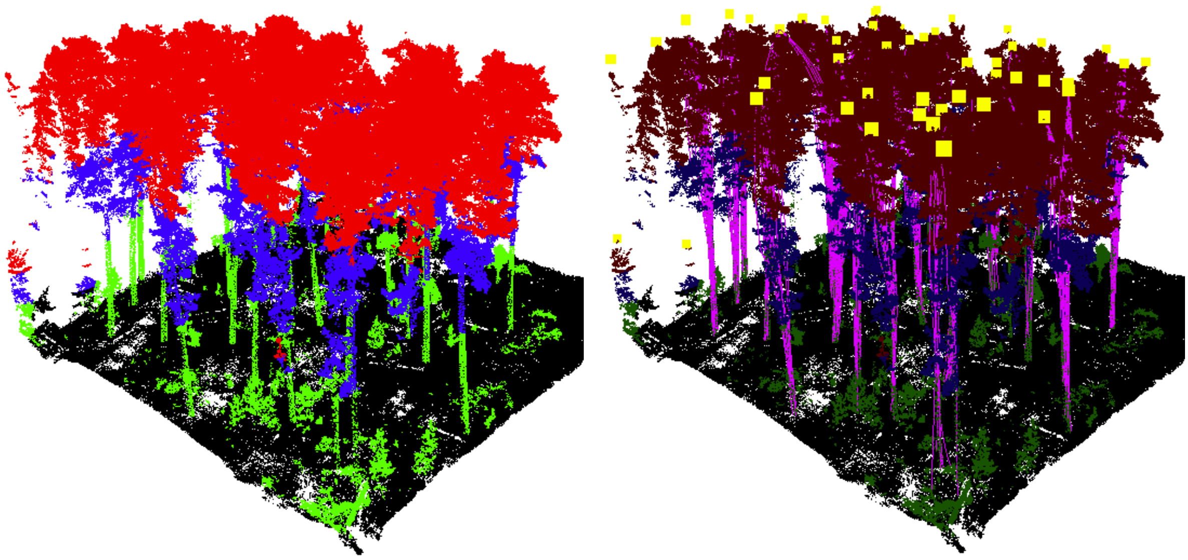

(a) (b)

Figure 4: (a) Original LiDAR pointcloud, coloured by height above ground, (b) pointcloud overlaid with detected canopy peaks (yellow) and detected cubic-spline fitted stems (purple)

Figure 4: (b) illustrates the resulting set of candidate tree stems that are detected from the cubic spline fitting process.

Combined Detection Algorithm

The resulting candidate tree stems are converted into a final set of stems by comparing and merging nearby stems. Stems that are found to be within a horizontal distance of 1m from each other, measured from the base of the tree are merged into a single stem. The number of fitting points in each vertical bin is compared, and the stem segment with the greatest number of fits for a given vertical bin is kept. Each stem is then defined by the diameters and segment of spline function of the remaining segments for each vertical bin.

Tree Detection and Segmentation Algorithms using a "Bottom-up" Approach: Cloud2Stem

In parallel to the "top-down" approach, a "bottom-up" approach for tree detection and reconstruction of stem profiles from dense LiDAR pointclouds was developed. The approach built upon existing algorithms and a SCION-developed software package "Cloud2Stem" that has been developed for processing TLS datasets. Development focussed on extending the approach to deal with lower-resolution scans (than TLS) and scans presenting occlusions that are representative of the dense aerially-acquired datasets collected so far.

Cloud2Stem is a command line software application which:

- Identifies stems in point clouds based on stacks of circles.
- Refine these stacks by "walking" the stem. This aligns the circles with the stem orientation to produce more diameter estimates (particularly diameter estimates within the canopy) and potentially more accurate diameter estimates.
- Stem modelling by creating a model of each stems based on the refined circle stacks. It may involve merging multiple stacks into one coherent stem model, for example when forked stems are encountered and/or sections of stem are missing as they have not been scanned.
- Crude stem height estimation based on the highest point found above the refined circle stack.
- Use a custom volume/taper function to predict whole stem volume and diameter at any level.
- Comparison of measured DBH's with estimated DBH's (i.e. those estimated from the point cloud).

Currently Cloud2Stem is designed to work with a circular area (defined by a centre and radius). Cloud2Stem does not identify or model the stem canopy/branches and only identifies stem diameters which are greater than approximately 100mm.

Cloud2Stem has been used with point clouds produced from terrestrial and aerial scanners including the ZEB1, FARO, Leica and VUX-1. The focus of recent work has been pointclouds produced by dense aerially acquired data, such as from the VUX-1 scanner (for example see Figure 1). Cloud2Stem has also been run on a point cloud generated by a UAS-borne Velodyne Puck laser scanner, flown by the University of Tasmania in September 2017. This was not successful due to the "noise" or error present in the point cloud and the low number of points on the stem beneath the canopy.

Volume/Taper Model

Given that a number of diameters can be measured by the algorithm on a given stem identified from a point cloud, it is necessary to augment this information so that diameter and volumes of any stem section, both over- and under-bark, can be predicted. This provides estimates of potential log size and yield which are the key variables of interest of any commercial forest assessment. The approach taken was to merge prior knowledge of stem shape with the empirical measurements of diameter taken from the stack of circles to fit a stem profile model (Van Laar & Akça, 2007). The resulting algorithm is robust and flexible but also efficient in the sense that it uses all the information that is provided to it and can exclude unreliable measurements.

Model of Stem Shape

The diameter of a tree's stem can be modelled as a monotonic curve which decreases from a maximum at ground level to reach zero at the tip of the tree (Larson, 1963). A stem’s diameter profile is approximately neiloidal in the lower third, conic in the central third and paraboloidal in the upper third of the stem. To model the profile of the diameter of the tree against height, a segmented approach (Max and Burkhart, 1976) was used with join-points at one-third and two-thirds of the stem height. The resulting curve is continuous but not strictly smooth.

Algorithm for Fitting the Model

The algorithm for fitting the model involves the following steps:

1. The lower curve is fitted via linear regression to all diameters below half height. If the fit fails due to insufficient, or very noisy, data, a fall-back approach is taken by estimating the ground-level diameter as the largest diameter found, and the rate of taper from the mean diameter in the lower half of the stem.
2. The upper curve is fitted via linear regression to all diameters above half height. If the fit fails due to insufficient or very noisy data, a fall-back approach is taken by assuming a paraboloid that intercepts at the stem height. The rate of taper is estimated from the mean diameter in the upper half of the stem.
3. A quadratic is used to cover the central third of the stem, passing through the mean diameter in this segment of the stem.
4. Any diameters which are more than P percent from the Step 1 curve estimates are now identified as outliers. The diameter data are filtered to exclude these points. P is a parameter to the algorithm.
5. If one or more outliers are found, the step 1 fitting process is repeated using the filtered data.

Volume Calculation

Volumes are calculated using a stepped approximation. A step length of 0.1 metres produces good accuracy without excessive calculation. Each section is treated as a frustrum of a cone. For example, the volume of a log from 0.27 metres to 5.77 metres above ground is calculated by summing the fifty-four section volumes from 0.3 to 5.7, then calculating and adding on the 0.27 to 0.3 and 5.7 to 5.77 volumes.

Bark Thickness

Pointclouds reflect the shape of the surface of objects, whereas foresters are often interested in the volume and diameters under-bark. To provide this information, a bark function is incorporated in the algorithm. A default set of parameters is provided but these can be over-ridden on construction. The default parameters were estimated for *radiata* pine (Gordon & Budianto, 1999).

Diameter Estimation

In some cases, there are insufficient points present to reliably estimate a diameter. Figure 5 shows a stem where the lack of points at the base of the stem is evident. Circles are colour coded by circumferential coverage. The bottom circle shown is approximately 1.8m above ground and in fact both the bottom two circles will be discarded due to having low scores.

Given cases like this, a 3 piece-wise curves to the stem profile has been developed. Diameters which are more than 15% different from the fitted (predicted) values are discarded, then the curve is re-fitted to the trimmed diameters. Therefore a continuous (but not necessarily completely smooth) curve from ground to tip is calculated, from which diameters, over- and under-bark, can be calculated.

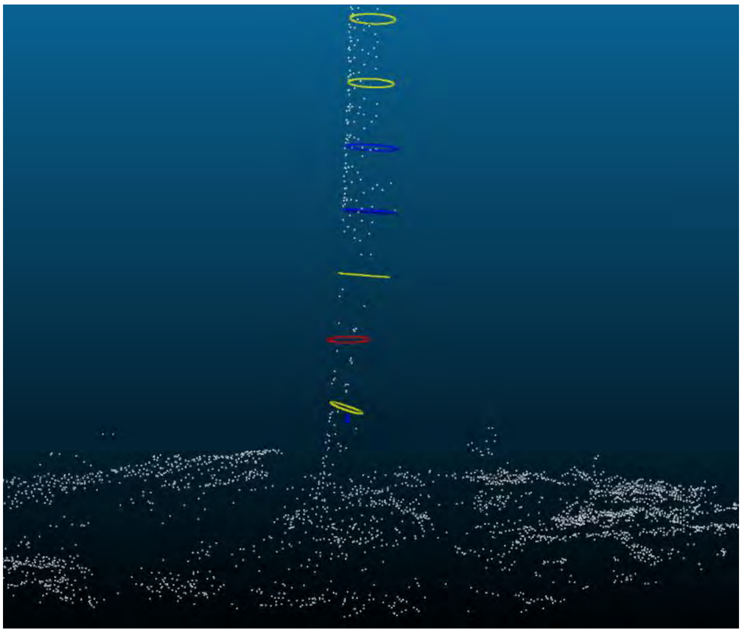

Figure 5: An example of a detected stem with very few LiDAR strikes (points) across one side at the base of the stem. Diameters fits on this section of the stem are inaccurate.

Recommendations for an Efficient Prototype Workflow Pipeline for Estimating Stem-level Data from Dense Aerially-acquired Pointcloud Data

Based on the current progress achieved in individual tree detection and stem modelling, we considered how the two different algorithms/workflows could be potentially merged into a single workflow that would allow for efficient processing of dense pointclouds for providing tree stem maps and basic inventory attributes over both plot-scale and larger areas as part of future work. Figure 6 presents a potential workflow including both modules that have currently been developed (in blue) and modules to be developed in future work (in green).

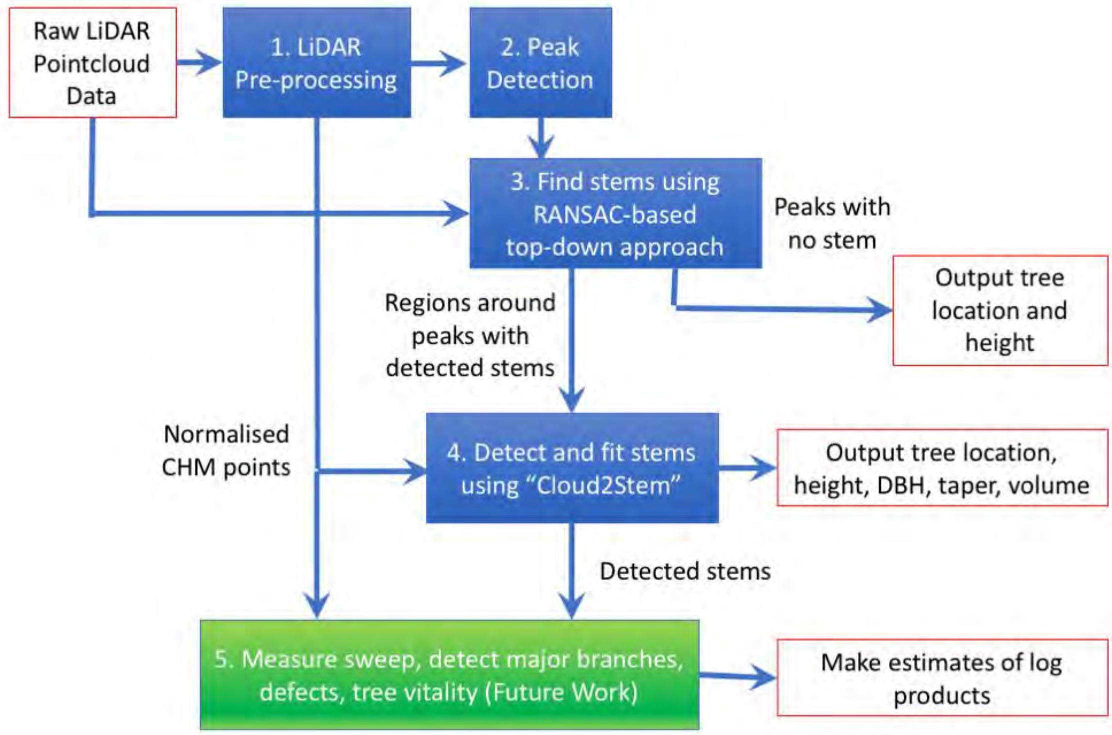

Figure 6: Proposed efficient prototype workflow pipeline for estimating stem-level data from dense aerially-acquired pointcloud data

The pipeline would perform the following steps:

1. **LiDAR pre-processing:** LiDAR pointclouds would be pre-processed by estimating a ground terrain model and generating both a set of normalised canopy height model points and assigning height above ground to the original LiDAR points (see Section 2.1)
2. **Peak Detection:** Local maxima would be detected in the canopy points and used to provide a crude estimate of crown locations and provide data for further processing steps (see section on "top-down" approach above)
3. **Find stems using "top-down" RANSAC-based approach:** Stems would be initially identified using RANSAC modelling-fitting algorithms (see section on "top-down" approach above) to provide candidate search regions that could be fed to Cloud2Stem for a refined search and extraction of stem properties. Data on crowns identified via peak points but not located using this step could be provided in the form of height and location, and stem-DBH models used to estimate the DBH of these stems.
4. **Detect and fit stems using Cloud2Stem:** Rather than searching across the entire pointcloud, Cloud2Stem (see section on "bottom-up" approach) could potentially be used in a more computationally efficient and scalable way by providing candidate search regions from stems identified in step 3, when applied to larger LiDAR datasets.
5. **Make estimates of additional variables necessary for estimates of log products:** Additional variables such as the sweep, position of major branches, defects and the vitality of the tree should be identified before feeding outputs to an external software package designed for making log product estimates. The estimation of these variables would form part of future work.

The overall idea of the workflow is to initially perform tree detection based canopy-based peak models and the RANSAC-based model fitting algorithms, which are potentially fast and scalable to larger LiDAR datasets. These detections could then provide refined candidate search regions in the pointcloud data that could be passed to Cloud2Stem for a more accurate and computationally-intense search for tree stems from which basic stem attributes could be extracted.

Results

"Top-down" Combined Detection Algorithm Results

Figure 7 illustrates results of the top-down RANSAC-based tree detection algorithm applied to a 65-by-65m section of VUX-1 LiDAR data collected at Tumut, NSW in 2016. Shown in purple are the remaining detected stem segments for each tree. Trees have varying numbers of reconstructed segments based on where an acceptable fit to the stem was found. Currently the algorithm detects and reconstructs stems for 27 of the 29 trees in this dataset.

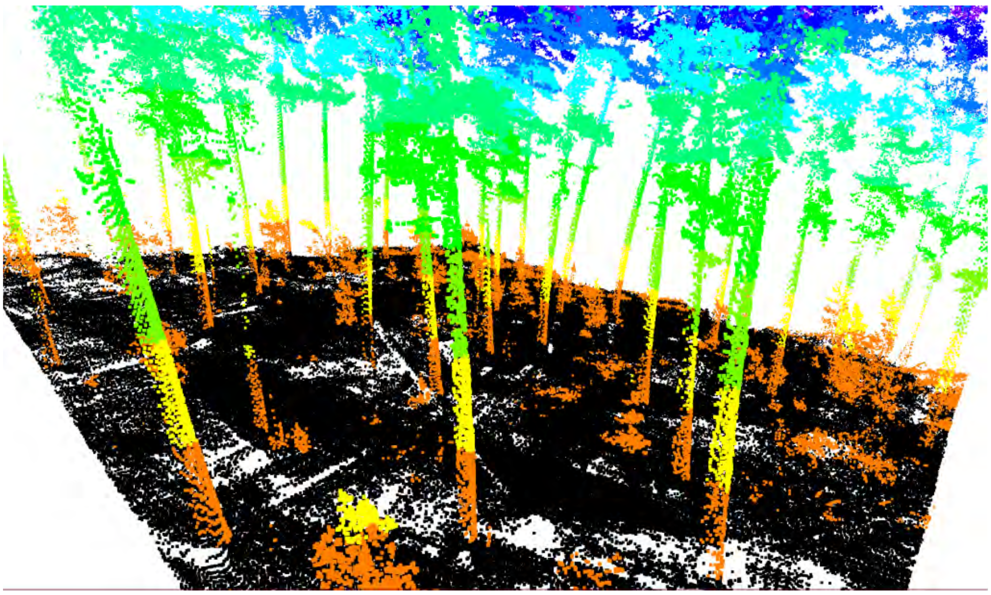

(a)

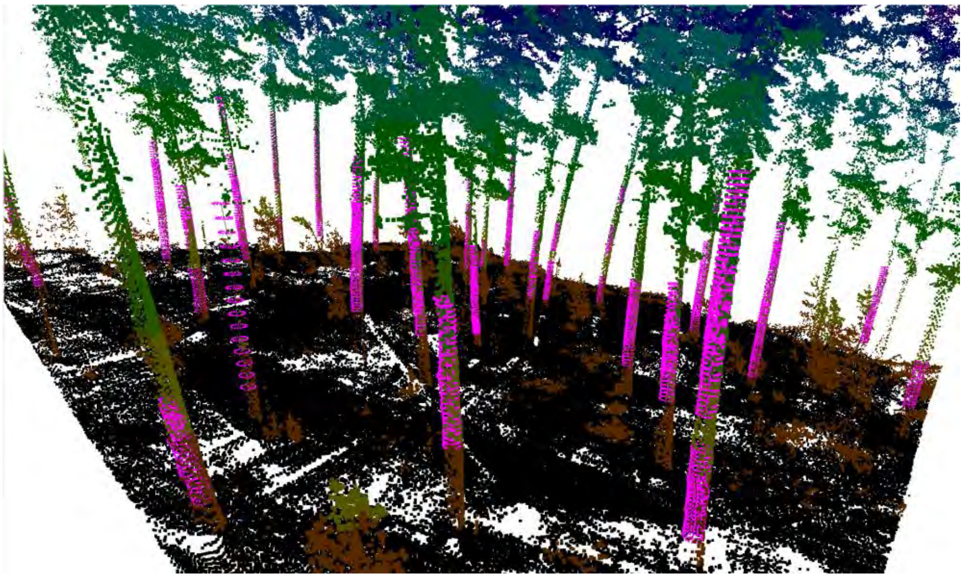

(b)

Figure 7: Stem detection and model-fitting results: (a) Original LiDAR pointclouds coloured by height, (b) detected stem sections (shown in purple) overlaid with LiDAR points

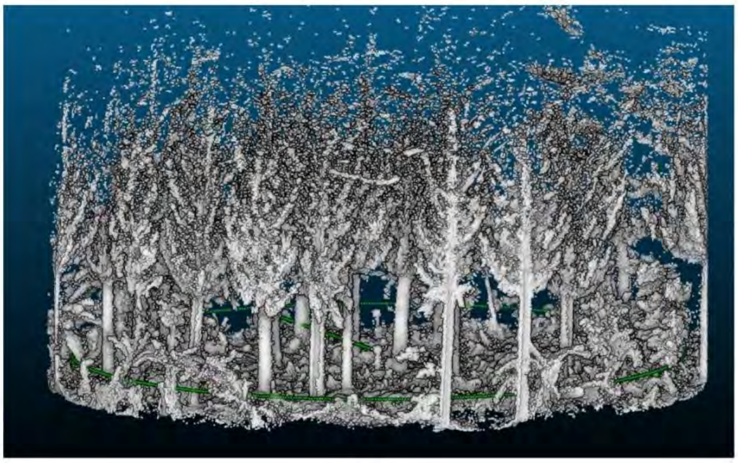

(a)

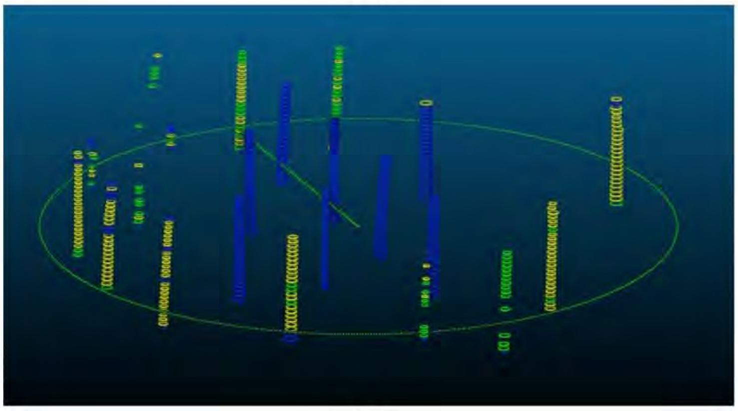

(b)

Figure 8: (a) TLS pointcloud of plot at Springfield, Tasmania with defined plot radius shown in green, (b) detected stem profiles using "Cloud2Stem". The large green circle near ground level identifies the boundary of a circular plot with a radius of 20m (a 3m buffer is present to allow for stems leaning out of the plot).

"Bottom-up"/Cloud2Stem Tree Detection and Stem Measurement Results Using TLS Data

TLS datasets of *Pinus radiata* plantation plots at the Springfield, Tasmania site, provided by Jon Osborn and researchers at the University of Tasmania were used initially to test algorithms within the "bottom-up", Cloud2Stem software. Figure 8 shows one of five 20 m radius TLS plots examined, with detected stems and stem profiles at a range of heights using "Cloud2Stem". All stems in the plot were identified correctly when compared to measurements taken in the field. Detected stem profiles were then used to extract DBH of each stem, and estimates of stem volume. Estimated DBH were then validated by comparing to DBH measurements made in the field (Figure 9). A strong correlation to field measurements was found with few outliers, which were manually investigated and found to be likely due to errors made during fieldwork.

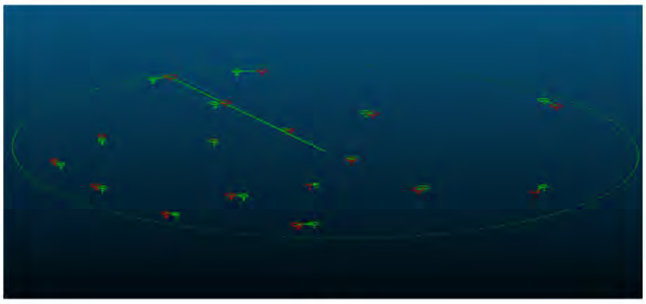

(a)

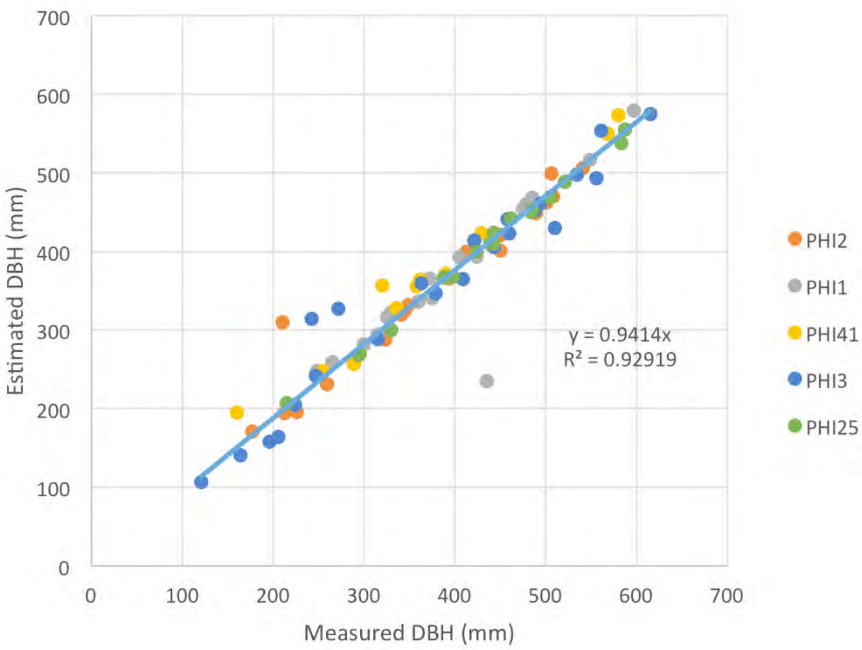

(b)

Figure 9: (a) Comparison of stem profiles detected using "Cloud2Stem" with stem locations and diameters (DBH) measured in the field. (b) Estimated DBH using "Cloud2Stem" versus field-measured DBH for six TLS plots at Springfield Tasmania.

"Bottom-up"/Cloud2Stem Tree Detection and Measurement Results Using VUX-1 Data

The Cloud2Stem software was used to detect and segment trees from aerially-acquired VUX-1 pointcloud data. Figure 10 shows a circular section of VUX-1 pointcloud data with corresponding fitted stem profiles (yellow, green and blue circles) using Cloud2Stem.

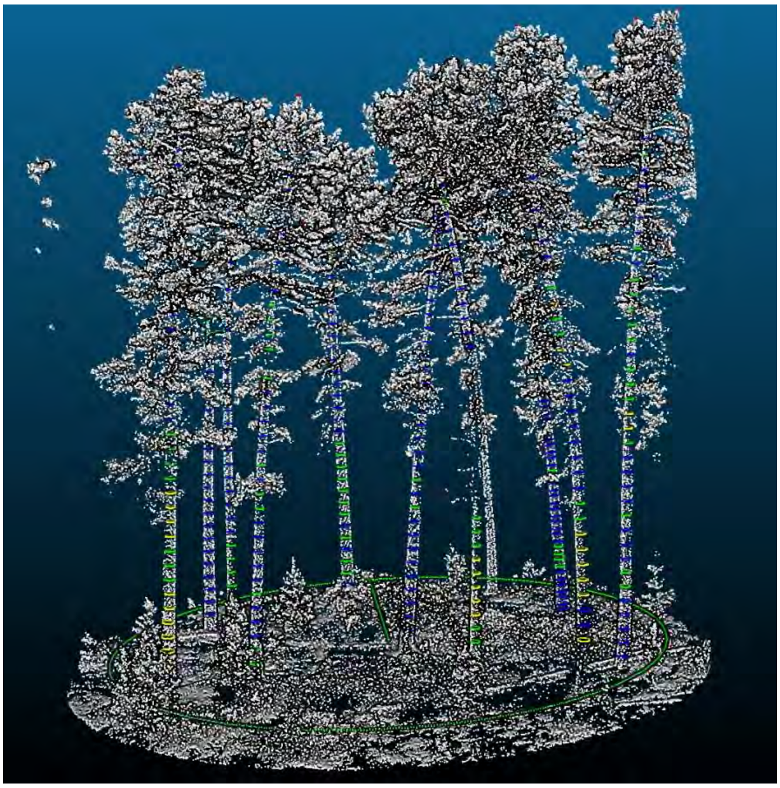

Figure 10: Identified stems superimposed over the normalised input point cloud produced by the VUX-1 scanner

Examples of Fitted Taper Curves

Figure 11 illustrates the initial tree diameters measured by the Cloud2Stem software taken from stacks of detected circles from the raw LiDAR pointclouds. Figure 12 shows a stem taper curve fitted to a well-formed set of diameters derived from the stacks. Outlier detection is set at 10% resulting in three diameters being excluded from the fit (at 10.9, 28.9 and 37.9m). Figure 13 shows a test case where only three diameters and stem height are measured. All three are in the lower half of the stem. The resulting curve is logical although supported by very few data points.

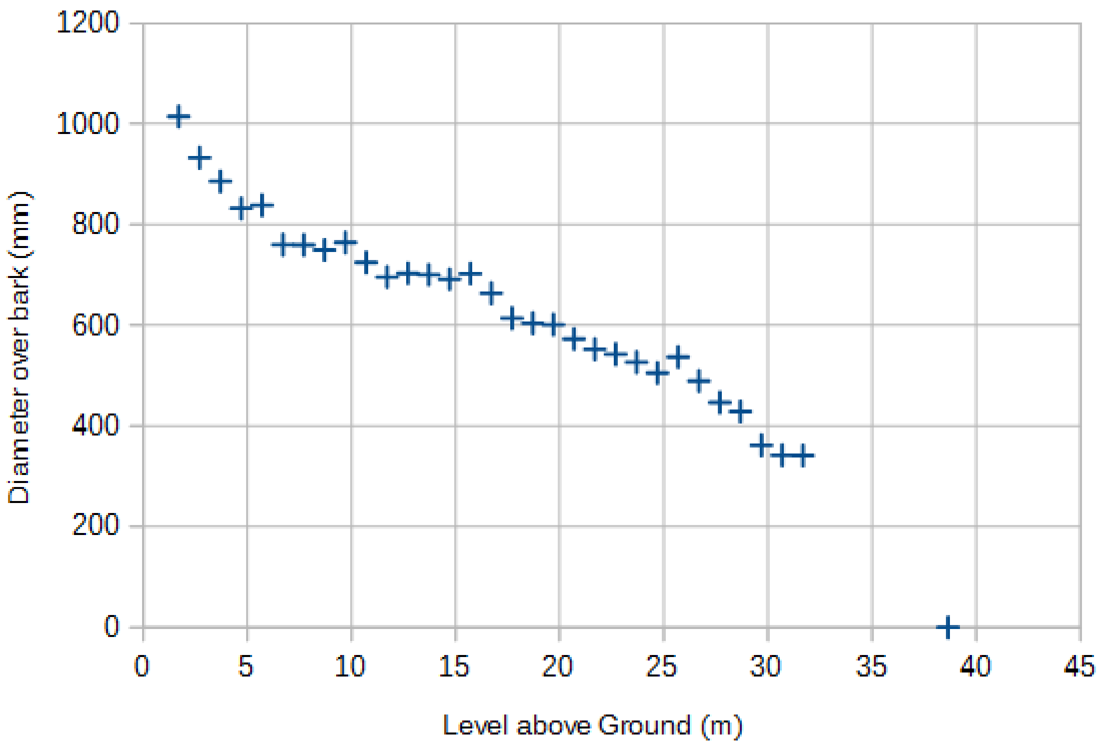

Figure 11: Example of stem diameters derived from a VUX-1 pointcloud

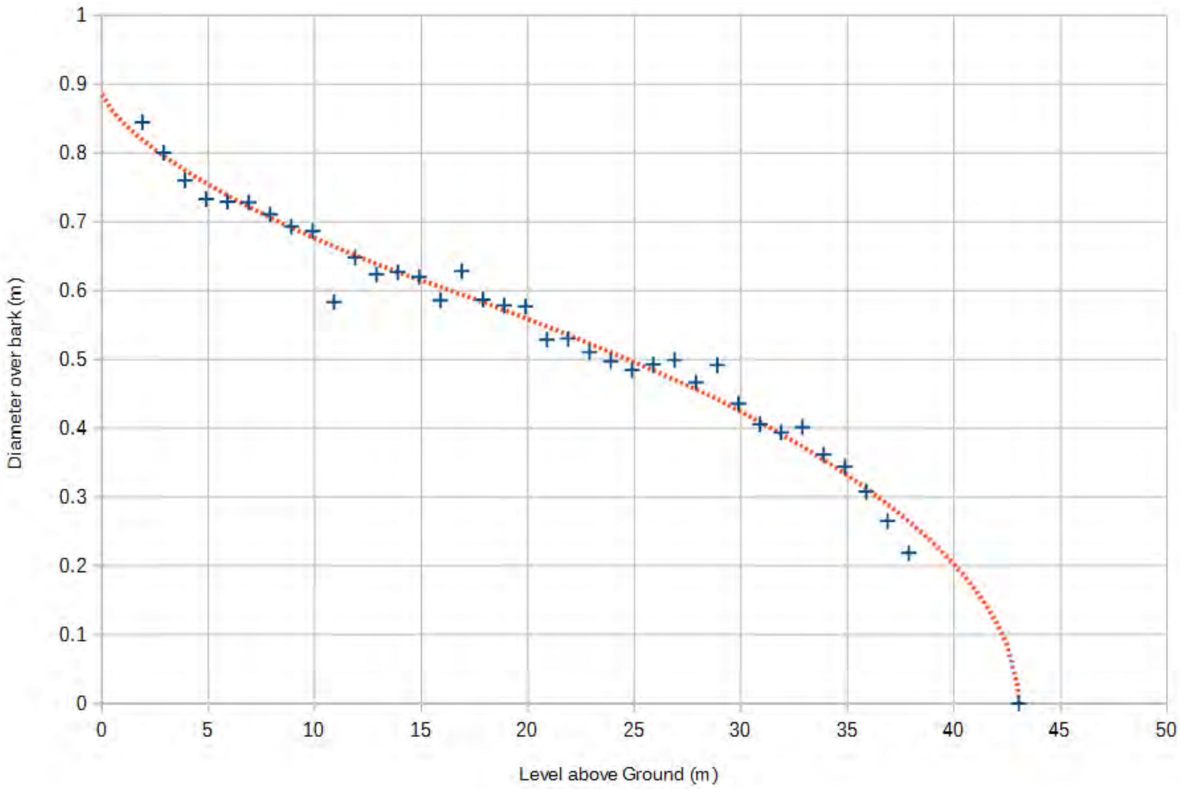

Figure 12: Taper curve fitted to diameters measured from VUX-1 pointcloud

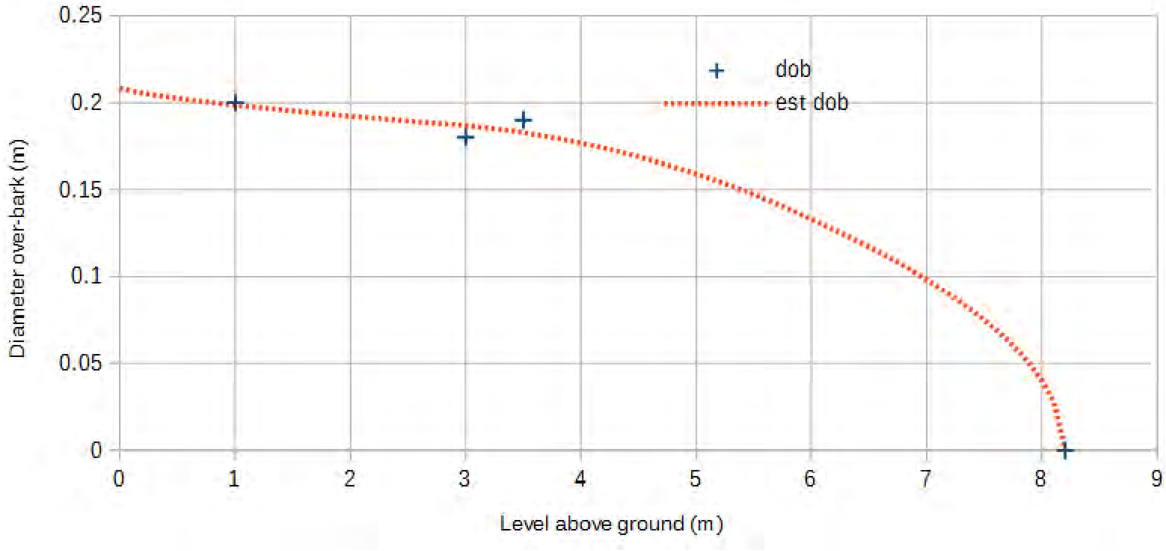

Figure 13: Taper curve fitted to test case with only three diameters and stem height

Example of Diameter Estimation

Figure 14 shows the upper and lower curves fitted to diameters derived from the point cloud for a particular stem using the 3 piece-wise curves to the stem profile. The un-trimmed diameters are present. The central curve (from H/3 to 2*H/3) is not shown.

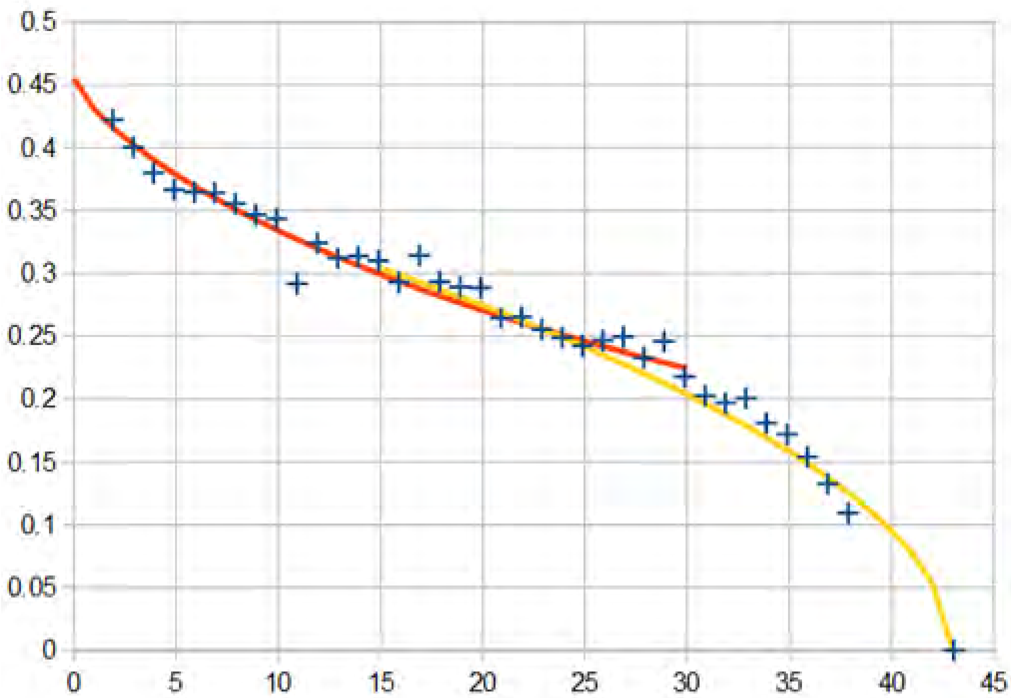

Figure 14: Upper and lower curves fitted to a set of diameters calculated from the VUX-**1** point cloud

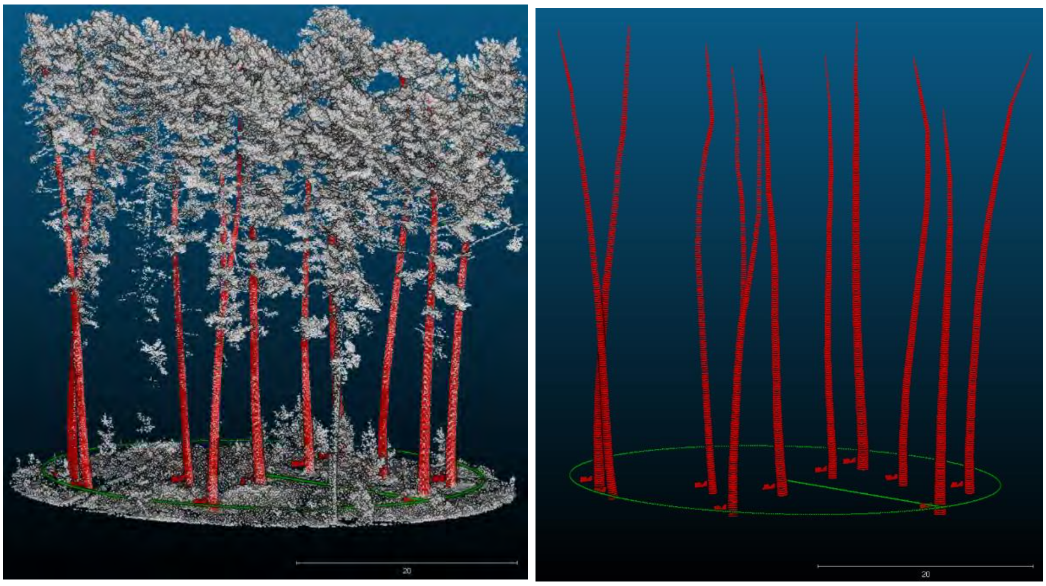

Figure 15: Diameters modelled over the entire stem

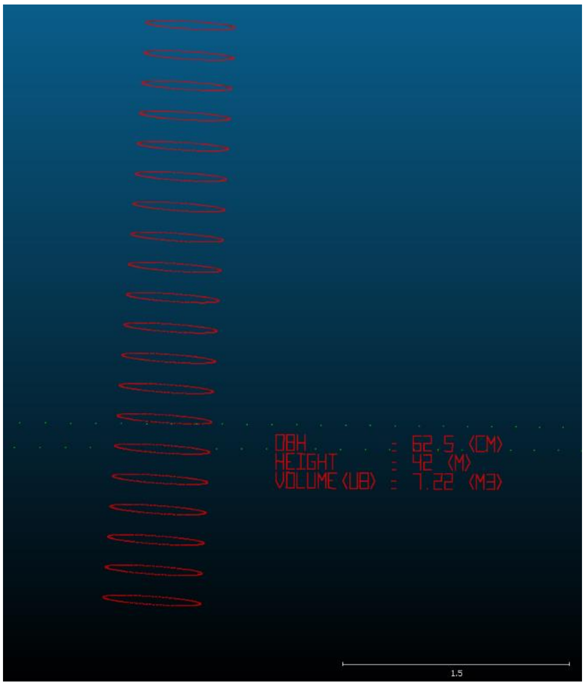

Figure 16: DBH, height and volume estimates displayed at the base of each stem

Final Stem Modelling Results: Detected, fitted stem sections

Figures 15 and 16 show red circles representing diameters modelled using the volume taper function calculated at regular intervals over the entire stem. These circles are superimposed over the original point cloud in the figure on the left. In the figure on the right the original point cloud is not shown and a fork is visible in the stem fourth from the left. An estimate of DBH, height and volume is written at the base of each stem and displayed alongside 3D models of the pointclouds and stem diameters (Figure 16).

Comparison with Measured Stems

Field measurements were taken of the scanned stems shown in Figure 10. All estimated stems were successfully matched with a corresponding measured stem. There was one omission (i.e. a measured stem was present which was not matched to a stem estimated by the Cloud2Stem software). In general, the DBH's were slightly under estimated by the Cloud2Stem software.

Stem Map Results

Figure 17 presents a resulting stem map showing the location of both measured (field measurements) and estimated stems within the plot for comparison. The large green circle is the plot boundary, while the green line is drawn from the plot centre to the plot boundary. The green circles represent measured stems, while the red circles represent estimated stems. A green line has been drawn from the centre of the measured stem to the corresponding estimated stem. On average the distance between centres is approximately 1.6m. The circles are at breast height (so represent DBH) and are to scale.

The red circles (i.e. estimated DBH's) are in general slightly smaller than the green (i.e. measured DBH's). Also, there is a green circle (i.e. measure stem) present in the top right of the figure which has no corresponding estimated stem.

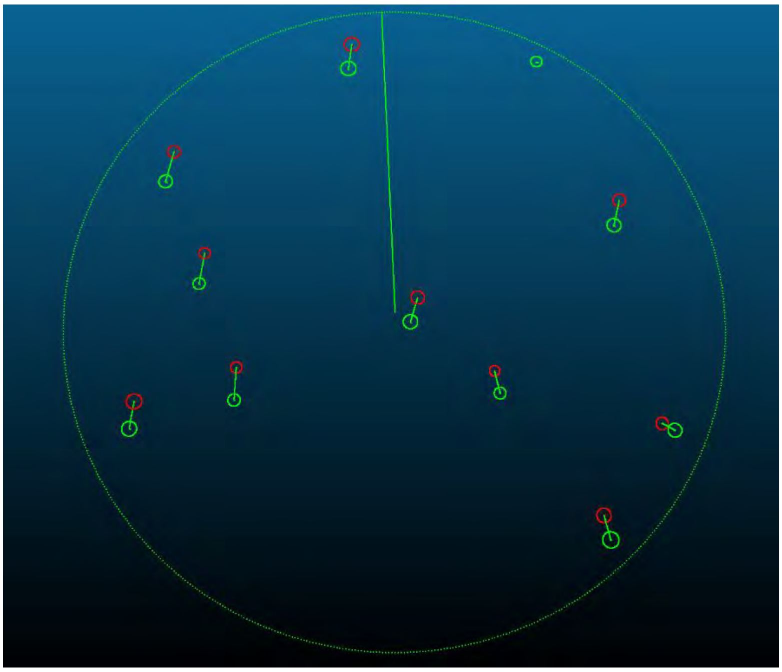

Figure 17: Stem map showing the location and size of all measured stems (green) and estimated stems (red)

On closer inspection, this missing estimated stem was identified by the software but was discarded as it was out of the plot. Figure 18 below shows the measured stem locations (green circles) superimposed over the point cloud produced by the VUX-1. The measured stem (in the right hand side of the figure below) has in fact been identified by the Cloud2Stem software, but as it is beyond the plot boundary (identified by the large green circle) it has been discarded.

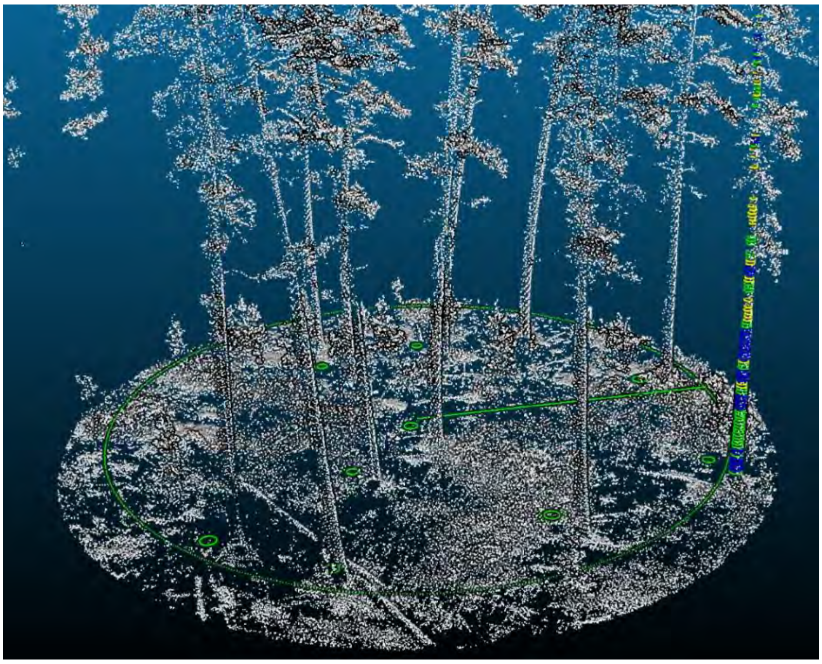

Figure 18: The omitted stem shown on the far right (identified by the stack of green, blue and yellow circles) is in fact beyond the plot boundary

This difference in stem locations may be caused by a difference in plot centre. If all the green circles in the stem map shown in Figure 17 were moved "up" by approximately 1.5m, (along the line drawn from the plot centre to the plot boundary), then the measured stem locations would closely match those of the estimated stems. Also, this would explain why the measured stem at the top right of the stem map was included, while the corresponding estimated stem was discarded as it fell outside the plot boundary.

It is important to note that errors in locating plot centre can cause differences in stocking estimates (as is the case with this plot).

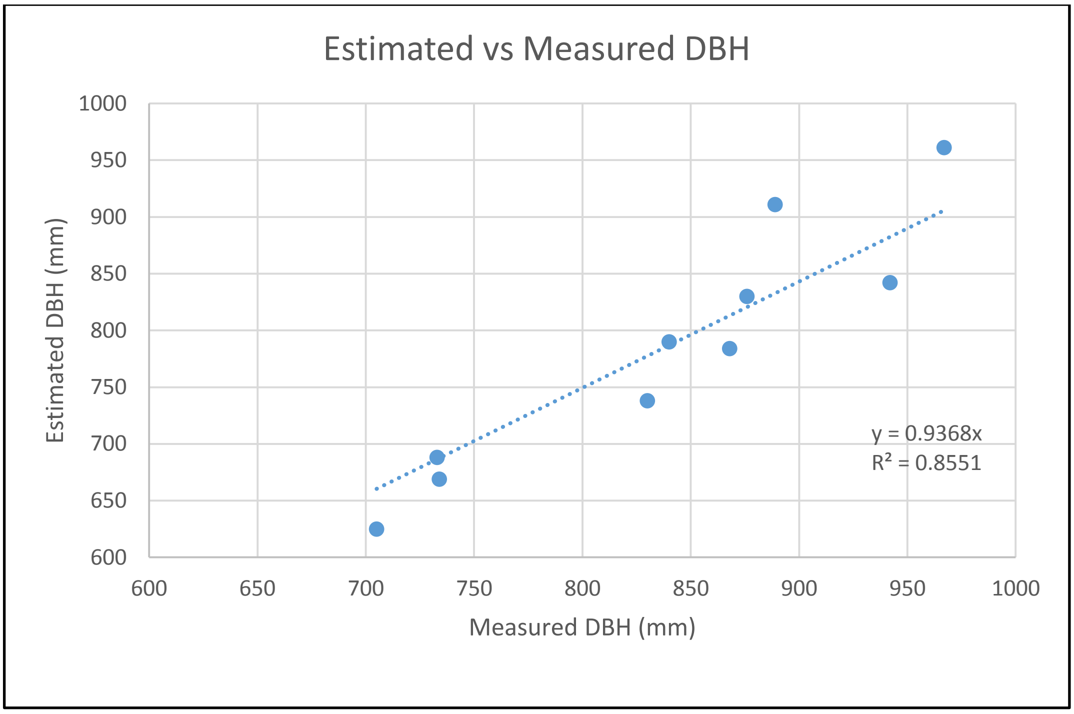

Figure 19: Comparison of ground-measured DBH to DBH estimated by Cloud2Stem for the 10 stems identified

Table 1: Comparison of Measured vs Estimated DBH.

Measured Stem No.	Estimated Stem No.	Measured Stem DBH (mm)	Estimated Stem DBH (mm)	Absolute Difference (mm)	Percentage Difference (%)
2	1	830	738	-92	-11.1
11	2	868	784	-84	-9.7
6	3	889	911	22	2.5
7	4	733	688	-45	-6.1
5	5	734	669	-65	-8.9
8	6	840	790	-50	-6
9	7	967	961	-6	-0.6
3	8	705	625	-80	-11.3
1	9	876	830	-46	-5.3
4	10	942	842	-100	-10.6
10		723			

DBH Comparison Results

Figure 19 and Table 1 show a comparison of the DBH of estimated stems with the DBH of field measured stems. On average the DBHs estimated from the point cloud are approximately 7% less than the measured DBHs.

Conclusion and Future Work

This chapter has described the development of algorithms and workflows for tree detection and individual tree-level estimates of diameter, volume and taper from high-resolution aerially-acquired LiDAR pointclouds. Algorithms were developed for a "top-down" detection of trees using a computationally-efficient RANSAC detection model and a "bottom-up" approach to circle detection, stacking and fitting algorithms, implemented in the software Cloud2Stem, for measuring stem position, diameter, volume and taper. A prototype workflow that combines the "top-down" and "bottom-up" processes and algorithms explored in this chapter was also proposed and described. This work flow would exploit the computational performance of a RANSAC-based detection system for initial detection of stems and the accurate stem modelling capabilities of the "Cloud2Stem" process to make estimates of stem diameters, volume and taper.

In order for the algorithms implemented in Cloud2Stem to work successfully, the input point cloud must have the following characteristics:

- A significant number of "stem hits" (i.e. points on the main stem below the canopy). Ideally there should be points on the main stem close to breast height so that an accurately assessment can be made of whether the stem's which are close to the plot boundary are to be included or excluded (particularly if the stems are leaning). For aerial scanners this involves penetrating the canopy (which can be particularly difficult with the dense canopy present in radiata pine stands)
- At least 50% circumferential coverage around the stem. This is important in order to estimate diameters reliably.
- A low level of positional error in the location of the points. This may lead to diameters being unreliable, or in some cases stems not being detected (particularly with small stems).

Most of these characteristics are related to the scanner used, whether or not the scanner is mobile and whether the scanner is terrestrial or aerial. For the aerially-acquired datasets using the VUX-1 scanner in this project, tree detection and diameter/volume calculations algorithms performed with a precision comparable results to field-based measurements. The nature of radiata pine and the stems being scanned most likely also affect the accuracy of estimated diameters and radii; radiata pine is not particularly uniform and the dense nature of needles makes it difficult for aerial scanners to penetrate the canopy or "see" the stem. When scanning radiata pine aerially the point clouds tend to contain a very high point density in the crown and few stem hits below the canopy.

Currently it is not possible for the algorithms presented here to produce log product estimates. The further estimation of log products relies on a number of pieces of information about stems that have not yet been successfully extracted using the currently developed approaches (such as the sweep, position of major branches, defects and the vitality of the tree). Tree sweep could potentially be measured from the cubic spline curves and direction and orientation of stem sections currently drawn out by Cloud2Stem. The detection of the position of major branches and defects in the tree requires additional work; potentially ideas for extracting this data include extending cubic spline fitting algorithms up into the canopy in a horizontal direction and the use of point segmentation algorithms to identify stem points for fine resolution modelling of stem surface geometry. These areas are left to future development.

References

Ayrey, E., Fraver, S., Kershaw, J.A., Kenefic, L.S., Hayes, D., Weiskittel, A.R., & Roth, B.E. (2017). Layer stacking: A novel algorithm for individual forest tree segmentation from LiDAR point clouds. *Canadian Journal of Remote Sensing* 43(1) 16-27.

Bienert, A., Scheller, S., Keane, E., Mohan, F., & Nugent, C. (2007). Tree Detection and Diameter Estimations by Analysis of Forest Terrestrial Laserscanner Point Clouds. *ISPRS Workshop on Laser Scanning and SilviLaser*, Espoo, Finland.

Dralle, K., & Rudemo, M. (1997). Stem number estimation by kernel smoothing of aerial photos. *Canadian Journal of Forest Research.* 26, 1228-1236.

Fischler, M.A., & Bolles. R.C. (1981). Random Sample Consensus: A Paradigm for Model Fitting with Applications to Image Analysis and Automated Cartography. *Comm. ACM.* 24(6): 381–395.

Gordon, A.D., & Budianto, M. (1999). A 3-point stem volume and taper equation for radiata pine. *Rotorua: Forest and Farm Plantation Management Cooperative*, Report No. 66 (Unpublished).

Gougeon, F.A. (1995). A crown-following approach to the automatic delineation of individual tree crowns in high spatial resolution aerial images. *Canadian Journal of Remote Sensing.* 21(3), 274-284.

Hyyppa, J., Kelle, O., Lehikoinen, M., & Inkinen, M. (2001). A Segmentation-Based Method to Retrieve Stem Volume Estimates from 3-D Tree Height Models Produced by Laser Scanners. *IEEE Trans. on Geoscience and Remote Sensing*. 39(5).

Lamprecht, S., Stoffels, J., Dotzler, S., Hab, E., & Udelhoven. T. (2015). aTrunk - An ALS-Based Trunk Detection Algorithm. *Remote Sensing*, 7, 9975-9997; doi:10.3390/rs70809975.

Larson, P.R. (1963). Stem form development of forest trees. *For. Abstr. Monogr.* 5:42.

Leckie, D., Gougeon, F., Tinis, S., Nelson, T., Burnett, C., & Paradine, D. (2005). Automated tree recognition in old growth conifer stands with high resolution digital imagery. *Remote Sensing of Environment* 94(3), 311-326.

Max, T.A., & Burkhart, H.E. (1976). Segmented polynomial regression applied to taper equations. *Forestry Science* 22:283–289.

Olofsson, K., Wallerman, J., Holmgren, J., Olsson, H. (2006). Tree species discrimination using Z/I DMC imagery and template matching of single trees. *Scandinavian Journal of Forest Research*. 21, 106-110.

Pollock, R. (1996). The automatic recognition of individual trees in aerial images of forests based on a synthetic tree crown model. PhD Thesis, Dept. of Computer Science. University of British Columbia.

Raumonen, P., Kaasalainen, M., Akerblom, M., Kaasalainen, S., Kaartinen, H., Vastaranta, M., Holopainen, M., Disney M., & Lewis, P. (2013). Fast Automatic Precision Tree Models from Terrestrial Laser Scanner Data. *Remote Sensing* 5(2), 491-520.

Reitberger, J., Schnorr, C.L., Krzystek, P., & Stillac, U. (2009). 3D segmentation of single trees exploiting full waveform LIDAR data. *ISPRS Journal of Photogrammetry and Remote Sensing* 64(6), 561-574.

Van Laar, A., & Akça, A. (2007). Forest Mensuration. Springer ISBN-13 978-1-4020-5991-9.

Wallace, L., Lucieer, A., & Watson, C.S. (2014). Evaluating Tree Detection and Segmentation Routines on Very High Resolution UAV LiDAR Data. *IEEE Trans. on Geoscience and Remote Sensing*, 52(12).

Wang, D., Kankare, V., Puttonen, E., Hollaus, M. & Pfeifer, N. (2017). Reconstructing Stem Cross Section Shapes from Terrestrial Laser Scanning. *IEEE Geoscience and Remote Sensing Letters* 14(2).

Weinacker, H., Kock, B., Heyder, U., & Weinacker, R. (2004). Development of filtering, segmentation and modelling modules for lidar and multispectral data as a fundament of an automatic forest inventory system. *Proceedings of the ISPRS working group VIII/2 laser scanners for forest and landscape assessment*, Frieburg, Germany, Vol. XXXVI. Part 8/W2.

Wulder, M., Niemann, K.O., & Goodenough, D.G. (2000). Local maximum filtering for the extraction of tree locations and basal area from high spatial resolution imagery. *Remote Sensing of Environment*, 73, 103–114.

Ziegler, M., Konrad, H., Hofrichter, J., Wimmer, A., Ruppert, G.S., Schardt, M., & Hyyppae, J.M. (2000). Assessment of forest attributes and single-tree segmentation by means of laser scanning. *Proceedings or Laser Radar Technology and Applications V*, Volume 4035; doi: 10.1117/12.397780.

4.2. Comparison of models describing forest inventory attributes using standard and voxel-based LiDAR predictors across a range of pulse densities

Pearse G.[1], *Watt M.S.*[2], *Dash J.P.*[1], *Stone, C.*[3]

[1]*Scion, Private Bag 3020, Rotorua, New Zealand*
[2]*Scion, P.O. Box 29237, Christchurch, New Zealand*
[3]*NSW Forest Science, NSW Department of Primary Industries Forestry, Locked Bag 5123, Parramatta, NSW, Australia*

Introduction

Light detection and ranging (LiDAR) is an established, active remote sensing technology that has been widely used in vegetation assessment. There has been a rapid uptake of lidar over the last two decades as this technology can finely characterise the three-dimensional structure of both the forest canopy and underlying terrain across broad spatial scales. Previous research has demonstrated the utility of LiDAR for a diverse range of applications such as habitat analysis (Hyde *et al*. 2005; Vierling *et al*. 2008; Palminteri *et al.* 2012), predicting forest inventory attributes (e.g. Nilsson 1996; Næsset & Okland 2002; Næsset & Bjerknes 2001; Popescu *et al*. 2002; Holmgren *et al*. 2003; Watt & Watt 2013), change detection (Hudak et al. 2012; Yu *et al.* 2004; Teo & Shih 2013) and estimation of wildland fire parameters (Hall *et al*. 2005; Mutlu *et al.* 2008a; Mutlu *et al*. 2008b). When included within a forest inventory framework, auxiliary data from LiDAR allows the spatial projection of forest inventory attributes and has been shown to markedly improve the inventory precision compared to conventional approaches with only plot data (Dash *et al*. 2015a; Næsset 2002, 2004; Naesset 2007). The use of airborne LiDAR surveys have become common practice for stand-wise forest inventories in several countries (e.g. Næsset *et al.* 2004) and this technology underpins several national forest inventories (Stephens *et al.* 2012).

Almost all LiDAR surveys use low (≤4 pulses/m^2) to moderate (4 − 20 pulses/m^2) density LiDAR collected from manned aircraft and little research has investigated the utility of high-density LiDAR (> 20 pulses m^2) for predicting forest inventory attributes. The development of LiDAR sensors that can be carried at low altitude by unmanned aerial systems (UAS) provide a means of acquiring far more detailed point clouds than is possible from manned aircraft. Typical point densities from these platforms range between 60 − 1,500 points/m^2 (Puliti et al. 2015) which exceeds the point densities that can ordinarily be collected from conventional fixed-wing aircraft by up to two orders of magnitude. Studies demonstrating the utility of LiDAR from UAS are still sparse but do demonstrate relatively accurate predictions of forest dimensions within a range of forest types using high (Brede et al. 2017) and moderately precise scanners (Wallace *et al.* 2016; Wallace *et al.* 2012; Wallace *et al*. 2014; Jaakkola *et al*. 2010).

Prevailing approaches to LiDAR analysis for forest inventory use standard statistical metrics derived from discrete return data. Standard metrics, which are obtained from LiDAR point cloud data, generally include height percentiles, distributional statistics, and estimates of canopy cover. These metrics have been previously used to predict stand height and volume with high precision (Watt & Watt 2013; Coops *et al*. 2007; Means *et al*. 2000; Means *et al.* 1999) basal area with moderate precision (Næsset 2004, 2005; Nord-Larsen & Schumacher

2012; Means *et al.* 1999; Means *et al.* 2000) and stand density with a low to moderate degree of precision (Næsset & Bjerknes 2001; Hall *et al*. 2005).

Another class of LiDAR metrics, termed voxel-based metrics, have emerged over the last decade (Sumnall *et al.* 2016). Using this approach, the LiDAR point cloud is sliced in both the vertical and horizontal dimensions into volumetric pixels (volume pixel or voxel) which can be visualised as an array of 3-D cubes. Voxel-based metrics are then created by describing the LiDAR point cloud data in relation to each voxel space. Compared to standard metrics, voxel-based predictors have the advantage of representing LiDAR point cloud information within different strata in the forest canopy and offer the potential to better characterise the fine-scale distribution of returns.

Voxel-based metrics have been used relatively widely with terrestrial laser scanning (TLS) data to predict forest inventory attributes (Moskal & Zheng 2011; Ehbrecht *et al.* 2016; Bienert *et al.* 2014) and leaf area index (Grau *et al*. 2017; Béland *et al.* 2014). However, less research has investigated the utility of voxel-based metrics from airborne LiDAR data. These predictors have been used to model above-ground biomass (Kim *et al*. 2016), canopy base height (Maguya *et al*. 2015; Popescu & Zhao 2008), leaf area index (Pearse *et al.* 2017) and canopy attributes (Sumnall *et al*. 2016). We are unaware of any research comparing the precision of voxel-based and standard metrics for predicting forest inventory attributes from airborne LiDAR data. Given that high-density LiDAR is becoming more commonly available and acquisition costs are decreasing, comparison of these approaches across a wide range of LiDAR pulse densities would be useful and timely.

Using high-density LiDAR acquired across 73 plots from a helicopter-mounted VUX-1 scanner, the objective of this study was to compare the precision of models predicting forest inventory attributes (top height, basal area, stand density and total stem volume) created using standard metrics, voxel-based metrics and both types of metrics at pulse densities ranging from 1 to 280 pulses m^{-2}.

Methods

Study Site and Plot Location

The study area, managed by the Forestry Corporation of New South Wales, is located in the Snowy Mountains in southeastern New South Wales, Australia. The plots were divided between two adjacent *Pinus radiata* D. Don plantations (Figure 1). Field plots (n = 73) were deliberately located to target a broad range of stand conditions within these two plantations (Table 1). Several of the included plots from the southern study area were part of a long-term trial block which had recently been measured. Differential GPS was used to determine the centre coordinates of each of the 0.13 ha bounded circular plots.

Table 1: Variation in summary statistics for the dataset. Shown are the mean, standard deviation and range for data from the 73 plots.

Variable	Mean	SD	Range
Age (years)	26.8	5.3	15.0 – 48.2
Top Height (m)	26.8	3.3	17.3 – 35.0
Basal Area (m2 ha-1)	34.5	11.8	4.14 – 63.9
Stand Density (stems ha-1)	422	304	33 – 1,683
Total Stem Volume (m3 ha-1)	312	119.8	58.1 – 692.8
Pulse Density (pulses m-2)	270	53	163 – 452
Point Density (points m-2)	436	99	260 – 800

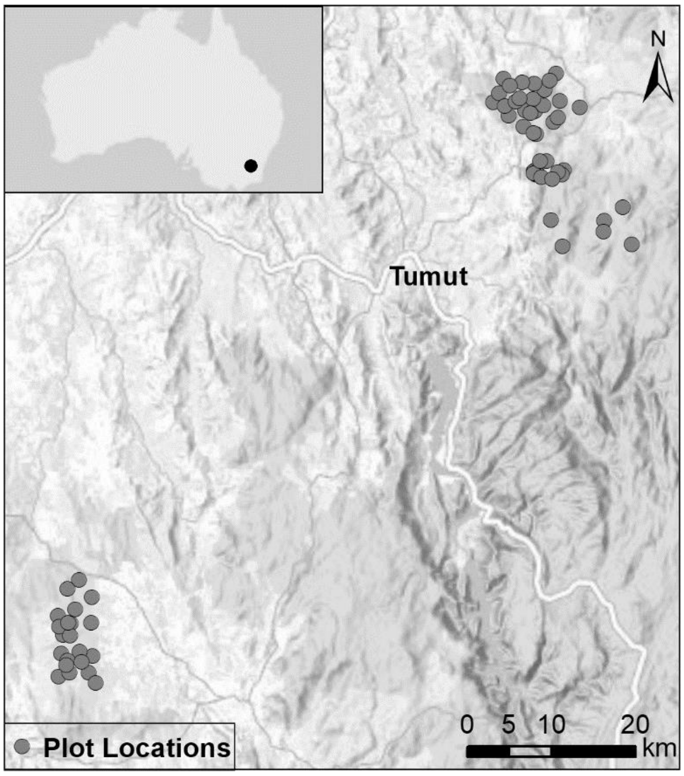

Figure 1: Map of the study plots (n=73) near Tumut, New South Wales, Australia.

Field Measurements

Plot measurements, which were taken during the latter half of 2016, included diameter at breast height, D, for all trees within the plot (1.3 m) and height, H, on a sub-sample of three trees, covering the D range within the plot. These measurements were used to fit a regression between D and H that was subsequently used to estimate H for all plot trees where H was not measured. Top Height was then calculated as the average height of the largest 100 trees per hectare, where largest was defined in terms of D. Plot basal area and stand density were calculated from the plot measurements. Total under-bark stem volume, V, was derived from height and diameter using the following volume function (Baalman 2003):

$$V = \exp(a)\, D^b \left(\frac{H^2}{H-1.3}\right)^c \tag{1}$$

where a, b and c are empirically determined coefficients.

Summary statistics for all of the plots included in the study (Table 1) show wide variation in forest inventory attributes and stand ages. Stand age varied three-fold, averaging 27 years and ranging from 15 − 48 years. Other forest inventory attributes also showed large variations that ranged from two-fold, 15 fold, 51-fold and 12-fold for top height, basal area, stand density and volume respectively.

Lidar Data

Lidar data were acquired using a VUX-1 (RIEGL, Horn, Austria) laser scanner mounted on a helicopter flying at < 8 m s^{-1} and an altitude of approximately 90 m above ground. A large buffer was defined around each plot and flight plans were designed to ensure high overlap and minimal occlusion of all trees within each buffered plot. The LiDAR data coincident with the plots were extracted, processed and, classified using LAStools (Rapidlasso GmbH, Gilching, Germany). The high scan rate (+- 200 scans per second) of the VUX-1 combined with a specified value of up to 5 returns per pulse generated extremely dense datasets (Figure 2). Up to three-fold variation in pulse density was observed in the final plot data (Table 1). This resulted from the combination of the scan rate and unavoidable variations in helicopter flight trajectories and inclusion of additional flight lines to avoid stem occlusion in difficult plots.

To determine the relative importance of pulse density and metric type, we thinned the LiDAR data. All plots were thinned to an initial, maximum pulse density of 280 pulses m^{-2} based on the lowest pulse density of the included plots. Target pulse densities of 260, 240, 220, …20, 15, 10, 5, and 1 were specified and an iterative algorithm was devised to systematically remove all returns associated with individual pulses until the target pulse density was achieved with a reasonable homogeneity of spacing.

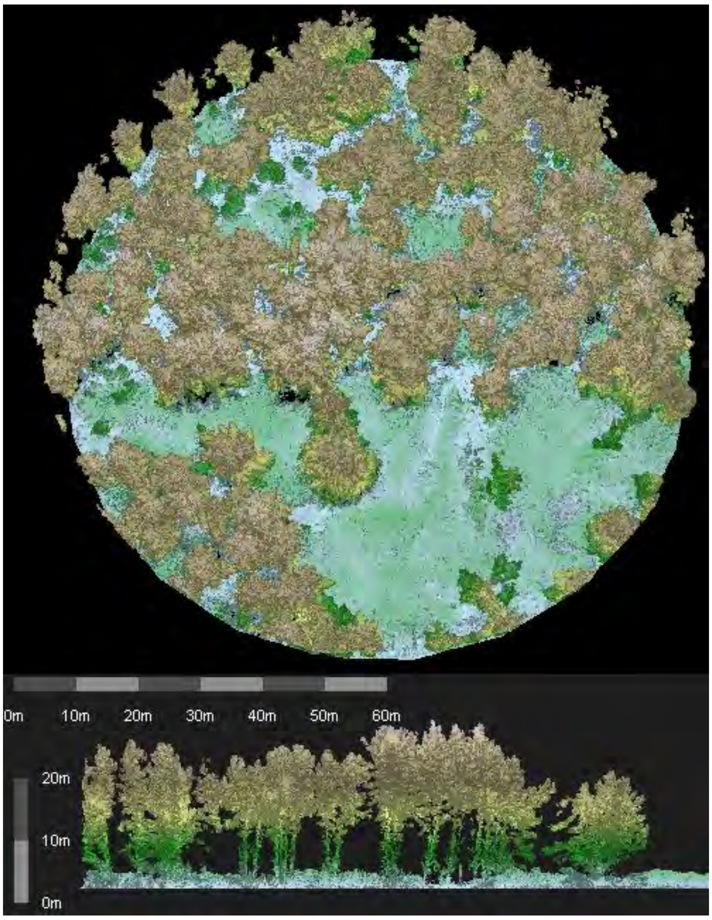

Figure 2: Example of lidar data acquired from the VUX-1 sensor in a stand of *Pinus radiata* (top). Cross-section (bottom) showing detail from a strip of 10 m width running North to South.

Variables Used

The very high pulse density provided by the VUX-1 scanner motivated an investigation of novel metrics for prediction of key forest plot attributes. Metrics proposed for use with TLS data and others proposed for the fine-scale characterisation of point clouds were identified for this purpose. For this study, descriptive metrics such as percentile heights, measures of skew, and other common metrics were termed 'standard' metrics (Appendix 1). These metrics have been widely used to predict forest attributes from LiDAR (Dash *et al.* 2015a; Naesset 2002) and are often available as outputs from widely used LiDAR processing software (Pearse *et al.* 2017; McGaughey 2015). The remaining metrics were termed 'voxelised' metrics on the basis that they required the division of the point clouds captured from each plot into voxels. The rationale and the method of construction for the selected metrics are provided in the sources listed in Appendix 2. Several common forms were used and these are described in the following section.

General Description of Voxelisation

The number of dimensions considered during the voxelisation process was a useful property for grouping the different metrics. The majority of metrics used regular, fixed-size voxels whereby the point cloud was divided into sub-voxels with each voxel having fixed dimensions of $X \times Y \times Z$ m - equivalent to a 3-dimensional histogram. The points falling within each cell formed the basis for further operations. For example, the variable sub-voxels (SVi) and variable density (Di) metrics (Kim *et al.* 2016; Sheridan *et al.* 2014) and the effective number of layers (ENL) defined by Ehbrecht *et al.* (2016) consider the density, proportion or distribution of different return types falling within each sub-voxel (Figure 3).

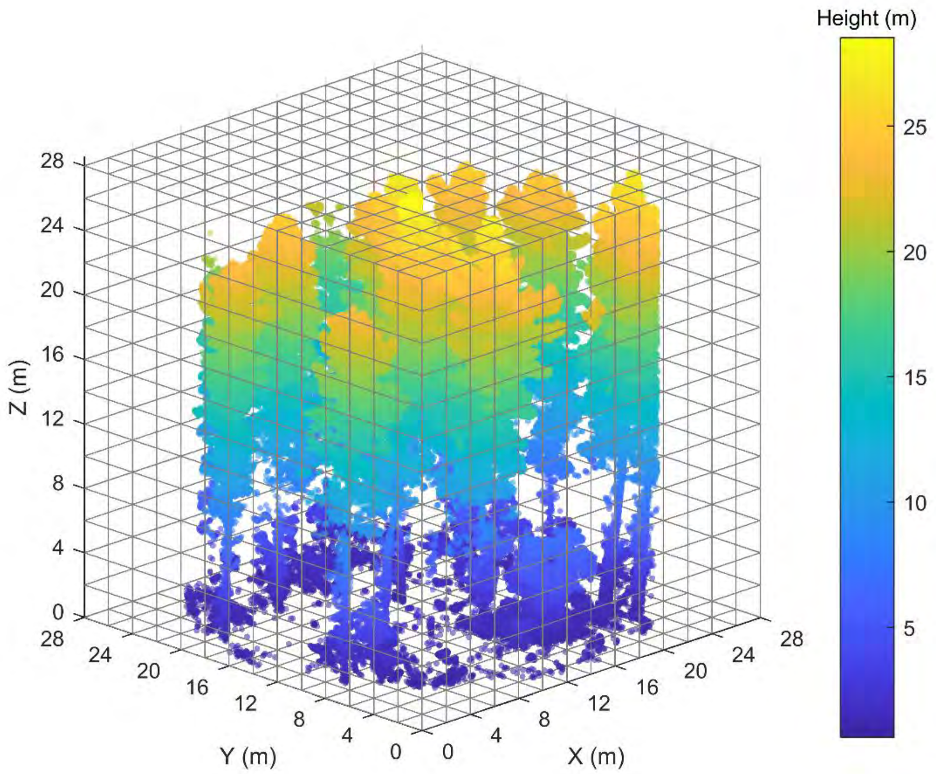

Figure 3: Example lidar data showing the division of the vegetation returns into regular, equal size voxels.

Metrics dividing the point cloud into two dimensions, similar to the canopy closure measure of Pope and Treitz (2013), allocate points to bins using only the x and y axes (bivariate histogram) before characterising the point cloud based on the distribution of returns within each sub-voxel (Figure 4).

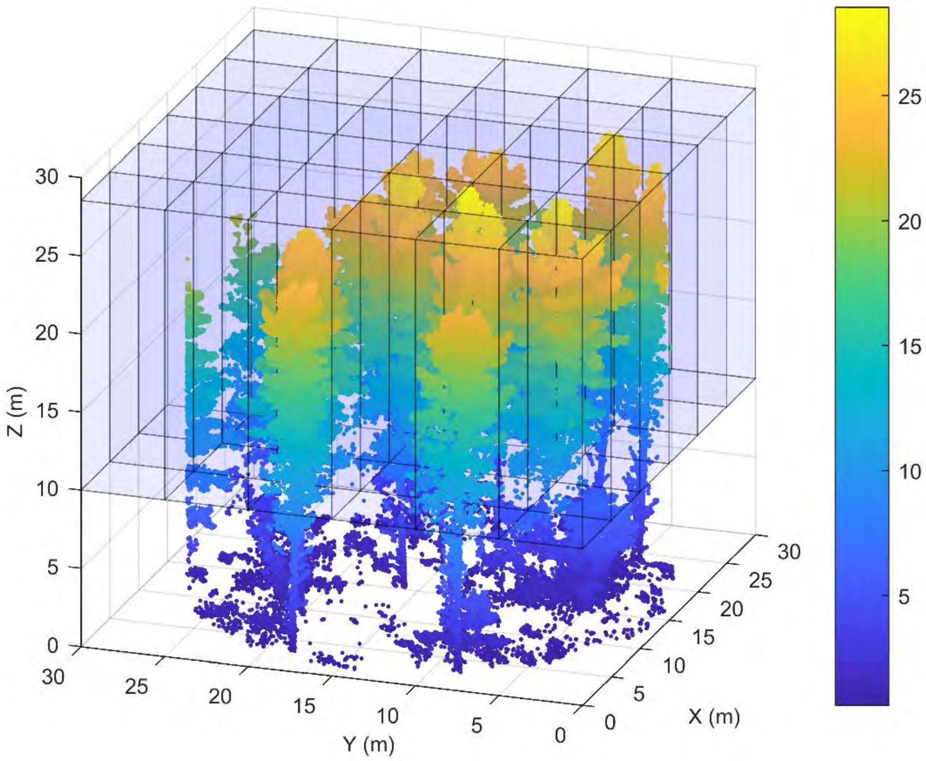

Figure 4: Example of bivariate voxel metric quantifying canopy closure as the fraction of empty voxels at 10 m height.

Unidimensional metrics such as the vertical complexity index (VCI) (Van Ewijk 2015) seek to characterise the evenness, or relative abundance of points using strata or layers of a fixed size (Figure 5).

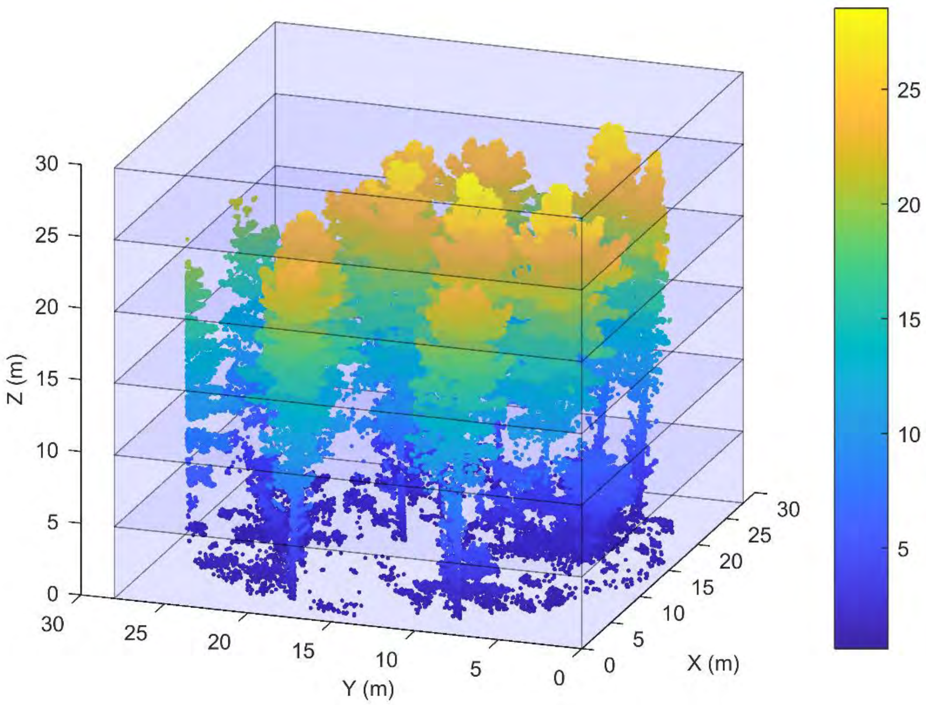

Figure 5: Division of the point cloud into layers (univariate voxelisation) as a precursor to calculating the relative abundance of points in each stratum.

The final class of metrics used a dynamic process to characterise the point cloud. For example, the moving-voxel metrics of Maguya *et al*. (2015) use an iterative searching process to identify gap sizes in 3-dimensions. Similarly, the variable sub-voxel metrics (SVM) of Kim *et al.* (2016) characterise the point cloud with reference to a specific sub-voxel of interest (e.g. sub-voxel with the median point density) that must first be identified (Figure 6A) before the distribution of points relative to the identified voxel are characterised (Figure 6B). Many of these processes require decisions around the appropriate sub-voxel size or methods of characterisation. In some cases, recommendations are available based on previous sensitivity analysis (e.g. Van Ewijk (2015)). However, in others research the choice has been subjective or multiple permutations of voxel-based metrics with different dimensions have been used simultaneously during model fitting (Kim *et al.* 2016; Pope & Treitz 2013). The values chosen for this analysis were partially informed by previous work in a similar context (Pearse *et al*. 2017). Where these values were indeterminate, several permutations were trialled e.g. voxels varying in size from 1, 2…, 5 m. To limit over-fitting and reduce dimensionality, a process of screening was then carried out to remove permutations with excessively high inter-correlation. The threshold for exclusion was defined as any permutation of a base metric with a Pearson's correlation coefficient greater than 0.9.

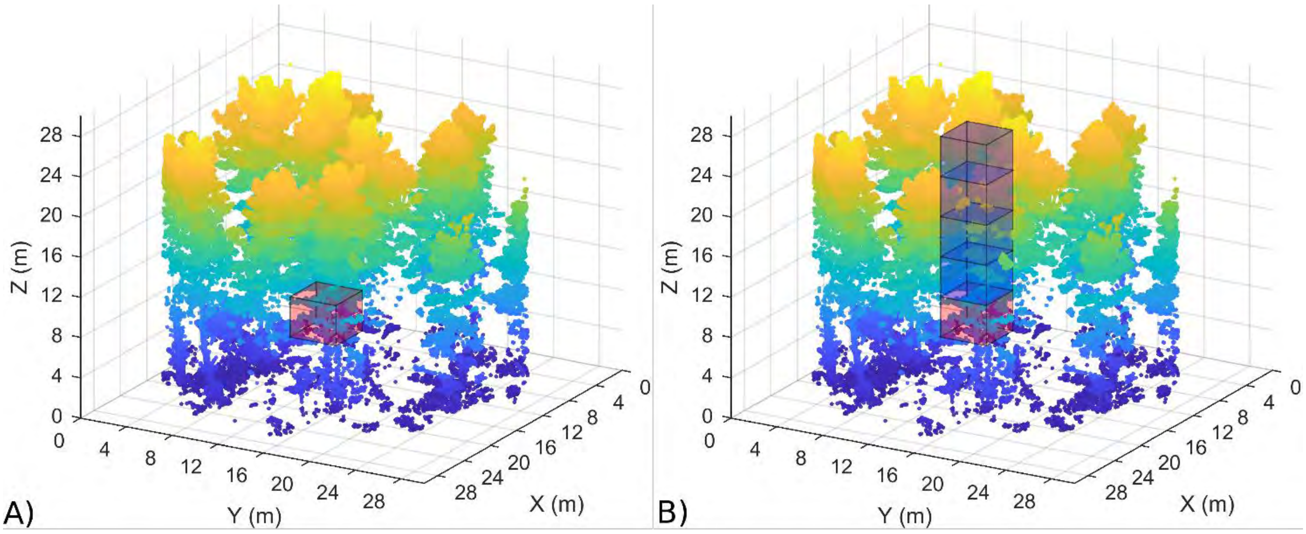

Figure 6: Adaptive voxelisation identifying the voxel with the median density (A) and the relative fraction of returns in the voxels above (B).

Statistical Analysis

The random forests algorithm was selected for modelling of plot attributes (Breiman 2001) and modelling was carried out using the package RandomForests (Liaw & Wiener 2002) in the R statistical language (R Core Team, 2016). Random forests is an ensemble learning algorithm that is well suited to both classification and regression. The algorithm grows a large forest of decision trees, utilising both random permutations of data available to each tree as well as permutation of variables at each splitting node. In this way, the algorithm avoids overfitting when dealing with a large number of covariates such as the LiDAR metrics assembled in this study. Random forests models were used to model mean top height, basal area, stand density and volume from standard LiDAR metrics (Appendix 1), voxelised metrics (Appendix 2) and both classes of metrics combined. Because data are withheld during construction of each tree, an estimate of model performance can be obtained by making predictions on the withheld 'out-of-bag' data during the model fitting process. However, we opted to include a strategy of 10-fold cross-validation combined with resampling (100 repeats). This approach was chosen to guard against overfitting, minimise fold effects and to produce conservative estimates of model precision. The model fitting process described was then repeated using LiDAR metrics constructed from the thinned datasets to assess the impact of pulse density on the choice of metrics and predictive accuracy of the models.

Comparisons of model precision for each of the four forest inventory attributes were made to determine the relative effect of pulse density and the type of LiDAR metrics included within the models. Precision was evaluated by the coefficient of determination (R^2) and the root-mean-square error (RMSE), which was normalised with respect to the overall mean of each of the four dimensions (y_m) as nRMSE = RMSE/y_m x 100. Variation in model precision between the three metric types was examined both at the highest pulse density and plotted against the complete range in pulse density to examine how thinning the dataset affected model precision.

Metric Importance

The importance of voxel-based and standard LiDAR metrics was evaluated for each of the four forest inventory attributes using the models that included all LiDAR metrics (voxel-based and standard). Random forests computes a measure of variable importance through random permutation of variable values in the withheld data. For regression, the importance of the variable is then scored by observing the increase in mean squared error (MSE) after permutation (Genuer *et al.* 2010; Liaw & Wiener 2002). At each pulse density, the variable importance scores obtained from the random forests algorithm were used to identify the most important predictors contributing to the model. While this measure had been widely used for variable selection, the absolute importance scores have been shown to be unreliable in some situations (Strobl *et al.* 2008). For this study, we were concerned only with patterns of variable importance between the two groups of voxel-based and standard metrics rather than the absolute importance of individual metrics. To evaluate potential trends, a threshold for importance was required to compare the many models obtained for each of the inventory attributes at each pulse density. Inspection of variable importance scores (not shown) showed that, for the majority of models, separating metrics above an importance score of 3 worked well. This value excluded nearly all metrics with similar, low importance scores for the different models while retaining the key variables that showed a marked increase in importance as assessed by a large increase in MSE after permutation. The number of these important variables within each group (voxel-based or standard) was then plotted against pulse density and averaged across all pulse densities to gain insight into which metric types were the most influential within the models for each of the four inventory attributes.

Results

Model Predictions at the Highest Pulse Density

At the highest pulse density, models created using standard LiDAR metrics had an R^2 of 0.72, 0.44, 0.34 and 0.53, respectively, for top height, basal area, stand density and volume (Fig. 7a). Use of voxel-based metrics substantially improved the R^2 of these models by 0.23, 0.24 and 0.22 respectively, for basal area, stand density and volume, but resulted in only a small improvement of 0.04 for top height. Use of all metrics in predictive models had little effect on predictive precision over models that included only voxel-based metrics (Figure 7a).

The pattern described above reflected changes in nRMSE (Figure 7b). Using standard LiDAR metrics, nRMSE was 7, 25, 60 and 25%, respectively, for top height, basal area, stand density and volume. Use of voxel-based metrics substantially improved the predictive precision of these models, for all dimensions apart from top height, reducing nRMSE by 0.6, 6, 12 and 7%, respectively, for top height, basal area, stand density and volume. Model precision using both types of LiDAR metrics was very similar to the precision of models that used only voxel-based metrics (Figure 7b).

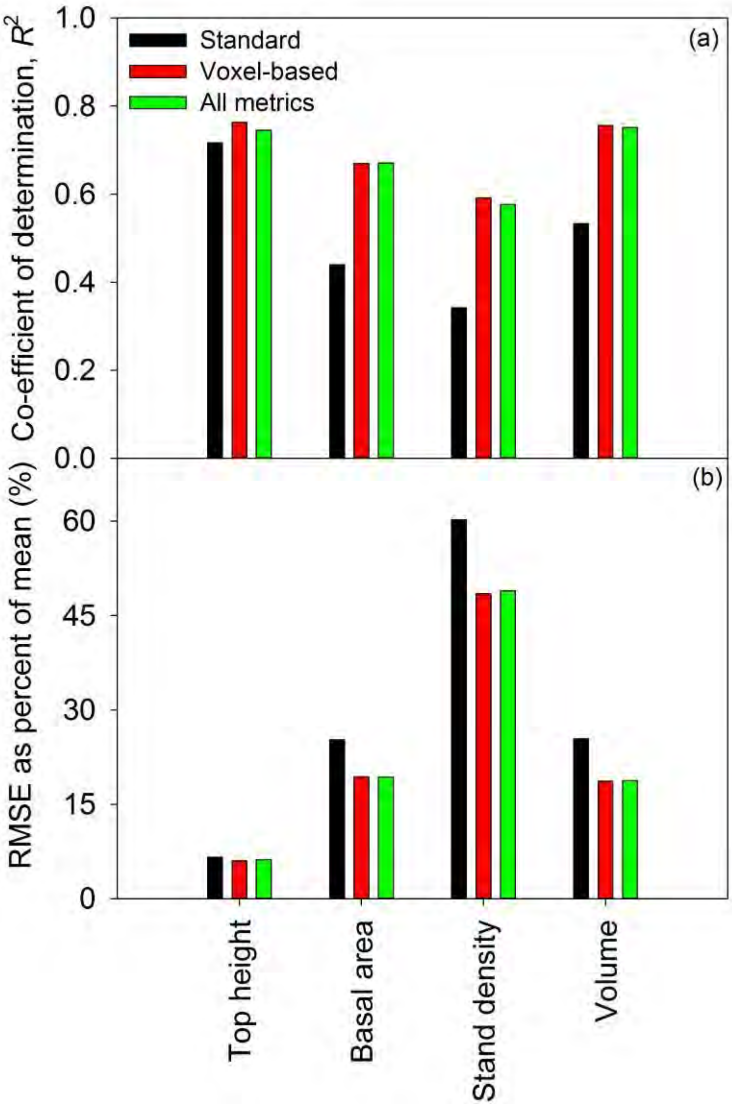

Figure 7: Influence of predictor type on model precision for the four stand metrics at the highest pulse density with results showing (a) RMSE as a percentage of the mean and (b) the coefficient of determination (R^2).

Effect of Thinning on Model Precision Between the Three Metric Groupings

With the exception of stand density, pulse density had little effect on model precision (Figure 8). When averaged across the three groups of independent variables, the R^2 for models of stand density gradually increased from 0.45 at 1 pulse m^{-2} reaching a maximum of 0.54 at 60 pulses m^{-2} before declining slightly (Figure 8c).

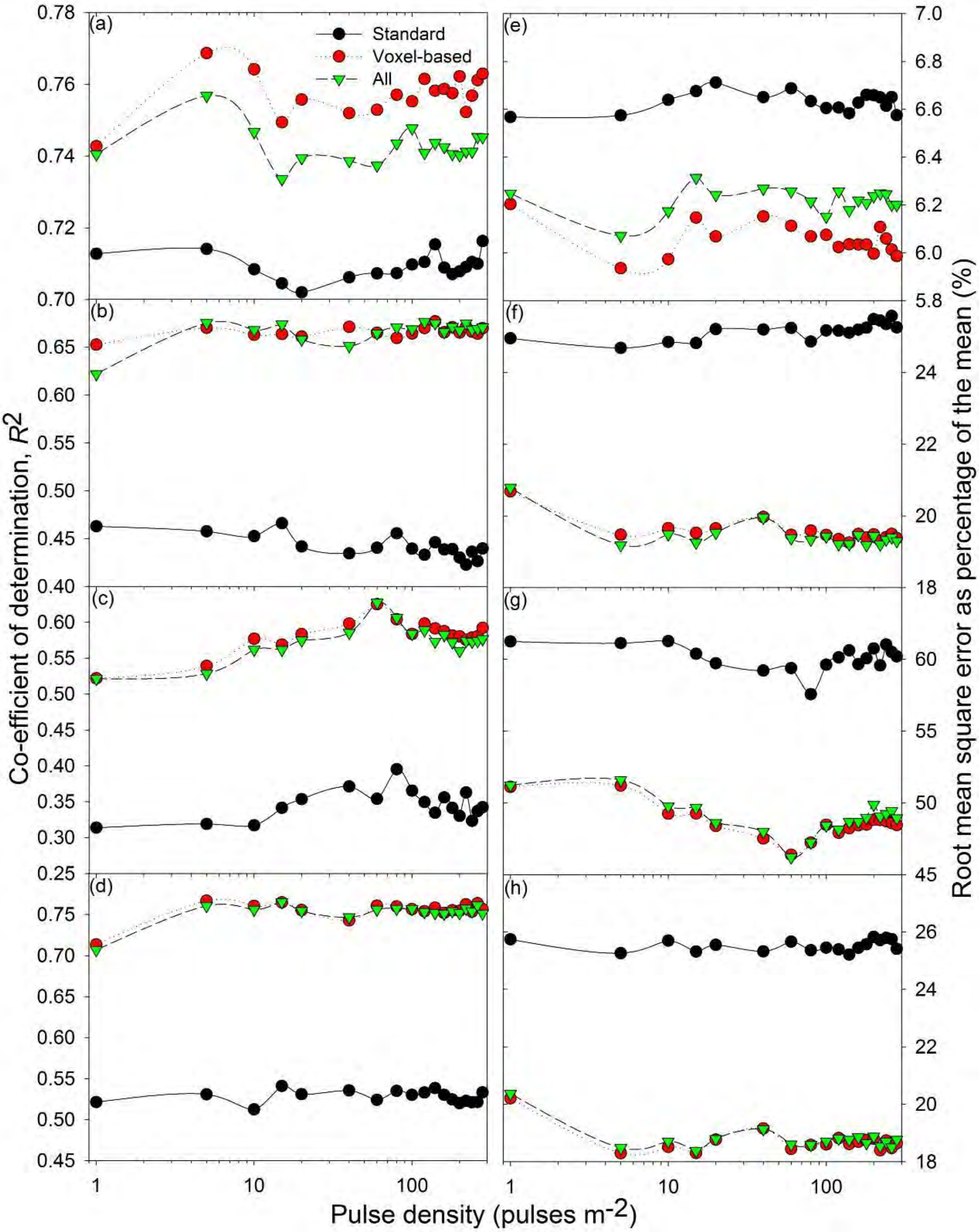

Figure 8: Variation in the (a-d) coefficient of determination, R^2, and (e-h) root mean square error as a percentage of the mean across the pulse density range for the three predictor groups (standard, voxel-based and all metrics) in models of (a, e) top height, (b, f) basal area, (c, g) stand density and (d, h) total stem volume.

Variation in mean R^2 for the three other forest inventory attributes across the pulse density range was only slight, ranging from 0.73 – 0.75 for top height (Figure 8a), 0.58 – 0.60 for basal area (Figure 8b) and 0.65 – 0.69 for volume (Figure 8c). Similar patterns were observed for nRMSE (Figures 8e – h). For all variables, apart from top height, the lowest mean precision was recorded at 1 pulse m^{-2}.Differences in predictive precision between the three groups of metrics remained relatively similar across the pulse density range (Fig. 8). Averaged across all pulse densities, the R^2 for models fitted using standard metrics were respectively, 0.71, 0.44, 0.34 and 0.53 for top height, basal area, stand density and volume. The use of voxel-based metrics resulted in average gains in R^2 for these four metrics of 0.05, 0.22, 0.24 and 0.23, respectively (Table 2). These gains had a relatively low range between pulse densities with gains varying from 0.03–0.06, 0.19–0.25, 0.21–0.27 and 0.19–0.25, respectively, for top height, basal area, stand density and volume. As data were thinned to the lowest pulse density (1 pulse m^{-2}), models constructed using voxel-based metrics showed a decline in predictive precision that contrasted models using standard metrics where precision did not change (Figures 8a – d). Consequently, exclusion of the lowest pulse density from these analyses further reduced the range in predictive precision across pulse densities to 0.04 – 0.06, 0.20 – 0.25 and 0.21 – 0.25, respectively for top height, basal area and volume but had little effect on the range for stand density.

Models that included all metrics had slightly lower mean R^2, than models with voxel-based metrics, for both mean top height (0.74 vs 0.76), stand density (0.57 vs. 0.58) and very similar R^2 values for both basal area and volume (Table 2). Changes in precision for models with all metrics across the pulse density range were very similar to models with voxel-based metrics (Fig. 8a – d).

As patterns of nRMSE were very similar to those already noted for R^2 only the key statistics are given below. The mean nRMSE for models that used standard metrics were, respectively, 6.6, 25.2, 60.1 and 25.5% for top height, basal area, stand density and volume (Table 2). Reductions in nRMSE for top height, basal area, stand density and volume were, respectively, 0.6, 5.6, 11.5 and 6.8% when voxel-based metrics were used and 0.4, 5.7, 11.1 and 6.7% when all metrics were used within models (Table 2).

Table 2: Variation in mean coefficient of determination and normalised root mean square error for models of top height, basal area, stand density and volume created using standard metrics, voxel-based metrics and all metrics. Values shown are the average of 18 pulse densities, ranging from 1 to 280 pulses m^{-2}.

	Coefficient of determination			Normalised RMSE (%)		
	Standard	Voxel-based	All metrics	Standard	Voxel-based	All metrics
Height	0.71	0.76	0.74	6.6	6.1	6.2
Basal area	0.44	0.67	0.67	25.2	19.6	19.5
Stand density	0.34	0.58	0.57	60.1	48.6	49.0
Volume	0.53	0.75	0.75	25.5	18.7	18.8

Metrics Included Within Models

The random forests variable importance scores, calculated through permuting of individual predictors, indicated that voxel-based metrics were important predictors of forest inventory attributes. Within the models that included all metrics, voxel-based metrics were far more common than standard Lidar metrics. When averaged across all pulse densities, voxel-based metrics constituted 73, 97, 94 and 98%, respectively of all important metrics for mean top height, basal area, stand density and volume. This ratio remained relatively constant across the range in pulse densities varying from 65 – 81%, 91 – 100%, 76 – 100% and 93 – 100%, respectively, for mean top height, basal area, stand density and volume. While general trends in the relative importance of metrics from different groups could be ascertained from the results, identification the best metric(s) from each model was not attempted due to known issues in the scoring of variable importance in the presence of correlated predictors such as those produced from LiDAR data (Pearse *et al.* 2017) which limited detailed analysis of individual variable importance. These issues are expanded on in the discussion.

Discussion

This research clearly demonstrates the utility of voxel-based metrics for the prediction of key forest inventory attributes. Gains in predictive precision afforded by voxel-based metrics over the use of standard LiDAR metrics were substantial for predictions of basal area, stand density and volume and moderate for predictions of top height. The relative invariance of model precision to pulse density demonstrated that precision gains can be achieved using voxel-based metrics at pulse densities typical of current operational LiDAR acquisitions.

Although the predictive precision of the four forest inventory attributes made using standard LiDAR metrics had a ranking that was consistent with previous research, the absolute values of precision reported here were generally lower than most previously reported values. The model coefficient of determinations for mean top height (R^2 = 0.71) and basal area (R^2 = 0.44) were lower than those previously reported within studies in coniferous forests, where values of R^2 ranged, respectively, between 0.82−0.99 (Watt & Watt 2013; Coops *et a*l. 2007; Means *et al*. 2000; Naesset 2002; Means *et al.* 1999; Watt *et al.* 2013b; Dash *et al.* 2015b) and 0.62−0.94 (Naesset 2004, 2005, 2002; Means *et al.* 1999; Nord-Larsen & Schumacher 2012; Dash *et al*. 2015b; Watt *et al.* 2013b). Similarly, the precision around the estimate of stand density (R^2 = 0.34) was lower than that of previous research, where R^2 values have been found to range from 0.42−0.84 (Naesset & Bjerknes 2001; Watt *et al.* 2013b; Næsset 2002; Dash *et al.* 2015b). The coefficient of determination for volume (R^2 = 0.53) was within the range cited by previous studies for coniferous species that vary from 0.46−0.97 (Means *et al.* 2000; Naesset 1997, 2002; Watt & Watt 2013; Watt *et al*. 2013b; Dash *et al.* 2015b).

The generally lower precision of our predictions was not attributable to any anomalies in the LiDAR or field plot data. The strength of single variable relationships in the fitting dataset was consistent with previously reported values. For instance, using the highest pulse density data, the relationship between top height and the 90th LiDAR percentile, had an R^2 of 0.87 (nRMSE = 5.0%) while basal area was most strongly related to a voxel-based cover metric (percentage canopy cover at 10 m) with R^2 = 0.68 (nRMSE = 19.4%). Instead, we attribute the lower precision of our models to the combination of cross-validation and the internal data splitting of the random forests algorithm on the available data. These two approaches would have acted in combination to limit the size of the training and test data used during construction of the regression trees. The high variability of the dataset could also be expected to impact the measures of model performance. In combination, these factors are likely to make the results presented conservative estimates of model precision achievable using this approach.

Voxel-based metrics provided significantly improved predictions of basal area, volume, and stand density than standard metrics. Given the importance of canopy percentiles in predicting tree height, it was somewhat surprising to see that voxel-based metrics provided greater predictive power than standard metrics. However, differences in predictive power between metric classes were moderate and it is worth noting that canopy percentiles were the most important variables amongst the top 22 variables when all metrics were used to predict top height (data not shown).

We are unaware of any research that has comprehensively investigated the utility of voxel-based metrics from ALS for predictions of forest inventory attributes used for inventory purposes in plantation forests. However, it is worth noting that ALS voxel-based metrics using the approaches shown in Figures. 3-6 and Appendix 2 have been successfully used to predict more ecological forest metrics such as above-ground biomass (Kim *et al.* 2016), canopy base height (Maguya *et al*. 2015; Popescu & Zhao 2008), leaf area index (Peduzzi *et al.* 2012; Pearse *et al*. 2017), and canopy attributes (Sumnall *et al.* 2016). Sheridan *et al.* (2014) also used standard LiDAR metrics and density metrics derived from height bins (univariate voxelisation), that covered the horizontal extent of the entire plot, to predict both volume and above ground biomass in natural forests within the United States (Sheridan *et al.* 2014).

Consistent with the gains attributable to use of voxel-based metrics, most important variables found in the model that included all metrics, were voxel-based. While it is desirable to identify key metrics, the method used to determine variable importance within random forests is known to produce biased values in the presence of correlated predictors (Strobl *et al*. 2008). Solutions utilising importance scores assessed conditionally on correlated predictors are available (Strobl & Zeileis 2008; Strobl *et al.* 2008); however, these are computationally intensive. It was not feasible to compute the conditional importance scores given the large number of models required to assess the impact of both pulse density and metric type. Switching to the use of conditional variable importance scores would be most likely to impact the relative rankings of predictors, but not the overall composition of the group of 'top' predictors that were usually clearly identifiable. This was confirmed by inspecting the fluctuations in the variable importance scores produced across several of the repeats.

We hypothesise that the greater predictive precision of models that include voxel-based metrics is due to their greater ability to represent complex canopy structure than standard metrics. This may be particularly true with respect to horizontal structure within the highly variable plots included in the study. The majority of the standard metrics described in Appendix 1 could be expected to adequately describe vertical structure and this would explain the high accuracy and increased importance of these metrics for predicting top height. In contrast, the improvements produced by using voxel-based metrics were largely constrained to attributes that could be expected to relate primarily to variation in the horizontal structure such as variations in basal area and stand density.

A key question that was not addressed in this study relates to the fine-tuning of the voxel-based metrics. Many of these metrics require selection of voxel size, height threshold to be considered, or selection of other metric-specific parameters. An assessment of the impact of these parameters on the usefulness of these metrics in different contexts is required to simplify future applications of this approach and potentially reduce both the computation and modelling times. In addition, further validation of voxel-based metrics should be trialled in larger studies with sufficient data to more closely examine the linkage between the structure of important voxel-based metrics and forest inventory attributes.

Models created using standard metrics were largely invariant to pulse density and showed little change in precision even at the lowest pulse density. This agrees with most studies in coniferous forest, including stands of *P. radiata*, that have found LiDAR can be reduced to pulse densities of 1 pulse m^{-2} or lower with little impact on the precision of forest inventory attributes predicted from standard LiDAR metrics (Jakubowski *et al*. 2013; Treitz *et al*. 2012; Watt *et al.* 2013a). Watt *et al.* (2014) found a higher threshold of 2 – 3 pulses m^{-2} when predicting forest inventory attributes of Douglas-fir. However, this is likely to be attributable to the dense canopy cover of this species that results in a low number of ground returns, compared to other coniferous species. This sparsity of ground returns impacts on the quality of the digital terrain model and consequently the precision of the above ground point cloud (Watt *et al*. 2014).

The precision of predictions made using voxel-based metrics was also largely invariant to pulse density; however, the lowest precision for all four forest inventory attributes was recorded at 1 pulse m^{-2}. This deterioration in precision at low pulse densities most likely reflects the sparsity of returns per voxel at a pulse density of 1 pulse m^{-2}. Voxel-based metrics are likely to be more sensitive than standard metrics at this pulse density as this latter group of metrics is able to utilise the greater number of points associated with the entire point cloud. We are unaware of any previous research that has examined the effect of data thinning on the precision of predictions made using voxel-based metrics.

It is important to note that although predictions from voxel-based metrics did not improve at greater pulse densities, higher density data are likely to have applications beyond the voxelised approach. There are many individual tree approaches currently in use or under development that may benefit from the high pulse densities used in this study (Dalponte & Coomes 2016; Dalponte *et al.* 2012). Higher pulse density is not only useful for delineation of individual trees but also increases the incidence of reflections from the lower and upper stem that can be used to directly characterise the stem shape.

Implementation of Voxelised Metrics Within LAStools

The voxelised metrics were originally implemented using modules within Numeric and Scientific Python. Although fast, these modules do not integrate easily into the traditional tile-based LiDAR analysis pipelines widely used in forestry. LAStools is the most popular application for processing and characterising LiDAR in Australasia and the 'lascanopy' feature is traditionally used to derive forestry metrics for use in e.g. k-Nearest Neighbour yield assessment within a tile-based processing chain. As a result of the analysis carried out for this work, Scion discussed with Dr Martin Isenberg of RapidLASSO the potential to implement voxelisation into LAStools. Recently, RapidLASSO has released a beta version of 'lasvoxel' to enable voxelisation of LiDAR within a tile-based processing chain. A brief comparison revealed nearly identical results between a set of simple voxel-based metrics computed using Numpy and Lasvoxel. While the results were nearly identical, the approach of lasvoxel differs significantly from other tools. Lasvoxel defines a flexible voxel size determined by two parameters defining the X&Y and Z voxel dimensions respectively. At present, return count per voxel is computed by default but further options are likely to be available in the future. A key advantage of the lasvoxel tool is the use of the LAS format to store voxelisation results. This has the advantages of 1) being highly compressible, 2) allowing other LAStools (and many other software packages) to process and visualise the voxelised outputs (Fig. 9 below). In this approach, the XYZ values for each 'return' in the LAS file store instead of the XYZ location of a voxel's centroid with the density or other metric stored in the intensity field. Empty voxels are not stored and the original voxel size is recorded in an additional field within the LAS file. Early testing suggests this approach works well within tile-based processing and analysis chains and joint use of other tools such as lascanopy allow more complex metrics to be derived. Conversion from LAS voxel to Numpy arrays is more complex but remains feasible.

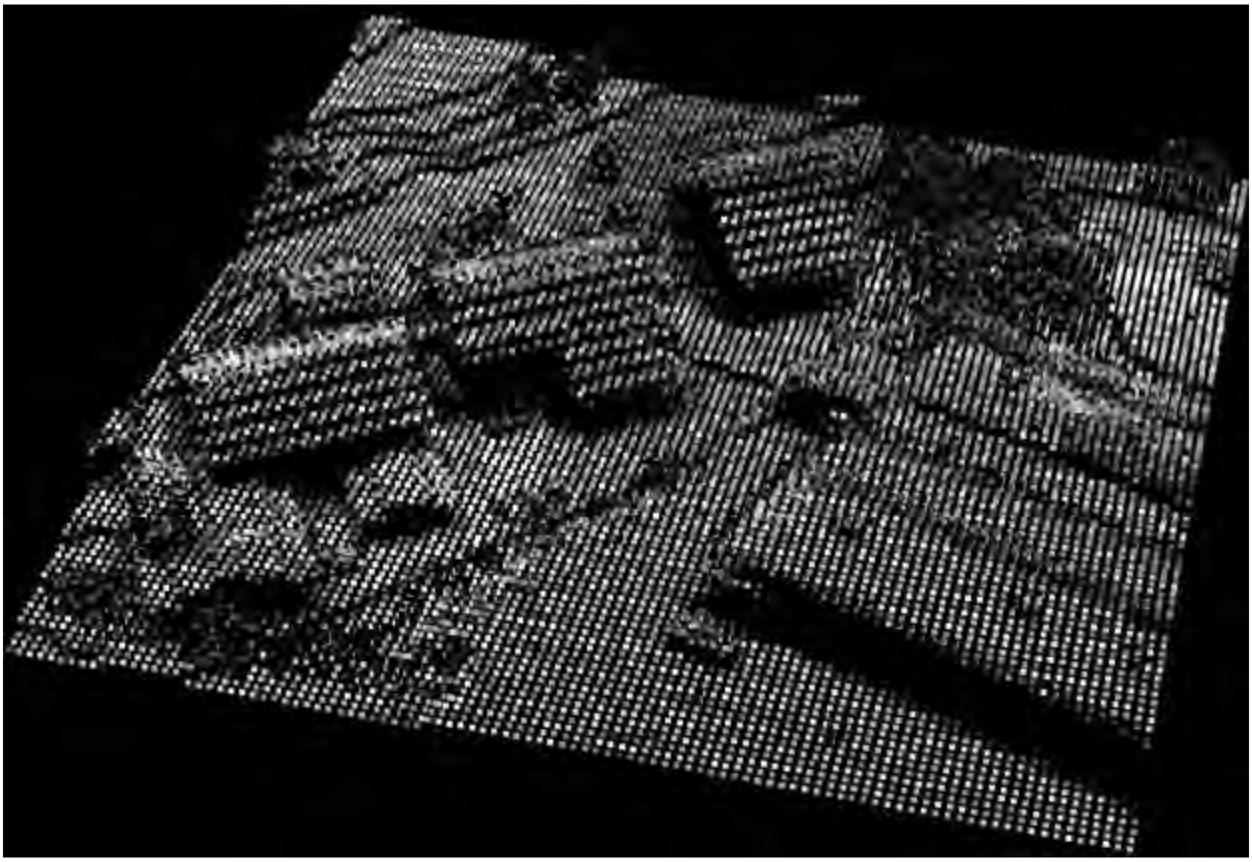

Figure 9: Example of LiDAR data voxelised with lasvoxel. XYZ attributes are used locate the voxel centroid and the intensity field is used to represent the chosen voxel metric (e.g. count of returns within voxel shown above).

Conclusions

The results presented here clearly show that voxel-based metrics have considerable potential for improving the precision of forest inventories. As extraction of voxel-based metrics does not greatly add to inventory cost, the significant precision gains demonstrated here are likely to markedly improve estimates of inventory attributes for a given cost, or allow equivalent accuracy at a lower cost. The invariance of precision gains to all but the lowest pulse density (1 pulse m^{-2}) suggests voxel-based metrics could be implemented using LiDAR captured at standard pulse densities associated with aerial capture allowing immediate and widespread implementation. Further research should be undertaken to verify these results and to examine how voxel-based metrics capture a greater proportion of the variance in forest inventory attributes than standard LiDAR metrics.

Acknowledgements

We appreciate financial support from Forest & Wood Products Australia (FWPA) and the Ministry for Business Industry and Employment (MBIE) Strategic Science Investment Fund (SSIF) for funding. We also appreciate the assistance of David Herries at Interpine Group who co-ordinated the collection of the dataset used in this project and Damien Petfield, Duncan Watt and Mike Sutton at Forestry Corporation of New South Wales for supplying inventory and ancillary data.

Appendices

Appendix 1. Standard LiDAR metrics included in models predicting stand variables.

Lidar Metric	Details
Avg	Average height of all returns
Qav	Quadratic mean height of all returns
Std	Std. deviation of all return heights
Ske	Skewness of all return heights
Kur	Kurtosis of all return heights
Percentiles	Height percentiles: p(1, 5, 10, 20,… ,90, 95, 99)
Deciles	Canopy densities: b(10, 20,… ,90)
Densities	Percentage of all returns within height bins d(0,1,… ,5)
Cover	Canopy cover from first returns above 10 and 20 m

Appendix 2: Voxelised metrics included in models predicting stand variables.

LiDAR Metric	Description	Classification	Source and definition
VCI	Vertical complexity index using bins of height vci_h(0.3, 0.5, 1, … 3).	Evenness	Van Ewijk (2015), Pope and Treitz (2013).
CC_above	Subpixel canopy closure at height: cc(6, 9,…, 21) m	Closure	Pope and Treitz (2013)
P_cc	Mean percentage canopy closure above: pcc_z(1.5, 5, 10, 15, 20) m	Closure	Griffin et al. (2008), Popescu and Zhao (2008).
VB Metrics	Biomass voxel metrics with sub-voxels at i(5,10,…, 45 m).	Multiple – Evenness / intensity	Kim et al. (2016)
SVi	Variable sub-voxel i		Kim et al. (2016)
Di	Variable density i		Kim et al. (2016)
SVM	Variable sub-voxel maximum		Kim et al. (2016)
ENL	Effective number of layers with 30 cm voxels.	Evenness	Ehbrecht et al. (2016)

References

Baalman, E. (2003). Tree volume and taper equations for New South Wales radiata pine. Technical Note 9, Resources Branch, Forests NSW.

Béland, M., Widlowski, J.-L., & Fournier, R. A. (2014). A model for deriving voxel-level tree leaf area density estimates from ground-based LiDAR. *Environmental Modelling & Software, 51*, 184-189.

Bienert, A., Hess, C., Maas, H., & von Oheimb, G. (2014). A voxel-based technique to estimate the volume of trees from terrestrial laser scanner data. *The International Archives of Photogrammetry, Remote Sensing and Spatial Information Sciences, 40*(5), 101.

Brede, B., Lau, A., Bartholomeus, H. M., & Kooistra, L. (2017). Comparing RIEGL RiCOPTER UAV LiDAR Derived Canopy Height and DBH with Terrestrial LiDAR. *Sensors, 17*(10), 2371.

Breiman, L. (2001). Random Forests. *Machine Learning, 45*, 5-32, doi:10.1023/A:1010933404324.
Coops, N. C., Hilker, T., Wulder, M. A., St-Onge, B., Newnham, G., Siggins, A., & Trofymow, J. A. (2007). Estimating canopy structure of Douglas-fir forest stands from discrete-return LiDAR. *Trees-Structure and Function, 21*, 295-310.
Dalponte, M., Bruzzone, L., & Gianelle, D. (2012). Tree species classification in the Southern Alps based on the fusion of very high geometrical resolution multispectral/hyperspectral images and LiDAR data. *Remote sensing of environment, 123*(Supplement C), 258-270, doi:https://doi.org/10.1016/j.rse.2012.03.013.
Dalponte, M., & Coomes, D. A. (2016). Tree-centric mapping of forest carbon density from airborne laser scanning and hyperspectral data. *Methods in Ecology and Evolution, 7*(10), 1236-1245, doi:10.1111/2041-210X.12575.
Dash, J. P., Marshall, H. M., & Rawley, B. (2015a). Methods for estimating multivariate stand yields and errors using k-NN and aerial laser scanning. *Forestry*, doi:10.1093/forestry/cpu054.
Dash, J. P., Watt, M. S., Bhandari, S., & Watt, P. (2015b). Characterising forest structure using combinations of airborne laser scanning data, RapidEye satellite imagery and environmental variables. *Forestry*, cpv048.
Ehbrecht, M., Schall, P., Juchheim, J., Ammer, C., & Seidel, D. (2016). Effective number of layers: A new measure for quantifying three-dimensional stand structure based on sampling with terrestrial LiDAR. *Forest Ecology And Management, 380*, 212-223.
Genuer, R., Poggi, J.-M., & Tuleau-Malot, C. (2010). Variable selection using random forests. *Pattern Recognition Letters, 31*(14), 2225-2236, doi:https://doi.org/10.1016/j.patrec.2010.03.014.
Grau, E., Durrieu, S., Fournier, R., Gastellu-Etchegorry, J.-P., & Yin, T. (2017). Estimation of 3D vegetation density with Terrestrial Laser Scanning data using voxels. A sensitivity analysis of influencing parameters. *Remote sensing of environment, 191*, 373-388.
Griffin, A. M., Popescu, S., & Zhao, K. Using LIDAR and normalized difference vegetation index to remotely determine LAI and percent canopy cover. In*, 2008 2008* (8th)
Hall, S. A., Burke, I. C., Box, D. O., Kaufmann, M. R., & Stoker, J. M. (2005). Estimating stand structure using discrete-return lidar: an example from low density, fire prone ponderosa pine forests. *Forest Ecology And Management, 208*(1-3), 189-209.
Holmgren, J., Nilsson, M., & Olsson, H. (2003). Estimation of tree height and stem volume on plots using airborne laser scanning. *Forest Science, 49*, 419-428.
Hudak, A. T., Strand, E. K., Vierling, L. A., Byrne, J. C., Eitel, J. U., Martinuzzi, S., & Falkowski, M. J. (2012). Quantifying aboveground forest carbon pools and fluxes from repeat LiDAR surveys. *Remote sensing of environment, 123*, 25-40.
Hyde, P., Dubayah, R., Peterson, B., Blair, J., Hofton, M., Hunsaker, C., Knox, R., & Walker, W. (2005). Mapping forest structure for wildlife habitat analysis using waveform lidar: Validation of montane ecosystems. *Remote sensing of environment, 96*(3), 427-437.
Jaakkola, A., Hyyppä, J., Kukko, A., Yu, X., Kaartinen, H., Lehtomäki, M., & Lin, Y. (2010). A low-cost multi-sensoral mobile mapping system and its feasibility for tree measurements. *ISPRS journal of Photogrammetry and Remote Sensing, 65*(6), 514-522.
Jakubowski, M. K., Guo, Q. H., & Kelly, M. (2013). Tradeoffs between lidar pulse density and forest measurement accuracy. *Remote Sensing of Environment, 130*, 245-253, doi:DOI 10.1016/j.rse.2012.11.024.
Kim, E., Lee, W.-K., Yoon, M., Lee, J.-Y., Son, Y., & Abu Salim, K. (2016). Estimation of Voxel-Based Above-Ground Biomass Using Airborne LiDAR Data in an Intact Tropical Rain Forest, Brunei. *Forests, 7*(11), 259.

Liaw, A., & Wiener, M. (2002). Classification and regression by randomForest. *R news, 2*(3), 18-22.

Maguya, A. S., Tegel, K., Junttila, V., Kauranne, T., Korhonen, M., Burns, J., Leppanen, V., & Sanz, B. (2015). Moving Voxel Method for Estimating Canopy Base Height from Airborne Laser Scanner Data. *Remote Sensing, 7*(7), 8950-8972.

McGaughey, R. J. (2015). FUSION. (3.42 ed.). Washington, USA: USDA.

Means, J. E., Acker, S. A., Fitt, B. J., Renslow, M., Emerson, L., & Hendrix, C. J. (2000). Predicting forest stand characteristics with airborne scanning LiDAR. *Photogrammetric Engineering and Remote Sensing, 66*(11), 1367-1371.

Means, J. E., Acker, S. A., Harding, D. J., Blair, J. B., Lefsky, M. A., Cohen, W. B., Harmon, M. E., & McKee, W. A. (1999). Use of large-footprint scanning airborne LiDAR to estimate forest stand characteristics in the Western Cascades of Oregon. *Remote Sensing of Environment, 67*(3), 298-308.

Moskal, L. M., & Zheng, G. (2011). Retrieving forest inventory variables with terrestrial laser scanning (TLS) in urban heterogeneous forest. *Remote Sensing, 4*(1), 1-20.

Mutlu, M., Popescu, S. C., Stripling, C., & Spencer, T. (2008a). Mapping surface fuel models using lidar and multispectral data fusion for fire behavior. *Remote sensing of environment, 112*(1), 274-285.

Mutlu, M., Popescu, S. C., & Zhao, K. (2008b). Sensitivity analysis of fire behavior modeling with LIDAR-derived surface fuel maps. *Forest Ecology And Management, 256*(3), 289-294.

Næsset, E. (2002). Predicting forest stand characteristics with airborne scanning laser using a practical two-stage procedure and field data. *Remote sensing of environment, 80*(1), 88-99.

Næsset, E. (2004). Practical large-scale forest stand inventory using a small-footprint airborne scanning laser. *Scandinavian Journal of Forest Research, 19*(2), 164-179, doi:Doi 10.1080/02827580310019257.

Næsset, E. (2005). Assessing sensor effects and effects of leaf-off and leaf-on canopy conditions on biophysical stand properties derived from small-footprint airborne laser data. *Remote sensing of environment, 98*(2-3), 356-370.

Naesset, E. (1997). Estimating timber volume of forest stands using airborne laser scanner data. *Remote sensing of environment, 61*(2), 246-253.

Naesset, E. (2002). Predicting forest stand characteristics with airborne scanning laser using a practical two-stage procedure and field data. *Remote sensing of environment, 80*(1), 88-99.

Naesset, E. (2004). Practical large-scale forest stand inventory using a small-footprint airborne scanning laser. *Scandinavian Journal of Forest Research, 19*(2), 164-179, doi:Doi 10.1080/02827580310019257.

Naesset, E. (2005). Assessing sensor effects and effects of leaf-off and leaf-on canopy conditions on biophysical stand properties derived from small-footprint airborne laser data. *Remote sensing of environment, 98*(2-3), 356-370.

Naesset, E. (2007). Airborne laser scanning as a method in operational forest inventory: Status of accuracy assessments accomplished in Scandinavia. *Scandinavian Journal of Forest Research, 22*(5), 433-442, doi:10.1080/02827580701672147.

Næsset, E., & Bjerknes, K. O. (2001). Estimating tree heights and number of stems in young forest stands using airborne laser scanner data. *Remote Sensing of Environment, 78*(3), 328-340.

Naesset, E., & Bjerknes, K. O. (2001). Estimating tree heights and number of stems in young forest stands using airborne laser scanner data. *Remote sensing of environment, 78*(3), 328-340.

Næsset, E., Gobakken, T., Holmgren, J., Hyyppä, H., Hyyppä, J., Maltamo, M., Nilsson, M., Olsson, H., Persson, Å., & Söderman, U. (2004). Laser scanning of forest resources: The nordic experience. *Scandinavian Journal of Forest Research, 19*(6), 482-499, doi:10.1080/02827580410019553.

Næsset, E., & Okland, T. (2002). Estimating tree height and tree crown properties using airborne scanning laser in a boreal nature reserve. *Remote Sensing of Environment, 79*(1), 105-115.

Nilsson, M. (1996). Estimation of tree heights and stand volume using an airborne LiDAR system. *Remote Sensing of Environment, 56*(1), 1-7.

Nord-Larsen, T., & Schumacher, J. (2012). Estimation of forest resources from a country wide laser scanning survey and national forest inventory data. *Remote Sensing of Environment, 119*, 148-157, doi:DOI 10.1016/j.rse.2011.12.022.

Palminteri, S., Powell, G. V., Asner, G. P., & Peres, C. A. (2012). LiDAR measurements of canopy structure predict spatial distribution of a tropical mature forest primate. *Remote sensing of environment, 127*, 98-105.

Pearse, G. D., Morgenroth, J., Dash, J. P., & Watt, M. S. (2017). Optimising prediction of forest leaf area index from discrete airborne LiDAR. *Remote Sensing and Environment*.

Peduzzi, A., Wynne, R. H., Fox, T. R., Nelson, R. F., & Thomas, V. A. (2012). Estimating leaf area index in intensively managed pine plantations using airborne laser scanner data. *Forest Ecology And Management, 270*, 54-65.

Pope, G., & Treitz, P. (2013). Leaf Area Index (LAI) Estimation in Boreal Mixedwood Forest of Ontario, Canada Using Light Detection and Ranging (LiDAR) and WorldView-2 Imagery. *Remote Sensing, 5*(10), 5040.

Popescu, S. C., Wynne, R. H., & Nelson, R. F. (2002). Estimating plot-level tree heights with lidar: local filtering with a canopy-height based variable window size. *Computers and Electronics in Agriculture, 37*(1-3), 71-95.

Popescu, S. C., & Zhao, K. (2008). A voxel-based lidar method for estimating crown base height for deciduous and pine trees. *Remote sensing of environment, 112*(3), 767-781.

Puliti, S., Ørka, H. O., Gobakken, T., & Næsset, E. (2015). Inventory of small forest areas using an unmanned aerial system. *Remote Sensing, 7*(8), 9632-9654.

Sheridan, R. D., Popescu, S. C., Gatziolis, D., Morgan, C. L., & Ku, N.-W. (2014). Modeling forest aboveground biomass and volume using airborne LiDAR metrics and forest inventory and analysis data in the Pacific Northwest. *Remote Sensing, 7*(1), 229-255.

Stephens, P. R., Kimberley, M. O., Beets, P. N., Paul, T. S. H., Searles, N., Bell, A., Brack, C., & Broadley, J. (2012). Airborne scanning LiDAR in a double sampling forest carbon inventory. *Remote sensing of environment, 117*, 348-357.

Strobl, C., Boulesteix, A.-L., Kneib, T., Augustin, T., & Zeileis, A. (2008). Conditional variable importance for random forests. *BMC Bioinformatics, 9*(1), 307, doi:10.1186/1471-2105-9-307.

Strobl, C., & Zeileis, A. (2008). Danger: High Power! – Exploring the Statistical Properties of a Test for Random Forest Variable Importance. In *Proceedings of the 18th International Conference on Computational Statistics, Porto, Portugal*.

Sumnall, M., Peduzzi, A., Fox, T. R., Wynne, R. H., & Thomas, V. A. (2016). Analysis of a lidar voxel-derived vertical profile at the plot and individual tree scales for the estimation of forest canopy layer characteristics. *International Journal of Remote Sensing, 37*(11), 2653-2681.

Teo, T.-A., & Shih, T.-Y. (2013). Lidar-based change detection and change-type determination in urban areas. *International Journal Of Remote Sensing, 34*(3), 968-981.

Treitz, P., Lim, K., Woods, M., Pitt, D., Nesbitt, D., & Etheridge, D. (2012). LiDAR Sampling Density for Forest Resource Inventories in Ontario, Canada. *Remote Sensing, 4*(4), 830-848, doi:Doi 10.3390/Rs4040830.

Van Ewijk, K. (2015). *Estimating Forest Structure from LiDAR and High Spatial Resolution Imagery for the Prediction of Succession and Species Composition*. Queen's University,

Vierling, K. T., Vierling, L. A., Gould, W. A., Martinuzzi, S., & Clawges, R. M. (2008). Lidar: shedding new light on habitat characterization and modeling. *Frontiers in Ecology and the Environment, 6*(2), 90-98.

Wallace, L., Lucieer, A., Malenovský, Z., Turner, D., & Vopěnka, P. (2016). Assessment of Forest Structure Using Two UAV Techniques: A Comparison of Airborne Laser Scanning and Structure from Motion (SfM) Point Clouds. *Forests, 7*(3), 62.

Wallace, L., Lucieer, A., Watson, C., & Turner, D. (2012). Development of a UAV-LiDAR system with application to forest inventory. *Remote Sensing, 4*(6), 1519-1543.

Wallace, L., Musk, R., & Lucieer, A. (2014). An assessment of the repeatability of automatic forest inventory metrics derived from UAV-borne laser scanning data. *IEEE Transactions on Geoscience and Remote Sensing, 52*(11), 7160-7169.

Watt, M. S., Adams, T., Aracil, S. G., Marshall, H., & Watt, P. (2013a). The influence of LiDAR pulse density and plot size on the accuracy of New Zealand plantation stand volume equations. *New Zealand Journal of Forestry Science, 43*(1), 15.

Watt, M. S., Meredith, A., Watt, P., & Gunn, A. (2013b). Use of LiDAR to estimate stand characteristics for thinning operations in young Douglas-fir plantations. *New Zealand Journal of Forestry Science, 43*(1), 18.

Watt, M. S., Meredith, A., Watt, P., & Gunn, A. (2014). The influence of LiDAR pulse density on the precision of inventory metrics in young unthinned Douglas-fir stands during initial and subsequent LiDAR acquisitions. *New Zealand Journal of Forestry Science, 44*(1), 1-9.

Watt, P., & Watt, M. S. (2013). Development of a national model of *Pinus radiata* stand volume from LiDAR metrics for New Zealand. *International Journal of Remote Sensing*.

Yu, X., Hyyppä, J., Kaartinen, H., & Maltamo, M. (2004). Automatic detection of harvested trees and determination of forest growth using airborne laser scanning. *Remote sensing of environment, 90*(4), 451-462.

5. Conclusions

This project has highlighted the increasing capacity of remote sensing systems to capture 3D dense point cloud data. These significant technological advancements permit the extraction of detailed 3D structural information that cannot be derived from LiDAR surfaces such as Canopy Height Models. A focus on the pointcloud data not only utilises the shape and structure of the canopy surface but allows access to much more sub-canopy information. In this report we have evaluated several remote LiDAR systems and provide specifications and procedures for optimal data acquisition.

Although results described in this report demonstrate significant utility from dense LiDAR data they clearly show that further research is required to fully utilise this data. Analyses using UAS LiDAR data demonstrate that the absolute accuracy of the Velodyne puck (3 – 7 cm) is sufficient to detect stems and crowns of individual trees but is unlikely to be sufficiently precise to measure tree dimensions such as stem diameters. Unlike, the Velodyne puck, the more expensive Riegl VUX-1LR is a survey-grade lidar sensor with a reported accuracy/precision of 15 mm and theoretically could be used to detect large branches. However, further research will be required to fully explore the capabilities of this sensor.

The authors of Section 4.1 plan to progress their evaluation of stem segmentation algorithms on the same high quality dataset used in Section 3.2 which was acquired with a Reigl VUX 1LR lidar sensor, under, what we believe to be superior acquisition specifications. This analysis has been included in a project proposal submitted for NIFPI funding.

Section 3.3. presents the first attempt of acquiring UAV stereo-camera imagery below a *P. radiata* canopy in order to capture tree stem information. The authors present a RMSE for DBH estimation of 5.0 cm which is likely to be inadequate for stem volume estimations. However, while the individual diameters may be less accurate than those obtained using a manual tape, a major advantage of this approach is that diameter estimates can be obtained at multiple locations along the tree stem. The approach of deriving multiple diameters and applying existing taper functions is developed further in Section 4.1 "Algorithms and 3D modelling techniques for tree detection and tree-level volume estimates".

Parallel to these advances made in system hardware has been the recent advances in software systems that can process, visualise and analysis these very large pointcloud datasets. We have demonstrated that these 3D datasets can be imported into an immersive virtual reality environment. A new FWPA project (PNC464-1718) is aimed at developing software tools that will allow the user to measure stem and tree structure interactively as well as integrating into the same VR environment algorithms that can automatically segment and reconstruct individual trees identified within the 3D point cloud data.

The accurate estimation of stem level attributes, however, requires not only dense point data but also very geospatially accurate data. A range of different UAV and ALS LiDAR systems now exist but there is a trade-off between the cost of the instrument and the quality of the acquired datasets. In all cases it is strongly recommended that the LiDAR systems are calibrated and appropriate ground control geo-registration is obtained. The application area and quality of information required determine the type of platform/sensor system chosen. For example, the remote assessment of reference tree stems (possibly replacing conventional inventory plot sampling strategies) will require dense, very high quality point data that can be provided by the survey-grade Riegl VUX1 systems. Cheaper LiDAR-UAS or new ALS systems can also acquire dense pointcloud data that can provide tree-level information such as accurate tree counts and the extraction of new 3D metrics such as voxel metrics. These parameters will improve inventory estimates when applied to existing ABA based modelling approaches.

Further research that analyses a sufficient number of datasets from a varying mix of sensors & platforms, acquisition specifications and stand conditions will be required to gain confidence around recommendations for operational specifications. Nevertheless, report findings do suggest that utilisation of dense point cloud data for characterisation of stand and tree-level attributes does look like a promising approach. As a result certain aspects of this project are now being progressed in new projects e.g. FWPA PNC464-1718. One area that requires particular attention and is the topic of future research plans will be the exploration of the potential of the VUX-1 LR lidar sensor to undertake detailed stem characterisations. An important issue which we did not address in this project was the potential cost benefits related to the trade-offs between estimation accuracies and cost of the sensor/platform systems.

Finally, a key operational constraint to UAS operations in any Australian forested environment is the compliance with current Civil Aviation Safety Authority (CASA) regulations, in particular the requirement for the UAS to be within visual line of sight. The Civil Aviation Authority (CAA) in New Zealand, however, permit a UAS to fly beyond the line of sight if the operator is appropriately certified (with 102 certification) by the CAA and the operator has prepared a flight plan to the required standards defined by the CAA. We recommend that the Australian UAS industry and the forestry industry continue to lobby CASA for beyond visual line of sight for operations within commercial forests.

Appendix 1 - Airborne Laser Scanner acquisition specifications for plantation inventory

Susana Gonzalez[1], David Herries[1], Christine Stone[2]

[1] *Interpine Group Ltd, Rotorua, NZ, Susana.Gonzalez@interpine.nz*
[2] *NSW Department Primary Industries - Forestry, Christine.Stone@dpi.nsw.gov.au*

Introduction and Discussion

LiDAR acquisition specifications are heavily influenced by the intended application. Requirements should consider the type of terrain, the complexity of the forest characteristics, and the required information. When writing a contract for the acquisition and delivery of LiDAR data, there are several survey specifications that need to be defined including: 1) data-acquisition parameters; 2) accuracy specifications; 3) Completeness and consistency of the data set; 4) spatial reference framework (datum, projections, etc.); 5) deliverables and 6) formats and data organization.

Several documents have recently been published that provide excellent advice on the specification considerations for forestry applications (e.g. White *et al*. 2013, Natural Resources Canada 2017; Mitchell *et al.* 2018). These guides tend to be relatively generic since forest environments vary and the technology evolves quickly. Therefore foresters need to select the specifications best suited for their information needs and budget.

The Area Based Approach (ABA) has become the standard procedure for processing Airborne laser Scanner (ALS) point cloud data for spatial metrics that can then be used to generate predictive models for inventory attributes (White *et al*. 2017). The ABA usually provides an estimation of forest inventory attributes of interest over a grid that typically corresponds to the size of the measured ground plots. The Report by White *et al*. (2017) provides excellent advice on the ABA data workflow procedure for modelling and mapping using ALS data for spatially explicit forest inventory. If however, the ALS data is sufficiently dense ($\geq$ 5 pulses/m^2), then individual tree crowns can be detected using the ALS point clouds, enabling tree-level attributes such as stocking to be accurately estimated. ALS technology, however, is advancing rapidly with new survey-grade laser sensors now capable much higher pulse rates. ALS sensors with pulse rates $\geq$ 500,000 pulses/second are now available in Australia and New Zealand. Increased pulse rates allow data vendors to fly aircraft at higher altitudes and faster speeds to obtain data within a specified pulse density target, which in turn reduces acquisition costs. In addition, it is these new sensors having very high pulse rates that provide the potential for stem reconstruction and segmentation. As usual there are the trade-offs between data quality and cost-efficiencies.

Most discrete return laser systems can now provide 4 or more returns per pulse. This occurs when the laser pulse intercepts an object through which it can penetrate, such that some of the energy will be returned to the instrument (first return), and some continue through the canopy and intercepts stems, branches, leaves before reaching the ground. The last returns are assumed to originate from the ground or objects near the ground. Full waveform systems, on the other hand, record the reflected energy from each pulse emitted as a continuous signal. The new Riegl laser sensors now capture full waveform data, however, discrete points are commonly extracted from the waveform using sophisticated algorithms to isolate targets at the highest peaks of reflectance along the wave. This technology provides the flexibility of extracting more or less discrete points from the wave based upon detection thresholds and range tolerances settings for best target estimation.

With ALS data, the vertical accuracy is always greater than the horizontal accuracy, with the absolute accuracy stating that the x, y, z, attributes of the return are within a certain limit in the real-world. For the large New Zealand acquisition campaigned managed by Interpine, they sought a vertical accuracy of =< 10 cm and a horizontal accuracy of =< 50 cm (Table 1). White *et al*. (2013) also point out that relative accuracy is also important for calibrating data from adjacent flight lines against each other (i.e. swath-to-swath matching).

The collection and processing of ground control points (GCPs) is highly recommended as they are used of undertaking data quality assurance and quality control (QA/QC) (refer to Section 3.2.2 in this Report). The GCPs are used for both survey calibration and assessment of absolute vertical accuracy. Strongly clustered GCPs are useful for the calibration process. It is also good practice to use ALS calibration arrays (usually at least three open, un-vegetated sites across an ALS block). These assist with identification and removal of systematic errors during the post-processing of raw ALS data. Differential GNSS can be used to acquire ground heights at each of the calibration arrays, which are incorporated into the ALS processing workflow to adjust the block of ALS data onto terrain.

For the coverage of large areas, the operating parameters of the LiDAR system are usually selected that optimize point density and area coverage rate. Table 1 presents the LiDAR data and delivery specifications that were defined by Interpine for a recent, very large acquisition campaign over hundreds of thousands of hectares in New Zealand. Key sensor parameters include: accuracy; pulse density; returns per pulse; scan angle; beam divergence; pulse repetition frequency; beam footprint and flight line overlap. Pulse density is a function of multiple sensor parameters including pulse rate, instrument energy, receiver sensitivity, flying height and speed and scan angles. As mentioned, pulse density per square metre affects what can be achieved from the derived metrics. Higher point densities enable an improved description of the forest stands. We have demonstrated in this FWPA project that ultra-high point densities provide the capability for stem reconstruction and segmentation (refer to Section 4.1 in this Report).

Forestry operations usually specify a relatively narrow scan angle (i.e. <± 15°). Narrow scan angles increase penetration through the canopy, support smaller footprints, and increase incident pulse energy. Conversely ground returns decrease as scanning angle increases.

Laser Beam divergence represents the angular spread of the laser pulse which is a combination of the height of the aircraft, scan angle and motion of the aircraft as well as the slope of the terrain. Narrow beam divergence improves the penetration rate into the canopy. Both the beam divergence and flying altitude influence footprint size, in turn, influence the footprint size of the laser pulse on the ground. For example, a laser at an altitude of 1000 m with a beam divergence of 0.3 mrad will have a footprint that is approximately 30 cm in diameter. Small footprints (< 30 cm) provide more information on canopy gaps and have greater ranging accuracy. Also small footprints with high pulse energy are preferred for individual tree feature extraction.

Pulse repetition frequency is the frequency of transmitted laser pulses. Newer systems are continually offering greater pulse frequencies. The pulse repetition frequency directly influences the ability of the laser pulses to penetrate the forest canopy. Flight line overlap or swath overlap is another important ALS acquisition specification and refers to how much overlap exists between scanning swaths. A total swath overlap of ≥ 50% is now requested. Fifty percent sidelap provides 100% total overlap, so each area is being scanned twice. Hence overlapping swaths enable higher pulse densities and multiple look angles, both of which increase the likelihood of ground returns in dense canopies but decrease data occlusions.

The planned LiDAR acquisition parameters should be designed and conducted with no data gaps and no data void areas except in those areas where low near infrared surface reflectance features are present, such as water. It is now also common for ALS aircraft to carry a 3-band camera which is acquired simultaneously with the LiDAR capture. These images can be provided as high spatial (10 – 20 cm) resolution imagery individual georeferenced and ortho-rectified frames.

In terms of data deliverables, all the discrete multi-return data are classified. All the above ground level features (e.g. vegetation, buildings, water etc.,) are filtered from the 'bare—earth' ground point data, using a schema based on the ASPRS (American Society for Photogrammetry & Remote Sensing) LAS standard. The current ASPRS LAS format standard is version LAS1.4. In addition to the point classification, each laser return is assigned the following values; x, y, z, intensity, return number, number of returns, flagged if overlap, scan angle and point source ID. The return intensity is a measure of the energy in the originating infrared pulse that returns to the sensor. Intensity data can be processed into an image corresponding to a non-calibrated infrared reflection that is like an orthophoto.

Interpine also define the required datum and map projection, the tiling, size and naming nomenclature of the data files, the data formats, how the data should be stored and supplied and the project acquisition metadata..

In conclusion, the LiDAR data specifications selected are dependent on the intended project objectives and associated information needs (e.g. stand level ABA versus individual tree level information). Therefore, forest managers need be aware of the specifications and capacity of currently available LiDAR systems while the ALS data vendor needs to be aware of the project-specific objectives and issues in order for a clearly worded ALS acquisition contract. Finally, once delivered, a process of quality assurance and control evaluation of the data is essential because errors in the quality of the data will directly influence parameter accuracies derived from imputation.

Table 1: ALS acquisition specifications for plantation inventory provided by Interpine Group Ltd

LiDAR Point Cloud Specifications

Ref	Specification	Expectation and Criteria
1.	Coverage	Wall-to-wall coverage required including a buffer to avoid edge effects. A 50m buffer is currently **included** in the area of interest provided.
2.	LiDAR Equipment	Riegl LMS-Q1560 or LMS-Q780 LiDAR Scanner (or equivalent scanner type, if outside of these units please provide a detailed specification and an example dataset over vegetation).
3.	Accuracy	Vertical =< 10 cm Horizontal =< 50cm
4.	Ground Survey Control and Network Accuracy	Additional ground control survey will be conducted.
5.	Pulse Density	Recording a **minimum** pulse density of four **(4)** outbound pulses per square metre.
6.	Returns Per Pulse	It is expected the supplier will work with the client to review full waveform datasets to result in an acceptable delivery of multiple discrete returns during post processing. It is important for the supplier to realise the data is capture over dense forest canopy.
7.	Pulse Intensity	Recording of intensity of each return is required.
8.	Scan Angle	• Flight line will be designed to ensure the scan angle is a maximum of 14° either side of nadir, with a total effective field of view of 28°. • It is acknowledged that the total field of view of the LiDAR unit deployed is 58-60° and that all flights will capture and deliver to the client the full dataset across this entire 58-60° field of view. By design this will result in an approximate total overlap of ~50%.
9.	Beam Divergence	Narrow beam divergence.
10.	Pulse Repetition Frequency (PRF)	Pulse repetition frequency good enough to ensure good LiDAR pulse penetration through the forest canopy.
11.	Beam Footprint	=<30cm
12.	Flight Line Overlap	• Based on the scan angle being a maximum of 14° either side of nadir, with a total effective field of view of 28°. • It is acknowledged that the total field of view of the LiDAR unit deployed is 58° and that all flights will capture and deliver to the client the full dataset across this entire 58° field of view. By design this will result in an approximate total overlap of ~50%. • Any data with gaps between the geometrically usable portions of the swaths will be rejected in QA.

13.	Cross Track	Ratio of cross track to down track point collection should not exceed a ratio of 2:3 in compliance with international standards.
14.	Data Voids	Data voids caused by system malfunctions, data dropout, clouds, or flight line data gaps, or excessive classification of withheld / overlap flagged points are considered unacceptable. These can be defined as Data Voids => 4x NPS^2 measured using 1st-returns only within a single swath are not acceptable, except: 1) where caused by water bodies 2) where caused by areas of low near infra-red (NIR) reflectivity such asphalt or composition roofing 3) where appropriately filled-in by another swath within the target scan angle from Nadir.
15.	Flight Conditions	Conditions for data capture should be: 1) Cloud and fog free between aircraft and the ground. 2) Flights should not be taken during periods of heavy smoke or haze. 3) Floodplain/wetland data must be captured during times of base-flow and outside of significant surface inundation due to natural events and /or regulated environmental flows.
16.	Aerial Photos	Acquisition of 3-band imagery simultaneously with LiDAR capture, processing and delivery of 10-20cm resolution imagery as individually georeferenced and ortho-rectified frames.

LiDAR Derivative Data Specifications

Ref	Specification	Expectation and Criteria
1	Output Formats	Output data will be provided in ASPRS LAS format files. 1) Discrete multi-return data with point classifications consistent with the ASPRS LAS standard. 2) Each laser return will have a minimum of: a. GPS times recorded as adjusted GPS time, at a precision sufficient to allow unique timestamps for each pulse. b. Easting, northing and elevation above sea level. c. Intensity d. Return number e. Number of returns f. Classification (including classification of all overlap) g. Overlap flagged as withheld point as not to be classified as Class 12 h. Scan angle. i. Channel 1 or 2 from dual channel sensor. j. Point source (flight path ID) 3) Minimum of version 1.4 LAS format in LAZ compression format (see notes on Classification). 4) Geo-referencing information in all LAS headers (as VLR to ASPRS standard). 5) Data will be supplied for the full fixed field of view of the scanner. 6) Full waveform will be provided in Riegl waveform formats or a format agreed by both parties (consideration of PulseWaves format will be discussed).
2	Datum and Map Projection	The coordinate system for all deliverables is the New Zealand Transverse Mercator 2000.

<table>
<tr><th>Ref</th><th>Specification</th><th>Expectation and Criteria</th></tr>
<tr><td></td><td></td><td>This includes the:

- Horizontal datum: New Zealand Geodetic Datum 2000
- Vertical datum: New Zealand Vertical Datum 2016
- Geoid Model: LINZ NZGeoid2016
Elevation will be provided above sea level, where geoid model above shall be used to derive orthometric heights from ellipsoidal data.</td></tr>
<tr><td>3</td><td>Tiling and
File sizes</td><td>Output should be split into tiles 500x500m (Larger tile sizes which maximise workflow efficiency will be considered, but files should contain no more than 20 million returns. The origin of the tile must be placed on a whole metre coordinate value of the south west corner of each tile. e.g. 426000mE_7243000mN

Tile Naming: ProjectYYYY_ProductType_xxxxxxx_yyyyyyy.laz
Example: HB2015_C2_1444000_5082000.laz

<table>
<tr><td>Project</td><td>Interpine</td><td>Project Name / Tile Owner</td></tr>
<tr><td>YYYY</td><td>2017</td><td>Year of Survey</td></tr>
<tr><td>ProductType</td><td>_C2 or _UNC</td><td>ICSM Classification level (C1, C2, C3, C4) or Unclassified (UNC).</td></tr>
<tr><td>xxxxxxx_yyyyyyy</td><td>_1444000_5082000
(1,444,000mE)
(5,082,000mN)</td><td>The full easting and northing value of the south-west corner of the tile.
A single “_” must be used to separate the remaining file name components.</td></tr>
</table></td></tr>
<tr><td>4</td><td>Data Storage and Supply</td><td>All data is to be provided on external HDD with a minimum 2TB capacity. Provisions for download from an online portal can be made available for initial data delivery to check data structure and specification compliance. External HDD supplied with be retained by the client.</td></tr>
<tr><td>5</td><td>Data Thinning</td><td>No data will be removed, and all points collected will be supplied.</td></tr>
<tr><td>6</td><td>Point Classification</td><td>Classification of the point data as follows:

1. Undertake automatic classification of all collected data (Level 1 (ICSM 2010))

2. Automatically remove any atmospheric points above all collected data (Level 1 (ICSM 2010))

3. Automatically classify all overage outside 28 degree FOV into a separate class (so that manual improvement of ground is not impeded by this additional data)

4. Manually improve the ground definition where required up to 28 degree FOV, then automatically reclassify overage data back to the appropriate classes and attach the withheld flag to any overage points. This will be provided to Level 2 (ICSM 2010) classification to achieve 98% accuracy levels for ground data classification. It is expected this is for ground surface improvement using automated and manual methods be used to obtain ground (2 and model key points).

5. Then automatically reclassify overage data back to the appropriate classes and attach the withheld flag to any overage points.

Minimum automated ASPRS classification scheme shown below. (ICSM 2011).

0 Unclassified (Created, never classified)
1 Default (Unclassified)</td></tr>
</table>

Ref	Specification	Expectation and Criteria
		2 Ground (Bare Ground) 3 Low Vegetation (0-0.3m, essentially sensor noise) 4 Medium Vegetation (0.3-2m) 5 High Vegetation (>2m) 6 Buildings and structures (buildings, houses, sheds, silos etc) 7 Low/high points (spurious high/low returns (unusable)) 8 Model key points (Reserved for 'model key points' only) 9 Water (any point in water) 10-11 Defined by supplier **12 DO NOT USE FOR OVERLAP IN FINAL DELIVERY – must be defined as withheld flag and overlap classified as part of step 5 in workflow above** 13-31 Defined by supplier *It is understood that through the process of Level 2 ground surface improvement that best practice stipulates level 1 classification is carried out to aid manual validation. Focus of level 1 classification should be on a "clean vegetation cloud" free of atmospheric clouds and noisy return data. It is however expected that there will be within the vegetation layer some misclassification of structures such as buildings, vehicles, and power cables due to the automated nature of level 1 classification.

Commination and Reporting Requirements

The LiDAR provider is expected to provide progress updates throughout all stages of the project, in the form of verbal conversations, email and formal reports.

- Progress Reports must be provided weekly via email and include a KML, GPX file of Shapefile of the captured flight lines. These reports will provide updates on progress of the capture and data processing tasks, whether tasks are still within timeframe expectations.
- A Final Project report will be provided with the delivery of the final data and derived products upon project completion.

Data Supply Specifications

Deliverable	Format	Notes
Classified point cloud	.LAS (.LAZ)	Classified dataset as outlined above in tiles.
Unclassified Point cloud	.LAS (.LAZ)	Full unclassified point cloud in tiles (raw return data prior to noise filtering and classification)
Full wavelength	PulseWaves Format	Full waveform in PulseWaves compression format.
1m Intensity Images	.TIF	Derived 1m resolution images of intensity.
1m Contours	ESRI Shape file	Derived 0.5m resolution contours.
1m DTM	.TIF	Derived 1m resolution DEM surface, from triangulated mesh from processed LiDAR ground points (class 2,8).
Aerial Photos	ECW & .TIF	0.10-0.20cm resolution (preference for 0.10cm)

Deliverable	Format	Notes
Flight Trajectory	ESRI Shape file	Actual flight lines including a minimum of date, time, altitude, point source ID.
Project Report	PDF	This report provides a single point of reference, describing the project, work undertaken, processing steps followed and dataset accuracy checks completed. For each supplied LiDAR data product this report should either include a metadata statement consistent with the ANZLIC Metadata Profile (Version 1.1) or supply the ANZLIC approved XML format. The ANZMET Lite metadata tool will be used to validate all XML records if these are being provided. http://www.anzlic.org.au/infrastructure_metadata.html Example of metadata information: 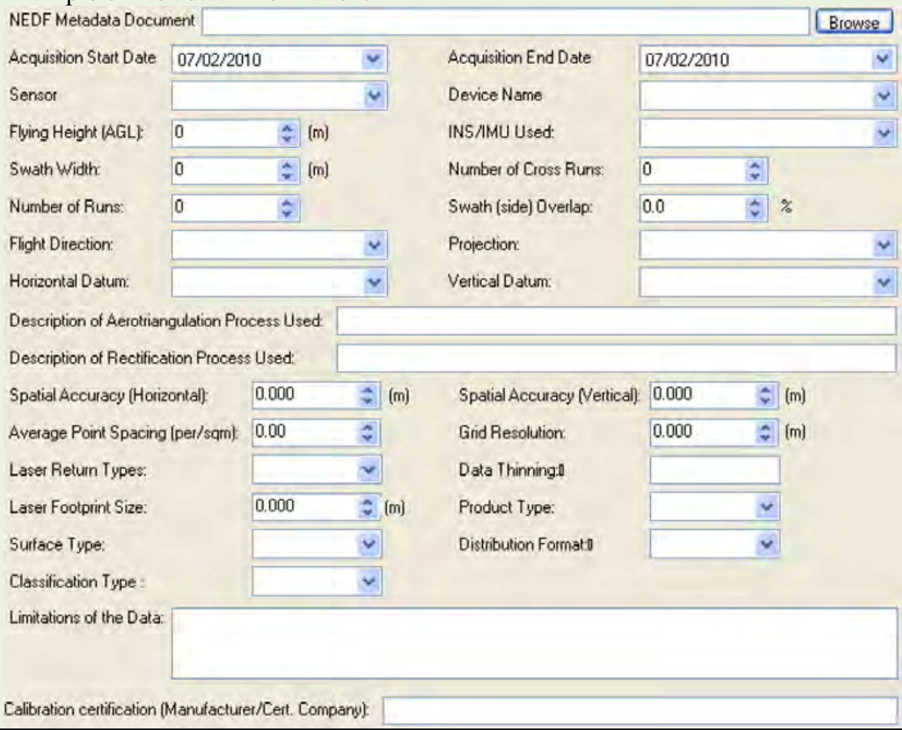 NEDF Metadata Document Browse Acquisition Start Date 07/02/2010 Acquisition End Date 07/02/2010 Sensor Device Name Flying Height (AGL): 0 (m) INS/IMU Used: Swath Width: 0 (m) Number of Cross Runs: 0 Number of Runs: 0 Swath (side) Overlap: 0.0 % Flight Direction: Projection: Horizontal Datum: Vertical Datum: Description of Aerotriangulation Process Used: Description of Rectification Process Used: Spatial Accuracy (Horizontal): 0.000 (m) Spatial Accuracy (Vertical): 0.000 (m) Average Point Spacing (per/sqm): 0.00 Grid Resolution: 0.000 (m) Laser Return Types: Data Thinning: Laser Footprint Size: 0.000 (m) Product Type: Surface Type: Distribution Format: Classification Type : Limitations of the Data: Calibration certification (Manufacturer/Cert. Company):
Tile Index Metadata	ESRI Shape file	Tile index polygon showing meta data including date of acquisition for the LiDAR dataset.

Finally, after all the data is received and a quality assurance (QA) is compete the data is sign off. Otherwise, the airborne LiDAR supplier has 30 days from final data delivery to ensure data products meet project standards.

For further information please contact:

Susana Gonzalez

Email : Susana.Gonzalez@interpine.nz

Mobile : +64 21 026 49733

Office: +64 7 3503209

Disclaimer

The information in this document has been prepared and approved by Interpine Group Limited (Interpine). Access to the information in this document is being given by Interpine specifically to the person(s) to whom it was intended. The information contained in this document remains the intellectual property of Interpine and may not be reproduced, distributed or published by any recipient for any purpose without the prior written consent of Interpine.

Although all reasonable care has been taken to ensure that the information contained in this document is accurate, neither Interpine nor its respective officers, advisers or agents makes any representation or warranty, express or implied as to the accuracy, completeness, currency or reliability of such information or any other information provided whether in writing or orally to any recipient or its officers, advisers or agents.

Interpine and its respective officers, advisers, or agents do not accept: any responsibility arising in any way for any errors in or omissions from any information contained in this document or for any lack of accuracy, completeness, currency or reliability of any information made available to any recipient, its officers, advisers, or agents; or any liability for any director or consequential loss, damage or injury suffered or incurred by the recipient, or any other person as a result of or arising out of that person placing any reliance on the infomation or its accuracy, completeness, currency or reliability.

Interpine Group Ltd
P.O. Box 1209, Rotorua
Telephone. (07) 345 7573
Email. info@interpine.co.nz
Website. www.interpine.com

References

Mitchell, B., Fisk, H., Clark, J., Rounds, E. (2018) LiDAR acquisition specifications for forestry applications. US Forest Service, Geospatial Technology & Applications Centre.

Natural Resources Canada (2017) Federal airborne LiDAR data acquisition guideline. Version 1.0. General Information Product 117e, Natural Resources Canada (https://doi.org/10.4095/304669)

White, J.C., Wulder, M.A., Varhola, A., Vastaranta, M. (2013) A best practices guide for generating forest inventory attributes from airborne laser scanning data using an area-based approach. Canadian Forest Service Information Report FI-X-010.

White, J.C., Tompalski, P., Vastaranta, M., Wulder, M.A., *et al*. (2017) A model development and application guide for generating an enhanced forest inventory using airborne laser scanning data and an area-based approach. Canadian Forest Service Information Report FI-X-018.